THE FLEXURAL SEISMIC RESISTANT DESIGN OF REINFORCED CONCRETE BRIDGE COLUMNS

by

OTTON LARA

Civil Engineer Instituto Tecnológico de Monterrey, Mexico 1968

M.Sc. University of California, Berkeley 1976

A THESIS SUBMITTED IN PARTIAL FULFILLMENT OF

THE REQUIREMENTS FOR THE DEGREE OF

DOCTOR OF PHILOSOPHY

in

THE FACULTY OF GRADUATE STUDIES
(Civil Engineering)

THE UNIVERSITY OF BRITISH COLUMBIA
(Vancouver)

DECEMBER 2011

ABSTRACT

Experimental studies about the cyclic response of reinforced concrete bridge columns designed to avoid shear failure and subjected to cyclic, reversible, and increasing displacements have been performed in several laboratories around the world. As a consequence there are several force-displacement relationships, called resultant models, that allow to predict the response of those columns. However, the use of the resultant models for earthquake response requires extensive calibration of several parameters.

In this investigation a Finite Fiber Element Model, FFEM, is obtained after calibrating first, the response of 30 circular reinforced concrete bridge columns tested under cyclic, reversible, and increasing displacements. Then a re-calibration is carried out in order to simulate the response of two additional columns shake table tested under two earthquake ground motions. After obtaining satisfactory results the FFEM was used to simulate the seismic response of three bridge columns designed according to the prescriptions of the new seismic design bridge code.

The FFEM is able to predict directly four flexural failure mechanisms: cracking and crushing of the unconfined and confined concrete, fracture of the longitudinal steel bars due to tension, P-Δ effects, and fatigue of the longitudinal steel bars. Indirectly, the FFEM is able to predict the possible buckling of the longitudinal bars by capturing the confined concrete strain time-history.

In order to capture the low-cyclic fatigue, the FFEM through inelastic dynamic analysis is able to calculate the number of cycles and the amplitude of the cyclic plastic strains so these quantities are introduced into the fatigue equation. The fracture of the bars due to low-cyclic fatigue is a failure mechanism that depends on the accumulation of damage along the severe ground motion. The way to estimate the loss of fatigue life in a steel bar is considering the effect of the duration in the calculations since the materials stress-strain relationships are independent of the duration of the ground motion.

In order to determine the accumulation of damage in the bridge column a Cyclic Damage Index is proposed here. The Index is based on the energy dissipated by the column at the end of the ground motion.

TABLE OF CONTENTS

LIST OF TABLES

LIST OF FIGURES

LIST OF SYMBOLS

β_c parameter that regulates the importance of the repeated cyclic displacements

δ code allowable drifts values

Δ lateral displacement

Δ_{max} maximum lateral displacement (for P-Δ effects)

ε strain

ε^* normalized steel strain in Giuffre, Menegotto and Pinto steel stress-strain relationship

ε_c concrete compressive strain

ε_{cc} confined concrete strain for the maximum confined concrete strength

ε_{co} unconfined concrete strain for the maximum unconfined concrete strength

ε_{cu} ultimate confined concrete strain

ε_i strain amplitude at each cycle of the strain history

ε_o, σ_o strain and stress at the beginning of yielding in Giuffre, Menegotto and Pinto steel stress-strain relationship

ε_p plastic steel bar strain

ε_r, σ_r strain and stress at the beginning of unloading or reloading in Giuffre, Menegotto and Pinto steel stress-strain relationship

ε_s steel bar strain

ε_{scycle} cyclic strain in a steel bar

ε_{sp} ultimate unconfined concrete strain

ε_{su} ultimate steel bar strain

ε_{sy} yielding steel bar strain

ε_y yielding steel bar strain in Giuffre, Menegotto and Pinto steel stress-strain relationship

ε_0 strain amplitude at which one complete cyclic on a virgin material will cause failure of a longitudinal steel bar

θ_Δ stability index to limit P-Δ effects

μ_c cyclic ductility ratio

μ_{cpe} enveloping cyclic ductility ratio

μ_{nc} non-cyclic ductility ratio

ξ fraction of critical damping

ρ percentage of longitudinal steel

ρ_s percentage of transverse steel

σ^* normalized steel stress in Giuffre, Menegotto and Pinto steel stress-strain relationship

σ_y yielding steel stress in Giuffre, Menegotto and Pinto steel stress-strain relationship

ϕ_p plastic curvature

ϕ_u ultimate curvature

ϕ_y yielding curvature

ω_n circular natural frequency of the structure in the elstic range

c damping coefficient

CDI cyclic damage index

C_y seismic coefficient

d column diameter

D overall damage causing fracture due to low-cyclic fatigue in one bar

d_b longitudinal bar diameter

D_i damage in one bar due to every strain amplitude ε_i of the time history response

E_c energy capacity of the column

E_H dissipated energy of the column

EPP elastic-perfectly plastic

EQ earthquake

EQ_s earthquakes

E_{sec} secant modulus of elasticity

E_{ucpe} envelope energy. It is the the energy dissipated by the new cyclic plastic displacements

E_{ucpr} repeated energy. It is the energy dissipated by the repeated cyclic plastic displacements

E_0 initial modulus of elasticity of the steel bar in Giuffre, Menegotto and Pinto steel stress-strain relationship

E_1 tangent modulus of elasticity for the plastic zone in Giuffre, Menegotto and Pinto steel stress-strain relationship

F shear capacity of the column

f_c concrete compressive stress

f'_c concrete compressive strength

f'_{cc} confined concrete compressive strength

f'_{ce} expected concrete compressive strength

FDI fatigue damage index with a value equal to D

FFEM fiber finite element model

f'_l confinement concrete strength

F_s resistance function

f_{ue} expected tensile strength

f_y yielding strength of longitudinal steel reinforcement

F_y yielding Strength

f_{ye} expected yielding steel strength

f_{yh} yielding strength of transverse steel reinforcement

F_0 elastic strength

g gravity

L column length

l_d development length

L_{end} length of the fiber finite element attached to the foundation

L_p plastic hinge length

l_{sp} strain penetration length

LSPL life safety performance level

m parameter for fatigue equation; it is the log of the total strain amplitude divided by the log of the number of cycles to failure

M mass for the equation of motion

M_{cap} flexural moment capacity

M_p plastic flexural moment

M_u ultimate flexural moment

n_i number of cycles at determined strain counted on the strain history of a steel bar

N_f number of constant strain amplitude cycles that cause failure of the steel bar

N_{fi} log of the number of cycles to failure

OpenSees Open System for Earthquake Engineering Simulation

P axial force

PBSE performance based seismic engineering

PGA peak ground acceleration

R strength reduction

R_c constant strength reduction factor given by codes

R_0, R_1, R_2 parameters to simulate the Bauschinger effect of the inelastic response

Sa spectral acceleration

SDC seismic design category, according to AASHTO

SDOF single degree of freedom

SDPL significant damage performance level

SF scale factor

t time

T natural period of the column

T_g earthquake predominant period

u displacement response

$\dot{u}$ velocity response

$\ddot{u}$ acceleration response

$\ddot{u}_g$ ground acceleration

u_c cyclic displacement

u_{cp} cyclic plastic displacement

u_{cpe} envelope cyclic plastic response

u_{cpr} repeated cyclic plastic response

$|u_m|$ maximum lateral displacement

u_{nc} non-cyclic response

u_{ncp} non-cyclic plastic displacement

u_{ncp1} non-cyclic plastic displacement at 2% drift

u_{ncp2} non-cyclic plastic displacement at the end of the test

u_p plastic lateral displacement

u_y structure yield displacement

$u_{y(envelope)}$ reference to calculate u_{ncp}; it is not the structure yielding displacement u_y.

u_0 elastic displacement

w_1 weighting factor used by the Gauss quadrature method of integration

ACKNOWLEDGEMENTS

The Natural Science and Engineering Research Council of Canada (NSERC) provided partial support for this study. The author would also like to recognize the support provided by The University of British Columbia in Vancouver, Canada, and, Escuela Superior Politécnica del Litoral (ESPOL) and the Universidad de Guayaquil, both in Guayaquil, Ecuador.

The author recognizes that this dissertation would not have been possible without the commitment of Professor Vitelmo V. Bertero. His constant mentorship along the years and his advice are gratefully appreciated and thanked.

Professor Carlos E. Ventura, a friend of many years, opened for me the doors of the University of British Columbia at Vancouver. He gave me all the support required to fulfill the need of learning.

Professors Liam Finn and Ricardo Foschi suggested important ideas for the dissertation.

Jose Centeno did his Civil Engineer thesis under my direction at ESPOL and that was the beginning of the dream. With the advice of Professor Bertero we approached the problem of cyclic response.

Dr. Vinicio Suarez introduced me to the OpenSeees framework.

Daniel Toro an assistant engineer at Sismica Consulting, helped me by running the programs.

DEDICATION

To my Mother

To my sons:
Luis Fernando,
Otton Francisco,
and Carlos Alberto

To my grandchildren

To my sisters and brothers

To Fabiola, my wife

1. GENERAL INTRODUCTION, SCOPE, ORGANIZATION

1.1 General introduction

Bridge seismic design codes such as those of the American Association of State Highway and Transportation Officials (AASHTO) (2007) and the California Department of Transportation (Caltrans) (2006) are based on limiting the demand of maximum lateral displacements to meet the life safety performance level (LSPL). This limit has been defined by those codes as the displacement capacity that corresponds to the maximum confined concrete compressive strain given by Mander et al. (1988); it is obtained from a pushover analysis of the bridge structure.

The demand is obtained after performing an elastic analysis of the structure subjected to a site response spectrum the ordinates of which have been previously reduced from the elastic code prescribed design spectrum for the site of the construction. The value of the reduction is not prescribed by the codes; it is chosen by the designer to meet the displacement capacity prescription. According to the codes the maximum lateral elastic displacement demand on the bridge structure is assumed to be equal to the maximum lateral inelastic displacement demand by virtue of the equal displacement concept.

Using elastic spectrum matching, new codes also allow for seismic design or for design checking using three compatible records and obtaining for each record inelastic time history displacement responses for the structure. The maximum lateral or peak displacement from these responses is compared with the lateral displacement capacity. It is also possible to use seven compatible records and compare the average lateral displacement demand with the displacement capacity.

Mahin and Bertero (1981), in their evaluation of inelastic seismic design spectra, pointed out that the lateral evaluation of displacements to control damage was not enough, since earthquakes induce several cycles of inelastic response; they proposed that the maximum actual lateral displacement should take into consideration the previous plastic displacement. They called this maximum displacement “the cyclic lateral displacement”. The study of the cyclic response is the motivation of this dissertation.

As will be shown later, even the cyclic lateral displacement proposed by Mahin and Bertero (1981) is not enough to evaluate structural damage, since all plastic strains induced by the cyclic plastic displacements contribute to the damage. Therefore, it is proposed here to use the complete cyclic plastic displacement time history to provide a more reliable measure of material damage.

In their report about the rate of loading effects on uncracked and repaired reinforced concrete members Mahin and Bertero (1972) demonstrated that in a cyclic response the new plastic displacements cause the major amount of damage in the materials and that each repetition of plastic displacement causes less damage. However, the number of cycles of repeated plastic displacements and their amplitudes will accumulate damage in the steel structure or in the longitudinal steel bars of reinforced concrete structures, diminishing their fatigue life and eventually resulting in the fracture of the steel due to low-cyclic fatigue.

Applying a simple algorithm to the hysteretic time history response of a structure makes it possible to determine the new plastic displacements located in the envelope of all hysteretic responses. The rest of the cycles contain the repeated plastic displacements.

The investigation is focused on the flexural seismic cyclic response of reinforced concrete bridge columns, and for this purpose a fiber finite element model (FFEM) is developed. The FFEM is able to simulate the response of the columns when four flexural failure mechanisms are considered: (1) crushing of the confined and unconfined concrete, (2) fracture of the longitudinal bars due to tension, (3) P-Δ effects, and (4) fracture of the longitudinal bars due to low-cyclic fatigue. In the proposed FFEM, the damage each plastic strain induces in the longitudinal steel bars and the accumulation of such damage are taken into account using the fatigue model presented by Uriz and Mahin (2008) and the Brown and Kunnath (2000) parameters.

1.2 Objectives

The main objective of this dissertation is to study the flexural seismic response of reinforced concrete bridge columns, taking into consideration the four flexural failure mechanisms mentioned above and particularly examining the damaging effect of low-cyclic fatigue on the longitudinal steel bars when the columns are subjected to earthquakes and aftershocks. This effect is not taken into account by new seismic bridge codes. Other objectives are to develop a

general FFEM to simulate such responses and to develop a cyclic damage index (CDI) to estimate the level of damage induced by the four flexural failure mechanisms mentioned above.

1.3 Scope

Performance-based seismic engineering (PBSE), defined in Structural Engineering Association of California (SEAOC) Vision 2000 (1995), establishes levels of performance based on damage at and after a structure reaches yielding level. PBSE emphasizes that there is damage even during elastic response, local buckling or structure vibration amplitudes larger than the human sensitivity limit, but this is not considered in this study, since its scope is beyond the objectives of this investigation.

The complete system to analyze for design should include the soil foundation and the environment around the construction, as indicated in SEAOC Vision 2000 (2003), but this dissertation focus only on the localized flexural damage of reinforced concrete code-designed fixed cantilever bridge columns under severe earthquakes.

It is understood that the crushing by tension of the unconfined cover concrete leaves the steel bar and the spiral without this support (Bertero et al., 1962). In addition, the vertical component of the ground motion increases the compression on the bridge column inducing its lateral expansion and the enlargement of the spiral leaving the longitudinal steel bar without this important lateral support. The plastic strains in the longitudinal steel bars induce fatigue of these bars, so that they lose part of their fatigue life with each plastic cyclic strain until fracture due to low-cyclic fatigue or buckling could occur. In addition, after crushing of the unconfined cover concrete and the enlargement of the spiral, the flexural shear is taken only by the fatigued longitudinal steel bars. This could induce the initiation of a crack in the confined concrete that could lead to a shear failure. The response of the column to the other horizontal component would increase this damage.

The use in this study of only the largest horizontal component of the ground motion without consideration of the other horizontal and the vertical components is another limitation of this investigation.

The study is in addition limited to modern designed reinforced concrete bridge columns where shear has been avoided by careful use of code recommendations. It should be mentioned that the 32 laboratory tested bridge columns the response of which is used to calibrate the FFEM proposed in this investigation were designed to avoid shear failure and that all of them failed by flexure during the tests. It also should be mentioned that in most of the laboratory tested columns fracture of the longitudinal bars due to low-cyclic fatigue and/or buckling of those bars occurred.

The CDI proposed in this investigation as a practical tool to evaluate the state of flexural damage of bridge columns or for the seismic design of new bridge columns is limited to earthquake ground motions generating several cycles of inelastic response. Ground motions with large pulses inducing a very small number of repeated plastic displacements dissipate very small amounts of energy; therefore, the CDI does not give reliable information about the damage. The response for this type of earthquake is close to a pushover.

1.4 Organization

Each chapter in the body of this thesis begins with an introduction and ends with a summary and conclusions.

Because bridge columns are an important part of any bridge it is important to understand the effects of plastic cyclic response of bridge columns that have been well designed to code. Therefore, it was decided to begin this dissertation by studying the seismic response of single degree of freedom (SDOF) systems for elastic perfectly plastic (EPP) force–displacement relationships. The results are presented in Chapter 2.

The time history responses of the EPP SDOF systems due to severe earthquake ground motions show the different cycles of displacement, including the elastic and plastic portions where the maximum positive and negative lateral displacements of the time history forming the extremes of the envelope of all hysteretic responses as well as the repeated cycles of displacements that remain inside the envelope can be observed. The hysteretic responses show the reduced yielding forces and all the loops of the inelastic responses.

The new and repeated plastic responses are considerable larger than the plastic part of the peak lateral response for any strength reduction factor used and for almost all periods considered, as seen in the time histories and in the response spectra comparisons shown in Chapter 2.

It will be seen that reduction factors used to obtain inelastic responses are not constants and that the displacement responses should be limited by cyclic or non-cyclic ductility ratios. This is the main role of the non-cyclic ductility ratios since they do not measure plastic displacements and are not measures of damage.

The results of Chapter 2 also allow the clarification that drifts still used by some codes for building design do not measure plastic displacements and are not measures of damage. They are simply limits based on earthquake experience imposed by some codes. The new AASHTO and Caltrans codes no longer use drifts and now use non-cyclic or traditional ductility ratios to limit the lateral response of low period structures.

In Chapter 2 another analysis is performed. It was decided to observe the variations of the strength reduction factors for cyclic and non-cyclic response.

The results show that the strength reduction factors vary with the period and the plastic displacements demanded by every ground motion. It will be seen that for non-cyclic response the strength provided to the structure is less than the strength required for cyclic response and that designing for non-cyclic response increases the potential damage.

The results clearly show that cyclic response deserves attention because seismic response is cyclic, the plastic cyclic displacements are considerable larger than the non-cyclic ones, and the required strength is larger than the one used for the non-cyclic response.

In addition, it is also shown in Chapter 2 that the potential damage due to cyclic or non-cyclic plastic response can be associated with the energy dissipated at the end of the excitation and that the total energy can be divided into that related to the new plastic displacements and that related to the accumulation of the repeated plastic displacements.

Chapter 2 also demonstrates that aftershocks increase the repeated plastic displacements, since in general aftershocks have lower accelerations than those of the main shock. If the stiffness of the structure has not been considerably affected during reversals of plastic displacements, aftershocks rarely induce increases of new plastic displacements.

Since all the above analysis was performed for EPP systems, it was decided to study the effects of cyclic response on bridge columns that deteriorate in stiffness and strength. The development of a model with such characteristics is the content of Chapter 3.

Although there are very good resultant models used successfully by several researchers to predict seismic responses, it was decided to use the fiber finite element contained in the Open System for Earthquake Engineering Simulation (OpenSees) framework to model a fiber finite element model to simulate seismic responses of cantilevered bridge columns.

The model has three beam-column elements. Element 1 simulates the tension strain effect on the reinforcement from the base of the bridge column under the foundation; because of the numerical procedure involved in the integration of stresses and strains it has a length equal to twice the strain penetration length. Element 2 contains the length of the plastic hinge and has a length two times the plastic hinge length. Element 3 goes from the end of element 2 to the top of the column and remains elastic. At the integration points of each element the beam-column elements are discretized into small fiber elements, each one with a constitutive relationship for the confined and unconfined concrete and for the steel bars.

In addition to the constitutive stress–strain relationships for the unconfined and confined concrete and for the steel bars, the FFEM contains materials properties such as the P-Δ effect and the low-cyclic fatigue of the longitudinal steel bars.

The FFEM, through the measurement of strains in the materials, is able to determine the four flexural failure mechanisms mentioned in section 1.1.

The FFEM developed in Chapter 3 was calibrated individually for each one of 30 reinforced concrete bridge columns tested in the laboratory under cyclic reversible and increasing displacements. In order to ensure that the model gives comparable results with the tests, the

dissipated energies were compared. Once the simulated energies were within 10% of the energies measured in the tests the simulation was accepted.

For earthquake response simulation the simulations for each of the 30 columns tested under cyclic displacements were recalibrated with respect to the shake table responses of two additional reinforced concrete bridge columns subjected to two different scaled ground motions tested by Hachem et al. (2003). The recalibration focused on the parameters that develop the steel stress–strain relationship used in the fiber finite element. After recalibration the comparison of the strain time history responses obtained with the FFEM and those of the two shake table tests was considered satisfactory.

One of the most common flexural failure mechanisms encountered in the laboratory and in the simulations for the 32 bridge columns is the fracture of longitudinal bars due to low-cyclic fatigue.

In Chapter 3 it is proposed that the occurrence of any one of the flexural failure mechanisms during the earthquake should be identified as a significant damage performance level (SDPL), since the damage will require retrofit that is difficult and costly to execute and can even require stopping traffic. The SDPL proposed in this investigation can be considered as a definition for the LSPL, since this limit state can vary from yielding to near collapse.

The simulations were performed using the OpenSees framework (Mazzoni et al., 2006; McKenna, 1997), which is an object-oriented finite element program.

Chapter 4 begins with the design of three bridge columns each with periods T = 0.5, 1.0, and 1.5 s, following AASHTO and Caltrans new prescriptions.

Once it is proved that the bridge columns meet code requirements, the AASHTO prescriptions for inelastic dynamic analysis are followed. To do so, it is necessary to select three ground motions with some similar characteristics. For this study, magnitude, soil type, and earthquake source were chosen. In addition, AASHTO requires that the elastic spectrum of each of the three ground motions matches the site code spectrum for the periods of each bridge column.

It is proved through the seismic simulations that the design of the columns meets the code requirements. However, in some cases the columns suffer fracture of the longitudinal bars due to low-cyclic fatigue; this is a flexural failure mechanism not considered in the new codes.

Later, the damaged columns are subjected to aftershocks that increase the damage either by fracturing more bars due to low-cyclic fatigue or by crushing the confined concrete due to an excessive lateral displacement larger than the code limits.

The accumulation of plastic strains causing damage by low-cyclic fatigue is captured for each bar for the duration of the strong motion. The accumulation of damage in each affected steel bar could carry it to fracture, decreasing the strength and stiffness of the bridge column. Bridge columns models using the present constitutive relations of the materials cannot capture this type of failure because those relations are independent of the duration of the ground motion.

The complexity of the analysis called for a simple tool to identify the four flexural types of damage. The simple tool is the cyclic damage index associated with the energy dissipated by the bridge column at the end of the ground motion. The base line of the CDI is the SDPL.

Chapter 5 focuses on the development and application of the CDI. The three bridge columns designed and analyzed in Chapter 4 are subjected to 28 earthquake records grouped in four bins of seven records each. Each bin has in common only one characteristic, the source mechanism. The following three sources were chosen: subduction, crustal, and near fault records. In addition, because of their particular response characteristic, soft soils records from subduction earthquakes were also considered for another bin. Other characteristics such as magnitude and soil type are not considered for any of the bins

The occurrence of low-cyclic fatigue for some main shocks and aftershocks gave rise to two questions that are investigated in Chapter 6. These are (1) for bridge columns well designed to new codes, what would be the seismic response if the low-cyclic fatigue is not considered as a flexural failure mechanism? and (2) in bridge columns well designed to new codes where low-cyclic fatigue induces fracture of the bars, how can the columns be designed to avoid this frequent flexural failure mechanism?

To answer the first question, the column property model of low-cyclic fatigue is deactivated from the FFEM. The result is that for bridge columns designed to new codes a ground motion rarely induces any of the flexural failure mechanisms incorporated into the FFEM and deterioration of strength is limited to the level of strain reached in the confined concrete. There is always deterioration of stiffness due to the Bauschinger effect on the steel bars.

Instead, when the low-cyclic fatigue is activated, the fracture of bars due to low-cyclic fatigue induces a considerable deterioration of strength.

This is clearly revealing that the effect of the strong motion duration of severe earthquake ground motions is to induce large plastic reversible strains and that the number of cycles during the response could be enough to induce the diminishing of the fatigue life of the longitudinal steel bars and the possible fracture of some of these bars due to low-cyclic fatigue.

To answer the second question, it was decided to redesign the T = 1.5 s column. The stiffness and the strength were considerably improved, so the main shock that induced the fracture of seven bars due to low-cyclic fatigue would not be able to fracture any bar.

Of course, there are many other ways to avoid the fatigue of the bars, such as the use of energy dissipaters, dampers, or vibration isolators, but it was decided to choose the redesign simply to call attention to the low-cyclic fatigue phenomenon that is not recognized at the moment by the seismic codes.

Chapter 7 gives discussion, final conclusions and recommendations for future studies.

2. IMPORTANCE OF SEISMIC CYCLIC REVERSIBLE PLASTIC RESPONSE ON STRENGTH, DISPLACEMENT, AND ENERGY DEMANDS

2.1 Introduction

This chapter is devoted to the understanding of the cyclic characteristic of seismic response to obtain a better estimation of earthquake damage. Cyclic response is achieved in this chapter using a single degree of freedom (SDOF) system and the elastic perfectly plastic (EPP) force–displacement relationship.

Experimental studies cited later demonstrate that seismic response is cyclic and that during strong motion there are plastic displacements causing damage and sign reversals of plastic displacements that cause even more damage to structural elements. A reversal of plastic displacement occurs when there is a change of sign. For example, in the hysteretic envelope shown in Figure 2.1 a, the changes of sign are from E to G and from K to L, so in that envelope there are two reversals of plastic displacements.

Therefore, it is proposed that damage control should include the estimation of not only the plastic part of the maximum lateral displacement $|u_m|$ as it has been traditionally measured but also all the other plastic displacements that can be measured in the time history response of the structural system.

For example, in Figure 2.4 a, $|u_m|$ = 19.8 cm, and since the yield displacement u_y is 0.57 cm, as seen in Figures 2.4 a and b, the traditional measure of damage or maximum plastic displacement in the time history response is $|u_m| - u_y$ = 19.2 cm. However, Figure 2.4 a shows several other plastic displacements in the positive and negative directions occurring before and after the measured 19.2 cm that are also causing damage. Therefore, the proposition is that all plastic displacements should be taken into account to have a better estimation of the total potential damage that a severe ground motion can induce in a structural system.

As seen in Figure 2.4 b, the envelope hysteretic cycle contains the new plastic displacements of the time history response, but at the interior of the envelope there are several smaller hysteretic cycles. The plastic displacements of these smaller cycles are repeated with respect to the new ones. Therefore, the hysteretic response shows that the plastic response includes not only the new plastic displacements but also the repeated ones, as Mahin and Bertero (1981) pointed out through their experimental work. They even found that the new plastic displacements induce the major damage, whereas each one of the repeated ones causes less damage. However, depending on the number of cycles and the amplitude of the plastic strains generated in the steel the structural element can fail owing to low-cyclic fatigue.

In the envelope hysteretic cycle of Figure 2.1 a, the new plastic displacements are from A to B, from D to G, from J to A, and from B to L. The repeated plastic displacement goes from A to B. Notice that in Figure 2.1 a there are no internal hysteretic cycles as shown in Figure 2.2.

Figure 2.1 b is a simplified representation of the experimental results given in Figure 2.2 that show several internal hysteretic cycles, i.e., repeated plastic displacements that do not appear in the example given in Figure 2.1 a.

The EPP model used in this chapter is only a very gross approximation to the nonlinear behavior of a structural system, as it does not account for other important aspects of seismic response, such as strength and stiffness degradation. On the other hand, the simplicity of the EPP model provides a significant insight into the cyclic response of a structure subjected to a single earthquake while also comparing it with the effects of possible aftershocks.

2.2 Definitions and observations

Laboratory tests on structural components and scaled frames subjected to quasi-static cyclic displacements (Krawinkler et al., 1971) or to scaled ground motions (Lignos et al., 2008) have shown that there are several levels of damage after the first yielding of the steel; therefore, plastic displacements represent structural damage. The tests also demonstrate that earthquake response is in general two sided and that during the dynamic response there are several cycles that include reversals of plastic displacements forming hysteretic responses. The area of all hysteretic responses is the total energy dissipated by the structure at the end of the ground motion, and that energy can be associated with a measure of damage. Based on experimental

evidence, the performance-based seismic design methodology proposed by the Structural Engineering Association of California (SEAOC) (1995) Vision 2000 establishes levels of seismic performance based on the damage at and after the structure reaches yielding level but does not consider the cyclic response.

Based on the available evidence, the following observations, definitions, and assumptions are introduced.

- Reversals of plastic displacements. Occur when the plastic displacement changes sign. The reversals are not recoverable.
- Physical ductility. The plastic displacement physically measurable on the envelope of the hysteretic response.
- Damage potential. In this chapter, it is difficult to quantify the structural or even the localized damage because the model is EPP and it does not capture strength and stiffness degradation. The phrase "damage potential" is associated with the plastic displacement demanded by the earthquake, which is also called physical ductility demand and according to experiments induces structural damage, i.e., the larger the physical ductility demand or the energy demand, the larger the potential damage.
- Damage. In this study, damage is associated to the stiffness and strength degradation induced by flexural failure. Damage as defined cannot be identified in EPP systems.
- Yield displacement, u_y. The displacement associated with the first or initial yielding of the steel, e.g., point A in Figure 2.1 a.
- Cyclic response. Any complete hysteretic response, including the reversals that close the cycle. Earthquakes induce several cycles of inelastic response except near fault records that induce few cycles after the large lateral displacements induced by the pulses contained in such records.
- New plastic displacements. Plastic displacements that follow a path that has not been followed up to the moment.
- Repeated plastic displacements. Plastic displacements that follow a path that was already traversed.
- Envelope cyclic plastic response $u_{cpe.}$ Summation of all new plastic displacements measured in both directions in the envelope of all hysteretic responses. From J to L and from D to G in Figure 2.1 a.

- Repeated plastic response u_{cpr}. Cyclic plastic displacements occurring repeatedly after the new plastic displacement. It is in general measured inside the envelope of all hysteretic responses. In Figure 2.1 a, the repeated plastic displacement is in segment AB when a second cycle beginning at A goes up to L. Figure 2.1 b shows several internal cycles located inside the envelope. Each one shows a repeated plastic displacement.
- Dissipated energy E_H. Energy absorbed through unrecoverable plastic displacements of the structure. Since severe earthquakes induce reversible plastic displacements, the energy absorbed dissipates through the hysteretic response of the structure. When the earthquake shaking ends and the structure reaches the at-rest position, the elastic strain energy approaches zero. What is left in the energy equation is the energy dissipated through hysteretic response, which represents the final amount of energy absorbed by the system (Christopoulos and Filiatrault, 2006). Using the results by Mahin and Bertero (1981), the total hysteretic energy will be divided into the one dissipated by the new plastic displacements, E_{ucpe}, and the one dissipated by all the repeated plastic displacements, E_{ucpr}. Figures 2.4 b and 2.5 b show the hysteretic responses where both dissipated energies are located. E_{ucpe} is the energy measured in the envelope of the hysteretic responses, and E_{ucpr} is the energy accumulated through the smaller hysteresis at the interior of the envelope. Eventually there can be a repeated cycle similar to the envelope. The new plastic displacements and the repeated ones as well as their amplitudes can also be detected following the time history responses, as shown for example in Figures 2.4 a and 2.5 a.
- Non-cyclic response u_{nc}. Traditionally known maximum positive or negative lateral peak response measured on the envelope of the hysteretic responses but with no relation to cyclic reversible displacements. It is from L to K or from G to E, whichever is larger, in Figure 2.1 a.
- Maximum lateral displacement $|u_m|$. Absolute value of the maximum lateral displacement. It is measured in the envelope of the hysteretic responses from the maximum absolute lateral displacement $|u_m|$ back to the last zero displacement crossing. It is the absolute value measured from L to K or from G to E, whichever is the larger in Figure 2.1 a.
- Non-cyclic lateral plastic displacement or non-cyclic lateral physical ductility u_{ncp}. Refers to the plastic part of $|u_m|$. Its measurement depends on the position of the envelope of all hysteretic responses with respect to the displacement axes. It is explained for all cases in section 2.4.

- Cyclic displacement u_c. Summation of $|u_m|$ and the previous plastic displacement, both completing the lateral cycle that is part of the complete envelope cycle. It is measured from $|u_m|$ back to the previous zero force crossing in the envelope of the hysteretic responses. It is from G to C or from L to H, whichever is larger in Figure 2.1 a.
- Cyclic plastic displacement u_{cp}. The plastic part of u_c.
- Non-cyclic ductility ratio μ_{nc}. Traditionally known ductility ratio relating the maximum lateral $|u_m|$ to the yield u_y displacements.
- Cyclic ductility ratio μ_c. Relationship between the maximum lateral cyclic u_c and the yield u_y displacements.
- Envelope cyclic ductility ratio μ_{cpe}. Relationship between the envelope plastic displacement u_{cpe} and yield displacement u_y.
- Strength reduction R. Value used to reduce maximum elastic strength demand on the basis that R is associated with ductility capacity. Under this concept, the strength reduction from the maximum elastic strength demand yields an inelastic system that will be subjected to a ground motion. The non-linear calculation of the solution will deliver a history of inelastic response and a demand of ductility that depends on the selected R.
- Strength reduction factor given by codes R_c. Fixed value selected by the designer from building codes for different types of structures. R_c reduces the prescribed elastic spectrum that is used later to analyze an elastic structure. The results are reduced internal forces and displacements of an elastic system. Therefore, R_c is not related to the ductility demanded by the earthquake on an inelastic structure.
- Elastic strength demand F_0 and corresponding elastic displacement demand u_0. Both obtained for a linear elastic structure of period T subjected to a ground motion or to an elastic spectrum.
- Yielding strength F_y and yielding displacement u_y. Both values depend on the selected R or R_c.
- Life safety performance level. A structure reaches damage in its critical sections but without causing danger to the safety of the occupants. The structure is still standing, but after the earthquake or the aftershock the structure could need a retrofit or perhaps it may need to be demolished because the damage is so severe. This performance level is not associated with a defined damage.

- Prescribed or target ductility ratio. A value for a ductility ratio that a designer selects to determine the performance of the system.

2.3 Assumptions

1. Total dissipated energy E_H is the product of F_y and the cyclic plastic displacements of all hysteretic responses.
2. Part of E_H is the envelope energy E_{ucpe}, which is the energy dissipated by the new plastic displacements u_{cpe} measured in the envelope of the hysteretic responses. The other part of E_H is E_{ucpr}, the energy dissipated by the repeated plastic displacements u_{cpr}: it is equal to the difference between the total dissipated energy and the envelope energy. The repeated displacements u_{cpr} can be measured in each of the hysteretic cycles within the envelope cycle or occasionally on the same envelope cycle. In Figure 2.1 b the internal hysteretic cycles contain plastic displacements that are a repetition with respect to the new plastic displacements. Since the ground motions used in this investigation are severe, depending on the amplitude of the plastic displacements and on the number of cycles, the structure could fail due to low-cyclic fatigue.
3. The energy dissipated by a well-designed structure during seismic response corresponds to a life safety performance level (LSPL), and the structure can be at a yielding limit state or even at a near collapse limit state. The damage for both limit states is very different.
4. As stated before, the system studied in this chapter is a SDOF system with an EPP force–displacement relationship.

2.4 Equations for calculation of cyclic and non-cyclic response

Figure 2.2 illustrates the cyclic behavior of a steel beam-column subassemblage under cyclic displacement (Krawinkler et al., 1971). Clearly, one can observe in Figure 2.2 several cycles of response that include reversals of plastic displacements and deterioration of the stiffness due to the Bauschinger effect that occurs during reversals after previous yielding.

Figure 2.1 b is an idealization of the envelope of the cyclic response shown in Figure 2.2. This simplification has been used in codes and in a large number of studies to calculate yielding strength and maximum lateral displacements.

The equations developed here are general for any damping and can be used for hysteretic responses of deteriorating force–displacement relationships.

As shown in Figure 2.1 b, the strength reduction factor is equal to the relation between the elastic and yielding strength and the elastic and yield displacements; see equation (2.1).

$$R = \frac{F_0}{F_y} = \frac{u_0}{u_y} \tag{2.1}$$

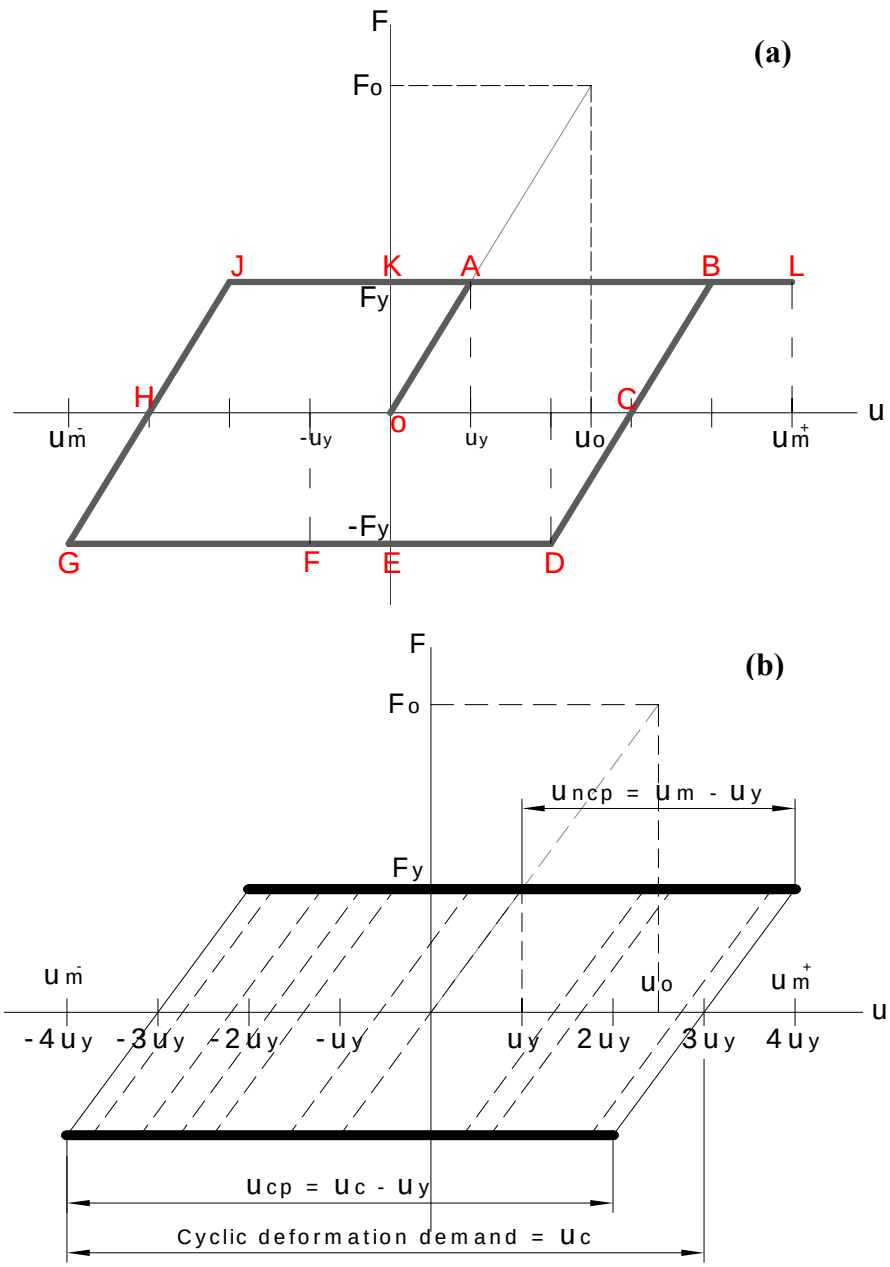

Figure 2.1 Elastic perfectly plastic idealization of cyclic response: (a) one cyclic response, (b) several cyclic responses

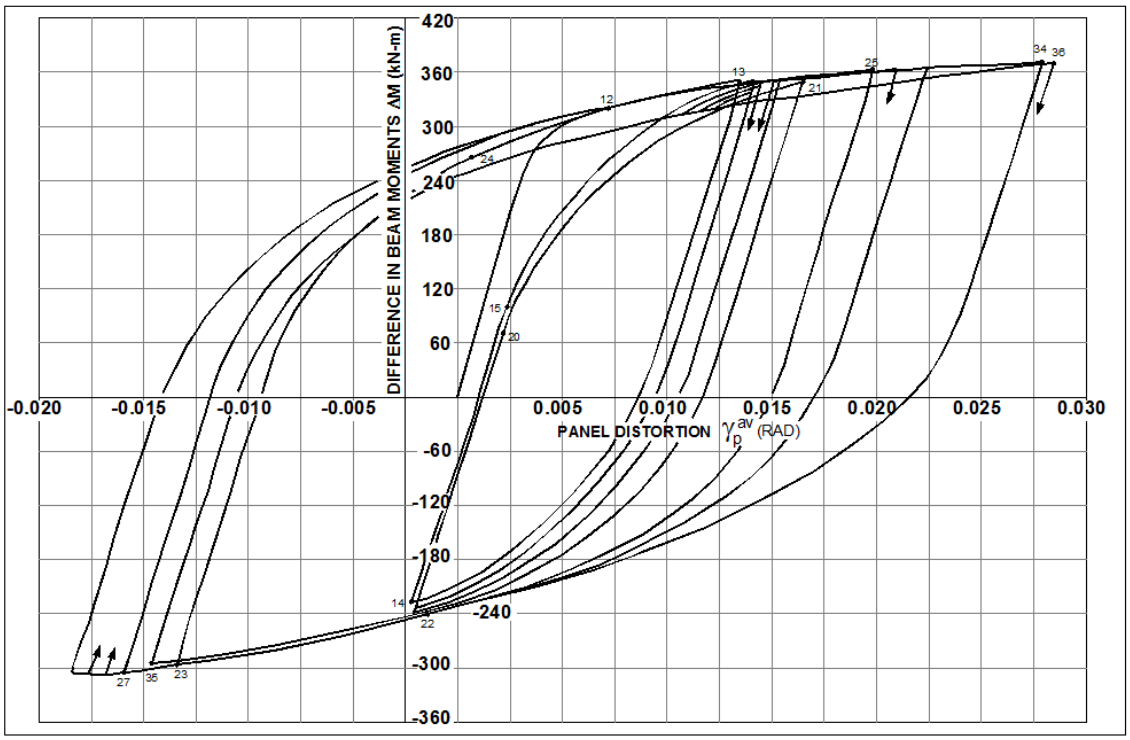

Figure 2.2 Force deformation relations for a steel beam-column subassemblage (Krawinkler et al., 1971)

The non-cyclic ductility ratio is

$$\mu_{\mathrm{nc}} = \frac{|u_{\mathrm{m}}|}{u_{\mathrm{y}}} = \frac{|u_{\mathrm{m}}|R}{u_0} \tag{2.2}$$

The traditionally known maximum lateral plastic displacement that in this investigation will be called non-cyclic plastic displacement and that represents lateral potential damage is

$$u_{\mathrm{ncp}} = |u_{\mathrm{m}}| - u_{\mathrm{y}} \tag{2.3}$$

If there is a reversal without crossing the zero displacement line represented by the force axis F in Figure 2.1 b, equation (2.3) gives the value for u_{ncp}. If the reversal crosses axis F but the new u_{m}, called $|u_{\mathrm{m}}|_{\mathrm{new}}$, is less than the previous $|u_{\mathrm{m}}|$, u_{ncp} will depend on the previous $|u_{\mathrm{m}}|$ and is given by equation (2.3).

When the reversal crosses axis F and $|u_{\mathrm{m}}|_{\mathrm{new}}$ is larger than the previous $|u_{\mathrm{m}}|$

$$u_{\mathrm{ncp}} = |u_{\mathrm{m}}|_{\mathrm{new}} \tag{2.4}$$

If the reversal crosses axis F but the yielding of the reversal of the envelope occurs after crossing axis F, as in the example of Figure 2.5 b,

$$u_{\mathrm{ncp}} = |u_{\mathrm{m}}| - u_{\mathrm{y(envelope)}} \tag{2.5}$$

where $u_{\mathrm{y(envelope)}}$ is the yielding displacement measured just before $|u_{\mathrm{m}}|$ in the envelope of the hysteretic responses. The value of $u_{\mathrm{y(envelope)}}$ is the reference to calculate u_{ncp}; it is not the structure yielding displacement u_{y}.

The cyclic ductility ratio (Mahin and Bertero, 1981) is

$$\mu_{\mathrm{c}} = \frac{u_{\mathrm{c}}}{u_{\mathrm{y}}} = \frac{u_{\mathrm{c}} R}{u_0} \tag{2.6}$$

The cyclic displacement u_{c} is equal to $|u_{\mathrm{m}}|$ when the reversal does not cross axis F, i.e., when the response is one sided and there are no reversals. If it crosses as seen in Figure 2.1 b,

$$u_{\mathrm{c}} = \left[\left(u_{\mathrm{m}}^{+} + u_{\mathrm{m}}^{-}\right) - u_{\mathrm{y}}\right] \tag{2.7}$$

The cyclic plastic displacement defined by Lara et al. (2007) illustrates the potential damage due to the lateral cyclic displacement. If the reversal does not cross axis F, Figure 2.1 b, the u_{cp} value would be

$$u_{\mathrm{cp}} = u_{\mathrm{ncp}} \tag{2.8}$$

If the reversal does cross axis F,

$$u_{\mathrm{cp}} = u_{\mathrm{c}} - u_{\mathrm{y}} \tag{2.9}$$

The envelope of the hysteretic responses represents the damage potential due to all new plastic displacements. The following relationship satisfies the EPP structures (Lara et al., 2007):

$$u_{\mathrm{cpe}} = \Sigma u_{\mathrm{cp}} \tag{2.10}$$

The corresponding enveloping cyclic ductility ratio is

$$\mu_{\text{cpe}} = u_{\text{cpe}} / u_{\text{y}} \tag{2.11}$$

2.5 Non-linear Response

The response of a nonlinear SDOF system with mass M, damping c, and resistance function F_s, subjected to earthquake ground acceleration $\ddot{u}_g(t)$ can be expressed as

$$\ddot{u} + 2\omega_n \dot{u}\xi + \frac{F_s}{M} = -\ddot{u}_g(t) \tag{2.12}$$

The resistance function for this investigation is assumed EPP, ω_n, is the circular natural frequency of the structure in the elastic range. ξ is the fraction of the critical damping in the elastic and inelastic range. The relative deformation, velocity, and acceleration responses are u, $\dot{u}$, and $\ddot{u}$, respectively. Newmark´s method, found in Newmark (1959), is used here for the numerical solution of equation (2.12).

2.6 Importance of cyclic and envelope cyclic responses compared with non-cyclic response

2.6.1 Cyclic and non-cyclic response: u_c vs. u_{nc}

In what follows the importance of cyclic response compared with non-cyclic is physically and numerically demonstrated by the analysis of two structures responses from the SCT-1 (E-W) record of the 1985 Michoacán, Mexico, earthquake, shown in Figure 2.3 (National Geophysical Data Center – NGDC website, 2008). In addition, energies demanded are compared.

Consider a structure with an elastic period T = 0.6 s subjected to the SCT-1 record. If a strength reduction factor R = 4, chosen independently of the cyclic or non-cyclic response, is used, it is possible to calculate an inelastic time history response as shown in Figure 2.4 a. The corresponding hysteretic behavior is shown in Figure 2.4 b.

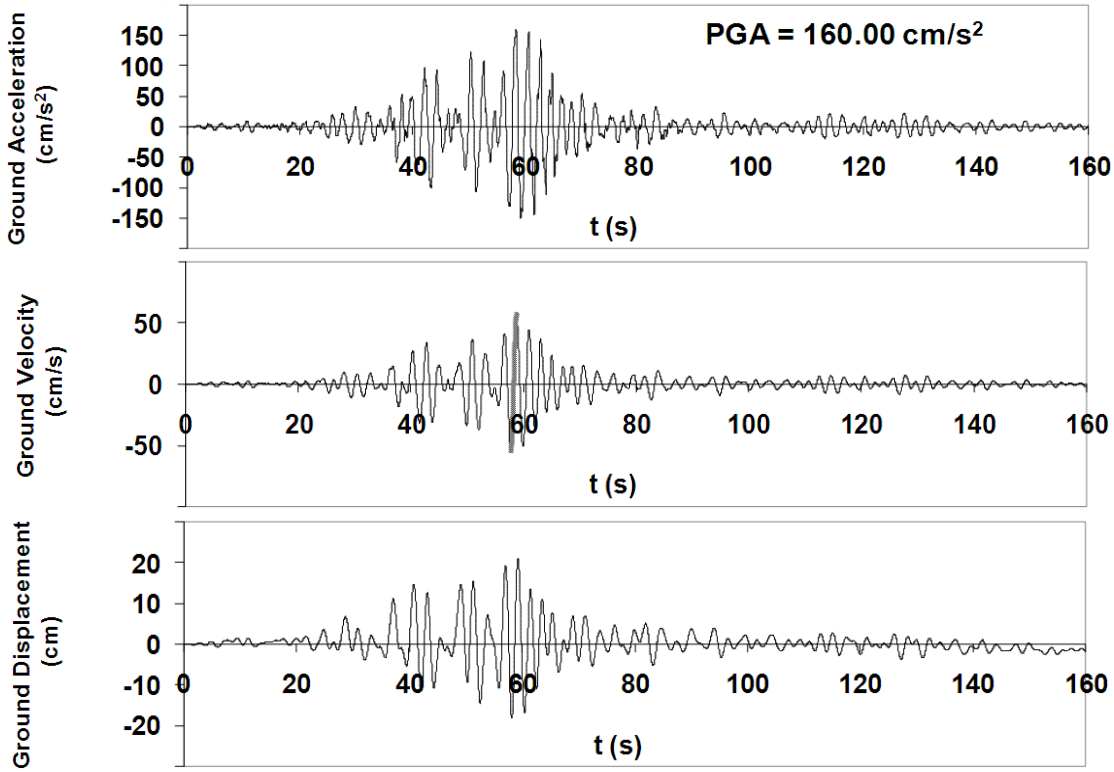

Figure 2.3 SCT-1 (EW) record, velocity and displacement of the 1985 Michoacán, Mexico, earthquake (National Geophysical Data Center, 2008)

Figure 2.4 a shows that there is one peak lateral displacement in each direction: u_m^- = 19.8 cm at 57.8 s and u_m^+ = 10 cm at 58.9 s. The traditional concept of maximum lateral displacements and drifts indicates that the maximum lateral displacement is $|u_m|$ = 19.8 cm. Since u_y = 0.57 cm, the non-cyclic plastic displacement calculated with equation (2.3) is u_{ncp} = 19.2 cm; this represents the potential damage but in just one direction.

In this example, according to equation (2.2) μ_{nc} = 34.7 for the chosen R = 4.

The cyclic response concept allows observing that the cyclic lateral displacement depends on the maximum positive and negative demand displacements. In Figure 2.4 a, u_m^- = 19.8 cm and u_m^+ = 10 cm. According to equation (2.7), since u_y = 0.57 cm, u_c = 29.2 cm. From Figure 2.4 b and equation (2.9), the damage caused by the cyclic lateral plastic displacement is u_{cp} = 28.6 cm.

From equation (2.6), μ_c = 51.2 for the chosen R = 4.

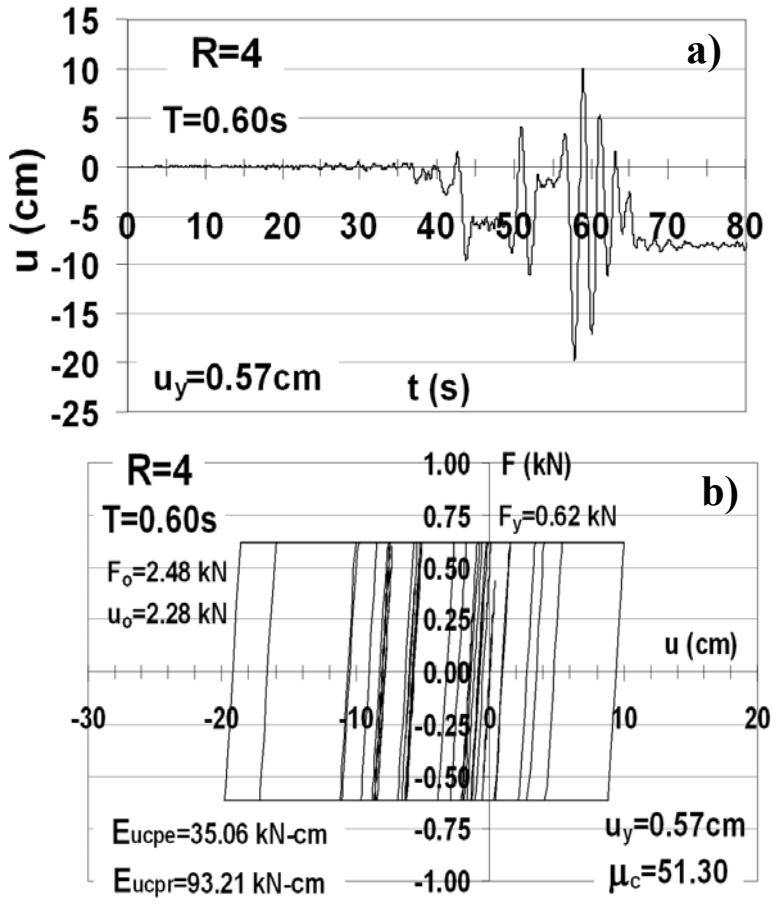

Figure 2.4 Response to the SCT-1 record of a *T*=0.6 s structure for the chosen *R* = 4: (a) time history response, (b) hysteretic response, ξ= 5%

Comparing non-cyclic and cyclic plastic lateral displacements u_{ncp} has not accounted for 9.4 cm of lateral plastic displacement. This value results from $u_{cp} - u_{ncp}$. However, as will be seen later, u_{cp} is not enough to make a reliable evaluation of damage.

Notice that for the same R = 4 the cyclic ductility ratio is larger than the non-cyclic one. Therefore, the ductility provided to the structure using only the u_{cp} demand will not be enough to supply the actual ductility demand given by the envelope of the cyclic plastic responses u_{cpe} and the fraction of the accumulated u_{cpr} demand.

Examine now the responses given in Figures 2.5 a and b for a T = 2.0 s structure subjected to the SCT-1 record, with all other parameters being the same as in the above example.

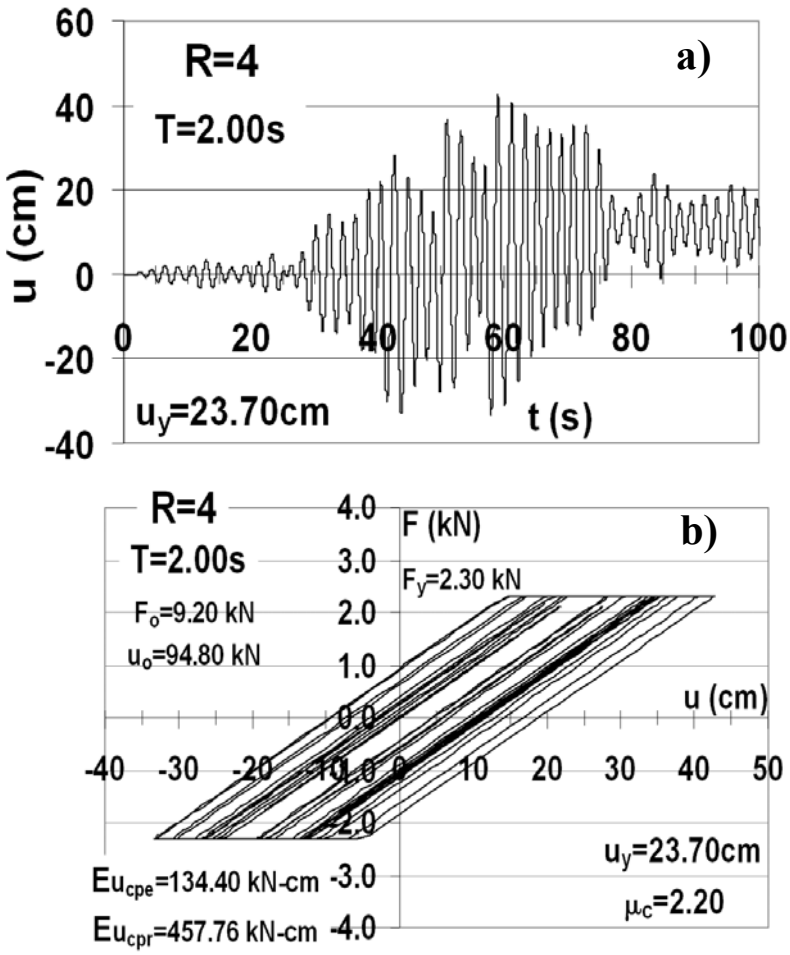

Figure 2.5 Response to the SCT-1 record of a *T*=2.0 s structure for the chosen *R*= 4: (a) time history response, (b) hysteretic response, ξ=5%

In Figure 2.5 a, for cyclic response at t = 57.8 s the negative peak is u_m^- = 33.4 cm, but at t = 58.9 s the positive peak is u_m^+ = 42.7 cm, both completing the lateral cycle. In Figure 2.5 b, the yielding displacement is u_y = 42.7 – 19 = 23.7 cm. Therefore, the value of u_c according to equation (2.7) is u_c = 42.7 + 33.4 – 23.7 = 52.4 cm and u_{cp} = 52.4 – 23.7 = 28.7 cm, that is the plastic part of u_c. Notice that this value is equal to u_{ncp} because of the position of the envelope, equation (2.8).

For the non-cyclic response the peak lateral displacement is $|u_m|$ = 42.7 cm, and since $u_{y(envelope)}$ = 14 cm (Figure 2.5 b), u_{ncp} = 42.7 – 14 = 28.7 cm, which is the plastic part of $|u_m|$ (equation (2.5)), and results equal to u_{cp} because of the position of the envelope in the coordinate system.

In this example $\mu_c = 2.2$ and $\mu_{nc} = 1.8$, but in both cases $R = 4$. Here μ_c is slightly larger than μ_{nc}. μ_c and μ_{nc} change drastically for both examples because they depend on u_c and $|u_m|$, respectively, and on u_y but they do not measure plastic displacements u_{cpe} or u_{ncp}.

2.6.2 Envelope cyclic and non-cyclic plastic displacements: u_{cpe} and u_{ncp}

The previous paragraphs show that u_c gives a better estimation of lateral displacements than $|u_m|$. However, in terms of potential damage, u_{cp} represents correctly only the damage corresponding to one-sided plastic displacement, and it is not sufficient for the general case.

In general, earthquake response induces complete cyclic displacements, as seen in Figures 2.4 and 2.5, that could induce large structural potential damage. Most of near fault earthquakes induce a pulse type of response, i.e. one side response.

When only the envelope cyclic plastic displacements shown in Figures 2.4 b and 2.5 b are considered and equation (2.10) is used, for the $T = 0.6$ s structure u_{cpe}= 57.2 cm, and for $T = 2$ s u_{cpe} = 57 cm. These values are the summation of all new plastic displacements measured in the envelope of the hysteretic responses of each structure, and they should be compared with u_{ncp}, which reaches 19.2 and 28.7 cm, respectively, or to u_{cp}, which reaches 28.6 and 28.7 cm, respectively.

Note that the repeated plastic displacements are ignored in the above calculations.

For the two-sided response while u_{cp} captures the half cycle including one reversal, u_{cpe} captures the complete envelope cycle including two reversals. For the one-sided response, u_{ncp} captures only the lateral displacement, which is about a quarter of a cycle when this is centered at the origin of coordinates. Thus, damage potential due to u_{cpe} is in general the most important and reliable quantity related to damage, and it is larger than u_{ncp} or u_{cp}.

In EPP systems that do not deteriorate, the contribution to damage from each of the repeated cyclic displacements or from the accumulated u_{cpr} is unknown. Thus, in this chapter u_{cpr} is considered only to calculate the energy dissipated by the repeated plastic displacements.

It can be argued that a large ductility ratio will represent more structural damage than a small value, but still it cannot give the designer a clear idea of the amount of cyclic plastic displacement response causing structural damage. What is needed to estimate damage is the physical amount of plastic displacement.

2.7 Energy dissipated

As indicated in Section 2.2, the energy dissipated is a more complete and conceptually more understandable measure of damage because the dissipation of energy is a function of the yielding resistance and the plastic displacements.

From the results shown in Figure 2.4 b for the T = 0.6 s structure, E_H = 128.3 kN cm, E_{ucpe} = 35 kN cm, and E_{ucpr} = 93.3 kN cm. Since E_{ucpr} is larger than E_{ucpe}, the repeated cycles containing plastic strains could lead to a failure by low-cyclic fatigue.

From the results shown in Figure 2.5 b for the T = 2.0 s structure, E_H = 592.1 kN cm, E_{ucpe} = 134.4 kN cm, and E_{ucpr} = 457.7 kN cm, which is significantly larger than E_{ucpe}. The tendency is similar to the T = 0.6 s structure, i.e., probable failure by low-cyclic fatigue. The values of the energy demand are considerably larger in the T = 2.0 s structure, since for that period the SCT-1 record shows the maximum energy demands as seen in Figure 2.6. The expected damage for the T = 2.0 s structure would be larger than that for the T = 0.6 s structure.

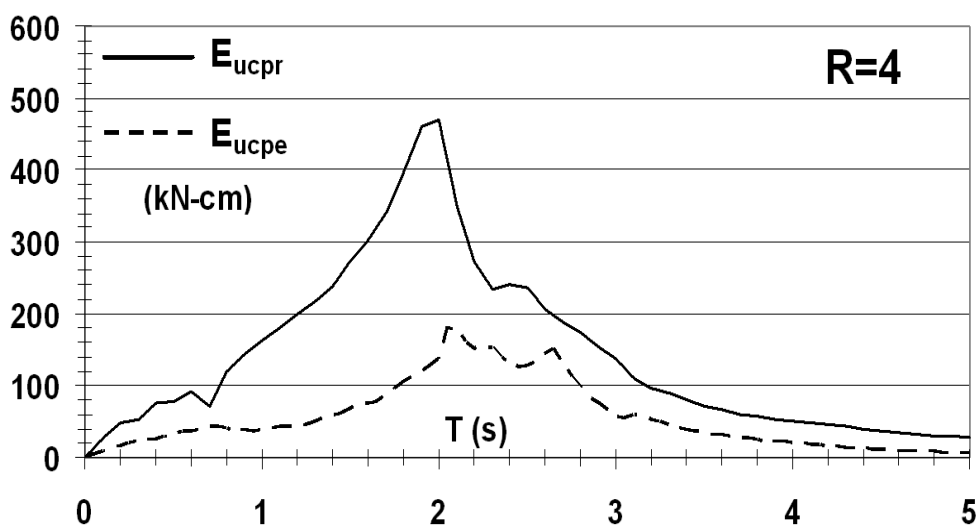

Figure 2.6 E_{ucpe} and E_{ucpr} spectra of SCT-1 record for R= 4

2.8 Comparisons of cyclic and non-cyclic strength and plastic displacements demand spectra

Appendix A.1 contains the comparison between cyclic and non-cyclic strength and displacement spectra obtained for different reduction factors. Appendix A.2 demonstrates that prescribed ductility ratios are not measures of plastic displacements. Appendix A.3 explains the differences between cyclic and non-cyclic strength demand spectra for target ductility ratios for soft soils. The Appendix A.3 also presents the differences between physical ductility demand spectra for target cyclic and non-cyclic ductility ratios for soft soils. Finally, this appendix shows the variation of the reduction factors with structure periods and the difference in the values of such reduction factors for cyclic and non-cyclic ductility ratios for one soft soil record. Appendix A.4 presents a comparison between cyclic and non-cyclic strength spectra for target cyclic and non-cyclic ductility ratios for firm soils and a comparison between strength reduction factors for target cyclic and non-cyclic ductility ratios for firm soils. Appendix A.4 also shows the physical ductility demand spectra and energy demands for target cyclic and non-cyclic ductility ratios for firm soils. Appendix A.5 explains the relationship between cyclic and non-cyclic ductility ratios with strength reduction factors and structure periods. Appendix A.6 shows the effects of aftershocks on the cyclic response.

2.9 Summary

Code provisions must be simple, but they cannot obscure the physical phenomena. Generally, the response to severe earthquakes is cyclic and two sided; therefore, it includes reversals of plastic displacements. In the case of severe earthquakes, seismic design requires reliable calculation of plastic deformation to make acceptable estimations of stiffness, strength, energy demand, and energy dissipation.

These cyclic characteristics have been acknowledged for several years through experimental research explaining that the observed damage after earthquakes due mainly to the reversible response could not be ignored (Bertero et al., 1962). Early studies also indicated the possibility of using plastic design to resist earthquakes based on the dissipation of energy (Housner, 1956).

The model used in this study is elastic perfectly plastic; therefore, it becomes difficult to estimate damage since this model does not deteriorate. However, the study clarifies the effect of cyclic reversible displacements on the strength required to sustain such large plastic displacements. It is

advisable to determine inelastic responses using systems in which stiffness and strength deteriorates as a result of the ground motion.

2.10 Conclusions

1. In this chapter, it has been demonstrated that the peak displacement during the dynamic response of a system subjected to earthquake shaking may not be enough to account for the demands that the system might experience. For design purposes, evaluation of its cyclic response would permit a better characterization of the demands of the system during the earthquake.

2.11 Remarks

1. Seismic response of EPP systems to severe earthquakes contains not only several elastic but also several elastic-plastic displacement peaks in a given direction, followed by peaks in the opposite direction, resulting in a cyclic response. At present, seismic codes do not consider the cyclic characteristic of the response, and design is based on only the maximum peak lateral response, i.e., non-cyclic response.

2. The time history response allows measurement of the new plastic displacements and the repeated ones. From the findings by Mahin and Bertero (1972) it follows that the total damage is due to the summation of all new plastic displacements and a percentage of all repeated plastic displacements. New cyclic plastic displacements u_{cpe} are measured in the envelope of the hysteretic responses, and the rest of the cyclic plastic displacements also measured in the envelope are the repeated ones u_{cpr}.

3. Since the model used in this chapter is EPP and there is no material degradation, it is not possible to estimate the damage. Therefore, the comparison between cyclic and non-cyclic response is limited to u_{cpe} and u_{ncp}.

4. Cyclic repeated plastic displacements u_{cpr} is not considered for the comparison.

5. The summation of the new plastic displacements u_{cpe} is always larger than the plastic part of the maximum lateral displacement u_{ncp} and larger than the traditional non-cyclic peak lateral displacement u_{nc}. This is true for any structure period.

6. The potential damage expected after an earthquake should be estimated from u_{cpe} and u_{cpr} and not just from u_{ncp}.

7. Knowing the yielding strength and u_{cpe} and u_{cpr} allows calculation of the energy dissipated at the end of the ground motion by both the new plastic displacements and the repeated ones. For u_{cpe}, the energy E_{ucpe} can be associated with the largest damage due to large lateral cyclic plastic displacements. For u_{cpr}, the energy E_{ucpr} can be associated with low-cyclic fatigue.

8. As discussed in Appendixes A.4 and A.5, the large demand of envelope plastic displacements represented by u_{cpe} requires larger strength in the structure than the one required by u_{ncp}; thus reduction factors for u_{cpe} are lower than for u_{ncp}. It follows that designs based on lateral displacements that depend only on $|u_m|$ as prescribed by the codes do not provide the appropriate strength to structures subjected to ground motions because the response is two sided.

9. When the strength reduction factor R is used in the sense of determining an inelastic structure that will be analyzed under an earthquake record, then R is a function of the period, the damping, the resistance function, and the capacity of the structure to dissipate the demanded energy through physical ductility. This would be the appropriate way to use R, since the designer could provide the structure with the cyclic physical ductility u_{cpe} and u_{cpr} demanded by the ground motion. However, for EPP systems there is no limit to the displacement demands resulting from the value of R chosen.

   Codes prescribe constant values for strength reduction factors R_c for all periods so the elastic spectra ordinates are reduced before applying them to an elastic structure. The result of the analysis will yield an elastic response that is not related to the results of an inelastic analysis. Therefore, the relationship of the factors R_c and the ductility capacity is questionable.

   In this case, R_c is associated only with the demanded physical ductility u_{ncp}, which is quite less than u_{cpe}.

The solution would be to limit the cyclic envelope displacements using cyclic ductility ratios. In this way, the strength demand will be associated with cyclic displacements demands.

10. The use of only maximum lateral displacements to determine the response of structures to earthquakes is correct for one-sided response, which is the case of pulse type records. When the response is two sided or cyclic, as for subduction, crustal, or soft soil records, the cyclic reversals accumulate plastic displacements increasing the potential damage.

11. Building codes prescribe drifts that put a limit only to $|u_m|$, i.e., only to u_{ncp}, the plastic part of $|u_m|$. Drift calculation ignores the two-sided plastic displacement and it is not directly related to the dissipation of energy. In addition, drifts also depend on R, the structure period, damping, and the ground motion, and they cannot be constant (Bozorgnia and Bertero, 2004). Therefore, drift does not seem appropriate to evaluate damage.

12. Damage increases with the increase of physical ductility demanded by the ground motion. Critical sections of structural elements with a large ductility demand will require a large capacity to deform plastically. This is a paradox, however, since the larger the ductility demanded by the earthquake shaking, the larger the damage (Bertero, 2009).

13. The parameters used to define structural damage, such as μ_{nc}, μ_c, and μ_{cpe}, do not seem to be the most appropriate damage indicators because damage depends on physical ductility and the energy dissipated through these plastic displacements. As demonstrated in this chapter, prescribed ductility ratios may not be a direct measure of plastic displacements and are only numbers that help to limit $|u_m|$, u_c, and u_{cpe}.

14. Aftershocks increase the demand of repeated plastic displacements. Therefore, the energy demand due to these displacements also increases and so does the danger of low-cyclic fatigue in steel structures.

15. Seismic response of structural systems depends on the dynamic characteristics of both the ground motion and the structure.

16. Dynamic characteristics of the structure are the fundamental period, the damping, the resistance function of the materials constitutive relation, and the capacity to dissipate energy through physical ductility. These characteristics can vary for each direction. In Chapter 2 a single degree of freedom steel structure with an elastic perfectly plastic (EPP) resistance function has been used.

17. Dynamic characteristics of the ground motion in each direction are the maximum acceleration, the frequency content, the duration of the main pulse, if any, and the duration of the ground motion.

3. FIBER FINITE ELEMENT MODEL OF REINFORCED CONCRETE BRIDGE COLUMNS TO SIMULATE EARTHQUAKE RESPONSE

3.1. Introduction

This chapter deals with the formulation of a single fiber finite element model (FFEM) for reinforced concrete bridge columns to identify four flexural failure mechanisms inducing damage during main earthquakes and aftershocks. These are (1) crushing of the confined, (2) P-Δ effects, (3) fracture of longitudinal bars due to tension, and (4) fracture of these bars due to low-cyclic fatigue.

The FFEM will measure the strain time-histories of the materials so that the analyst will be able to recognize when the crushing of the confined concrete occurs or when the cover concrete spalls. The crushing of the confined concrete is related to the possible enlargement or even fracture of the spirals and triggering of buckling of the longitudinal bars, Mander et al. (1988).

The occurrence of any of the four failure mechanisms will have important structural consequences in bridge columns, and if retrofitting is a solution, it could be costly and difficult and even require stopping of traffic over a period of time. Therefore, it is proposed in the chapter to define a significant damage performance level (SDPL) related to the occurrence of any of the four mechanisms mentioned. SDPL could be seen as a more precise indication of damage for the life safety performance level.

The proposed FFEM results after individual calibration to simulate first the response of 30 bridge columns tested in the laboratory under cyclic lateral reversible and increasing displacements and a recalibration to simulate the response of two additional columns to one horizontal component of two earthquake ground motions.

The information regarding the 30 laboratory tested reinforced concrete bridge columns chosen to calibrate the FFEM are in the database compiled by Berry et al. (2004). The recalibration of the FFEM is performed using the calibrated results of the 30 columns mentioned above but now

subjected to the two earthquakes used by Hachem et al. (2003) on two bridge columns tested in a shake table. Strains and displacements are compared.

3.2. Importance of the fiber finite element on modeling bridge columns

Several hysteretic relationships were developed from results of laboratory tests on reinforced concrete bridge columns under cyclic increasing and reversible displacements. These include, among others, tests by Ibarra et al. (2005), Kunnath et al. (1997), and Saatcioglu, et al. (1991). They defined backbone force–deformation relationships and loading, unloading, and reloading rules. The resulting models allow the successful determination of the force–displacement response of a bridge column, but the calibration of the hysteretic backbone and the parameters that simulate stiffness and strength degradation may require "extensive testing and fitting", as mentioned by Hachem et al. (2003). Figure 3.1 shows some of these resultant models.

Hachem et al. (2003) established that cyclic increasing loading tests "may not produce the same damage occurring during more erratic seismic loading conditions, and they may not provide information needed to define analytical models that are required to simulate these more complex response histories". In addition, they mentioned that the rate of loading effects might change failure or other behavior modes.

Hachem, et al. (2003) tested four flexural designed circular bridge columns on a shake table subjected to scaled ground motions. The experimental results were then compared with the predicted response of analytical models using linear elastic and inelastic methods. A FFEM with three elements and distributed plasticity was determined to be the best analytical model to predict the responses of the tested columns.

Thus, a FFEM appears to be a more appropriate model, since it allows the introduction of realistic material and structural element characteristics to calculate seismic response.

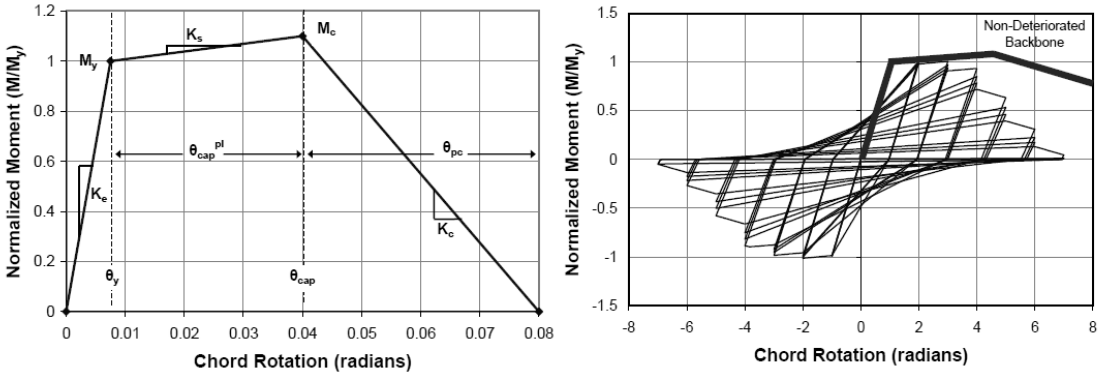

Monotonic and cyclic behavior of a structural element based on Ibarra, Medina and Krawinkler model (Haselton, Liel, Taylor and Deierlein, 2008)

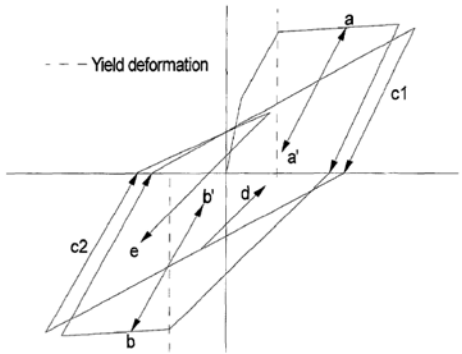

Proposed model of local hysteresis loops (Kunnath, El-Bahy, Taylor and Stone, 1997)

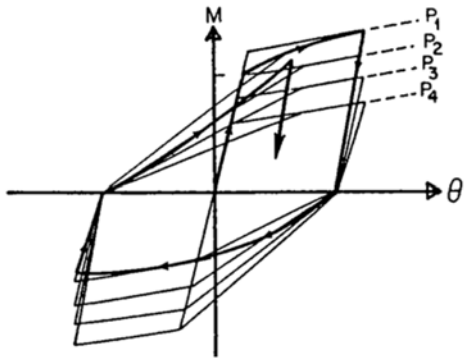

Axial force-moment interaction model (Saatcioglu, 1991)

Figure 3.1 Resultant models to simulate hysteretic response of a structural element

Additional important features of the FFEM include the following. First, it allows the obtainment of the strain response of the materials, unconfined or confined concrete and reinforcing steel, at the critical sections of the bridge columns, at any time of the response and at the end of the main shock or the aftershock. Second, the designer can identify the significant damage and its location and the flexural failure mechanisms that induced damage. Third, he/she will be able to study design alternatives in a three-dimensional model.

A variation of the analytical model presented by Hachem et al. (2003) is calibrated for each of the 30 laboratory tested circular reinforced concrete bridge columns subjected to cyclic reversible and increasing displacements to simulate their individual response. The responses are then studied, recalibrated, and validated to define a single FFEM that can be used to simulate the flexural response of reinforced concrete bridge columns subjected to main shocks and aftershocks.

One of the conclusions given in Chapter 2 regarding the importance of cyclic response of structures says that potential damage is associated with the energy dissipated at the end of the excitation. Thus, in the development of the model, the total energy dissipated in the simulated response of the bridge columns and the energy obtained in the laboratory are continuously compared during calibration of the variable parameters participating in the response until the difference in energies is lower than 10%.

The investigation uses the Open System for Earthquake Engineering Simulation (OpenSees) framework (Mazzoni et al., 2006); McKenna, 1997), which contains fiber beam-column elements and structural properties such as length of the plastic hinge, P-Δ effects, and low-cyclic fatigue, all required to model reinforced concrete bridge columns.

The OpenSees framework is an object-oriented finite element program. This framework is being developed at the Pacific Earthquake Engineering Research Center (PEER) in the Earthquake Engineering Research Center of the University of California, Berkeley, as an open source computer code that allows quantifying the flexural failure mechanisms by using finite elements to calculate strains and force–displacements relationships in the elastic and plastic range.

3.3. Significant damage performance level

Priestley et al. (2007) define the section limit states to relate member and structure limit states. This relation helps in understanding the link between structure response levels and seismic performance levels. The buckling of the longitudinal bars is included within the section limit states.

However, in this study, a SDPL at the critical sections of a bridge column is proposed. The rationality for this proposal follows.

In modern flexural designed bridge columns subjected to severe earthquakes, the proposed SDPL in a critical section can occur because of one or all of the flexural failure mechanisms mentioned above.

In this study, the crushing of the cover concrete occurs when it reaches the ultimate unconfined concrete strain of 0.004. The crushing of the confined concrete occurs when it reaches the ultimate strain given by Mander et al. (1988). The external flexural moment given by the product of the axial load and a large lateral displacement can cause instability of the column. This is called the P-Δ effect, and in this dissertation, following new code recommendations, the product is limited to a value equal to or lower than 0.25 times the flexural moment capacity of the column. Fracture of longitudinal bars due to tension occurs when the steel strain reaches the maximum cyclic strain that, according to new codes, varies with the diameter of the bar. Fracture of the longitudinal bars can also occur when the bars lose their fatigue life.

Kunnath et al. (1997) establish that when a longitudinal bar of a bridge column initiates buckling there is a substantial increase of strains that reduces fatigue life and that when fracture of the bar begins the strength and stiffness of the bridge column deteriorates rapidly. The reduction of fatigue life induces this failure mechanism, known as low-cycle fatigue, on flexural well designed bridge columns. Low-cycle fatigue can fracture one or more longitudinal bars, reducing with each fracture the strength and stiffness of the column. Uriz and Mahin (2008) arrived at similar conclusions after studying the response of steel bracings.

Another conclusion given by Kunnath et al. (1997) is that for low amplitude cycles the confining spiral will fail prior to the fracture of the longitudinal bars, but for high amplitudes like those during severe earthquakes inelastic cycles will fracture the longitudinal bars before confinement failure. The tests performed by Kunnath et al. are on a group of bridge columns subjected to cyclic displacements and on another group subjected to random cyclic displacements. Low amplitude cycles are those that keep the steel bars essentially elastic, whereas high amplitude cycles are those inducing cyclic plastic strains.

As will be seen in this and the following chapters, every cyclic plastic strain occurring during seismic response damages the steel bar, decreasing by a percentage the fatigue life of one or more of the longitudinal steel bars until fracture could occur, depending on the number of cycles

and the amplitude values of plastic strains. In addition, when crushing of the unconfined concrete and enlargement of the spiral occurs, the fatigued and damaged bar could buckle.

The failure by low-cyclic fatigue is not considered in the new bridge codes. In addition, the performance levels prescribed in SEAOC Vision 2000 (1995) or the SEAOC Revised Interim Guidelines Performance-Based Seismic Engineering (2003) do not give any prescription to avoid this type of flexural failure.

3.4. Selection of material modeling and bridge column properties

3.4.1. General remarks

A great majority of experimental research projects on bridge columns have used histories of cyclic displacements to study the behavior of the reinforcing detailing as well as that of the column. The results allowed development of numerical models for earthquake response and determination of the capacity of the bridge column.

However, as indicated above, cycling increasing and reversible displacements applied to the column are completely different from random seismic loads, so under earthquake loads structural damage may be different, and to predict response analytical models may be different. In addition, the rate of loading effects may change the type of behavior and even the failure mechanism (Hachem et al., 2003).

Therefore, the present investigation proposes a FFEM to simulate the response of the 32 bridge columns tested in the laboratory.

3.4.2. Materials modeling

(a) Concrete modeling. For the confined and unconfined concrete, the FFEM uses the Kent and Park (1971) and Scott et al. (1982) model as modified by Taucer et al. (1991) and incorporated in OpenSees. To simulate the response of the laboratory tested bridge columns, after several trials it was necessary to introduce the increased maximum strength and ultimate strain of the confined concrete resulting from the model given by Mander et al. (1988) into the model modified by Taucer et al. (1991), Figure 3.2 and equations (3.1) and (3.2)). These equations represent the stress–strain curves obtained after confined reinforced concrete columns are tested

at a fast strain rate of 0.013ε/s. Previously, Mahin and Bertero (1972) incorporated the rate of loading effects on tested specimens at similar and at larger strain rates to study the behavior of materials under the expected strain rate during earthquakes. The unconfined concrete follows the model shown in Figure 3.2.

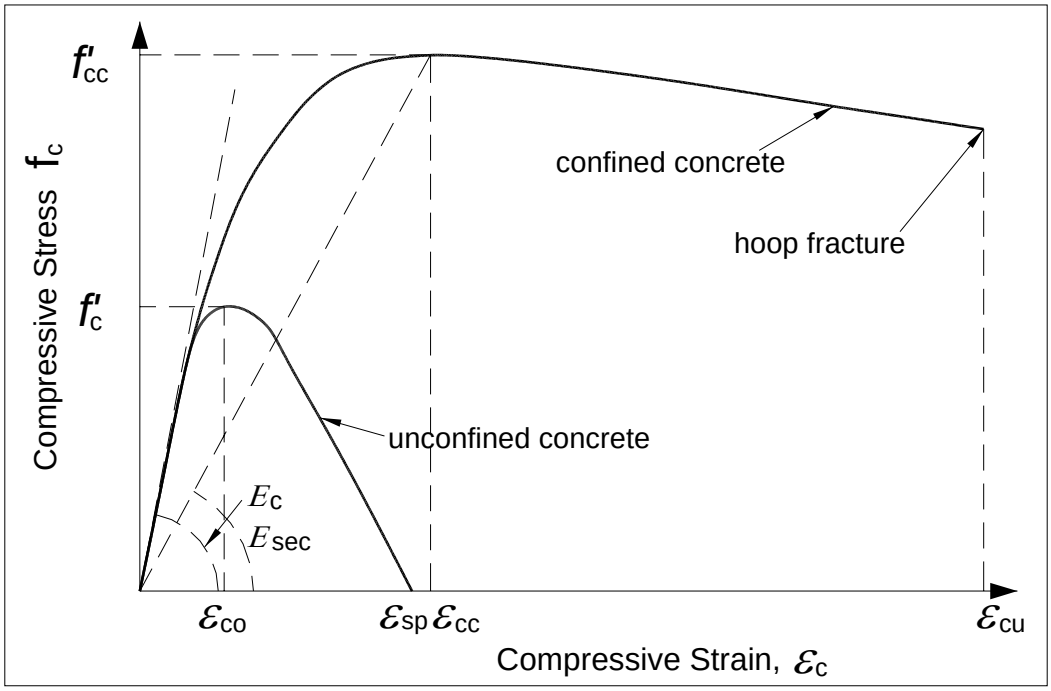

Figure 3.2 Stress–strain model for concrete in compression (Mander et al., 1988)

$$f'_{cc} = f'_c\left(2.254\sqrt{1+\frac{7.94\,f'_l}{f'_c}} - \frac{2\,f'_l}{f'_c} - 1.254\right) \tag{3.1}$$

$$\varepsilon_{cu} = 0.004 + \frac{1.4\rho_s f_{yh}\varepsilon_{su}}{f'_{cc}} \tag{3.2}$$

Most of the terms in equations (3.1) and (3.2) are in Figure 3.2. In addition, f_l' is the confinement concrete strength, ρ_s is the percentage of transverse steel, f_{yh} is the yielding strength of the transverse steel reinforcement, and ε_{su} is the maximum monotonic transverse steel strain. All these parameters are defined by Mander et al. (1988).

In the proposed FFEM, the confined concrete strain history is monitored at locations previously defined and that are very close to the longitudinal bars that are also monitored. The ultimate

confined concrete strain ε_{cu}, equation (3.2), can be reached at any moment during the inelastic response and is measured at any of those locations.

(b) Reinforcing steel modeling. The FFEM uses the Giuffre and Pinto (1970) and Menegotto and Pinto (1973) model incorporated into OpenSees; this has a bilinear stress–strain curve so there is no yielding plateau. The model considers the Bauschinger effect, which accounts for the stiffness degradation observed during reverse reloading after first yielding of the longitudinal steel during cycle response, as seen in Figure 3.3 a. Regarding the simulation of the Bauschinger effect the authors above mentioned indicate that after each reversal of the cyclic response the curvature is reduced because of the previous plastic excursion. This reduction is controlled by three parameters, R_0, R_1, and R_2, which will be calibrated in this study, Figure 3.3 b.

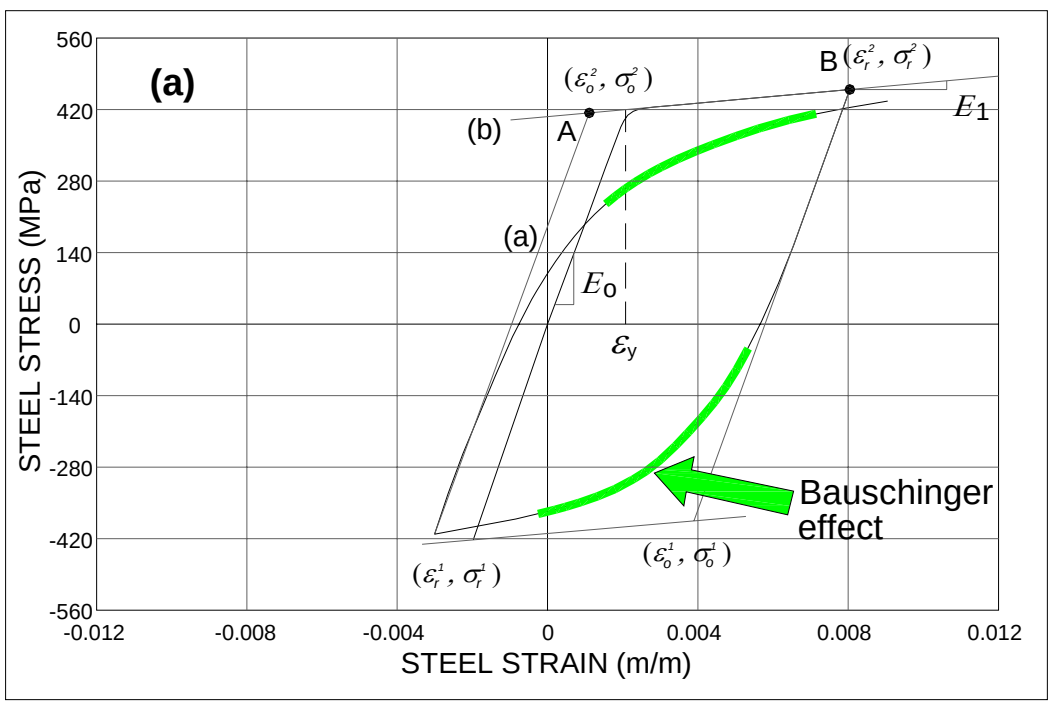

Figure 3.3 Giuffre–Menegotto–Pinto stress–strain model for reinforcing steel

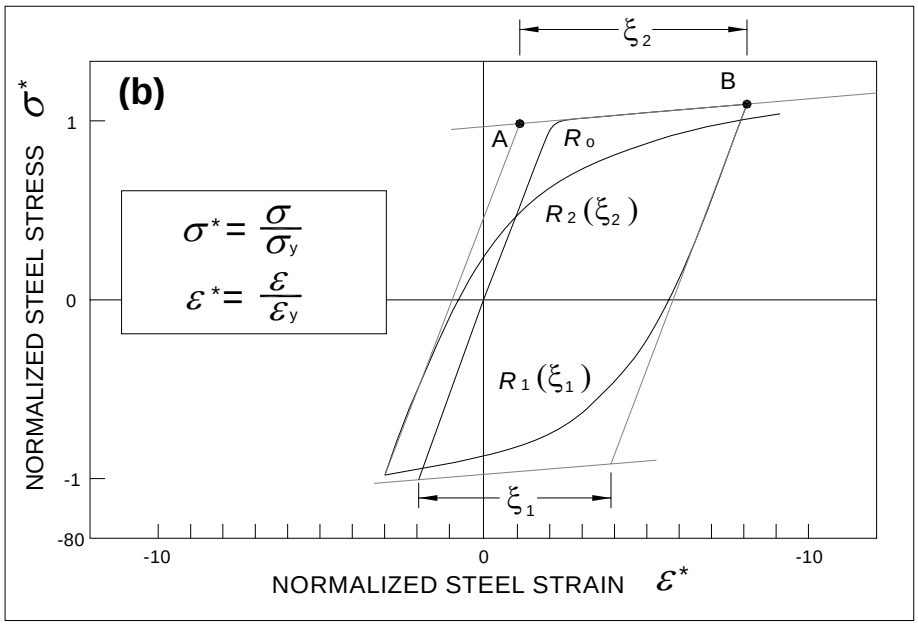

Figure 3.3 (cont.) Giuffre–Menegotto–Pinto stress–strain model for reinforcing steel

3.4.3 Bridge columns properties

(a) Length of the plastic hinge modeling. The displacements of a cantilever bridge column are calculated by integrating the moment-curvature along the length of the bridge column to obtain the force–displacement response. However, this procedure does not give the results obtained from experiments for several reasons, as indicated in Priestley et al. (2007). Among them is that the shear that induces diagonal tension shifts up the reinforcement tension strain, that there is no consideration of strain penetration into the foundation, and that spalling of the cover concrete increases curvature as the moment decreases. The use of the plastic hinge length, L_p, is a simplified approach to solve these problems under the assumption that along L_p strain and curvature are considered equal to the maximum values at the base of the bridge column. The plastic hinge length given by Priestley et al. (1996), equation (3.3), is calculated for each tested bridge column simulation as a function of the length of the bridge column L and includes the strain penetration of the steel under the foundation, which is a function of the yielding strength of longitudinal reinforcement f_y and the diameter of the vertical bar d_b.

$$L_p = 0.08L + 0.022 f_y d_b \text{ (MPa)} \tag{3.3}$$

(b) Fracture of the longitudinal bars caused by low-cyclic fatigue and fatigue material modeling. Fatigue is a physical phenomenon for which there are no prescriptions in any reinforced concrete seismic design code. Fatigue is the result of cumulative damage of the steel bars due to cyclic response.

From a phenomenological approach, during earthquake response every plastic cyclic strain damages one or more bars of a reinforced concrete bridge column, and as both the number of cycles of plastic response and their amplitude increase during a severe earthquake the damage also increases. This accumulation of damage induces the fracture of the fatigued steel bars. Therefore, beginning with the first cyclic plastic strain, the steel bar suffers damage that can be seen as the loss of a percentage of the fatigue life of the bar.

Small earthquakes induce several cycles of response in reinforced concrete bridge columns, but the longitudinal steel bars remain essentially elastic although the unconfined cover concrete could reach cracking. As long as the steel bars remain elastic, several hundreds of cycles will be necessary to cause fracture in those bars due to the accumulation of elastic strains.

New bridge codes allow, for seismic design, the reduction of the elastic strength demand so that bridge columns can respond plastically under severe earthquakes. The severe ground motions induce cycles of response with large plastic strains in those columns. For large amplitudes of the cyclic reversible plastic strains, few cycles are necessary to fracture the bar. This is called flexural failure by low-cyclic fatigue. Even the nonreversal cycles could cause fatigue, but a large number of cycles are required to fracture the bar.

Numerically, damage due to fatigue may be modeled as the ratio of the number of cycles with some plastic strain amplitude to the number of cycles of that amplitude that cause fracture of the bar. The summation of those quotients along the dynamic plastic response of the column allows calculation of a fatigue damage index. Once it reaches a value of 1.0, the bar fractures due to low-cycle fatigue. This means that the number of cycles of a fixed value of plastic strain equals the number of cycles of that amplitude necessary to cause fracture of the bar. This flexural failure mechanism can be captured by the FFEM developed in this chapter through the material modeling developed by Uriz and Mahin (2008) to simulate fatigue of the longitudinal bars.

It should be indicated that the calculation of the cumulative damage due to fatigue is the only physical way to take into consideration the effects of the duration of the strong part of the motion, where important amplitude cycles occur. In addition, fatigue of the longitudinal bars is the only way to capture the deterioration of the strength of the bridge column because once a bar fractures the strength of the column decays.

The steel and confined concrete materials enter into the FFEM with their stress–strain constitutive relations that are independent of the duration of the earthquake. The stress–strain curve of the steel allows stiffness deterioration of the bridge column critical section due to the Bauschinger effect, and the stress–strain curve of the confined concrete allows some deterioration of the strength of the critical section, depending on the level of the strain.

The damages occurring along the duration of the strong motion do not affect the monotonic strength–strain relationships of the materials introduced into the FFEM but do affect the response of the column.

This is another reason why the demand of physical ductility cannot be defined only for the maximum lateral displacement. It is necessary to consider, in addition, the effect of the cyclic plastic strains.

Several experimental studies have proved the effects of low-cyclic fatigue on bridge columns showing degradation of the stress–strain relationship of the section studied.

Brown and Kunnath (2004) did fatigue tests on bars under the assumption that during load reversals the unconfined concrete will spall at strains below the yielding strain of the longitudinal bars, so that the bars are in the air with no surrounding concrete. They established that eventually the longitudinal bar can buckle, weakening it and reducing its fatigue life.

It was already mentioned that the experiments on low-cyclic fatigue of reinforced concrete columns by Kunnath et al. (1997) showed that for high amplitudes of applied lateral displacements the inelastic cycles fractured the longitudinal bars by low-cyclic fatigue before buckling because of confinement failure.

The tests and the results of the FFEM show that once the fracture of the bar begins the strength and stiffness of the bridge columns deteriorates rapidly. The reduction of fatigue life induces the failure mechanism on flexural designed bridge columns known as low-cycle fatigue, which can fracture one or more longitudinal bars.

Fatigue material modeling. This material model considers the effects of low-cycle fatigue in the longitudinal steel bars. The model developed by Uriz and Mahin (2008) incorporated in the FFEM uses the OpenSees fiber model.

The fiber model is able to track strains in each fiber; therefore, the cyclic counting model presented by Uriz and Mahin (2008) is based on the strain time-history within each fiber to predict fracture due to low-cyclic fatigue. However, the Uriz and Mahin model does not consider fracture mechanics propagation of cracks, strain concentration, and effects of local buckling.

The linear relation given by Manson (1953) and by Coffin (1954) in equation (3.4) allows calculation of the strain amplitude at each cycle ε_i, using the number of constant amplitude cycles to failure N_f and the strain amplitude ε_0 at which one complete cyclic on a virgin material will cause failure of the longitudinal steel bar. The parameter m is the log of the total strain amplitude divided by the log of the number of cycles to failure. Figure 3.4 shows the typical cycle considered in the model.

$$\varepsilon_i = \varepsilon_0 \, (N_f)^m \tag{3.4}$$

The value of the parameter m is given in equation (3.5).

$$m = \frac{\log \varepsilon_i}{\log N_{fi}} \tag{3.5}$$

Equation (3.4) represents a straight line relating the log of the strain ε_i in the ordinate and the log of the number of cycles to failure N_{fi} in the abscissas, so for one cycle $N_{fi} = 1$ and $\varepsilon_i = \varepsilon_0$.

According to Uriz and Mahin (2008) it is unlikely that the cyclic strain is of constant amplitude during the response, as shown in Figure 3.4. In addition, ε_i considerably increases the damage when only large cycles are present in the response history.

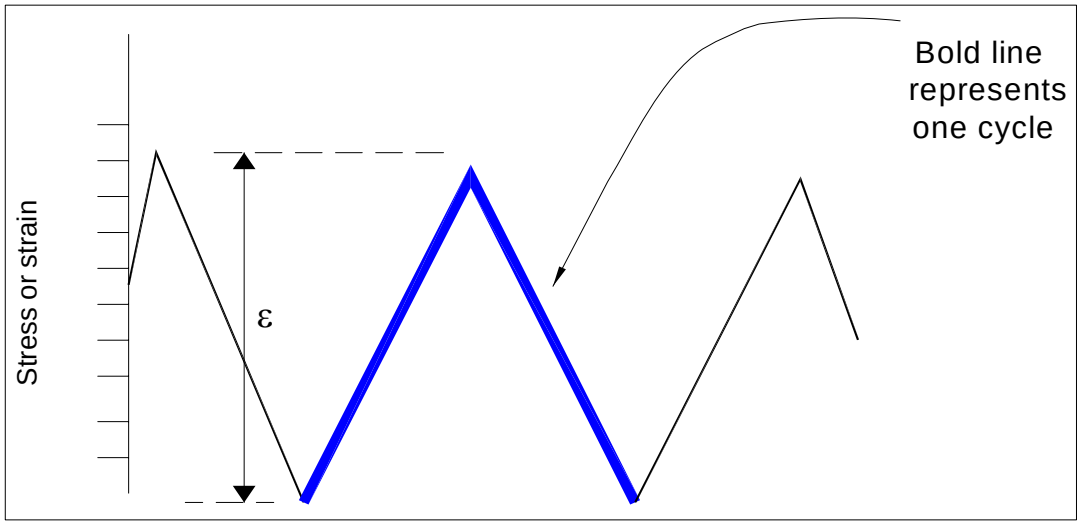

Figure 3.4 Illustration of a typical cycle considered in the model (Uriz and Mahin, 2008)

The rainflow cycle counting method standardized by the American Society for Testing and Materials (ASTM) considers the amplitude of each cycle and the number of cycles at each strain amplitude.

Uriz and Mahin (2008) presented a modification of the rainflow cyclic counting method.

The modified counting method uses the rule proposed by Miner (1945) for the calculation of the damage. The damage corresponding to every strain amplitude within a cycle, D_i, is calculated by dividing the number of cycles at that amplitude (n_i) existing in the strain time history by the number of constant strain amplitude cycles (N_{fi}) of that same amplitude that cause fracture, equation (3.6). The overall damage D causing fracture due to low-cyclic fatigue in one bar is equal to the summation of the damage D_i due to every strain amplitude ε_i of the time history until $D = 1.0$, so the bar is dismissed. D is given in equation (3.7).

$$D_i = \frac{n_i}{N_{fi}} \tag{3.6}$$

$$D = \sum \frac{n_i}{N_{fi}} \tag{3.7}$$

In equation (3.6), if a complete cycle shows a strain amplitude ε_i, then $n_i = 1$. If there is a one-half cycle at strain ε_i, then $n_i = 1/2$. In addition, the accumulation of damage shown in equation (3.7) indicates that the sequence of each cycle has no effect on the calculation of the fatigue life.

From equation (3.4), N_{fi} is given by

$$N_{fi} = 10^{m^{-1} \log \frac{\varepsilon_i}{\varepsilon_0}} \tag{3.8}$$

Uriz and Mahin (2008) propose that N_{fi} is the number of constant strain amplitude cycles causing failure with an amplitude equal to that of the cycle n_i under analysis. Therefore, N_{fi} does not represent the number of constant amplitude cycles along the time-history response but just the n_i cycles considered each time the strain amplitude changes. This is the conceptual modification of the Coffin (1954) and Manson (1953) equation (3.4) proposed by Uriz and Mahin (2008).

Miner's rule, as well as other methods, analyzes the total strain history to identify and count the cycles. Uriz and Mahin (2008) proposed that the amplitude of each cycle and the number of cycles of that amplitude be accounted for using the modified cycle counting method proposed, since it will save computer time.

It consists of using the three most recent peaks since the beginning of the strain history as long as the initial strain amplitude is shorter than the final strain amplitude of the one-half cycle formed by the three peaks. In this case, a one-half cycle is assigned to calculate the cumulative damage. When the final amplitude of the half cycle is shorter than the initial one, the counting method uses the four more recent peaks (Figure 3.5) and assigns a full cycle to the calculation of the cumulative damage. The method accounts for the shortest amplitudes of the one-half cycles, and at the end of the strain history it accounts for the large ones that were left behind if necessary. However, it does not keep track of all strain amplitudes, as do Miner's rule and other methods recognized by the ASTM.

According to Uriz and Mahin (2008) the number of cycles and amplitudes considered in their accounting method gives results identical in many cases to the ASTM rainbow method and requires less computer effort.

The Uriz and Mahin (2008) fatigue model implemented in OpenSees works as a material wrapper that wraps any uniaxial material where strains are monitored, such as the steel bars of a reinforced concrete column where the parameters m and ε_0 in equation (3.4) are known. This fatigue model is incorporated into the FFEM developed here.

Fracture of the bars due to low-cyclic fatigue reduces the strength of the column and leaves it vulnerable to more bar fractures and consequently more reduction of the strength because of severe aftershocks or future severe earthquakes.

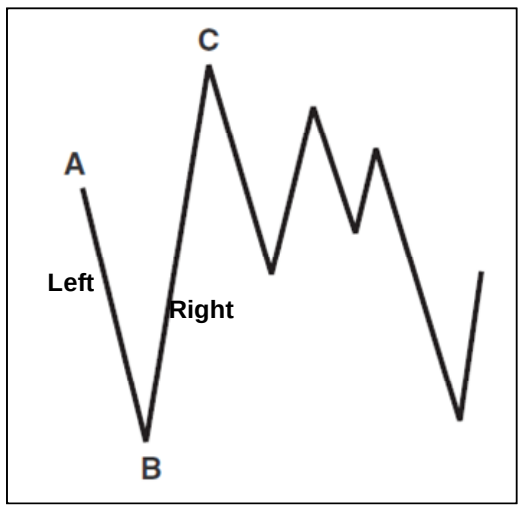

Figure 3.5 Illustration of one step of the cycle counting method (Uriz and Mahin, 2008)

(c) *P*-Δ effects. When the lateral displacement response Δ_{max} becomes too large and the stability index θ_Δ given in equation (3.9) is larger than 0.085, as indicated by Priestley et al. (2007), the vertical load P on top of the bridge column induces an additional flexural moment $P\Delta_{max}$ to that due to the applied displacement history or due to a ground motion.

$$\theta_\Delta = \frac{P\Delta_{max}}{M_{cap}} \leq 0.085 \tag{3.9}$$

It is recognized that the vertical component of the ground motion will cause an increase of the axial load, but although the FFEM is three dimensional, the effect of the vertical component is not studied in this investigation.

This additional moment increases the demand; thus the flexural capacity M_{cap} of the column may not be able to satisfy the increasing demand. The P-Δ effect decreases the column shear capacity F in equation (3.10). L is the height of the column measured at the center of mass.

$$F = \frac{M_{cap} - P\Delta_{max}}{L} \tag{3.10}$$

Owing to this shear reduction caused by the P-Δ moment, the shape of the hysteretic response changes because the plastic displacement stiffness becomes negative. In addition, there is a reduction of the stiffness of the bridge column, since the large lateral displacement induces a change of geometry called geometric non-linearity that has a significant effect on the dynamic response of the column.

The vertical load does not change in direction during the response; therefore, it is a conservative force. The geometric non-linearity that results in a vertical displacement of the deformed column, as seen in Figure 3.6, reduces the potential energy of the load so the product P-Δ_{max} becomes negative. Dividing equation (3.10) by L and recognizing that M_{cap}/L is the initial shear force, the additional P-Δ_{max} effect is to reduce the initial stiffness of the column (Clough and Penzien, 1975).

OpenSees, through the P-Δ transformation command, performs a linear geometric transformation of the column stiffness and the shear resistance force from the element system to the global coordinate system considering the second order P-Δ effects. The command allows accounting for the effects of axial load on the lateral capacity of the bridge column by subtracting from the shear resistance force a force equal to the axial load times the lateral displacement of the column divided by its length.

It should be mentioned that the vertical component of the ground motion could increase the value of the vertical load, increasing the P-Δ effect, since the axial load is not only the weight of

the mass because the bridge column will vibrate due to the vertical component of the ground motion.

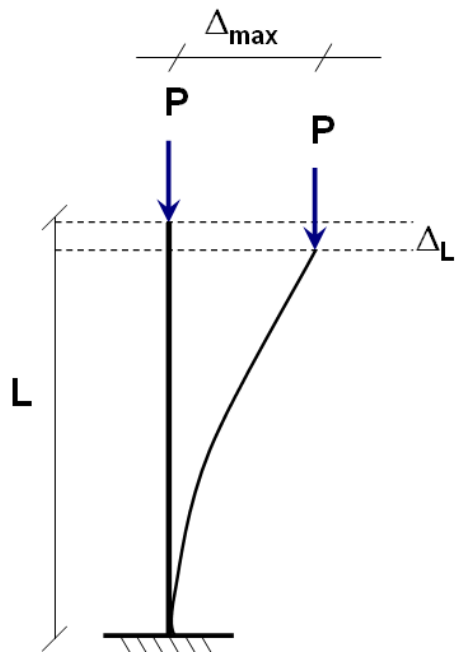

Figure 3.6 *P*-Δ effect. Vertical displacement of the column reduces the potential energy

3.5. Reinforced concrete bridge columns modeling

3.5.1 Non-linear beam-column element

To predict the response of the bridge columns the FFEM contains the beam-column element developed by Taucer et al. (1991) that uses fiber element sections to model section response. To integrate displacements along the length and to be able to capture the spread of the plasticity over the length of the bridge column, the element uses the Gauss–Lobato procedure in several integration points.

The beam-column element is a line element, and any flexural response at each integration point is determined from the fiber section assigned to the integration point. The element is based on force formulation, considers that plasticity can spread over the element, and is included in OpenSees (Figure 3.7).

The advantage of using a FFEM based on the beam-column element is that the incorporated material and column models allow the fiber element to capture the change of properties due to external loads along the length of the column. Fiber elements capture the changes in axial load, so a moment–curvature curve is calculated for each step during the response of the FFEM.

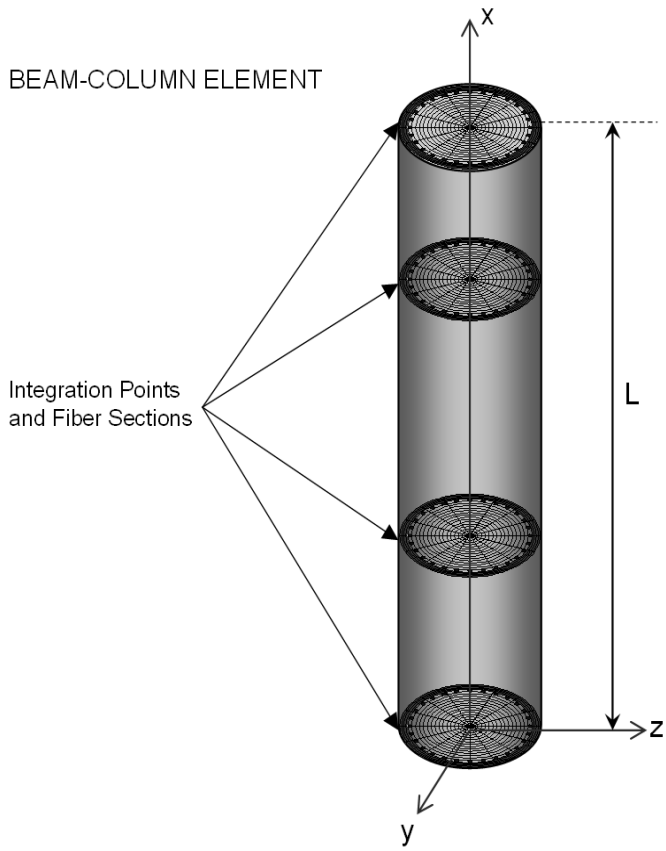

Figure 3.7 Beam-column element and fiber sections

The bridge columns tested in the laboratory are cantilever structural elements; the plastic behavior occurs at the fixed end where two of the integration points are located. It should be noted that the model shown in Figure 3.8 does not account for the vertical and the transversal component of the ground motion.

From virtual work (Figure 3.8) the plastic part of the top displacement, u_p, of the bridge column is

$$u_p = (\phi_u - \phi_y)L_p(L - L_p/2) \tag{3.11}$$

With the Gauss quadrature method of integration for the cantilever bridge column, the plastic part of the top displacement is approximated as (Hachem et al., 2003)

$$u_p = (\phi_u - \phi_y)L^2 w_1 \tag{3.12}$$

where w_1 is the weighting factor used by the method.

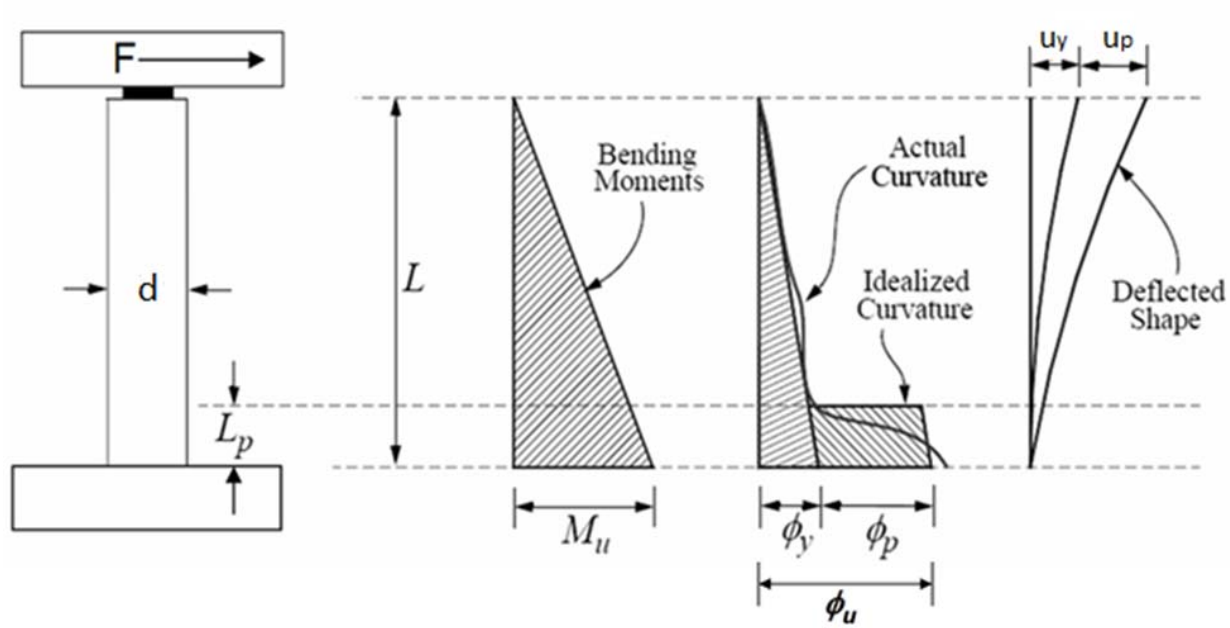

Figure 3.8 Elastic and plastic displacement for the cantilever bridge column

Equating (3.11) and (3.12),

$$w_1 = (L_p / L^2)(L - L_p) \tag{3.13a}$$

Assuming that $(L - L_p)$ is approximately equal to L and replacing in equation (3.13a) gives

$$w_1 = L_p / L \tag{3.13b}$$

According to Hachem et al (2003), if equation (3.13b) is not satisfied the fiber element will provide incorrect curvatures for a given deformation, so the column may be divided into two or more elements as long as the section weights of the edge fiber element satisfies equation (3.14a).

$$w_1 = (L_p / L_{end} L)(L - L_p) \tag{3.14a}$$

and

$$w_1 = L_p / L_{end} \tag{3.14b}$$

L_{end} is the length of the fiber finite element attached to the foundation.

If two integration points are selected at symmetrical positions within L_{end}, w_1 = 0.5 for each section; thus, in equation (3.14b)

$$L_{end} = 2L_p \tag{3.15}$$

The results given in the report by Hachem et al. (2003) indicate that a fiber model with three elements provides a top displacement corresponding to the ultimate curvature in monotonic tests. Two of the elements with length $2L_p$, each with two integration points, should be located at the ends of the column, and the third element should joint the two extreme elements (Figure 3.9). The monotonic test uses the plastic hinge method.

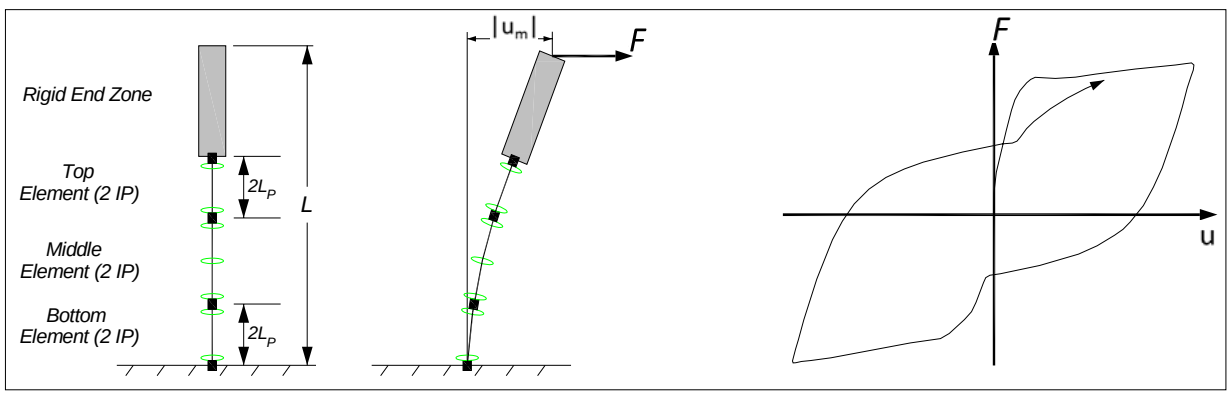

Figure 3.9 Three element model

For this study, a variation of the fiber model used in Hachem et al. (2003) is proposed. Only one end is considered fixed because only cantilever columns tested in the laboratory are simulated here.

The model has three fiber beam-column elements. The end element, called element 2, is attached to the base of the bridge column and has a length of $2L_p$ with two integration points. Element 3, which goes from element 2 to the top of the column, has two integration points. Inclusion of element 1 in the FFEM deserves an explanation, as given below.

In general, modeling of reinforced concrete bridge columns ignores strain penetration length l_{sp}, implying that the curvature goes to zero below the foundation. Actually, the reinforcement tension strain drops to zero at a depth equal to the development length l_d of the reinforcement,

inducing a pullout of the steel bar at the foundation that can be calculated using equations (3.16) and (3.17) (see Figure 3.10).

$$l_{\mathrm{sp}} = \int_0^{l_{\mathrm{d}}} \varepsilon_{\mathrm{y}} \left(1 - \frac{x}{l_{\mathrm{d}}}\right) \mathrm{d}x = \varepsilon_{\mathrm{y}} \frac{l_{\mathrm{d}}}{2} \tag{3.16}$$

According to Priestley et al. (2007)

$$l_{\mathrm{sp}} = 0.022 f_{\mathrm{y}} d_{\mathrm{b}} \tag{3.17}$$

The pullout known as bond slip induces an additional lateral displacement of the bridge column that can increase due to cyclic loading because the reversals induce more bond deterioration. To model bond slip, Filippou et al. (1992) used a rotational spring that connects the column to the foundation. The spring can be calibrated using moment-slip rotation data from experiments (Hachem et al., 2003).

In this study, instead of using a resultant model, a beam-column element of length equal to twice the strain penetration length given in equation (3.17), with two integration points, is used to simulate the tension strain effect on the reinforcement from the base of the bridge column under the foundation. The use of the element allows spreading OF the plasticity into the foundation and accounts for the rotation occurring along the strain penetration length l_{sp} due to bond deterioration. A restriction to lateral displacement that allows rotation is located between elements 1 and 2.

Figure 3.10 shows the scheme of the FFEM proposed and used in this investigation to simulate the 32 laboratory tested bridge columns. Figure 3.10 also shows the number of integration points at each section of the fiber finite element where responses are measured.

To obtain an accurate simulation of the bridge column, the fiber element sections can be discretized into small fibers, each one with the constitutive relation for the confined and unconfined concrete as well as for the steel.

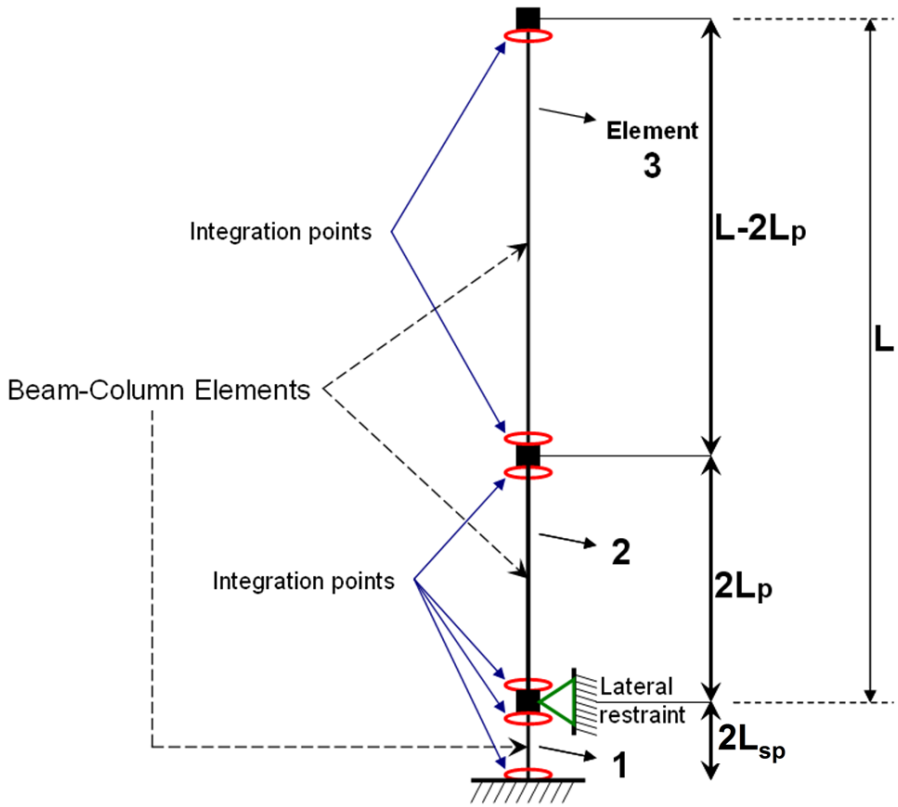

Figure 3.10 Proposed three element model including strain penetration

Appendix B.1 shows 15 different discretizations of the sections of the FFEM for bridge column 328. The comparison between tested and simulated dissipated energies shows small variations. However, only the first three discretizations give good results; the other 12 tend to produce convergence errors in the simulation. In this study, the first one is chosen.

The model to be calibrated for every column in this study shows the discretization of the section of the column with 16 core circumferential divisions, 16 core radial divisions, 16 cover circumferential divisions, and 4 cover radial divisions for a total of 320 fibers (Figure 3.11). To this number as many fibers as longitudinal steel bars exist in the column are added to the beam-column elements. For the column shown, there are 28 bars.

The effect of confinement of the spirals is considered in the FFEM through the calculation of the ultimate confined concrete strain ε_{cu} given by Mander et al. (1988).

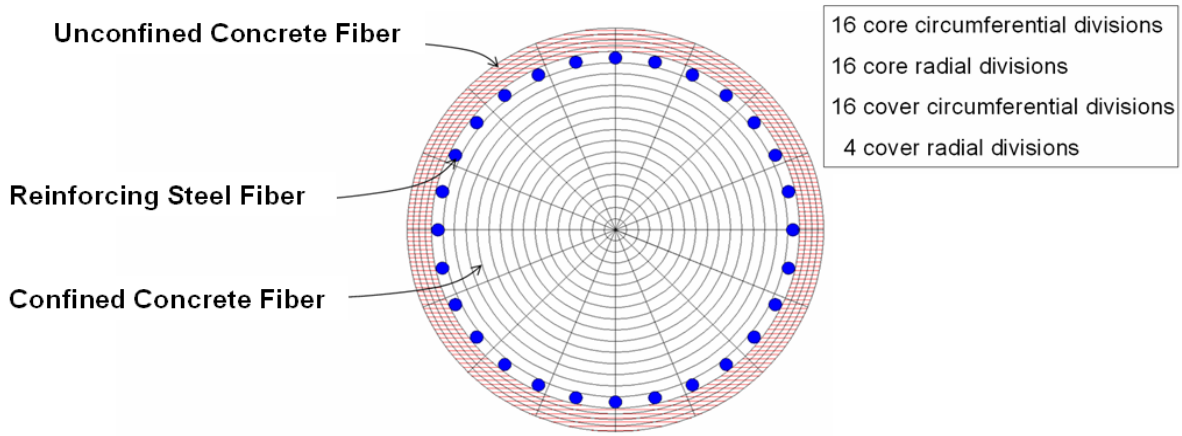

Figure 3.11 Discretization of the section of the bridge column

3.6. Calibration of the finite element model for each laboratory tested column

3.6.1 Procedure

The procedure for the calibration of the FFEM to simulate the response of each of the 30 reinforced concrete bridge columns that was tested at the Earthquake Engineering Research Center of the University of California at Berkeley for the PEER project and that fails by flexure is explained in detail for one of the columns.

Figure 3.12 shows the geometry, axial load, vertical and transverse reinforcement, as well as the material characteristics of a bridge column tested by Calderone et al. (2001), who named it as column 328. Table 3.1 shows all these characteristics for the 30 columns studied, including the name of the column and the authors of the test.

The five parameters to calibrate for each column are L_p, ε_0, R_0, R_1, and R_2, and the calibration is performed by a trial and error procedure. Appendix B.2 shows the process.

The length of the plastic hinge, L_p, is calculated for each column using equation (3.3) (Table 3.2). For column 328 L_p is 0.19 times the height L of the column.

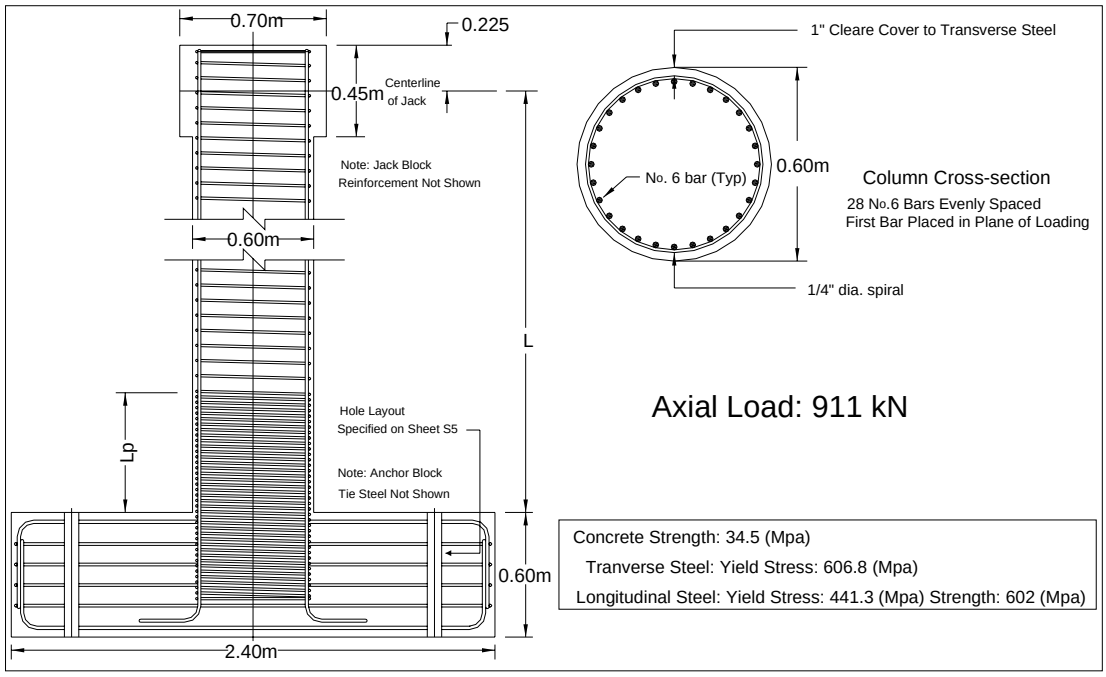

Figure 3.12 Specimen 328 tested at laboratory (Calderone et al., 2001)

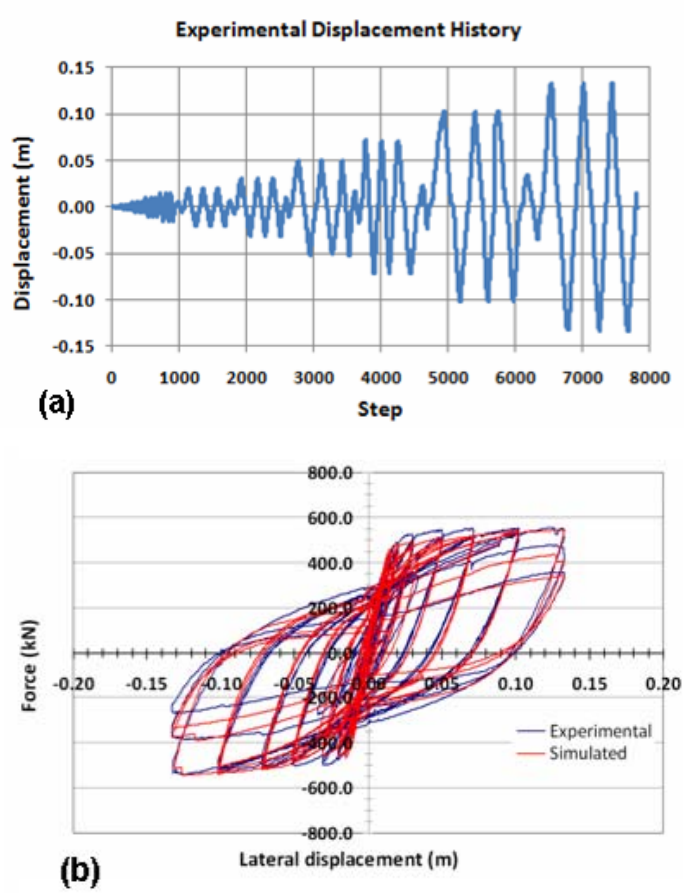

Figure 3.13 Test response and simulation of column 328 (Calderone et al., 2001)

Table 3.1 Characteristics of the 30 columns studied

COLUMN ID NUMBER	COLUMN (TEST ID)	AUTHORS	GEOMETRY			MATERIALS				LONGITUDINAL REINFORCEMENT			TRANSVERSE REINFORCEMENT				LOADING	
			Diameter, d (mm)	Length, L (mm)	L/d	Concrete Strength (MPa)	Long. Steel Yield Stress (MPa)	Long. Steel Strength (MPa)	Transv. Steel Yield Stress (MPa)	Diameter (mm)	Number of bars	Longitudinal reinforcement Ratio, ρ	Diameter Spiral (mm)	Hoop Spacing, Sv (mm)	Cover (mm)	Transverse Reinforcement Ratio, ρ_s	Axial Load (kN)	Axial Load Ratio
1	328	Calderone et al. 2000	609.6	1828.8	3.0	34.5	441.3	602.0	606.8	19.0	28.0	0.0273	6.4	25.4	28.6	0.89	911.84	0.091
2	407	Lehman et al. 1998	609.6	2438.4	4.0	31.0	462.0	630.0	606.8	15.9	11.0	0.0075	6.4	31.8	22.2	0.70	653.86	0.072
3	415	Lehman et al. 1998	609.6	2438.4	4.0	31.0	462.0	630.0	606.8	15.9	22.0	0.0149	6.4	31.8	22.2	0.70	653.86	0.072
4	415p	Henry, 1998	609.6	2438.4	4.0	37.2	462.0	-	606.8	15.9	22.0	0.0149	6.4	31.8	22.2	0.70	1308.00	0.120
5	415s	Henry, 1998	609.6	2438.4	4.0	37.2	462.0	-	606.8	15.9	22.0	0.0149	6.4	63.5	22.2	0.35	654.00	0.060
6	815	Lehman et al. 1998	609.6	4876.8	8.0	31.0	462.0	630.0	606.8	15.9	22.0	0.0149	6.4	31.8	22.2	0.70	653.86	0.072
7	828	Calderone et al. 2000	609.6	4876.8	8.0	34.5	441.3	602.0	606.8	19.0	28.0	0.0273	6.4	25.4	28.6	0.89	911.84	0.091
8	1015	Lehman et al. 1998	609.6	6096.0	10.0	31.0	462.0	630.0	606.8	15.9	22.0	0.0149	6.4	31.8	22.2	0.70	653.86	0.072
9	T3	Chai, Priestley, and Seible 1991	609.6	3657.0	6.0	32.6	315.1	497.8	351.6	19.0	26.0	0.0254	6.4	127.0	20.0	0.17	1779.00	0.187
10	UCI1	Hamilton, 2002	406.4	1854.2	4.6	36.5	458.5	646.0	691.5	12.7	12.0	0.0117	4.5	31.8	15.0	0.53	0.00	0.000
11	430	Lehman et al. 1998	609.6	2438.4	4.0	31.0	462.0	630.0	606.8	15.9	44.0	0.0298	6.4	31.8	22.2	0.70	653.86	0.072
12	A2	Kunnath et al. 1997	305.0	1372.0	4.5	29.0	448.0	690.0	434.0	9.5	21.0	0.0204	4.0	19.0	14.5	0.94	200.00	0.094
13	SRPH1	Hose et al. 1997	610.0	3660.0	6.0	41.1	455.0	746.0	414.0	22.2	20.0	0.0266	9.5	57.0	27.8	0.89	1780.00	0.148
14	N1	Wong et al. 1990	400.0	800.0	2.0	38.0	423.0	577.0	300.0	16.0	20.0	0.0320	10.0	60.0	20.0	1.42	907.00	0.190
15	NIST FS Flexure	Cheok and Stone	1520.0	9140.0	6.0	35.8	475.0	-	493.0	43.0	25.0	0.0200	15.9	89.0	58.7	0.63	4450.00	0.069
16	N1	Pontangaro a et al. 1979	600.0	1200.0	2.0	28.4	303.0	409.0	300.0	24.0	16.0	0.0243	10.0	75.0	25.0	0.75	1920.00	0.227
17	N4	Pontangaro a et al. 1979	600.0	1200.0	2.0	32.9	303.0	409.0	423.0	24.0	16.0	0.0243	10.0	70.0	25.0	0.80	3785.00	0.386
18	N5a	Pontangaro a et al. 1979	600.0	1200.0	2.0	32.5	307.0	414.0	280.0	24.0	16.0	0.0243	16.0	55.0	28.0	2.61	3385.00	0.349
19	N3	Ng et al. 1978	250.0	930.0	3.7	33.0	294.0	396.0	207.0	12.0	10.0	0.0218	4.3	10.0	10.2	2.48	550.00	0.322
20	NIST FS Shear	Cheok and Stone	1520.0	4570.0	3.0	34.3	475.0	-	435.0	43.0	25.0	0.0200	19.1	54.0	60.3	1.49	4450.00	0.071
21	N2	Ng et al. 1978	250.0	1340.0	5.4	35.1	305.0	411.0	263.0	13.0	10.0	0.0256	4.4	14.0	10.8	1.87	16.90	0.009
22	A9	Kunnath et al. 1997	305.0	1372.0	4.5	32.5	448.0	690.0	434.0	9.5	21.0	0.0204	4.0	19.0	14.5	0.94	222.00	0.093
23	A10	Kunnath et al. 1997	305.0	1372.0	4.5	27.0	448.0	690.0	434.0	9.5	21.0	0.0204	4.0	19.0	14.5	0.94	200.00	0.101
24	Con-1	Lim et al. 1990	152.0	1140.0	7.5	34.5	448.0	-	620.0	12.7	8.0	0.0559	3.7	22.0	10.2	1.45	151.00	0.241
25	A4	Kunnath et al. 1997	305.0	1372.0	4.5	35.5	448.0	690.0	434.0	9.5	21.0	0.0204	4.0	19.0	14.5	0.94	222.00	0.086
26	C-4	Soderstrom, 2001	419.0	1968.5	4.7	69.6	429.5	717.0	413.7	22.2	8.0	0.0213	10.0	50.8	55.8	1.93	987.50	0.098
27	IC-1	Sritharan et al. 1995	600.0	1800.0	3.0	31.4	448.0	739.0	431.0	22.2	14.0	0.0192	9.5	97.0	30.2	0.54	400.00	0.045
28	Kow-1	Kowalsky and Moyer, 2001	457.2	2438.4	5.3	32.7	565.4	696.4	434.4	19.0	12.0	0.0198	9.5	76.2	12.7	0.92	231.30	0.041
29	Kow-2	Kowalsky and Moyer, 2001	457.2	2438.4	5.3	34.2	565.4	696.4	434.4	19.0	12.0	0.0198	9.5	76.2	12.7	0.92	231.30	0.039
30	1028	Calderone et al. 2000	609.6	6096.0	10.0	34.5	441.3	602.0	606.8	19.0	28.0	0.0273	6.4	25.4	28.6	0.89	911.84	0.091

Figure 3.13 a shows the cyclic reversible displacements applied to the columns in the laboratory, and Figure 3.13 b shows both the laboratory hysteretic response of column 328 and the simulation using the calibrated parameters.

The cyclic steel strain ε_0 in equation (3.4) is calibrated for each column, as seen in Table 3.2. For column 328, ε_0 is 0.158.

The calibrated parameters controlling the stress–strain relation for the longitudinal steel bars shown in Figure 3.3 are listed in Table 3.2. For column 328 these are R_0 = 15, R_1 = 0.93, and R_2 = 0.15.

Table 3.2 Calibrated parameters for simulation of the 30 columns response

COLUMN ID NUMBER	COLUMN (TEST ID)	AUTHORS	L_p/L	ε_0 for reinforcing steel model	Giuffre-Menegotto-Pinto Model Parameters for Bauschinger effect		
					R_0	R_1	R_2
1	328	Calderone et al. 2000	0.19	0.158	15.0	0.930	0.15
2	407	Lehman et al. 1998	0.13	0.128	17.0	0.915	0.15
3	415	Lehman et al. 1998	0.15	0.130	16.0	0.905	0.15
4	415p	Henry, 1998	0.15	0.118	18.0	0.915	0.15
5	415s	Henry, 1998	0.15	0.110	14.0	0.910	0.15
6	815	Lehman et al. 1998	0.12	0.125	20.0	0.900	0.15
7	828	Calderone et al. 2000	0.20	0.100	17.0	0.915	0.15
8	1015	Lehman et al. 1998	0.11	0.100	13.0	0.890	0.15
9	T3	Chai, Priestley, and Seible 1991	0.12	0.075	15.0	0.925	0.15
10	UCI1	Hamilton, 2002	0.15	0.135	13.0	0.910	0.15
11	430	Lehman et al. 1998	0.15	0.140	13.0	0.930	0.15
12	A2	Kunnath et al. 1997	0.15	0.178	12.0	0.920	0.15
13	SRPH1	Hose et al. 1997	0.14	0.150	17.0	0.900	0.15
14	N1	Wong et al. 1990	0.25	0.130	14.0	0.900	0.15
15	NIST FS Flexure	Cheok and Stone	0.12	0.130	17.0	0.925	0.15
16	N1	Pontangaroa et al. 1979	0.21	0.120	18.0	0.920	0.15
17	N4	Pontangaroa et al. 1979	0.21	0.080	20.0	0.890	0.15
18	N5a	Pontangaroa et al. 1979	0.21	0.080	21.0	0.880	0.15
19	N3	Ng et al. 1978	0.16	0.100	19.0	0.890	0.15
20	NIST FS Shear	Cheok and Stone	0.17	0.170	14.0	0.930	0.15
21	N2	Ng et al. 1978	0.15	0.090	14.5	0.910	0.15
22	A9	Kunnath et al. 1997	0.16	0.140	14.0	0.920	0.15
23	A10	Kunnath et al. 1997	0.16	0.130	14.0	0.920	0.15
24	Con-1	Lim et al. 1990	0.19	0.120	16.0	0.930	0.15
25	A4	Kunnath et al. 1997	0.16	0.180	14.0	0.920	0.15
26	C-4	Soderstrom, 2001	0.20	0.150	18.0	0.930	0.15
27	IC-1	Sritharan et al. 1995	0.20	0.185	12.0	0.950	0.15
28	Kow-1	Kowalsky and Moyer, 2001	0.18	0.130	13.0	0.940	0.15
29	Kow-2	Kowalsky and Moyer, 2001	0.18	0.190	13.0	0.930	0.15
30	1028	Calderone et al. 2000	0.13	0.165	20.0	0.890	0.15
AVERAGE				0.131	15.717	0.915	0.150
STANDARD DEVIATION				0.0317	2.6316	0.0167	0.0000

Table 3.3 shows the envelope and repeated hysteretic dissipated energies and the summation of both for the tested columns. In addition, Table 3.3 also shows those energies after simulation using the calibrated FFEM. In all cases, the error average between the hysteretic energy in the test and in the simulation is less than 10%.

Table 3.3 Test and simulated columns dissipated energy

	COLUMN		TEST COLUMN DISSIPATED ENERGY (kN-m)			SIMULATED COLUMN DISSIPATED ENERGY (kN-m)			ERROR		
	COD.	AUTHOR	HYSTERETIC	ENVELOPE	REPEATED	HYSTERETIC	ENVELOPE	REPEATED	HYSTERETIC	ENVELOPE	REPEATED
1	328	Calderone et al. 2000	921.30	163.67	757.64	938.44	153.78	784.66	1.86%	-6.04%	3.57%
2	407	Lehman et al. 1998	179.98	42.75	137.23	177.65	42.95	134.70	-1.29%	0.47%	-1.84%
3	415	Lehman et al. 1998	443.67	106.10	337.57	490.55	99.55	391.01	10.57%	-6.17%	15.83%
4	415p	Henry, 1998	381.64	97.88	283.76	407.13	89.90	317.23	6.68%	-8.16%	11.80%
5	415s	Henry, 1998	324.55	89.32	235.23	352.41	80.10	272.31	8.59%	-10.32%	15.76%
6	815	Lehman et al. 1998	635.69	139.23	496.46	639.67	129.53	510.14	0.63%	-6.96%	2.75%
7	828	Calderone et al. 2000	1044.21	200.67	843.54	1055.60	191.33	864.26	1.09%	-4.65%	2.46%
8	1015	Lehman et al. 1998	496.63	141.42	355.22	435.10	119.73	315.37	-12.39%	-15.34%	-11.22%
9	T3	Chai, Priestley, and Seible 1991	261.81	61.18	200.64	255.16	55.87	199.29	-2.54%	-8.68%	-0.67%
10	UCI1	Hamilton, 2002	107.67	16.04	91.63	109.76	15.70	94.06	1.94%	-2.11%	2.65%
11	430	Lehman et al. 1998	708.31	179.08	529.23	734.87	163.47	571.40	3.75%	-8.72%	7.97%
12	A2	Kunnath et al. 1997	79.25	11.10	68.16	86.14	10.80	75.35	8.69%	-2.69%	10.55%
13	SRPH1	Hose et al. 1997	1355.26	230.21	1125.06	1300.16	204.50	1095.66	-4.07%	-11.17%	-2.61%
14	N1	Wong et al. 1990	223.68	37.42	186.26	240.43	35.28	205.15	7.49%	-5.73%	10.14%
15	NIST FS Flexure	Cheok and Stone	14321.52	1830.03	12491.49	13561.34	1508.24	12053.09	-5.31%	-17.58%	-3.51%
16	N1	Pontangaroa et al. 1979	208.62	60.28	148.34	220.83	59.55	161.27	5.85%	-1.20%	8.72%
17	N4	Pontangaroa et al. 1979	166.18	48.68	117.50	153.12	46.06	107.06	-7.86%	-5.38%	-8.89%
18	N5a	Pontangaroa et al. 1979	135.83	40.45	95.38	140.32	37.69	102.63	3.30%	-6.84%	7.60%
19	N3	Ng et al. 1978	18.72	4.88	13.85	18.91	4.52	14.39	1.02%	-7.32%	3.95%
20	NIST FS Shear	Cheok and Stone	10460.72	2379.24	8081.48	10487.99	2098.60	8389.39	0.26%	-11.80%	3.81%
21	N2	Ng et al. 1978	20.24	5.62	14.62	19.65	5.70	13.96	-2.91%	1.31%	-4.52%
22	A9	Kunnath et al. 1997	66.32	12.43	53.89	70.00	11.94	58.06	5.55%	-3.96%	7.75%
23	A10	Kunnath et al. 1997	63.90	12.12	51.78	67.87	11.77	56.10	6.21%	-2.83%	8.33%
24	Con-1	Lim et al. 1990	16.41	3.84	12.57	17.20	3.64	13.56	4.81%	-5.25%	7.89%
25	A4	Kunnath et al. 1997	125.85	7.81	118.04	123.59	7.32	116.28	-1.79%	-6.34%	-1.49%
26	C-4	Soderstrom, 2001	364.13	59.12	305.01	396.82	56.92	339.90	8.98%	-3.73%	11.44%
27	IC-1	Sritharan et al. 1995	502.28	104.71	397.57	507.64	97.69	409.94	1.07%	-6.70%	3.11%
28	Kow-1	Kowalsky and Moyer, 2001	291.25	58.58	232.67	264.55	53.26	211.29	-9.17%	-9.08%	-9.19%
29	Kow-2	Kowalsky and Moyer, 2001	340.44	50.43	290.01	371.45	47.89	323.56	9.11%	-5.03%	11.57%
30	1028	Calderone et al. 2000	2199.06	423.60	1775.46	2089.76	358.06	1731.70	-4.97%	-15.47%	-2.46%
								ERROR AVERAGE	1.51%	-6.78%	3.71%

3.6.2 Simulations

Figures 3.14 a to 3.14 e show the simulated hysteretic response of the 30 bridge columns using the FFEM with the calibrated parameters described above for each column (Table 3.2). The simulation is drawn on top of the reported response of the tested columns. Clearly, the simulations are satisfactory with respect to the results of the tests, as shown in these figures and according to the comparison of energies indicated above.

The inclusion of the fiber finite element 1 in the FFEM to simulate strain penetration as seen in Figure 3.10 allowed simulating satisfactorily the stiffness of every bridge column subjected to the applied displacement history, as will be seen later in Figures 3.23 a and b.

Tests for bridge columns Con-1 and C-4 (Table 3.1) are performed with an actuator located on the top of the column to simulate axial load so the P-Δ effect is activated in the FFEM for only these two columns. It can be observed in Figures 3.14 d and 3.14 e, respectively, that while the simulation for column Con-1 does not reach the test strength, the simulation for column C-4 is satisfactory.

The P-Δ effect modifies the hysteretic response of columns Con-1 and C-4, reducing the shear resistance and the initial stiffness, particularly in C-4.

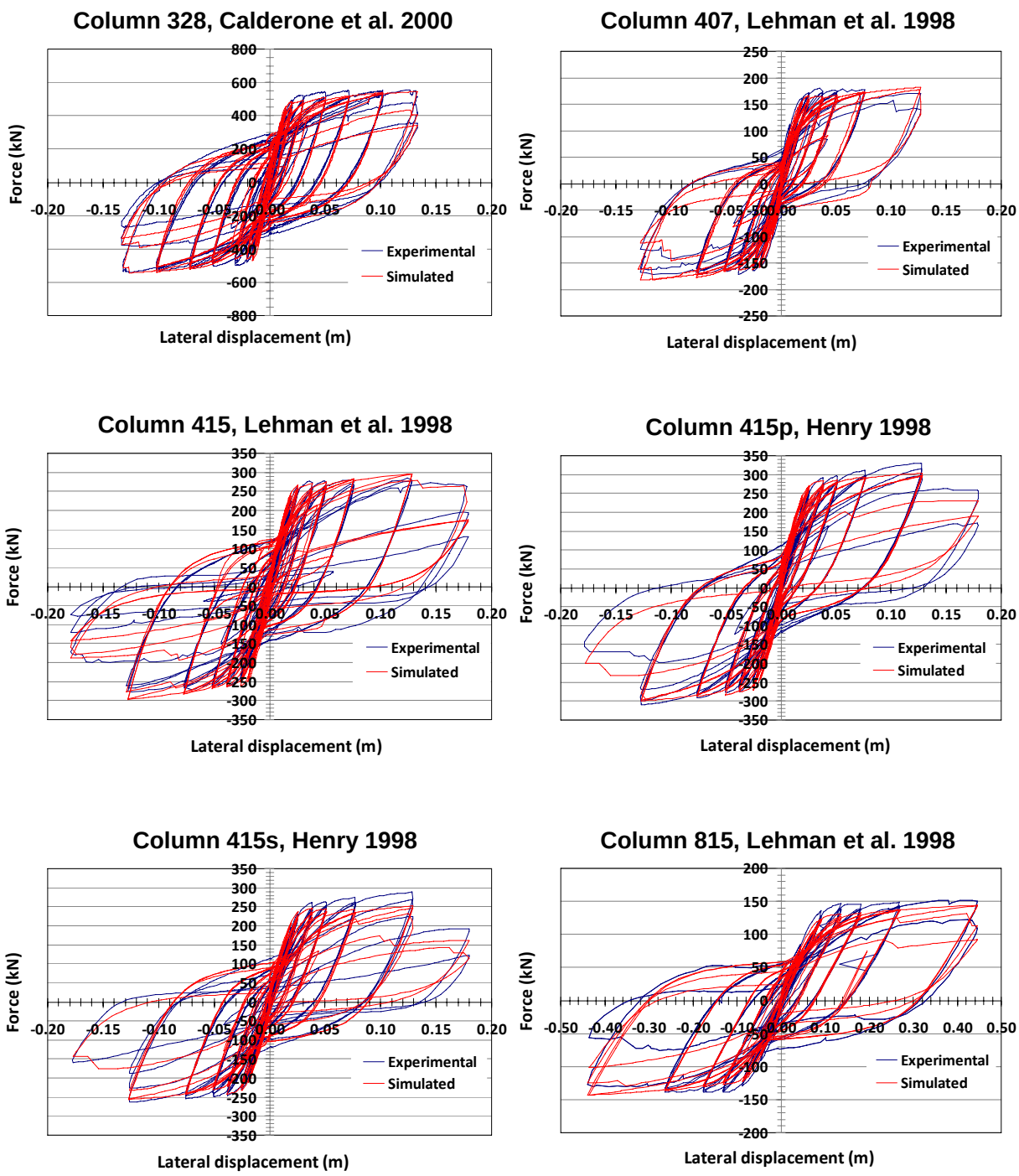

Figure 3.14 a. Experimental vs. simulated hysteretic response of the columns studied

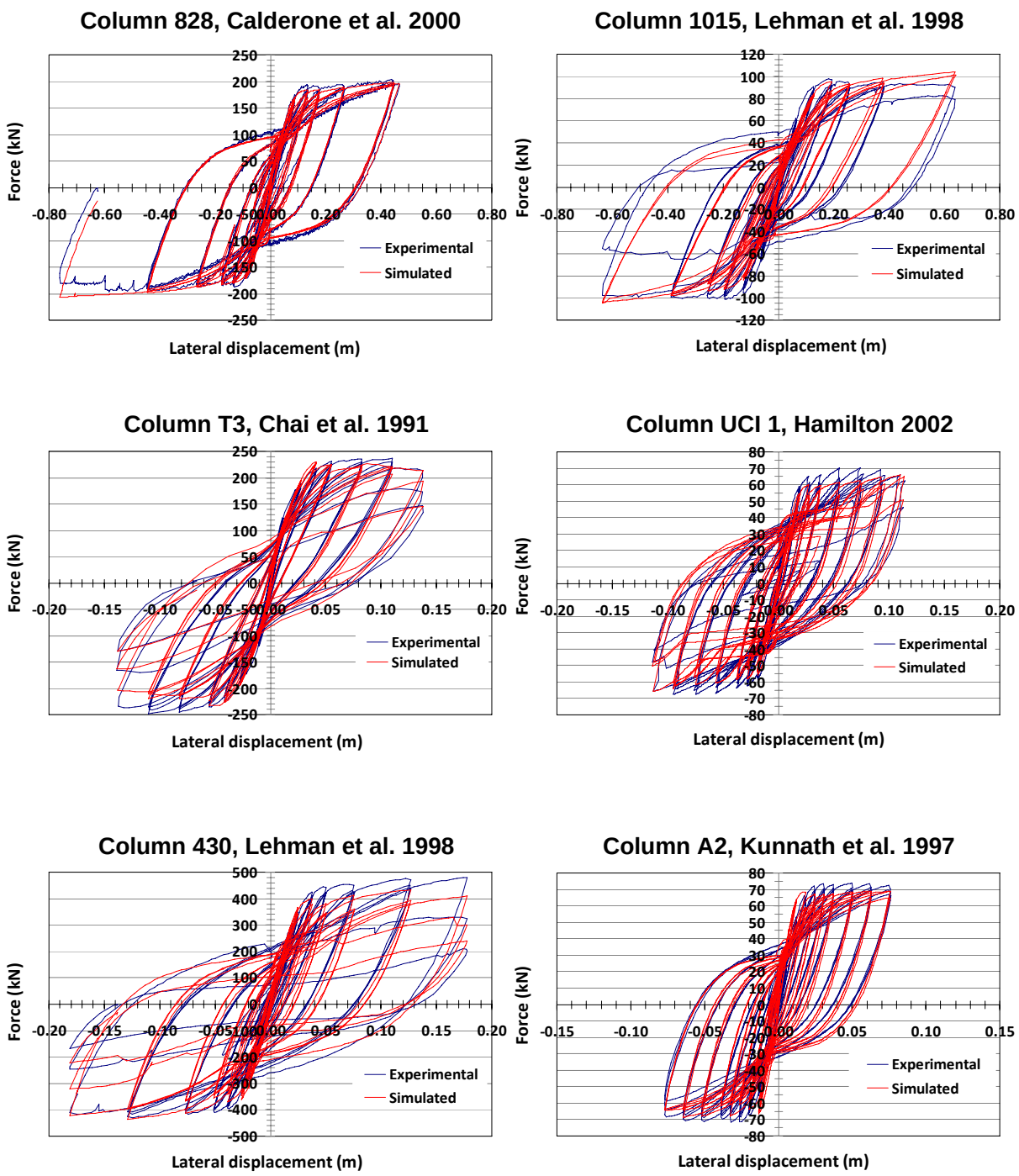

Figure 3.14 b. Experimental vs. simulated hysteretic response of the columns studied

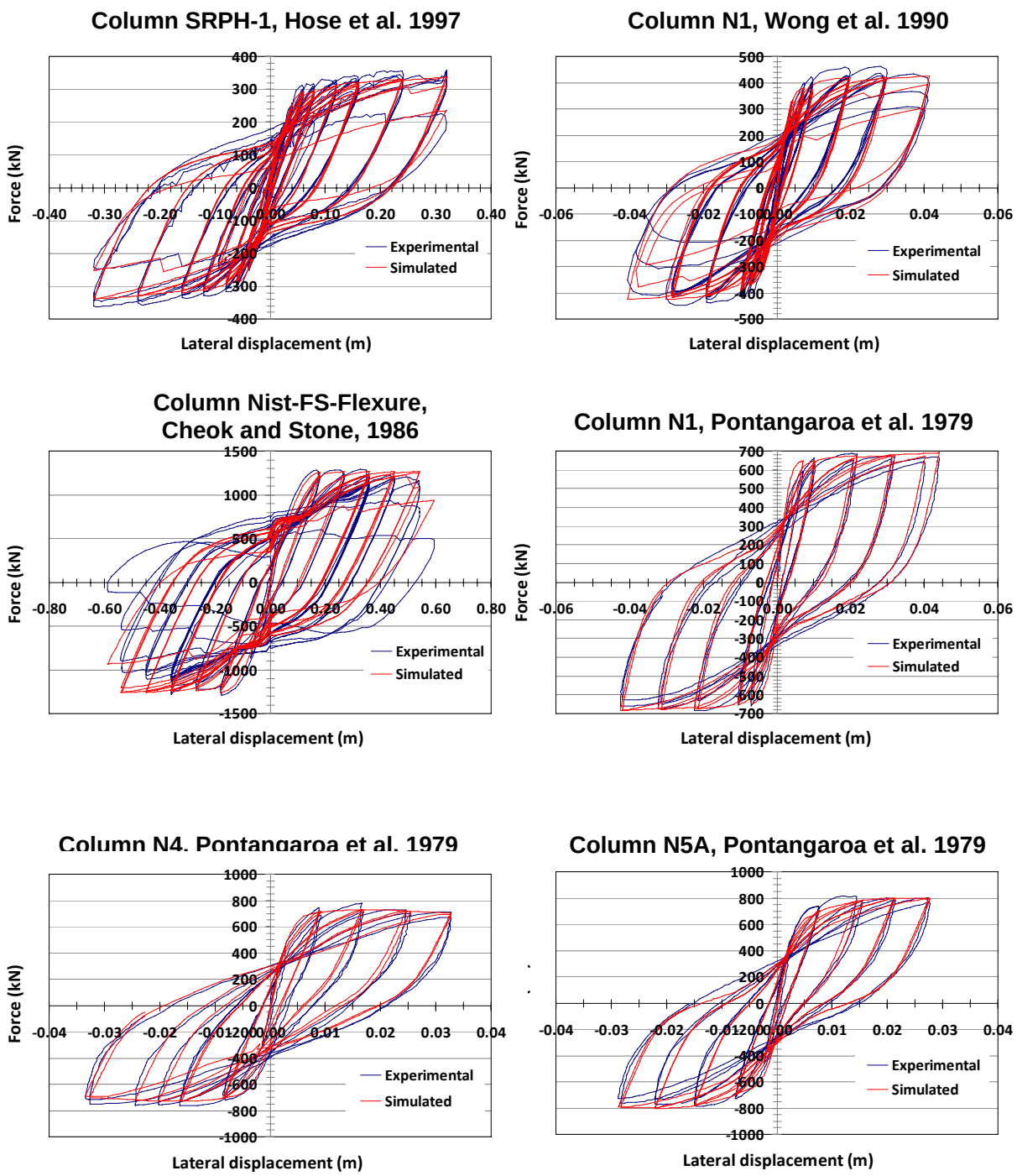

Figure 3.14 c. Experimental vs. simulated hysteretic response of the columns studied

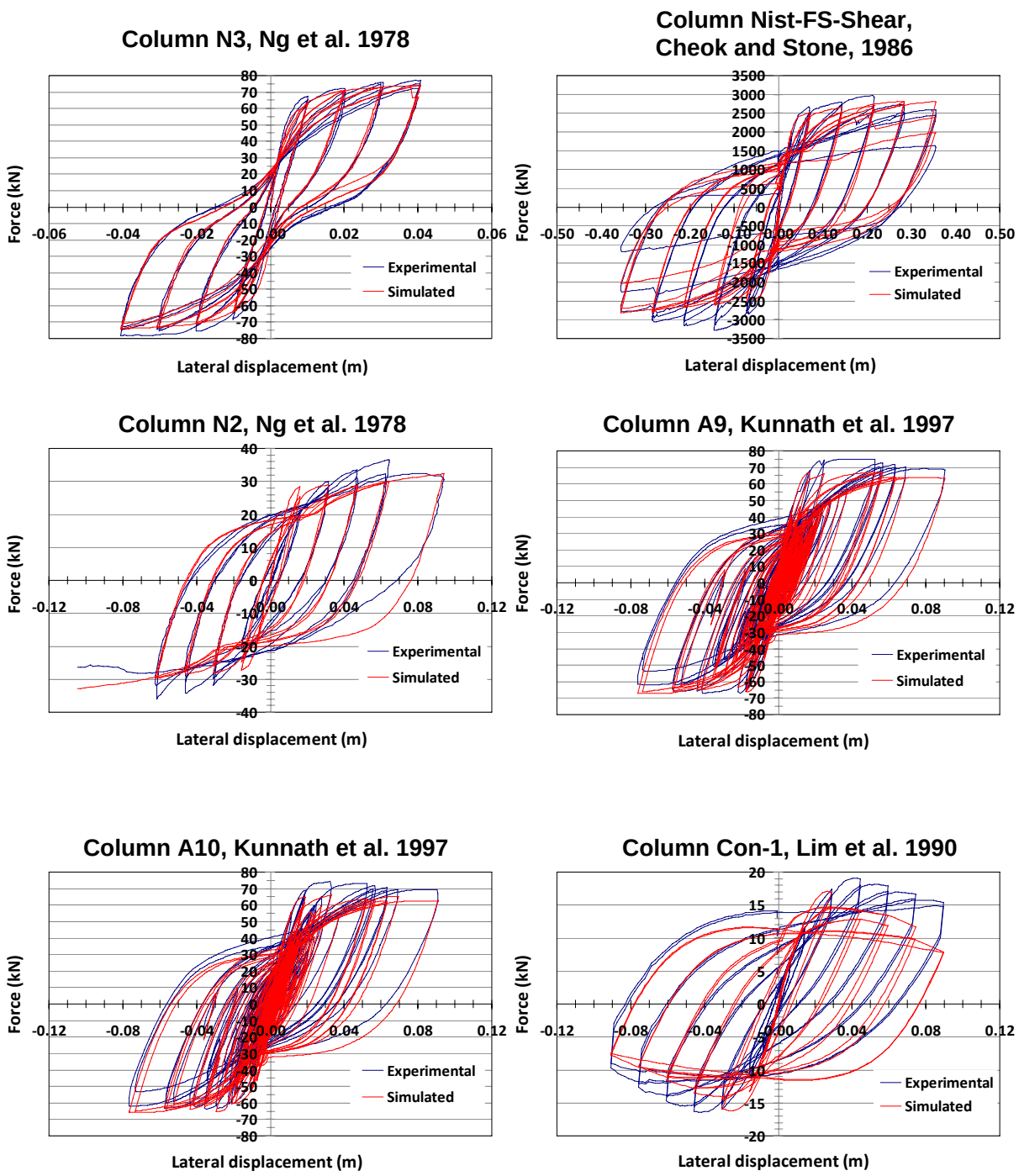

Figure 3.14 d. Experimental vs. simulated hysteretic response of the columns studied

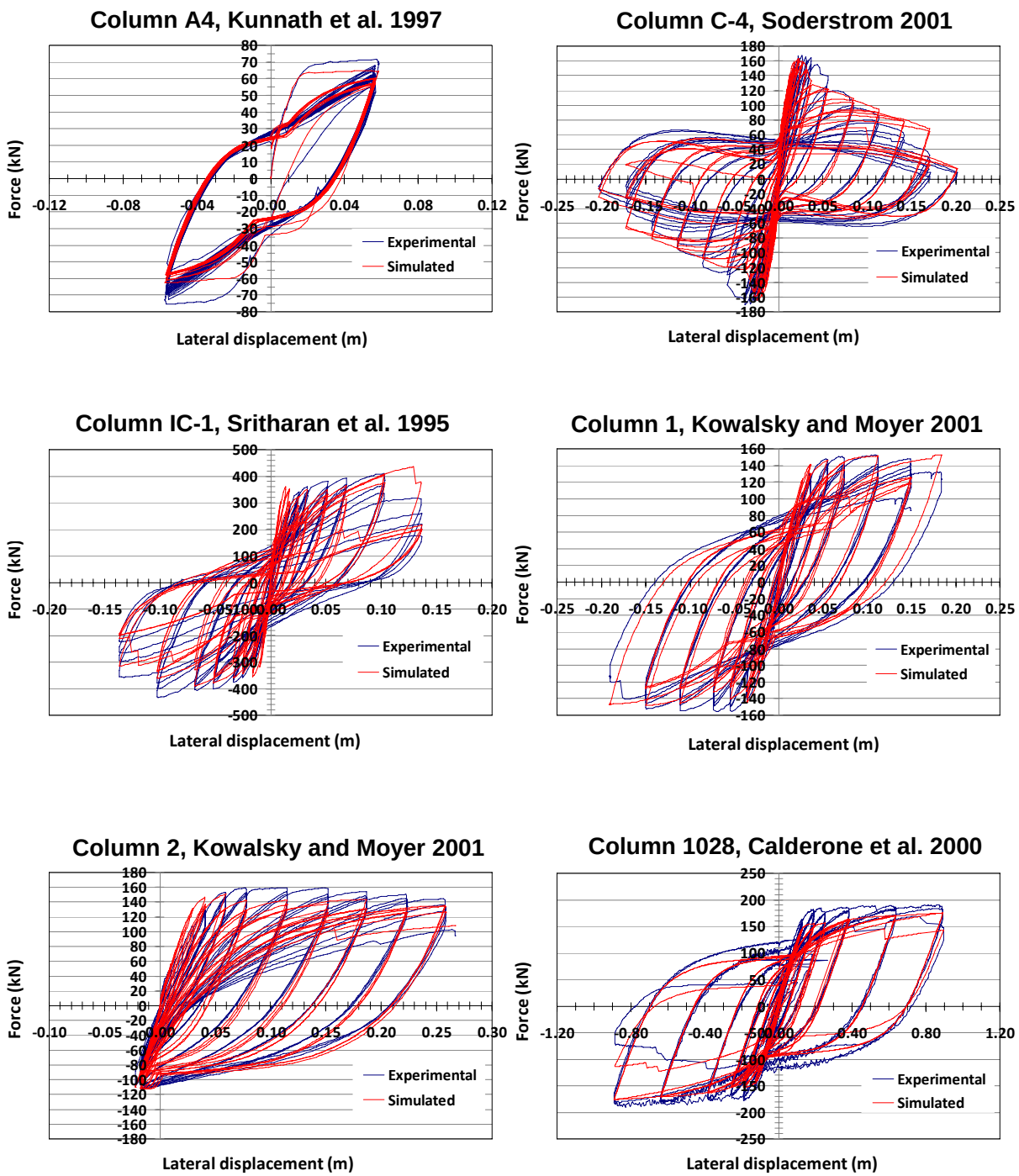

Figure 3.14 e. Experimental vs. simulated hysteretic response of the columns studied

3.7. Discussion of the simulation results for the 30 bridge columns tested in the laboratory under cyclic reversible and increasing displacements

Table 3.4 shows the non-cyclic plastic displacements, steel and concrete strains, and fatigue bar damage index at two levels of responses for the 30 bridge columns. The fatigue damage index, FDI, measures the accumulation of damage D_i, equation 3.7, and when FDI = 1.0 the bar fractures inducing a decrease of the strength of the column.

The first level corresponds to a traditional 2% maximum drift occurring during the application of the third and fourth group of the cyclic displacement history (Figure 3.13 a). Here, the non-cyclic plastic response at level 1, u_{ncp1}, is in general slightly larger than u_y.

The second level corresponds to a larger drift than the first level for each column when SDPL occurs for the fifth and sixth groups of applied displacements, as seen in Figure 3.13 a and Table 3.5.

Figure 3.15 a shows a simplified hysteretic response of a reinforced concrete column that deteriorates in strength and stiffness. To calculate the energies attributed to the new plastic displacements and to the repeated plastic displacements, how to separate both displacements is shown in Figure 3.15 a. The new plastic displacements go from A to B, from E to F, from H′ to J′, from K′ to K, and from T′ to T. The repeated plastic displacements go from J′ to K′, from M′ to P, and from Q to T′. The yielding value is obtained using the intersection of the tangents to the reversal and to the plastic deformation. In this figure, the yielding points are at A′, D, H, M, and R.

Table 3.4 Displacements and strains simulations at two levels of non-cyclic plastic deformations

					First Level 2% Drift					Second Level Large Drift					
	COLUMN	AUTHORS	Height (m)	u_y (m)	u_{ncp1} (m)	Steel Strain (u_{ncp1})	Concrete Strain (u_{ncp1})	Bar Damage Index (u_{ncp1})	u_{ncp2} (m)	u_{cpe} (m)	u_{cpr} (m)	Max Steel Strain (final of test)	Max Concrete Strain (final of test)	Bar Damage Index (final of test)
1	328	Calderone et al. 2000	1.828	0.014	0.037	0.014	-0.005	0.032	0.133	0.496	5.209	0.0650	-0.0230	1.0800
2	407	Lehman et al. 1998	2.238	0.020	0.045	0.017	-0.005	0.062	0.129	0.476	3.898	0.0630	-0.0160	1.0000
3	415	Lehman et al. 1998	2.238	0.020	0.045	0.015	-0.005	0.051	0.179	0.674	6.262	0.0770	-0.0280	1.0000
4	415p	Henry, 1998	2.438	0.020	0.049	0.013	-0.005	0.041	0.179	0.670	5.106	0.0654	-0.0231	1.0000
5	415s	Henry, 1998	2.438	0.020	0.049	0.015	-0.004	0.048	0.180	0.670	5.113	0.0710	-0.0200	1.0000
6	815	Lehman et al. 1998	4.677	0.080	0.094	0.005	-0.002	0.008	0.446	1.600	15.441	0.0591	-0.0177	1.0000
7	828	Calderone et al. 2000	4.877	0.060	0.098	0.004	-0.002	0.007	0.762	2.304	16.144	0.0552	-0.0208	1.0150
8	1015	Lehman et al. 1998	6.096	0.100	0.122	0.003	-0.002	0.005	0.640	2.350	16.922	0.0466	-0.0135	1.0800
9	T3	Chai, Priestley, and Seible 1991	3.457	0.025	0.069	0.011	-0.006	0.069	0.139	0.528	5.317	0.0258	-0.0172	1.0000
10	UCI1	Hamilton, 2002	1.854	0.015	0.037	0.014	-0.002	0.045	0.114	0.426	5.024	0.0546	-0.0066	1.0000
11	430	Lehman et al. 1998	2.438	0.022	0.049	0.013	-0.005	0.024	0.181	0.670	6.113	0.0655	-0.0223	1.0400
12	A2	Kunnath et al. 1997	1.222	0.019	0.024	0.012	-0.005	0.035	0.077	0.282	3.724	0.0502	-0.0168	0.8320
13	SRPH1	Hose et al. 1997	3.460	0.050	0.069	0.007	-0.004	0.010	0.320	1.174	12.663	0.0536	-0.0258	1.0000
14	N1	Wong et al. 1990	0.800	0.004	0.016	0.010	-0.006	0.069	0.041	0.154	1.695	0.0431	-0.0213	1.0000
15	NIST FS Flexure	Cheok and Stone	9.140	0.080	0.183	0.009	-0.003	0.006	0.593	2.172	31.148	0.0466	-0.0137	1.0000
16	N1	Pontangaroa et al. 1979	1.100	0.004	0.022	0.020	-0.011	0.013	0.044	0.166	0.704	0.0428	-0.0243	0.7260
17	N4	Pontangaroa et al. 1979	1.200	0.004	0.024	0.016	-0.014	0.099	0.033	0.124	0.534	0.0212	-0.0221	0.6230
18	N5a	Pontangaroa et al. 1979	1.100	0.004	0.022	0.017	-0.013	0.175	0.029	0.106	0.475	0.0231	-0.0163	0.6917
19	N3	Ng et al. 1978	0.880	0.005	0.018	0.012	-0.009	0.011	0.041	0.155	0.808	0.0330	-0.0200	1.0000
20	NIST FS Shear	Cheok and Stone	4.570	0.030	0.091	0.016	-0.005	0.008	0.356	1.360	8.833	0.0794	-0.0211	1.0000
21	N2	Ng et al. 1978	1.340	0.010	0.027	0.011	-0.003	0.005	0.105	0.380	1.284	0.0545	-0.0121	0.6118
22	A9	Kunnath et al. 1997	1.272	0.017	0.025	0.011	-0.005	0.005	0.091	0.310	4.785	0.0518	-0.0183	0.7869
23	A10	Kunnath et al. 1997	1.272	0.017	0.025	0.011	-0.005	0.005	0.091	0.310	4.764	0.0545	-0.0181	1.0000
24	Con-1	Lim et al. 1990	1.140	0.020	0.023	0.003	0.003	0.002	0.091	0.320	2.222	0.0189	-0.0147	0.5825
25	A4	Kunnath et al. 1997	1.372	0.015	0.027	0.011	-0.005	0.000	0.059	0.204	5.306	0.0271	-0.0097	0.8788
26	C-4	Soderstrom, 2001	1.769	0.020	0.035	0.009	-0.004	0.037	0.203	0.168	9.888	0.0580	-0.0248	1.0000
27	IC-1	Sritharan et al. 1995	1.600	0.015	0.032	0.017	-0.005	0.025	0.137	0.282	5.571	0.0837	-0.0226	1.0000
28	Kow-1	Kowalsky and Moyer, 2001	2.238	0.030	0.045	0.008	-0.003	0.008	0.190	0.690	5.677	0.0510	-0.0127	1.0000
29	Kow-2	Kowalsky and Moyer, 2001	2.238	0.030	0.045	0.008	-0.003	0.004	0.267	0.516	7.731	0.0720	-0.0205	1.0000
30	1028	Calderone et al. 2000	5.796	0.098	0.116	0.003	-0.002	0.000	0.894	3.342	32.189	0.0671	-0.0257	1.0000

Table 3.4 shows that the concrete strains corresponding to the non-cyclic plastic displacements for level 1 response, u_{ncp1}, are just less than, equal to, or slightly larger than the maximum unconfined concrete strain ε_{cc} = 0.004 given by Mander et al. (1988). Only columns N1, N4, N5a, and N3 appear, with confined concrete strains demands reaching 0.011, 0.014, 0.013, and 0.09; these are larger than ε_{cc} but still lower than ε_{cu} (Mander et al., 1988). The value of ε_{cu} equation (3.2), is the crushing strain given in Table 3.6. The main difference between these columns and the others is the high axial load ratios that reach 0.227, 0.286, 0.349, and 0.322, as seen in Table 3.1.

For the level 1 response, the fatigue damage index given in equation (3.7) shows some damage for the longitudinal bars. The largest one in Table 3.4 is 0.175 for one bar of bridge column N5a. These results indicate that for the u_{ncp1} there is no SDPL in any of the 30 bridge columns. Since the values for u_{ncp1} correspond to a 2% drift, the results clearly indicate that drifts do not measure plastic displacements and are not measures of structural damage, as stated in Chapter 2, but can be a limit for non-structural damage in building structures (Priestley et al., 2007) although there is already damage due to low-cyclic fatigue.

In Table 3.4, for the second level of responses the non-cyclic plastic displacements for level 2 response, u_{ncp2}, are considerable larger than u_y, varying between 3.9 and 12.6 times u_y. The damage observed on 15 columns during the seventh group of applied displacements (Figure 3.13 a), is shown in Table 3.5.

For seven of the columns there is no report of damage, and for three of them only spalling of the unconfined concrete is reported (Brown and Kunnath, 2000). The report for the other 20 columns show that SDPL occurred in the columns in the form of crushing of the confined concrete, fracture of the spiral, buckling of the longitudinal bar, or fracture of the longitudinal bars due to low-cycle fatigue; this agrees with the results of the FFEM (Tables 3.4 and 3.5).

Figure 3.15 b shows the confined concrete strains at coordinates located very close to the longitudinal steel bar 1 and the steel strains at the position of bar 1 for column 328.

Table 3.5 Damage observed during the tests

	COLUMN	AUTHORS	TEST DISPLACEMENT (mm)					SIMULATION DISPLACEMENT (mm)	
			Crushing	Spalling	Buckling	Long. Bar fracture	Spiral fracture	Long. Bar fracture	Spiral fracture
1	328	Calderone et al. 2000	30.0	-	133.0	132.0	132.0	132.0	132.0
2	407	Lehman et al. 1998	38.0	38.1	127.0	127.0	127.0	127.0	127 (90% of ε_{cu})
3	415	Lehman et al. 1998	38.1	-	129.0	178.0	135.0	178.0	178.0
4	415p	Henry, 1998	-	-	127.0	135.0	127.0	127.0	135.0
5	415s	Henry, 1998	-	-	127.0	-	127.0	127.0	127.0
6	815	Lehman et al. 1998	133.0	178.0	445.0	445.0	445.0	445.0	445 (94% of ε_{cu})
7	828	Calderone et al. 2000	178.0	-	600.0	-	750.0	750.0	750.0
8	1015	Lehman et al. 1998	191.0	254.0	635.0	635.0	635.0	635.0	635 (70% of ε_{cu})
9	T3	Chai, Priestley, and Seible 1991	-	-	-	-	-	110.0	110.0
10	UCI1	Hamilton, 2002	-	-	-	-	-	110.0	-
11	430	Lehman et al. 1998	38.1	50.8	178.0	-	178.0	178.0	178.0
12	A2	Kunnath et al. 1997	-	40.0	64.5	-	76.2	-	76.2 (93% of ε_{cu})
13	SRPH1	Hose et al. 1997	60.0	80.0	320.0	320.0	-	320.0	240.0
14	N1	Wong et al. 1990	6.0	9.6	41.4	-	40.0	40.0	40.0
15	NIST FS Flexure	Cheok and Stone	179.0	269.0	538.0	538.0	538.0	538.0	538.0
16	N1	Pontangaroa et al. 1979	10.0	20.0	-	-	-	-	40.0
17	N4	Pontangaroa et al. 1979	7.5	15.0	-	-	-	-	32.0
18	N5a	Pontangaroa et al. 1979	-	-	-	-	-	-	-
19	N3	Ng et al. 1978	10.0	20.0	-	-	-	40.0	40.0
20	NIST FS Shear	Cheok and Stone	-	142.0	285.0	356.0	356.0	356.0	356.0
21	N2	Ng et al. 1978	-	-	-	-	-	-	-
22	A9	Kunnath et al. 1997	-	63.0	63.0	-	90.0	-	90.0
23	A10	Kunnath et al. 1997	32.0	50.0	90.7	-	82.0	90.0	90.0
24	Con-1	Lim et al. 1990	-	-	-	-	-	-	-
25	A4	Kunnath et al. 1997	-	-	-	-	57.0	-	-
26	C-4	Soderstrom, 2001	-	-	-	-	-	200.0	200.0
27	IC-1	Sritharan et al. 1995	-	-	-	-	-	136.0	100.0
28	Kow-1	Kowalsky and Moyer, 2001	73.7	-	149.9	186.7	-	186.7	-
29	Kow-2	Kowalsky and Moyer, 2001	55.9	-	261.6	299.7	-	266.7	223.0
30	1028	Calderone et al. 2000	254.0	-	889.0	-	889.0	889.0	889.0

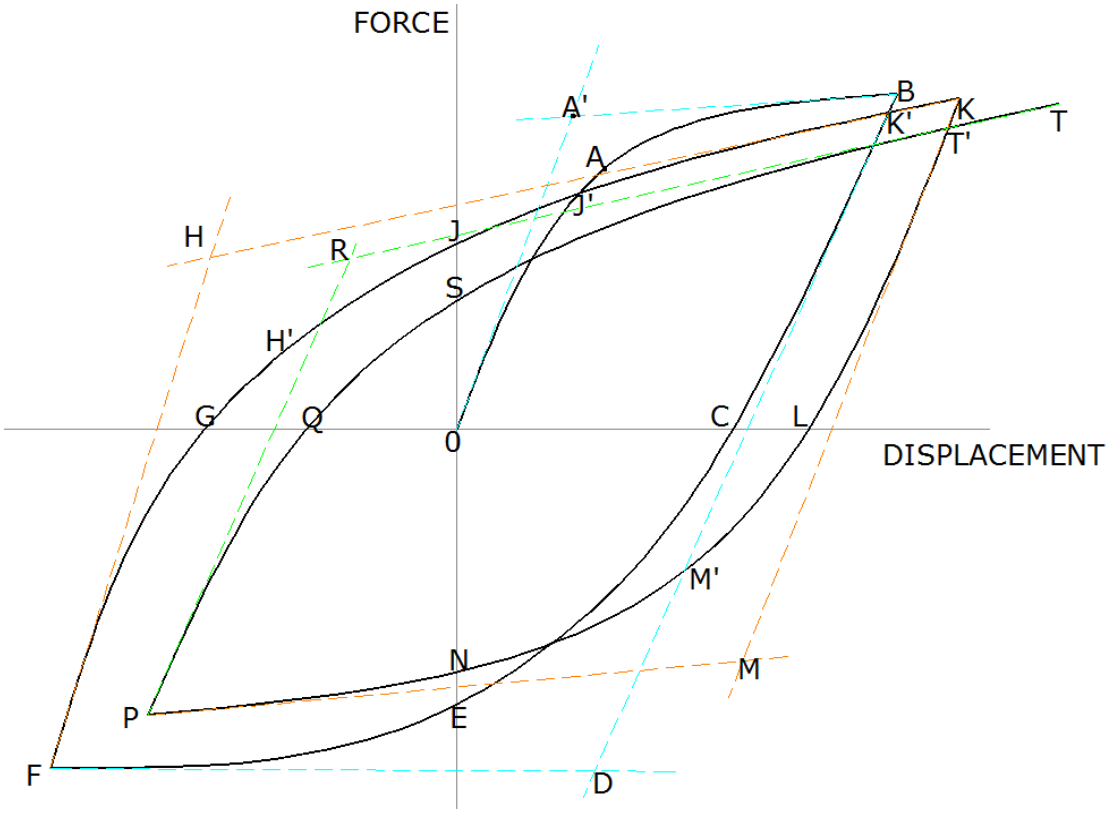

(a)

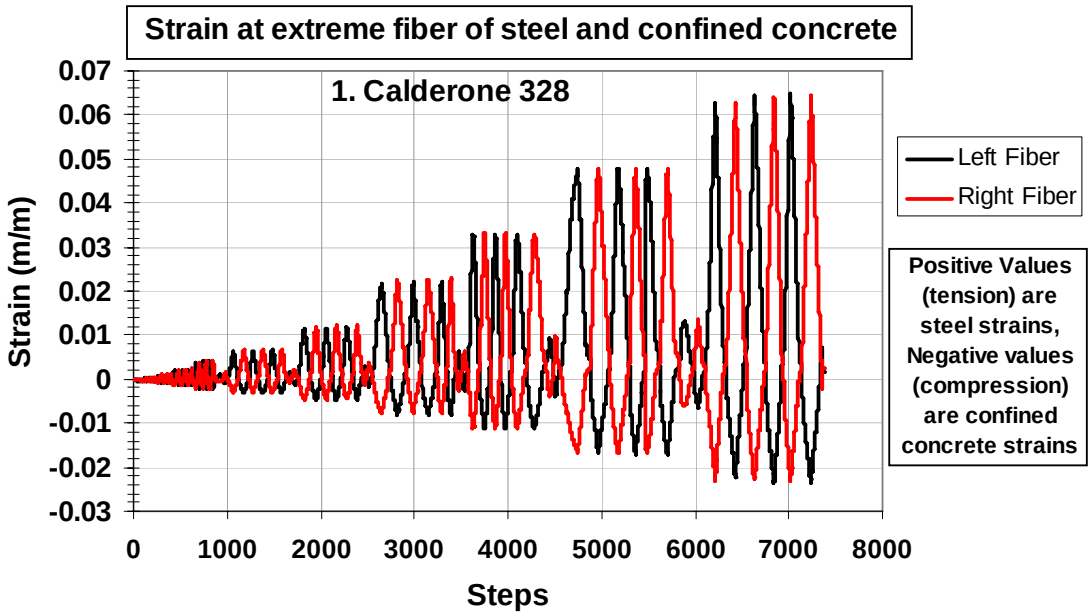

(b)

Figure 3.15 Column 328 simulation: (a) plastic response, (b) strain history response, (c) position of steel bars

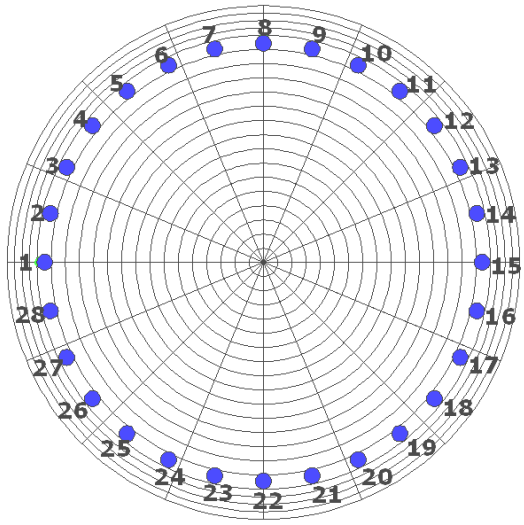

(c)

Figure 3.15 (cont.) Column 328 simulation: (a) plastic response, (b) strain history response, (c) position of steel bars

With regard to confined concrete and steel strains for the second level, Table 3.6 shows the relations between the demanded confined concrete strain and ε_{cu} calculated according to equation (3.2) and according to $1.5\varepsilon_{cu}$, as indicated in Priestley et al. (1996) for each column. In most of the cases the demand is equal or larger than ε_{cu}, and in just a few cases the demand is equal or larger than $1.5\varepsilon_{cu}$ or lower than ε_{cu}. This means that, in general for the 30 bridge columns and for the applied displacement history, the crushing of the concrete occurs at ε_{cu} and not at $1.5\varepsilon_{cu}$. In addition, the steel strains shown in Table 3.4 are equal to or lower than the recommended maximum cyclic steel strain, ε_{su} = 0.09 (Priestley et al., 2007), but the demands are larger than ε_y = 0.002.

For the second level of response, the damage index of the longitudinal steel bars for the last group of the displacement history applied is equal to one in the majority of the bridge columns, showing that there is fracture of these bars due to low-cycle fatigue. This is seen in Table 3.4, coinciding with the tests shown in Table 3.5. Figure 3.16 shows the history of the fatigue damage index for bars 1, 2, 3, 27, 28, and 15, Figure 3.15 c for column 328. The damage accumulates along the history of applied displacements.

The value of the strain at which the bar fractures by low-cycle fatigue in only one cycle ε_0 used to calculate the bar damage according to equation (3.6) for each simulation is the calibrated one,

which according to Table 3.2 has an average value of 0.131. As will be seen later, in the proposed FFEM the value recommended for ε_0 to simulate earthquake response depends on the bar diameter, and for typical diameters used in construction it can be lower than 0.131. Therefore, fracture of the longitudinal steel bars due to low-cyclic fatigue appears to be a very important flexural failure mechanism occurring frequently, inducing SDPL in the column.

The cyclic envelope plastic displacement corresponds to the new plastic excursions u_{cpe} that cause the larger amount of damage, as mentioned in Chapter 2. The repeated plastic displacements u_{cpr} cause less damage for each repetition, but depending on the number of cycles and amplitude of u_{cpr} its summation can lead to low-cyclic fatigue of the column, as stated in Chapter 2. In the second level, in Table 3.4, in column 328, u_{ncp2} = 0.133 m, u_{cpe} = 0.496 m, and u_{cpr} = 5.20 m, showing that u_{cpe} is 3.7 times the traditional lateral non-cyclic plastic displacement u_{ncp2}, and u_{cpr} is considerably larger.

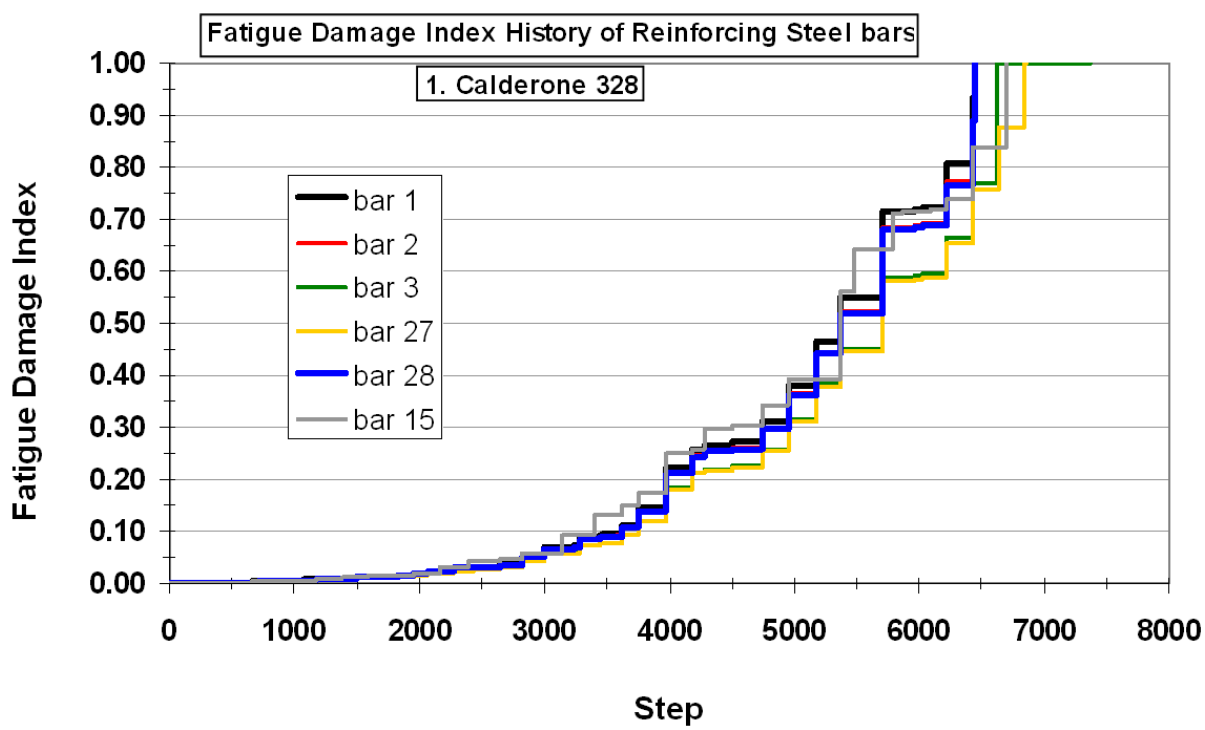

Figure 3.16 Fatigue damage index history for column 328

Table 3.6 Relations between maximum measured strains and ε_{cu} at u_{ncp2}

	COLUMN	AUTHORS	ε_{cu}	$\frac{\varepsilon(u_{ncp2})}{\varepsilon_{cu}}$	$\frac{\varepsilon(u_{ncp2})}{\varepsilon_{cu}*1.5}$
1	328	Calderone et al. 2000	-0.0208	1.106	0.738
2	407	Lehman et al. 1998	-0.0188	0.851	0.567
3	415	Lehman et al. 1998	-0.0188	1.491	0.994
4	415p	Henry, 1998	-0.0168	1.375	0.917
5	415s	Henry, 1998	-0.0112	1.790	1.194
6	815	Lehman et al. 1998	-0.0188	0.942	0.628
7	828	Calderone et al. 2000	-0.0206	1.011	0.674
8	1015	Lehman et al. 1998	-0.0188	0.719	0.479
9	T3	Chai, Priestley, and Seible 1991	-0.0065	2.627	1.751
10	UCI1	Hamilton, 2002	-0.0157	0.422	0.281
11	430	Lehman et al. 1998	-0.0187	1.191	0.794
12	A2	Kunnath et al. 1997	-0.0180	0.935	0.623
13	SRPH1	Hose et al. 1997	-0.0137	1.884	1.256
14	N1	Wong et al. 1990	-0.0150	1.419	0.946
15	NIST FS Flexure	Cheok and Stone	-0.0137	1.000	0.667
16	N1	Pontangaroa et al. 1979	-0.0130	1.868	1.245
17	N4	Pontangaroa et al. 1979	-0.0159	1.389	0.926
18	N5a	Pontangaroa et al. 1979	-0.0233	0.701	0.467
19	N3	Ng et al. 1978	-0.0176	1.135	0.757
20	NIST FS Shear	Cheok and Stone	-0.0209	1.010	0.673
21	N2	Ng et al. 1978	-0.0174	0.694	0.463
22	A9	Kunnath et al. 1997	-0.0168	1.087	0.725
23	A10	Kunnath et al. 1997	-0.0187	0.967	0.644
24	Con-1	Lim et al. 1990	-0.0281	0.523	0.349
25	A4	Kunnath et al. 1997	-0.0160	0.606	0.404
26	C-4	Soderstrom, 2001	-0.0162	1.527	1.018
27	IC-1	Sritharan et al. 1995	-0.0124	1.815	1.210
28	Kow-1	Kowalsky and Moyer, 2001	-0.0153	0.831	0.554
29	Kow-2	Kowalsky and Moyer, 2001	-0.0149	1.374	0.916
30	1028	Calderone et al. 2000	-0.0206	1.249	0.833

Figure 3.17 a shows the hysteretic response of the confined concrete in bridge column 328 during the last group of applied displacements, and Figure 3.17 b shows the hysteretic response of the steel. Notice in Figure 3.17 b that when the steel bar 1 reaches a compression strain of –0.019, the bar fractures because of low cycle fatigue, and it is not able to withstand any more stresses (see Tables 3.4 and 3.5 and Figure 3.16).

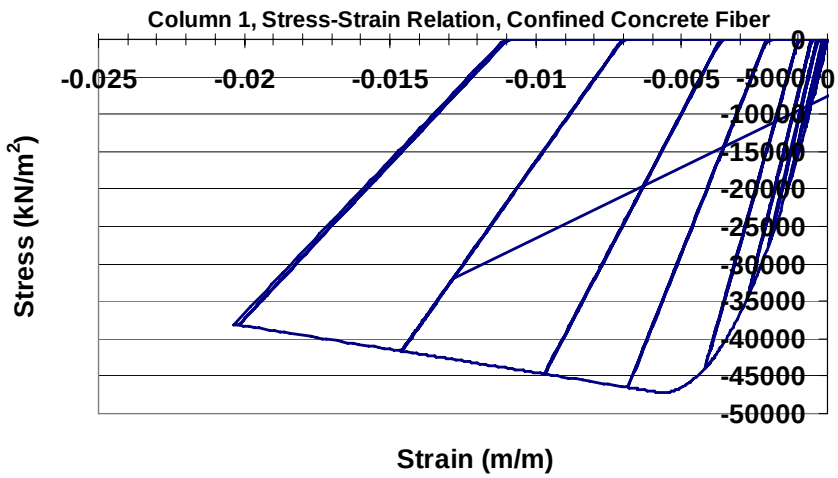

(a)

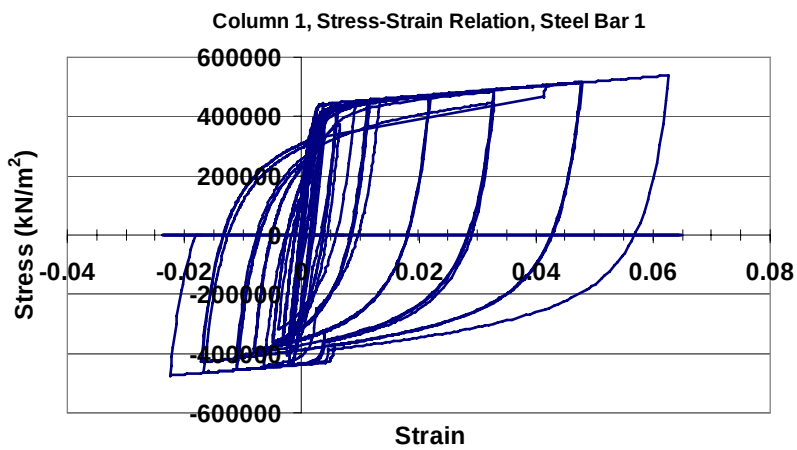

(b)

Figure 3.17. Column 328, stress–strain relations for (a) confined concrete and (b) steel bar 1

3.8. Study of steel bars parameters and validation of a single fiber finite element model for earthquake response of code designed bridge columns

Once the 30 bridge columns have been satisfactorily modeled, it is now necessary to re-calibrate the parameters that vary for the simulation of each column to define a single FFEM for earthquake response. This attempt has two parts.

The first part is a discussion based on steel properties of ε_0 because of its primary importance to strength degradation due to low-cycle fatigue.

Table 3.2 shows the calibrated values for ε_0 used for the simulation. The average is 0.131, and there are values as large as 0.19 and as small as 0.075. This clearly indicates that most of the uncertainties and limitations regarding the tests and the calibration of the 30 FFEMs are concentrated in ε_0. The re-calibration values are close to Brown and Kunnath values (2000).

According to Brown and Kunnath (2000) the value of ε_0 varies with the diameter of the steel bar, as shown in Table 3.7; therefore, for the large diameter (≥25 mm) longitudinal bars frequently used in design of bridge columns, the appropriate value for ε_0 decreases from 0.09 for 25 mm bar diameter to 0.07 for 28.6 mm bar diameter. For the single FFEM it is recommended to use the values indicated in Table 3.7 for ε_0. It is also recommended to use the values given in Table 3.7 for the exponent m in equation (3.5).

Table 3.7 Fatigue life equations obtained (Brown and Kunnath, 2000)

$\varepsilon_p = 0.16(2N_f)^{-0.57}$	for No. 6 bars (19.05mm)
$\varepsilon_p = 0.13(2N_f)^{-0.51}$	for No. 7 bars (22.23mm)
$\varepsilon_p = 0.09(2N_f)^{-0.42}$	for No. 8 bars (25.4mm)
$\varepsilon_p = 0.07(2N_f)^{-0.37}$	for No. 9 bars (28.58 mm)

The second part concerns the parameters R_0, R_1, and R_2 (Figure 3.4). The average calibrated values seen in Table 3.2 are 15.717, 0.915, and 0.15, respectively.

Filippou et al. (1983) studied the steel stress–strain relation to investigate the cyclic deterioration of bond that results in relative slippage of the steel bars with respect to the concrete, inducing concentrated rotations at the beam-column interface. Filippou et al. (1983) considered that the steel model indicated in Giuffre and Pinto (1970) and Menegotto and Pinto (1973) offered numerical efficiency and agreed very well with cyclic testing of steel bars. In Giuffre and Pinto (1970) the stress–strain relationship depends on the parameter R that influences the shape of the transition stress–strain curve and simulates the Bauschinger effect. In addition, according to Filippou et al. (1983) R depends on R_0, that is, the value for R during first loading and on R_1 =

a_1/R_0 and $a_2 = R_2$ where a_1 and a_2 are parameters obtained experimentally (Filippou et al., 1983). The model in Filippou et al. (1983) used the following parameters, $R_0 = 20$, $R_1 = 0.925$, and $R_2 = 0.15$, which are approximately the same as used in Giuffre and Pinto (1970) and Menegotto and Pinto (1973). The results of the analytical model compared with experimental cyclic tests were very satisfactory.

The average value for R_2 obtained through the calibration of the 30 bridge columns is the same as the experimental value given in Filippou et al. (1983); therefore, $R_2 = 0.15$ is recommended for the FFEM.

For R_1 the average value is 0.915, whereas the experimental value (Filippou et al., 1983) is 0.925. Table 3.2 shows that bridge columns 415p and 828 have the same calibrated value for R_1, that is, 0.915, which is equal to the average of the 30 calibrated columns. In order to check the differences between using $R_1 = 0.915$ or 0.925, the simulated hysteretic loops are compared. Figures 3.18 a and 3.18 b show the simulation with $R_1 = 0.915$ and with $R_1 = 0.925$, respectively, for bridge column 415p. When R_1 increases the loops become thinner with respect to the test hysteretic loops, but the differences are very small, as proven by the calculated hysteretic energies. For bridge column 415p the simulated hysteretic energy when $R_1 = 0.915$ is 407.13 kN m, but when $R_1 = 0.925$ it decreases to 379.73 kN m. The dissipated hysteretic energy at the end of the test is 381.64 kN m. For bridge column 828, seen in Figures 3.17 c and 3.17 d, when R_1 increases from 0.915 to 0.925, the hysteretic energy decreases from 1055.6 to 1014.96 kN m. The hysteretic energy after the test is 1044.21 kN m. The ε_0 values used for the comparison are the ones indicated in Table 3.2.

Table 3.2 show columns with values for R_1 lower than 0.9 that are going to be affected more if $R_1 = 0.925$ is used. These are columns 1015, N4, N5a, N3, and 1028. For columns 1015 and 1028, the ratios L/D are 8 and 30 and the axial load ratios are 0.091 for both columns, as seen in Table 3.1. Bridge columns N4, N5a, and N3 have in common high axial load ratios that reach 0.386, 0.349, and 0.322 and low L/D ratios that equal 2.0 for columns N4 and N5a and 3.72 for column N3, as shown in Table 3.1. The other parameters do not present large variations as seen in Table 3.1; therefore, it appears that the large L/D values for columns 1015 and 1028 and the large axial loads of the other columns diminish the value for R_1.

The average of the other 25 values for R_1 is 0.92; therefore, the recommended value for the single FFEM is the one found in Filippou et al. (1983), i.e., $R_1 = 0.925$.

The parameter R_0 has the largest variation with respect to the other R values. The average is 15.717, but Table 3.2 shows that there are calibrated values as large as 21.0 and as low as 12.0. The experimental value in Filippou et al. (1983) is 20.0.

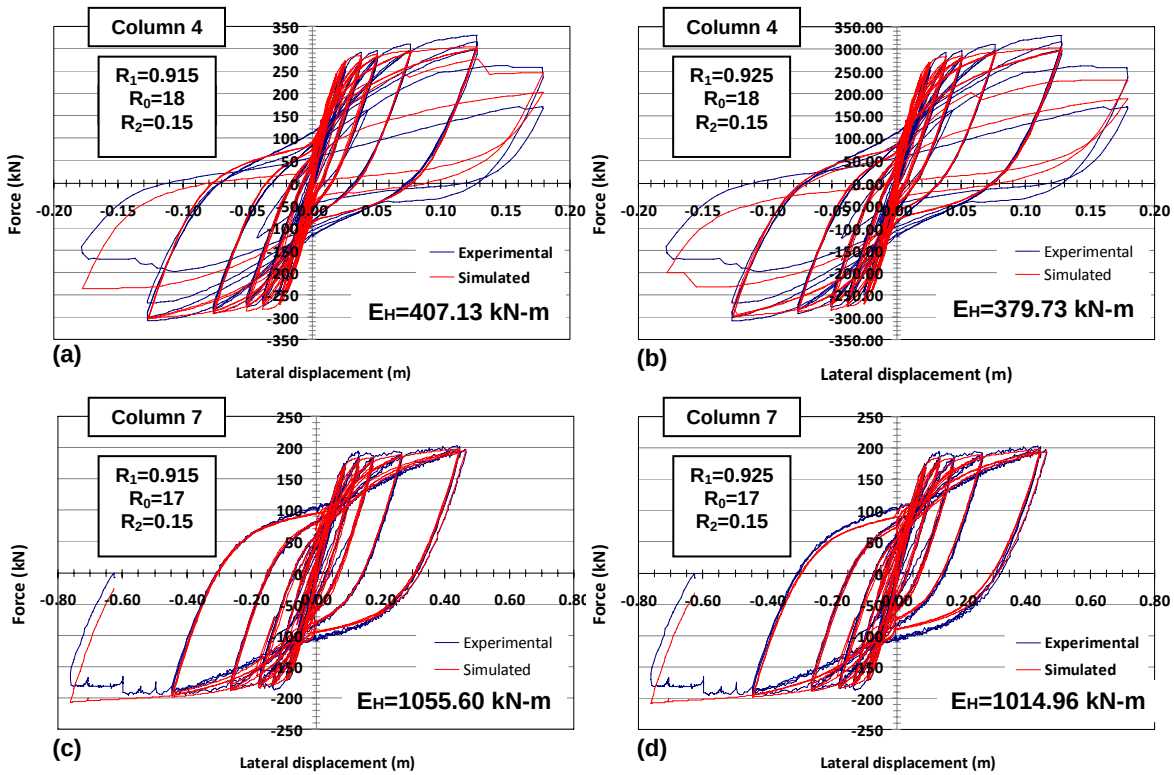

Figure 3.18. Hysteretic responses for columns 415p and 828, varying parameter R_1

Bridge column 328 has the following calibrated parameters, $R_0 = 13$, $R_1 = 0.94$, and $R_2 = 0.15$, and the hysteretic loops of the calibrated column are seen in Figure 3.19 a. If R_1 and R_2 are kept constant as R_0 increases from 13.0, which is the calibrated value for bridge column 328, the loops become wider with respect to the test hysteretic response, as seen in Figures 3.19 b to 3.19d. If R_0 decreases from 13.0 the loops become thinner (Figure 3.19 e). The values of ε_0 for these columns are those of Table 3.2.

COLUMN 28 (KOW 1, Kowalsky and Moyer, 2001)

R_0=13 R=0.94 R_2=0.15

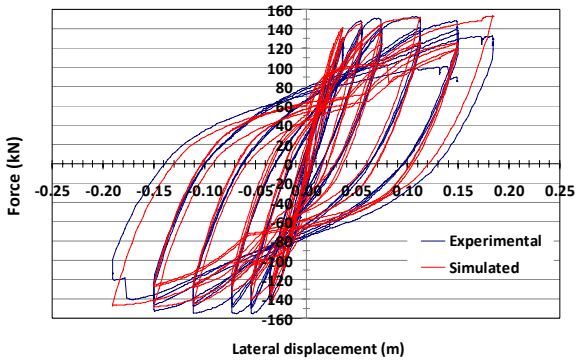

SIMULATED COLUMN DISSIPATED ENERGY (kN-m)		
HYSTERETIC	ENVELOPE	REPEATED
264.55	53.26	211.29

(a)

R_0=15 R_1=0.94 R_2=0.15

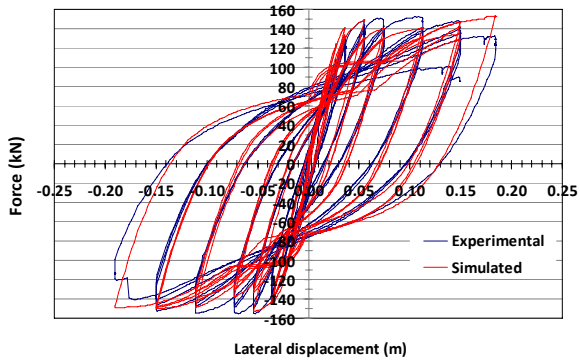

SIMULATED COLUMN DISSIPATED ENERGY (kN-m)		
HYSTERETIC	ENVELOPE	REPEATED
289.87	57.28	232.59

(b)

R_0=18 R_1=0.94 R_2=0.15

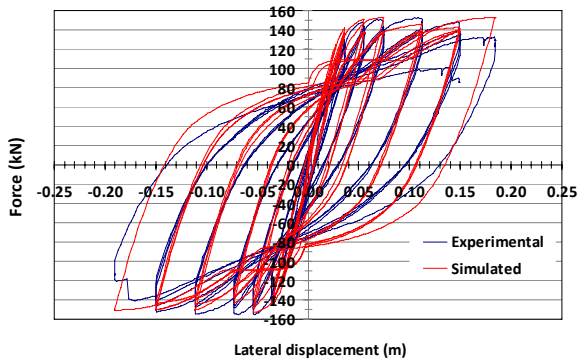

SIMULATED COLUMN DISSIPATED ENERGY (kN-m)		
HYSTERETIC	ENVELOPE	REPEATED
317.71	62.66	255.05

(c)

R_0=20 R_1=0.94 R_2=0.15

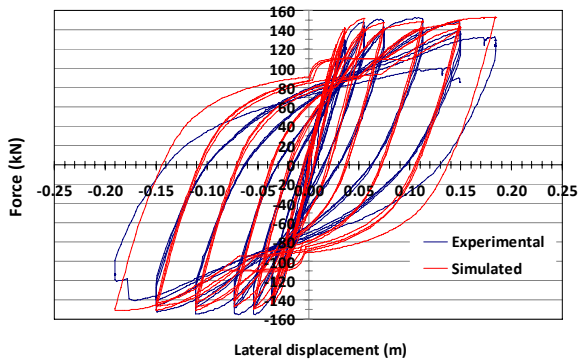

SIMULATED COLUMN DISSIPATED ENERGY (kN-m)		
HYSTERETIC	ENVELOPE	REPEATED
332.42	65.08	267.34

(d)

R_0=10 R_1=0.94 R_2=0.15

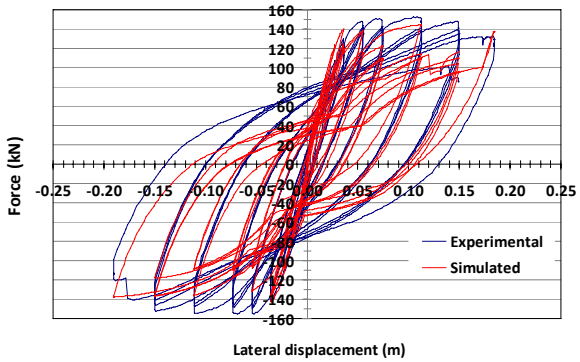

SIMULATED COLUMN DISSIPATED ENERGY (kN-m)		
HYSTERETIC	ENVELOPE	REPEATED
207.05	44.01	163.04

(e)

TEST COLUMN DISSIPATED ENERGY (kN-m)		
HYSTERETIC	ENVELOPE	REPEATED
291.25	58.58	232.67

Figure 3.19 Hysteretic responses for column 328, varying R_0

3.8.1 Calibration of R_0 and validation of a single model for seismic response

Because of the large variation of R_0, it was decided to calibrate this parameter by modeling Specimens A1 and B1 of Hachem et al. (2003) (Figure 3.20 a), using the proposed FFEM and varying R_0. This procedure will not only allow calibrating the parameter R_0 but also serve to validate a single FFEM proposed in this investigation to simulate earthquake response. The FFEM will include P-Δ effects, mass, and damping. The mass used is the one indicated in Hachem et al. (2003), the damping was assumed mass proportional, and values of 2% and 3% were used to calibrate the damping for the dynamic response.

In Hachem et al. (2003), the shake table model of bridge column A1 was subjected to the scaled Olive view record of the Northridge 1994 earthquake and column B1 to the scaled Llolleo record of the 1985 Valparaíso earthquake. The scales are $\sqrt{4.5}$ for the duration of the records, and the maximum accelerations were amplified 1.09 for Northridge and 1.29 for Llolleo, which according to Hachem et al. (2003) are the design values for bridge columns specimens A1 and B1. With the use of the same time and acceleration scales used in Hachem et al. (2003), Figures 3.20 b and 3.20 c show the Northridge and the Llolleo scaled records input to the shake table, the shake table output that is the excitation over the column in Hachem et al. (2003), and on top of them the scaled records used here. Clearly, there are small differences that could affect the responses.

There is a limitation on the comparison. The simulation using the proposed FFEM corresponds to a single degree of freedom (SDOF) system , whereas the shake table model in Hachem et al. (2003) includes the rotational degree of freedom due to the mass of the column head. Therefore, the system has two DOFs. In addition, the top of each of the two bridge columns tested in the laboratory is embedded in the column head (Figure 3.20 a), whereas in the proposed FFEM the column is free to move.

The average $\varepsilon_0 = 0.13$ was used for the columns, $R_1 = 0.925$ and $R_2 = 0.15$ were chosen, R_0 with two values, 15 and 20, and the viscous damping varying between 2% and 3%.The results are discussed below.

Figures 3.21 a to 3.21 d show the relative displacements responses for 2% and 3% damping ratio of the shake table model used in Hachem et al. (2003) and of the proposed FFEM with all inclusions mentioned applied to specimen A1 due to the Northridge record.

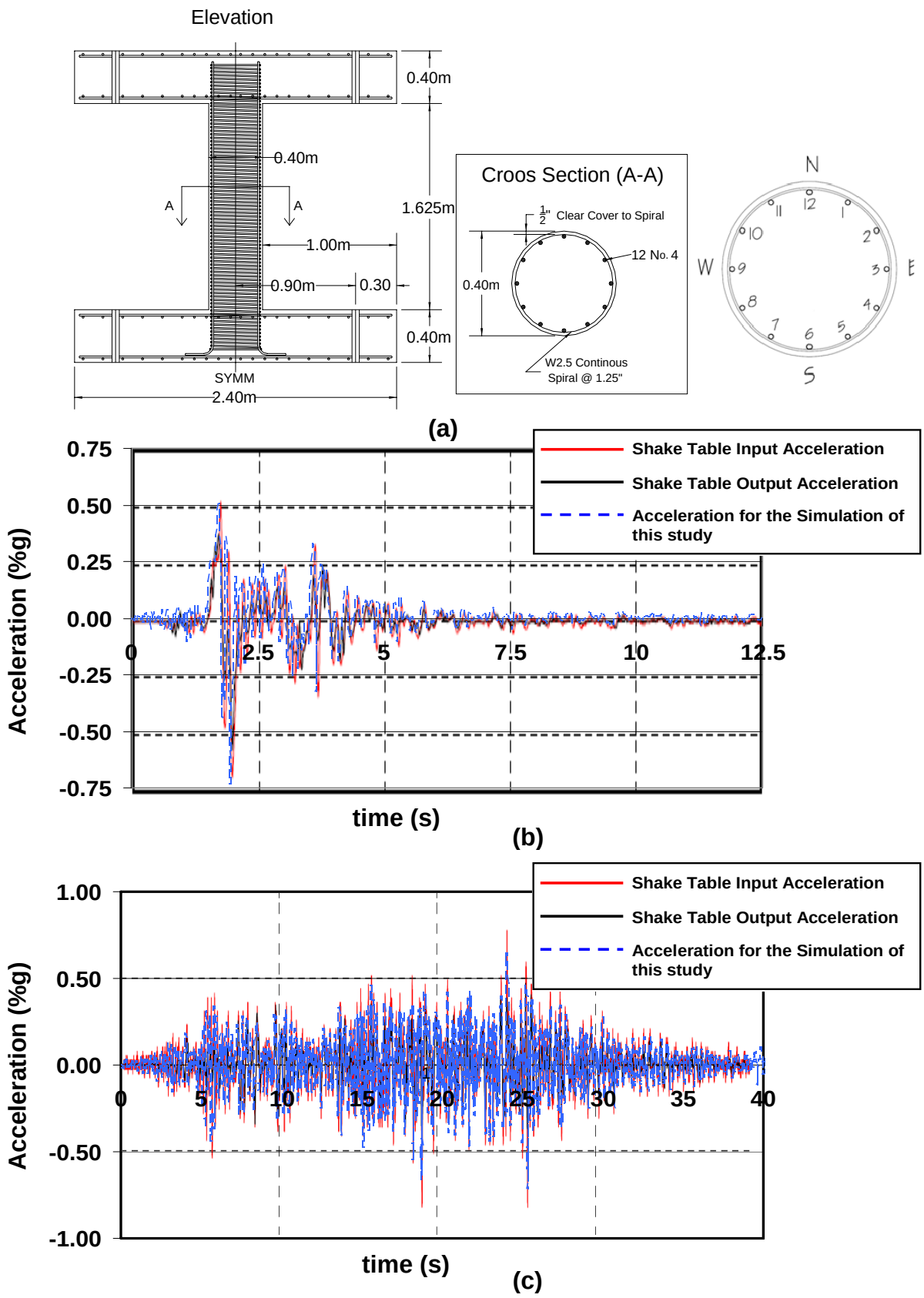

Figure 3.20 Shake table and FFEM input motions

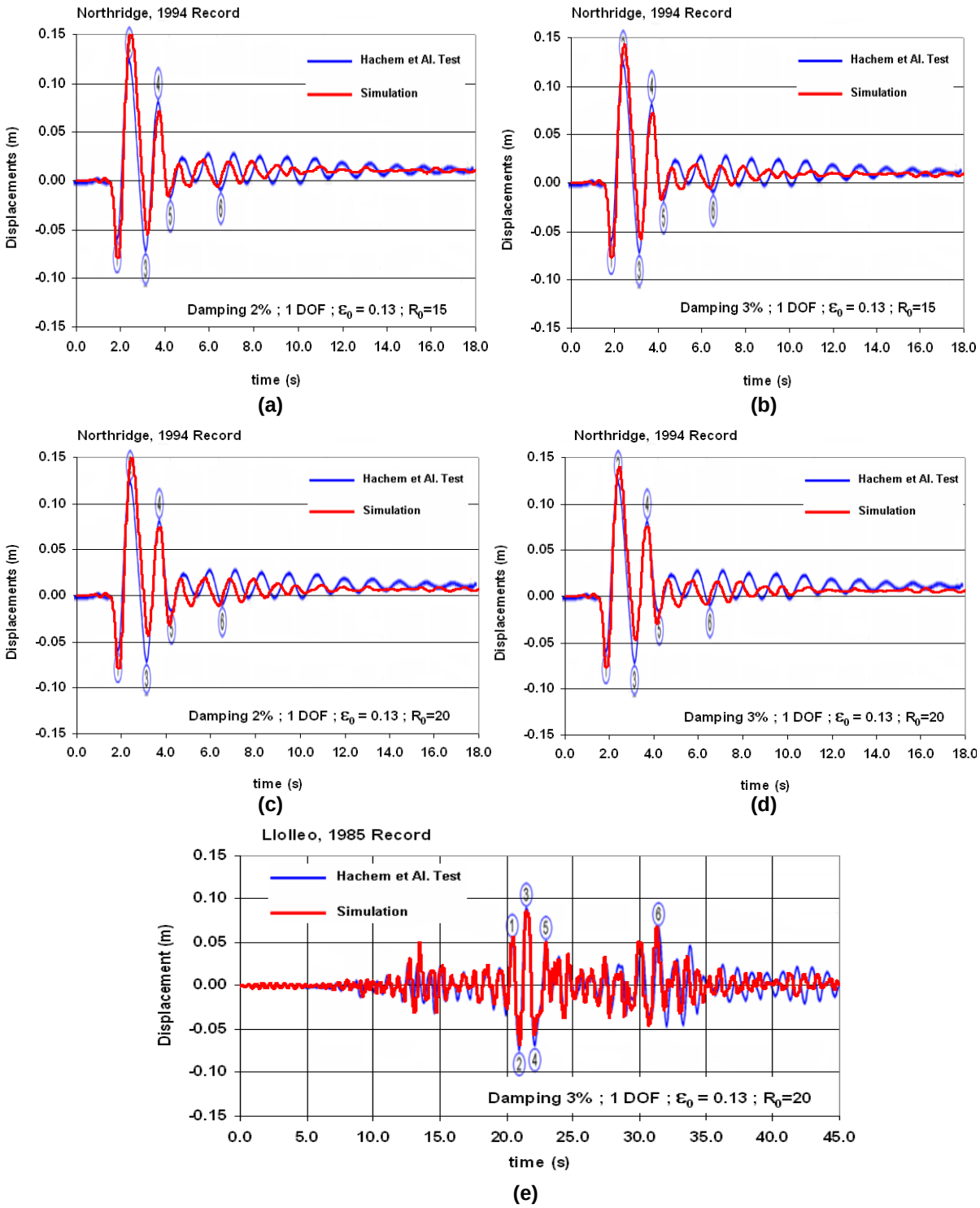

Figure 3.21. Experimental and simulated displacement responses of specimens A1 and B1 for 2% and 3% damping: (a), (b), (c), and (d) Northridge record, (e) Llolleo record on column B1

For 2% damping response, in Figure 3.21 a peaks 1, 2, 4, and 5 are larger in the simulation than in the shake table, while peak 3 of the simulation is smaller than in the test. The free vibration response of the FFEM is smaller than that in the shake table, and both are out of phase after the

fifth peak. In addition, the period of the free vibration in the simulation is slightly lower than that of the test, showing that the stiffness of the damaged column in the simulation is slightly more rigid than in the test.

Keeping all parameters equal and changing the damping ratio to 3% decreases the response of the proposed FFEM with respect to that with 2% damping, but it is still larger than the shake table response (Figure 3.21 b). The stiffness of the damaged column in the simulation continues to be slightly larger than that of the test.

The procedure is repeated, but R_0 is changed to 20. The proposed FFEM response for 2% damping (Figure 3.21 c), is similar for the first two peaks to that for the same damping with R_0 = 15 (Figure 3.21 a), but it is still larger than the shake table response. Also, peak 3 decreases and peak 4 is almost equal.

For 3% damping there is an improvement of the response with respect to all the others although it is slightly larger than the shake table response for peaks 1, 2, and 5, slightly less for peak 3, and similar for peak 4. However, all occur at the same time (Figure 3.21 d). The slight increase in the final stiffness of the simulated damaged column continues.

When the scaled Llolleo record is applied to column B1, the responses on the shake table and on the proposed FFEM are very similar in time and amplitude except at the end during the free vibration motions (Figure 3.21 e). This figure shows these responses for R_0 = 20 and 3% damping ratio. All the main peaks are similar and occur at the same time for both responses. After the fifth peak, the free vibration response is slightly out of phase up to the end of the time history. In addition, the stiffness of the damaged structure in the simulation is still slightly larger than in the test.

Figure 3.22 shows the steel strains comparisons for Column B1 subjected to the scaled Llolleo record. In this figure the strains measured during the shake table test using strain gages have their ordinates a little less than the calculated strains using the moment–curvature relationship (Hachem et al., 2003). The proposed FFEM gives steel strains ordinates very close to the test-measured strains.

The results of both simulations for the earthquake response of bridge columns A1 and B1 are very similar; therefore, the model proposed in this study will give satisfactory approximations to the earthquake response of code-designed reinforced concrete bridge columns.

After the above analysis, the following parameters are recommended for using in the proposed FFEM to simulate responses of reinforced concrete bridge columns subjected to earthquake ground motions in the OpenSees framework: R_0 = 20, R_1 = 0.925, and R_2 = 0.15. These values are the same as those recommended in Filippou et al (1983) and Menegotto and Pinto (1973). The length of the plastic hinge can be calculated using equation (3.3) (Priestley et al., 1996) and ε_0 and m according to Table 3.7. The FFEM contains three beam-column elements, each with two integration points, and the model is a single DOF system. The mass is the one specified in the design, and 3% mass proportional damping ratio, as is also used in Hachem et al. (2003), is recommended.

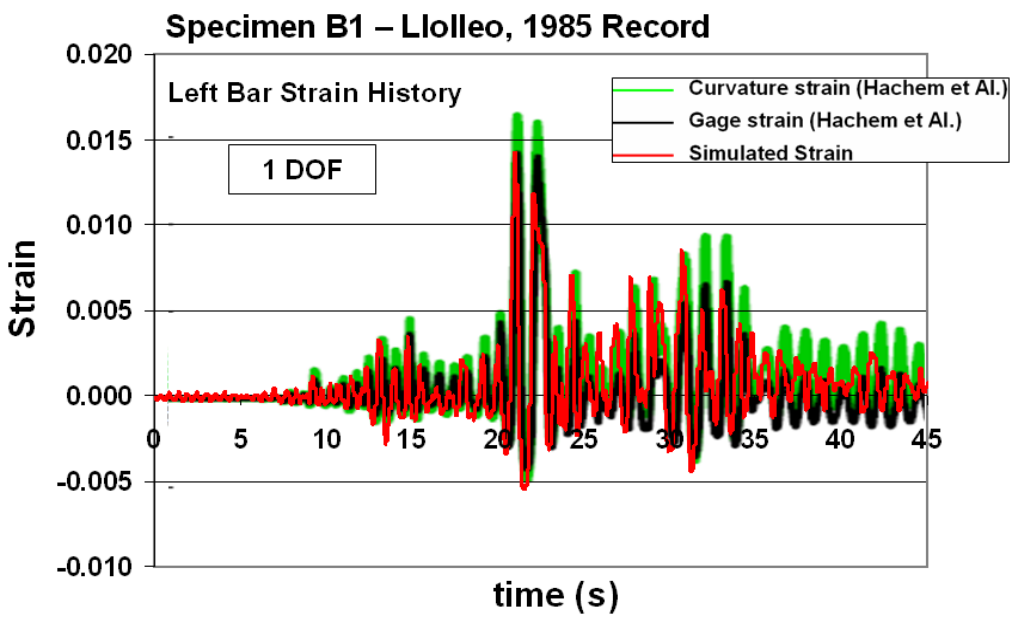

Figure 3.22 Strain comparison for column B1

The inclusion of element 1 (Figure 3.10) in the FFEM allows simulation of the tension strain at the base of the bridge column and at the end of element 1 of length l_{sp} (equation (3.16)). Figure 3.23 a shows that the maximum tension strain at the base of bridge column B1, called section 2, under the scaled Llolleo record is 0.0138. The steel strain history is recorded at bar 1, seen in Figure 3.15 b and, for the concrete, very near to this bar. This strain indicates that the concrete has cracked and the steel is yielding. Figure 3.23 b shows for the same column and the same

record but for section 1, at the end of element 1 (Figure 3.10), that the tension strain reaches 0.002; so the steel is just beginning to yield and the concrete is cracked. In addition, it is noted that, as expected, the tension strain decreases from the top to the bottom of element 1; its length, equal to twice the strain penetration, is given in equation (3.16).

To establish the effects of the rotation of the head column a rotational DOF was incorporated in the proposed FFEM and the previously recommended parameters are used.

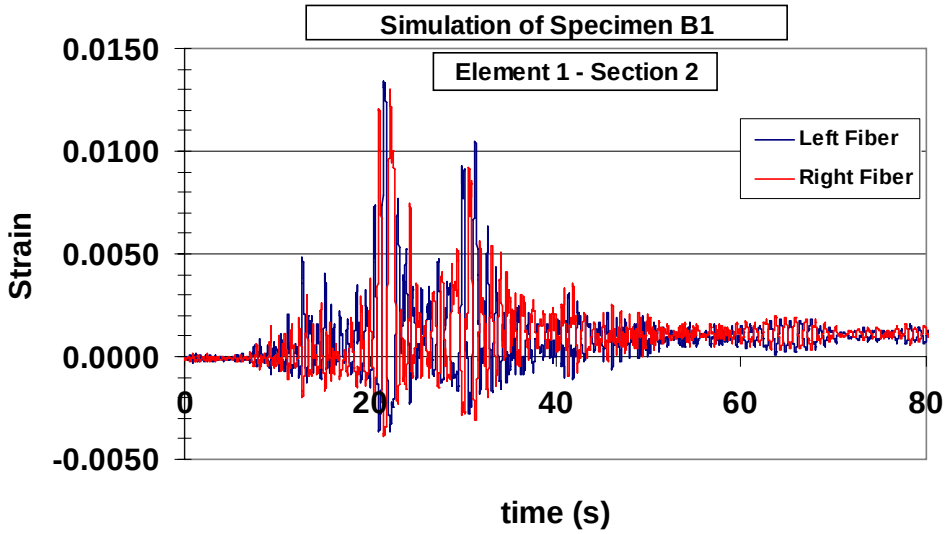

(a)

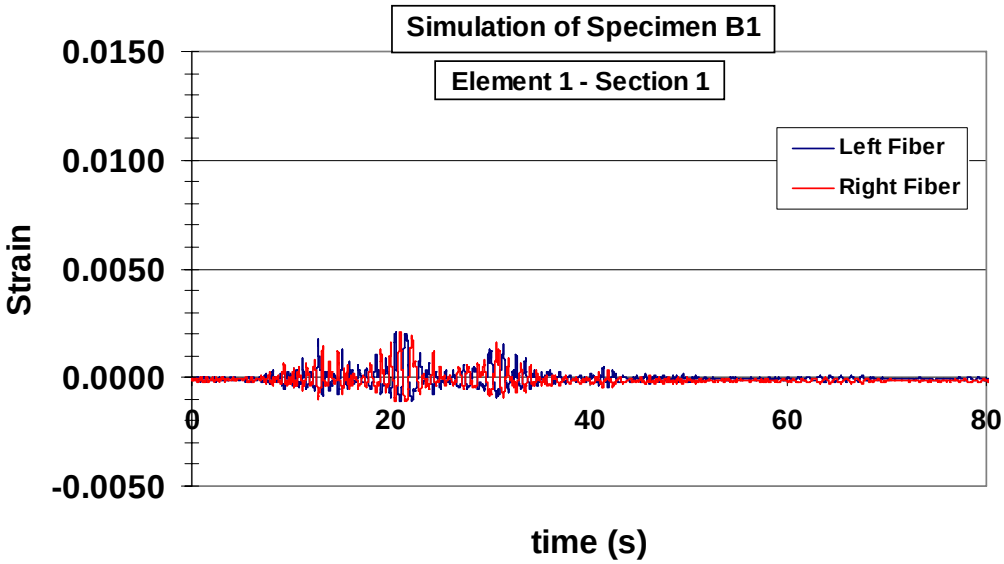

(b)

Figure 3.23 Simulated strains history of specimen B1: (a) strains at the base of the column B1. Element 1, section 2, (b) strains at the end of the element 1, section 2

Figure 3.24 a shows the response of the FFEM with two DOF and the shake table response of the column due to the scaled Northridge earthquake. Except for the free vibration part of the response, both responses look very similar, and the inclusion of the rotational degree of freedom further improves the response of the FFEM. Figure 3.24 b shows the responses of the FFEM and of the shake table due to the Llolleo record. Both look similar and just slightly different from the SDOF FFEM (Figure 3.21 e).

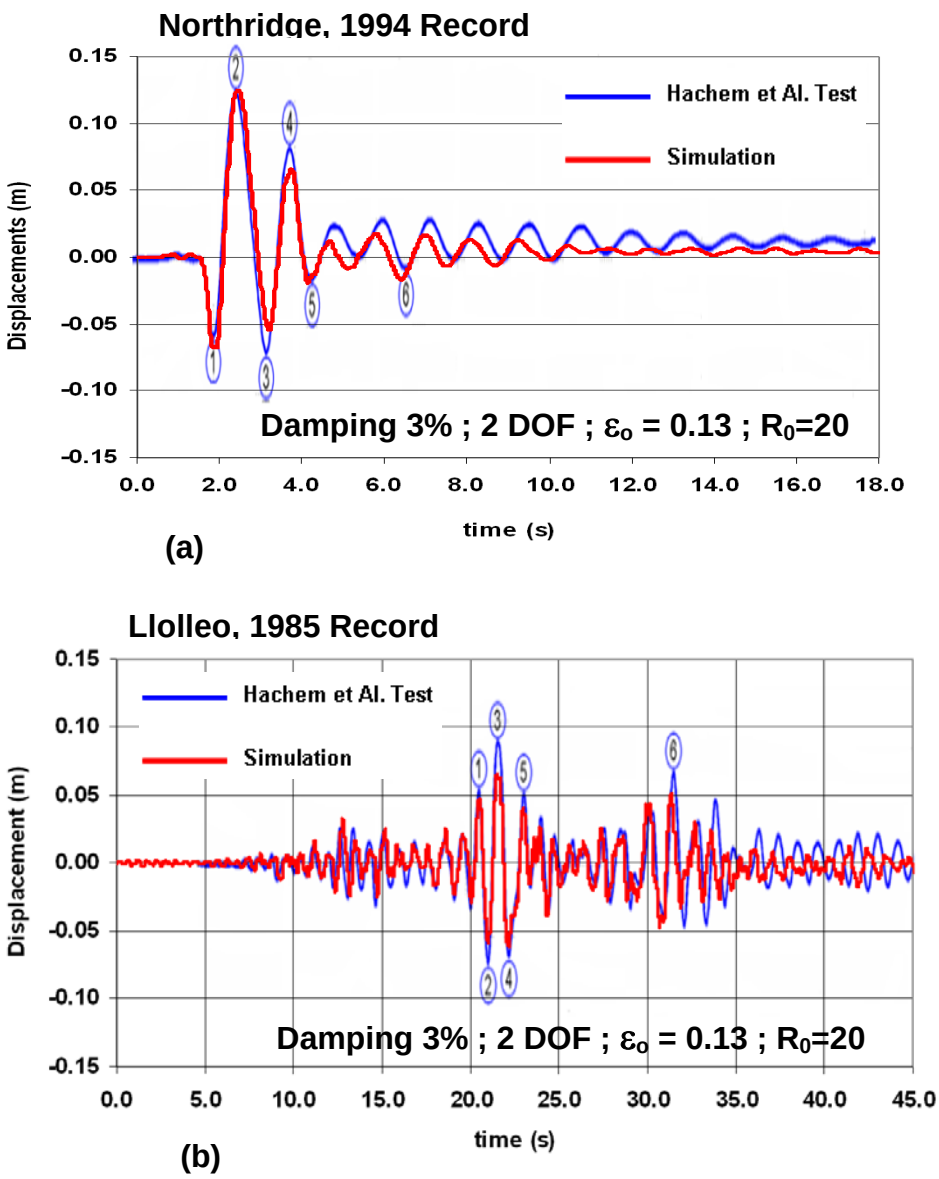

Figure 3.24 Responses of columns A1 and B1 (Hachem et al., 2003) for two degrees of freedom

Figure 3.25 shows the strain comparison similar to that shown in Figure 3.22 but for a FFEM with two DOF. The results are for column B1 subjected to the Llolleo record. Again, the results of the FFEM and the test-measured strains are similar.

The procedure for designing bridge columns can be followed as indicated in the codes stated by AASHTO (2007) and Caltrans (2006). To determine if the pre-designed column has reached any SDPL, the FFEM of a SDOF system with the recommended parameters can help to identify the material strains as well as the damage index of the longitudinal steel bars. For pre-designs, the inclusion of the rotational DOF in the proposed FFEM could be considered optional.

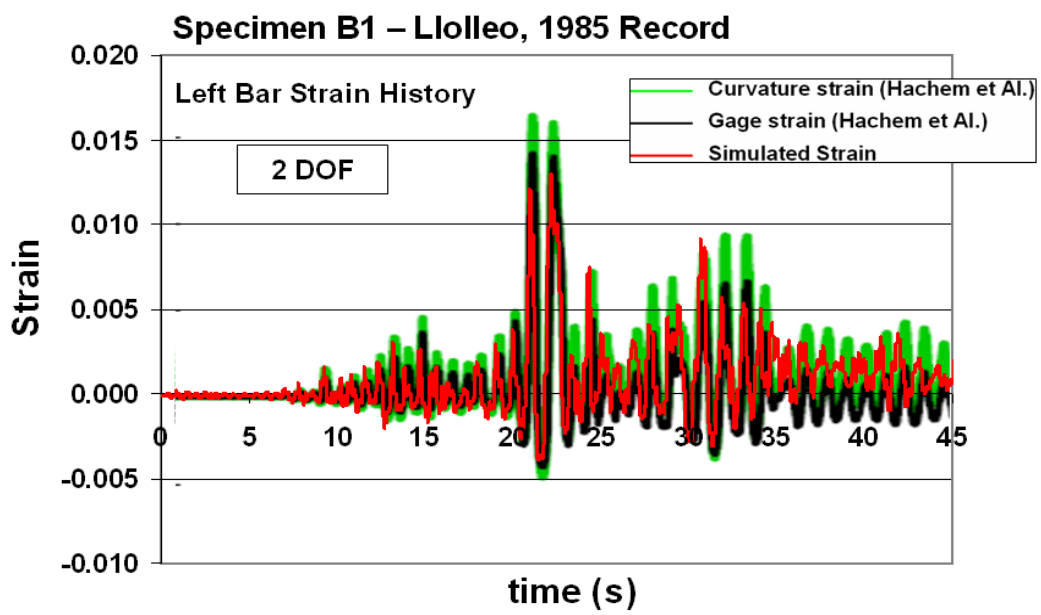

Figure 3.25 Strain comparison for column B1

3.8.2 Comparison of fatigue results using the calibrated FFEM with shake table tests

The simulations performed by Hachem et al. (2003) on their own shake table tests using the fatigue model proposed by Mander et al. (1985) did not show fracture of the longitudinal bars due to low-cyclic fatigue, as shown in Figure 3.26 b and 3.26 d. The more fatigued bars are bar 9 for column A1 and bar 3 for column B1, reaching 88% and 58% loss of their fatigue life, respectively. Hachem et al. (2003) bar numbering is also shown in Figure 3.26.

However, according to Hachem et al. (2003), in the laboratory specimen A1 shows fracture of bars 9 and 3 in that order at run 8 and in specimen B1 bars 3, 9, and 4 fracture in that order at run 9. Both runs are the last ones exciting the columns.

In order to simulate the Hachem et al. (2003) tests as closely as possible, the column introduced in the proposed FFEM is fixed at the foundation and free at the upper end, but the rotational mass is included. Thus the model has two degrees of freedom.

According to Brown and Kunnath (2004) small diameter bars require a larger ε_0 to fracture in one cycle; the smaller diameter bar that they tested for low-cyclic fatigue is bar6, which corresponds to a diameter of 19 mm. For this diameter Brown and Kunnath (2004) recommend $\varepsilon_0 = 0.16$ and $m = -0.57$ (Table 3.7), which are the values introduced in the proposed FFEM for the 12 mm bar used in the tests by Hachem et al. (2003). The Mander et al. (1985) fatigue model used by Hachem et al. (2003) uses fixed values of $\varepsilon_0 = 0.08$ and $m = -0.50$, and as indicated, it shows no fatigue for any of the bars of the tested columns.

The simulations of Hachem et al. (2003) tests using the proposed FFEM and the calibrated parameters as well as the Brown and Kunnath (2004) values are shown in Figures 3.26 a and 3.26 c. It is seen that at runs 8 and 9 the fatigue life lost is 65% for bar 9 in specimen A1 and 100% for bars 3 and 9 and 90% for bar 4 for specimen B1. The calibrated single FFEM gives satisfactory simulations of the shake table tests, particularly for column B1, which is subjected to the scaled Llolleo record of the 1985 Valparaíso earthquake.

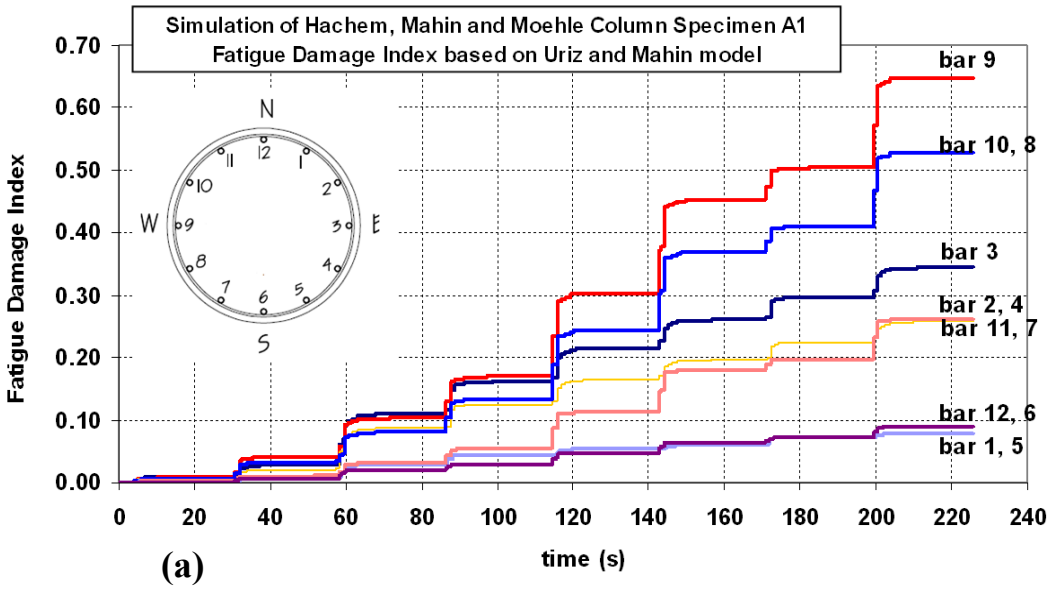

(a)

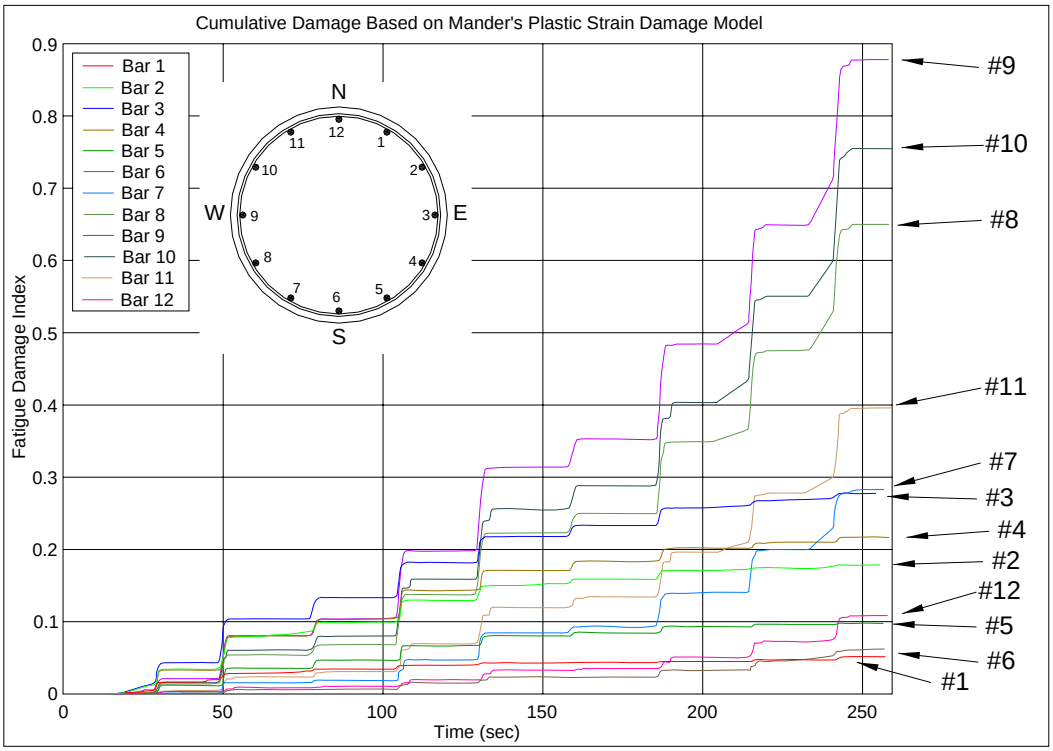

(b)

Specimen A1

Figure 3.26 Fatigue damage index of all bars. Comparison between FFEM and Hachem et al. (2003) results

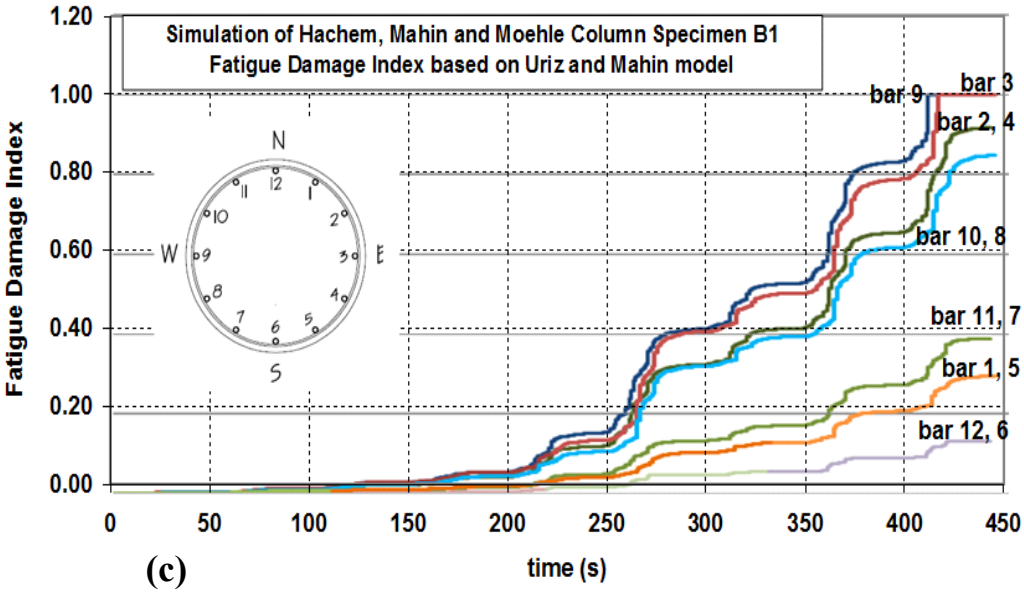

(c)

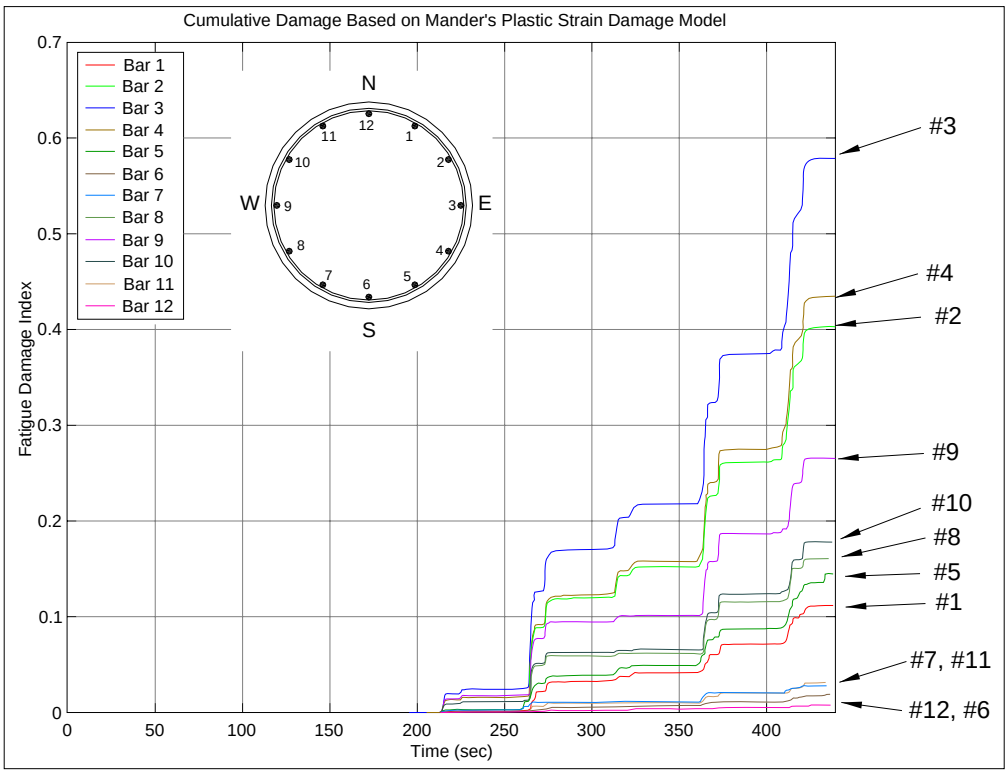

(d)

Specimen B1

Figure 3.26 (cont.) Fatigue damage index of all bars. Comparison between FFEM and Hachem et al. (2003) results

3.9. Summary

1. A fiber finite element model (FFEM) for each of the 30 reinforced concrete bridge columns tested in the laboratory and chosen for this study is calibrated to simulate their responses under cyclic reversible increasing displacement history.

2. The FFEM uses three beam-columns elements with two integration points each. The characteristics of the materials for the confined concrete and for the steel bars are introduced in the elements so that the variations of the materials force–deformation relationships are considered in the response calculation.

3. Some of the characteristics of the materials need to be calibrated for each bridge column. These are the longitudinal steel bars parameters, R_0, R_1, R_2, and ε_0 and m. The mass proportional damping was calibrated at 3%. The simulations are very similar to the test responses. The simulated dissipated energies and those of the tests are within 10% difference.

4. In addition to the characteristics of the materials, the following bridge column characteristics are introduced into the FFEM. These are length of the plastic hinge, low-cycle fatigue, length of the strain penetration, and the P-Δ effect. The lengths of the plastic hinge and of the strain penetration are also calibrated in the FFEM.

5. OpenSees does not contain flexure–shear interaction or bond deterioration; therefore, only flexural damage is considered in this study.

6. A re-calibration of a FFEM with respect to two bridge columns tested on a shake table under scaled ground motions is performed in order to propose a model that can be used for seismic response of columns. The re-calibration is satisfactory.

3.10 Conclusions

1. For the flexural design of reinforced concrete bridge columns, AASHTO specifies that the designer must meet the requirements for three mechanisms of flexural failure: (1) crushing of the confined concrete, (2) P-Δ effects, and (3) fracture of the longitudinal bars due to tension. The experimental studies by Mahin and Bertero (1972) demonstrated that the repetitions of cyclic plastic response induce fatigue on the steel bars. Therefore, a fourth flexural failure

mechanism was incorporated in this study to account for the reduction of fatigue life of the bars or possible fracture of the bars due to low-cyclic fatigue.

2. The seismic response of columns is obtained using a single fiber finite element model (FFEM) for reinforced concrete bridge columns. The FFEM identifies the four flexural failure mechanisms above mentioned. The FFEM measures the strain time-histories of the materials so the analyst will be able to recognize when the crushing of the confined concrete occurs or when the cover concrete spalls. Buckling is not modeled in the FFEM. However, according to Mander et al. (1988) crushing of the confined concrete is related to the possible enlargement or even fracture of the spirals and triggering of buckling of the longitudinal bars. The analyst is then able to identify the initiation of buckling looking at the strains given by the FFEM.

3. Eight parameters were necessary to calibrate for the FFEM. Three to simulate the inelastic hysteretic behavior of the steel bars, two for the lengths of the plastic hinge and the strain penetration, one for the cyclic strain to produce fracture due to fatigue of the bar in one cycle, one for a parameter included in the fatigue formulation, and one for the mass proportional damping. The values of the calibration of the lengths of the plastic hinge and the strain penetration are close to those calculated using the equations given by Priestley et al. (2007). The calibrated parameters for fatigue are close to those determined by Brown and Kunnath (2004). The equations given by Priestley et al. (2007) and the values given by Brown and Kunnath (2004) were used in the FFEM and the results of the simulations were considered satisfactory.

4. The calibrated parameters were re-calibrated for dynamic response using the results of two columns tested in a shake table under two different earthquakes. The re-calibration was necessary since the results of the simulation using the first calibration differed considerably from those of the shake table experiment. The simulations with the re-calibrated parameters using the FFEM were also satisfactory.

5. A significant damage performance level (SDPL) is presented to identify the first occurrence of damage on the column due to one of the above mentioned flexural failure mechanisms.

6. In order to obtain a better approximation of the displacements demanded by the ground motions on the columns it is necessary to include the strain penetration in the FFEM.

3.11 Remarks

1. The FFEM proposed requires the introduction of material and component characteristics, offering a great advantage for the calculation of inelastic responses of structures.

2. The introduction of a fiber finite element of length equal to twice the strain penetration of the tension steel into the foundation allowed satisfactorily simulating this effect and permitting the spread of plasticity between this element and the contiguous element of length equal to twice the length of the plastic hinge.

3. To improve accuracy of the proposed FFEM one integration point is assigned at the two extremes of each of the three elements used to model the bridge columns. In each integration point the section of the column is discretized into 328 fibers plus an additional number of fibers equal to the number of longitudinal steel bars.

4. The results obtained with the proposed FFEM are displacements, concrete and reinforcing steel stresses and strains, damage accumulation measured by a fatigue damage index, and time history responses.

5. The recommended parameters for simulation of the initial stiffness, Bauschinger effect, and degrading stiffness of the steel bars are $R_0 = 20$, $R_1 = 0.925$, and $R_2 = 0.15$. The steel strain at which the bar fractures by low-cycle fatigue after one cycle and the parameter m corresponding to equation (3.4) are given in Table 3.7 (Brown and Kunnath, 2004), according to the diameter of the bar. Both the length of the plastic hinge calculated using equation (3.3) and the length of strain penetration (equation (3.7)) have given satisfactory results in all simulations. The calibrated damping ratio is 3%.

6. The proposed FFEM can be easily transformed. In effect, the addition of a rotational degree of freedom to the proposed single degree of freedom FFEM because of the mass attached to the bridge column at the top of the component in the two shake table tested columns under scaled earthquakes improved both responses.

7. Design is an iterative procedure; therefore, it is advisable to pre-design bridge columns using the displacement based design procedure proposed by the new codes and then use the proposed FFEM to check if there is significant damage performance level (SDPL) and calculate the cyclic damage index at the critical section. If any of the flexural failure mechanisms occur, the designer can re-design the column and try again using the FFEM. The final design should be checked for aftershocks, since they increase the number of cyclic plastic displacements.

8. The OpenSees framework helped to identify the flexural mechanisms that can induce SDPL; so this framework is a great step ahead in earthquake research. Further investigation is required to solve some limitations, such as the flexure–shear interaction.

4. STUDY OF THE EFFECTS OF LOW-CYCLIC FATIGUE ON SEISMIC CODE-DESIGNED REINFORCED CONCRETE BRIDGE COLUMNS

4.1. Introduction

This chapter compares the new seismic code design requirements for three reinforced concrete bridge columns with the seismic demands induced by three ground motions scaled following prescriptions of AASHTO (2007) for inelastic dynamic analysis; the proposed FFEM was used for this analysis. The three bridge columns studied here are designed according to AASHTO (2007) and Caltrans (2006) and have different periods: 0.5, 1.0, and 2.0 s.

The FFEM predicts whether the responses of the code-designed columns are or are not within the limits of the code prescriptions, and it also predicts the loss of fatigue life that is not prescribed by the codes.

According to AASHTO (2007) the design of the bridge columns can be performed using a combination of displacement based design with an elastic analysis, using elastic spectra specified for different types of seismic zones. The code also allows for checking or for designing the use of three compatible acceleration records scaled to match the code spectral acceleration at the column period. Using the FFEM developed in Chapter 3 shows that although the columns meet the design code prescriptions, they suffer the fracture of one or more longitudinal steel bars due to low-cyclic fatigue either for the code scaled ground motions or for the aftershocks.

4.2. Study of code-designed bridge columns under compatible earthquake ground motions

Three bridge columns of different bridges are designed according to the new AASHTO (2007) and Caltrans (2006) proposed regulations and studied in order to verify if their design procedures cover the demands induced by any of the three ground motions chosen according to AASHTO (2007) prescriptions.

4.2.1. Present measures of damage for design

Recent proposed design specifications for reinforced concrete bridge column earthquake design given by AASHTO (2007) include seismic design category (SDC) D, which is the one assigned for high seismicity zones.

The design procedure proposed by the codes is based on a combination of displacement based design and elastic spectra. It consists of doing the elastic analysis of the pre-designed bridge using the code assigned elastic spectrum for the category and comparing the maximum elastic displacement with the maximum lateral displacement capacity obtained through a pushover analysis of the pre-design column. The comparison is based on the equal displacement concept applied to the elastic analysis. The pushover ends when the strain in the concrete reaches the ultimate strain ε_{cu} given by Mander et al. (1988) or when the steel reaches its ultimate cyclic tensile strain ε_{su}. In addition, the pushover makes it possible to obtain the yielding displacement.

The pre-design is accepted as a final design when the elastic displacement demand is less than or equal to the maximum lateral displacement capacity. For short period structures the demand is increased by means of a factor that includes the noncyclic ductility ratio μ_{nc}, as defined in Chapter 2. AASHTO (2007) and Caltrans (2006) indicate that the specifications apply to normal bridges of conventional superstructure and with spans not exceeding 150 m to resist earthquake motions, implying that the code is limited to ordinary bridges and that the design is controlled by the lateral displacement causing crushing of the concrete. There is some consideration of the cyclic plastic displacements through a limitation of the maximum steel bar flexural strain, as will be seen later.

4.2.2. Bridge columns designed according to AASHTO displacement based design

The columns are designed according to AASHTO (2007). The expected magnitude at the site of the bridge is 8, the soil is alluvium classified as type D, the rupture mechanism is subduction of the Nazca plate under the South American plate off the coast of Ecuador, and the expected rock acceleration for a return period of 475 years is 0.25*g*, as required by the Ecuadorian Society for Earthquake Engineering code for the City of Guayaquil (2005).

Figure 4.1 shows both the selected site elastic response spectrum derived from Caltrans (2006) and the SDC D AASHTO (2007) spectrum, which are similar. The damping is $\xi = 5\%$.

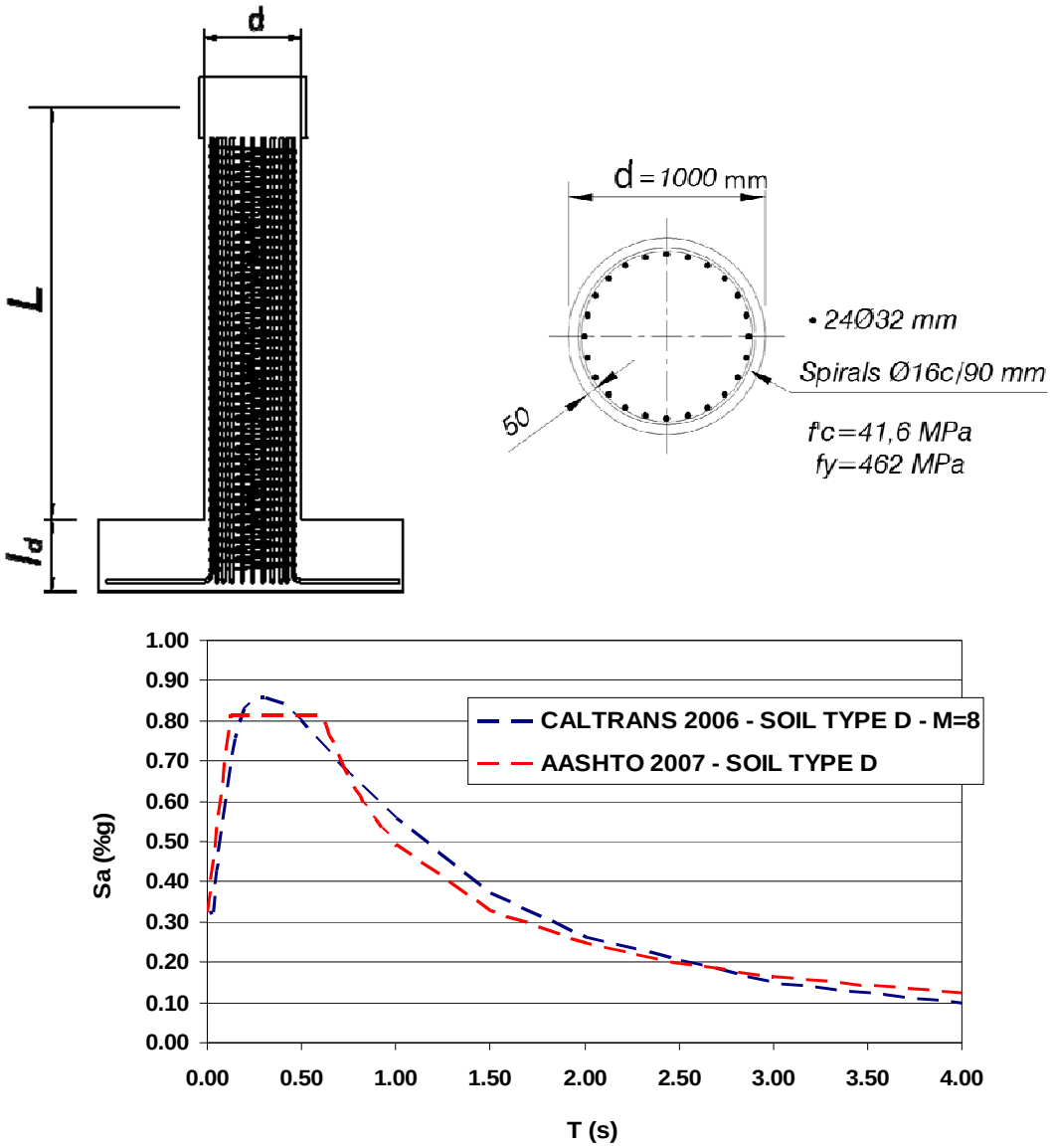

Figure 4.1 Column design and codes spectra

To calculate the moment–curvature of the critical section of the columns the material properties introduced in the FFEM are increased according to AASHTO (2007). The expected concrete compressive strength is $f'_{ce} = 1.3f'_c$, where $f'_c = 42$ MPa, and the expected yielding steel strength is $f_{ye} = 1.1f_y$, with $f_y = 420$ MPa. The expected tensile strength is $f_{ue} = 1.6f_y$. The expected ultimate flexural steel strains vary according to the bar diameter and are indicated in AASHTO (2007), Table 8.4.2-1, for steel bars meeting ASTM A 706. In this design $\varepsilon_{su} = 0.12$ for the spiral, and for the longitudinal bars the reduced ultimate steel tensile strain due to cyclic response is $\varepsilon_{su} = 0.09$, as prescribed in AASHTO (2007). In addition, the parameters that allow simulation of the Bauschinger effect and the changes in stiffness of the bars are those studied and

suggested in Chapter 3 and introduced in the FFEM. The parameters for the calculation of the strain amplitude leading to fatigue of the longitudinal bars are indicated later.

After several design trials to meet code requirements, the design was forced to be similar for the three columns; it is shown in Figure 4.1. This was done to compare the responses of the three columns to the same earthquakes and later to the same aftershocks. In this way the difference between the columns is the period only; therefore, the effects of the ground motions and aftershocks can be compared.

Figure 4.2 a shows the monotonic moment–curvature curve for the designed columns calculated using the FFEM and the material properties described above. The prescribed end of the curve is marked in Figure 4.2 a for the curvature associated with the ultimate monotonic strain of the confined concrete, ε_{cu} = 0.018, previously calculated according to Mander et al. (1988). This strain occurs before the steel reaches its ultimate reduced tension flexural strain ε_{su} = 0.09, as prescribed in AASHTO (2007).

Figures 4.2 b, c, and d also show the lateral displacement capacity of each column for ε_{cu} = 0.018 and their yield displacements, which are 13.8 and 1.0 cm for the column with period T = 0.5 s, 24 and 2.4 cm for the T = 1.0 s column, and 38 and 4 cm for the T = 1.5 s column, respectively.

The reduction of the elastic shear strength demand for the final design of the T = 0.5 s column is 3.6, for the T = 1.0 s column it is 6.0, and for the T = 1.5 s column it is 8.0. The elastic shear strength demand considered for all columns is 6620 kN

With the reduced strength the maximum lateral elastic displacement demand due to the SDC D AASHTO (2007) spectrum must be lower than the monotonic lateral displacement capacities indicated above for each bridge column, and the P-Δ product for each column must be less than $0.25M_p$.

The shear strength and the development length are provided to the column according to the prescriptions given in AASHTO (2007).

From the elastic spectral analysis of the structure the maximum lateral elastic displacement demands of the each column are u_m = 2.1 cm for the T = 0.5 s column. For the T = 1.0 s column, u_m = 6 cm, and for the T = 1.5 s column, u_m = 9 cm. According to AASHTO (2007) the T = 0.5 s column is a low period column and the displacement should be increased by a factor of 1.4; thus, the displacement becomes 3.0 cm. Also, according to AASHTO (2007) the displacements for the two large period columns are not affected by any multiplier.

Owing to the equal displacement concept used in AASHTO (2007) and Caltrans (2006), the elastic displacements indicated above become the maximum lateral displacement demands. They are all less than the lateral displacement capacities.

Also, because of the equal displacement concept in both codes, the strength reduction is equal to the traditional ductility ratio. It was pointed out in Chapter 3 that the traditional noncyclic ductility ratio is not a measure of damage and it does not take into consideration the cyclic plastic reversible response of structures due to earthquakes.

Since AASHTO (2007) retains the concept of the noncyclic ductility ratio and limits it to a maximum value of 6.0, it is necessary to calculate such ratios for each column. For the T = 0.5 s column it is 3.0/1.0 = 3.0, for the T = 1.0 s column, it is 6/2.4 = 2.5, and for the T = 1.5 s column this ratio is 9/4 = 2.2. All these values are less than 6.0.

AASHTO (2007) limits the reduction of the moment capacity due to the P-Δ effect to $0.25M_p$. For the T = 0.5 s column, the moment capacity is M_p = 4200 kN m (Figure 4.2 a) and P = 2850 kN. From the spectral analysis, Δ = 3.0 cm, so that the product P-Δ in this case is $0.02M_p < 0.25M_p$. For the T = 1.0 s column, the moment capacity is M_p = 4200 kN m (Figure 4.2 a). Since Δ = 6 cm and P = 2850 kN, the product P-Δ is $0.04M_p < 0.25M_p$. Finally, for the T = 1.5 s column, M_p = 4200 kN m (Figure 4.2 a) and Δ = 9 cm; therefore, P-$\Delta = 0.05Mp < 0.25M_p$.

The elastic spectral design of the three columns meets both code requirements. Thus, according to AASHTO (2007) and Caltrans (2006), it is accepted.

There are, however, some facts regarding this acceptance that should be discussed.

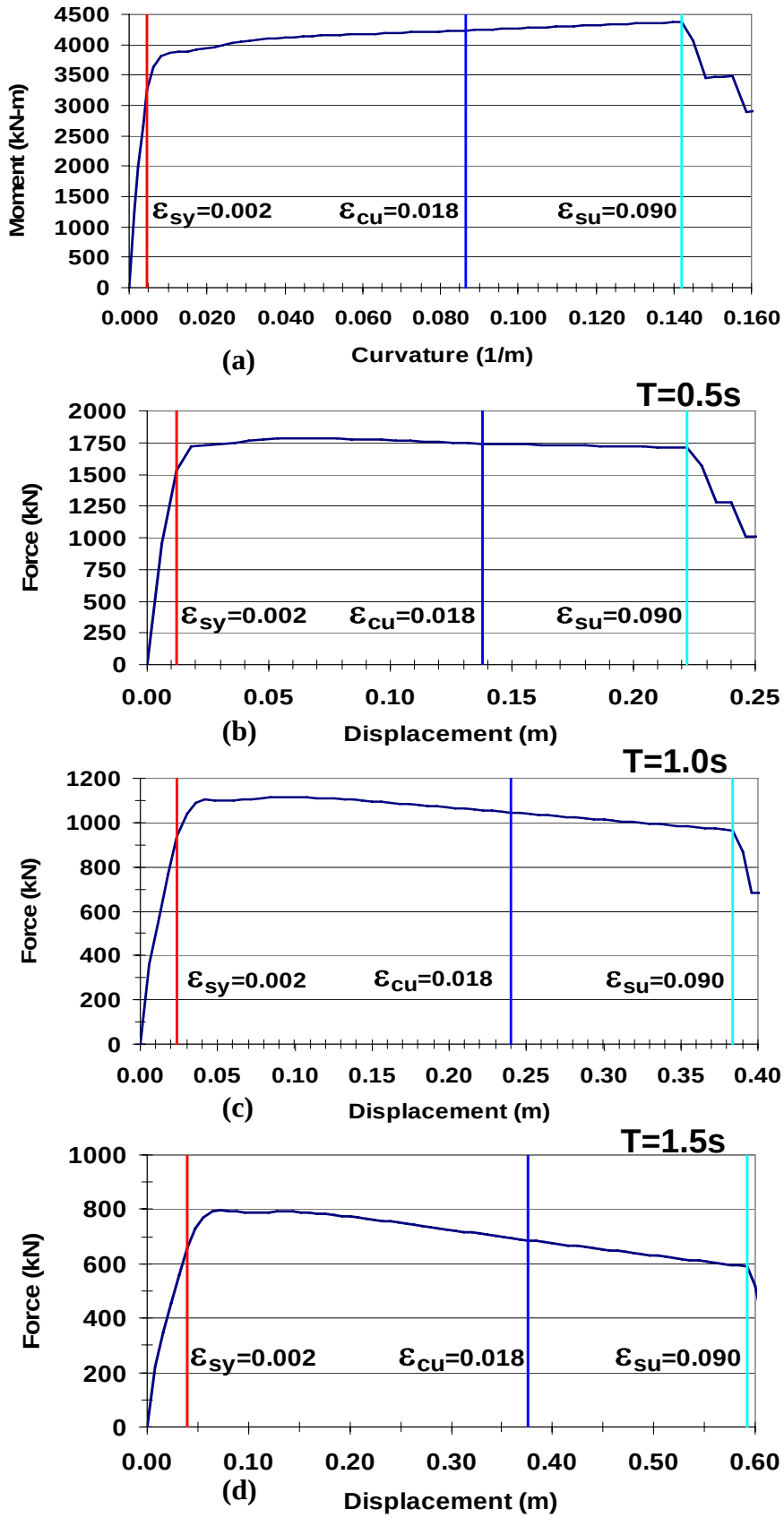

Figure 4.2 Moment curvature for the design section and force–displacement curves for the three columns

4.3. Seismic verification of code-designed bridge columns using the fiber finite element model

Structural components respond cyclically to earthquakes, and materials do have a memory of the plastic reversible deformations, as pointed out by Krawinkler et al. (1983). For a steel bar the memory of the materials keeps adding the value of the cyclic plastic strains that provoke a continuous decreasing of fatigue life until fracture of the bar could occur. This mechanism is not considered in the prescriptions given in the codes.

To verify the occurrence of low-cyclic fatigue of the longitudinal bars, Brown and Kunnath (2004) experimentally defined values for the parameters involved in the calculation of the constant strain amplitude at each cycle ε_i given in equation (3.4). For the 32 mm bar diameter used in this study, they determined that the steel strain inducing fracture of this bar in one cycle is $\varepsilon_0 = 0.08$ and the parameter that appears in equation (3.4) to calculate fatigue of the 32 mm bars is $m = -0.4$. Both are introduced in the FFEM, as recommended by Brown and Kunnath, for this bar diameter.

4.3.1 Materials and column modeling introduced into the proposed FFEM

The material properties introduced into the FFEM are those already mentioned here and recommended in AASHTO (2007). The length of the plastic hinge and the strain penetration into the foundation, both introduced into the FFEM, are calculated according to Priestley et al. (2007). The parameters to simulate low-cyclic fatigue using the FFEM are the ones indicated in section 3.8.1.

The FFEM is three dimensional, and it accepts different support conditions at both ends. Because of the design support conditions shown in Figure 4.1, the model is fixed supported at one end and free at the upper end.

According to AASHTO (2007), to carry out an inelastic dynamic analysis as an alternative to the elastic spectral analysis, three ground motions should be used and the design should meet the maximum demands obtained from any of the three records. The records selected are the Pisco main shock record of the 2008 Perú earthquake (Lara and Centeno, 2007), the Caleta record of the Michoacán, Mexico, 1985 earthquake (National Geophysical Data Center – NGDC website,

2008), and the Melipilla record of the 1985 Chile earthquake (National Geophysical Data Center – NGDC website, 2008).

They are chosen because they were recorded in alluvium and the magnitude is 8.0 for the first two records and 7.8 for the Chilean earthquake. In addition, the Pisco and Melipilla records are products of a subduction process off the South American west coast while the Caleta record is due to the subduction off the Mexican west coast.

In what follows, the response of the three bridge columns under the three selected ground motions is simulated by the proposed FFEM, considering only a SDOF for the bridge columns. The results are discussed.

4.4. Performance of a bridge column with period T = 0.5 s

Figure 4.3 shows that the AASHTO (2007) SDC D spectrum for ξ = 5% reaches 0.813g at the period T = 0.5 s of the column; therefore. according to AASHTO the acceleration for each record is scaled to match the spectral acceleration of 0.813g for T = 0.5 s, as shown in the same figure.

Figure 4.3 also contains the spectrum derived from Caltrans (2006), which is similar to that of AASHTO (2007). Figure 4.4 shows the three original records.

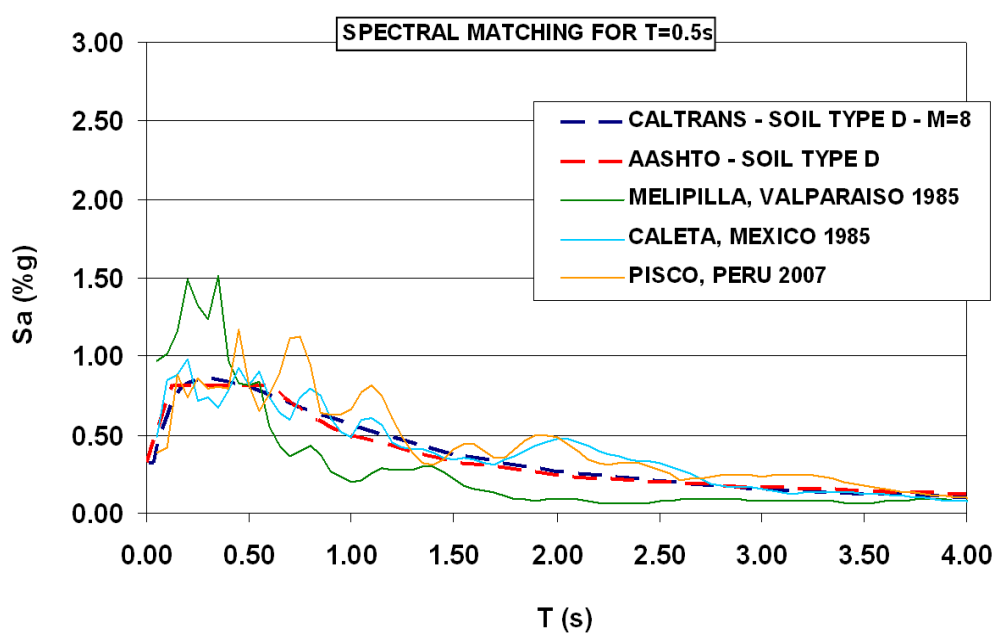

Figure 4.3 Spectral matching for T=0.5 s column

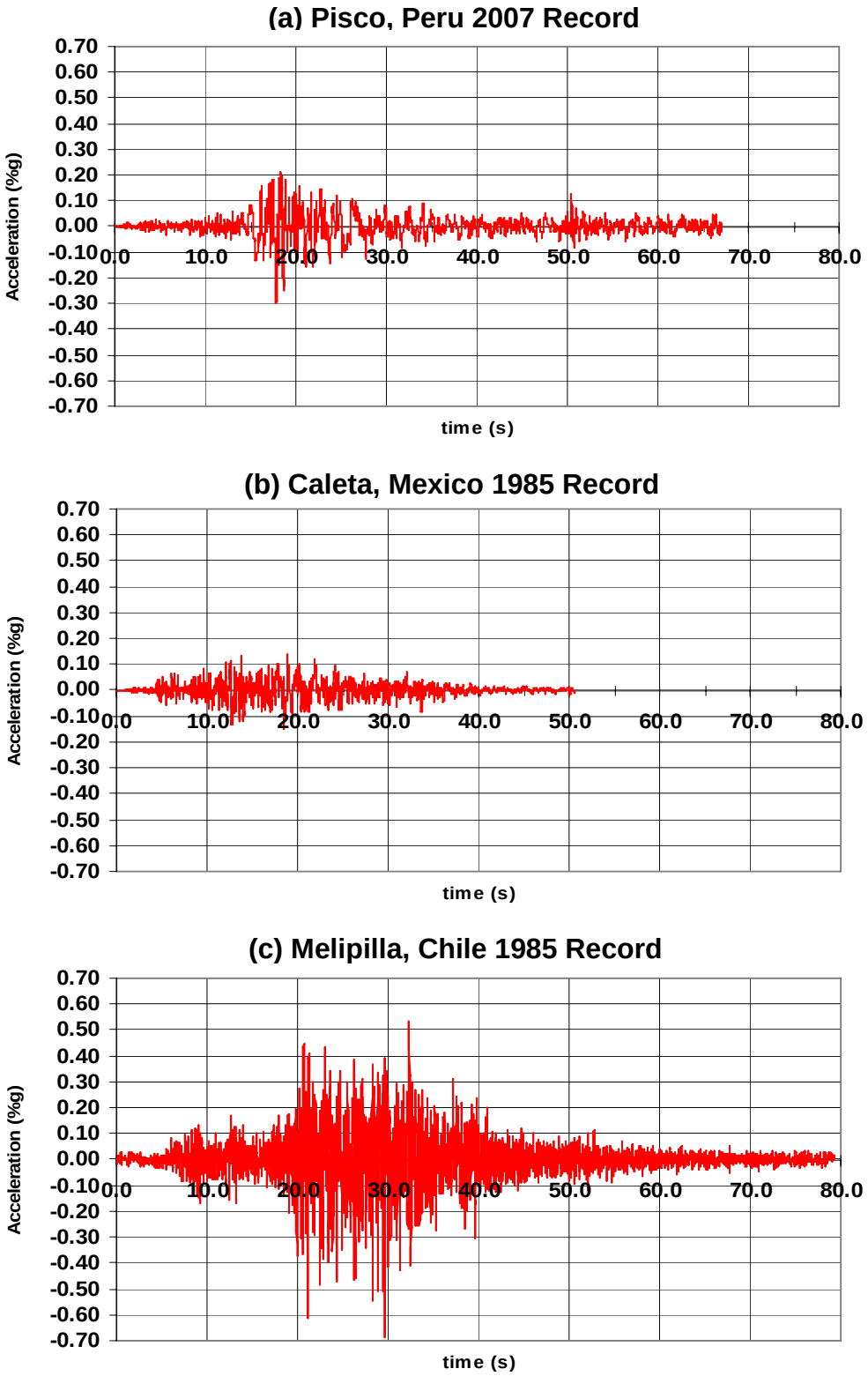

Figure 4.4 Original records used for matching with code spectrum (National Geophysical Data Center, 2008)

4.4.1. General results

Table 4.1a shows the duration, the peak ground acceleration (PGA), the period calculated through the Fourier transform function, the scale factor to match the AASHTO spectral acceleration of each record at T = 0.5 s, the spectral acceleration amplitude of the unscaled records at T = 0.5 s, the scaled spectral acceleration of the records matching the code spectral acceleration of 0.813g for T = 0.5 s, and the demanded dissipated energies E_{ucpe} and E_{ucpr} defined in Chapter 2 for each record.

Table 4.1a Analysis for records scaled to the AASHTO spectral acceleration at T=0.5s

COLUMN T = 0.5s SCALING FOR MATCHING WITH AASHTO SPECTRUM								
EQ	Duration (s)	PGA (%g)	Tg (s)	Scale Factor (SF) (for matching)	Sa (%g) for T=0.5s Spectral Acceleration (original record)	Matching Sa (%g) for T=0.5s Spectrum Acceleration	Enveloping Energy, Eucpe (kN-m)	Repeated Energy, Eucpr (kN-m)
Pisco,2007 (Perú)	67.00	0.300	0.82	1.27	0.638	0.813	554.06	1063.78
Caleta,1985 (México)	50.63	0.154	1.05	2.26	0.359	0.813	481.64	1011.05
Melipilla,1985 (Chile)	79.32	0.686	0.35	0.79	1.026	0.813	142.63	236.48

The repeated cyclic energies E_{ucpr} for the Pisco and Caleta scaled records shown in Table 4.1a are high compared with the new plastic energies E_{ucpe} measured in the envelope hysteretic response. This is an indication of possible low-cyclic fatigue failure for the columns, as proposed in Chapter 2. In effect, 12 bars for the scaled Pisco record and 7 bars for the scaled Caleta record fracture because of low-cyclic fatigue, as will be seen later. Instead, both E_{ucpe} and E_{ucpr} are low for the scaled Melipilla record.

Table 4.1b shows the failures type occurring along the strong motion duration of each record, the time at which the maximum lateral displacement is reached after first and additional failures occur, the time at which this maximum is reached, the total number of bars fractured due to low-cyclic fatigue along the strong motion durations, the initial and final times where fracture by fatigue takes place, and the maximum confined concrete and longitudinal steel strains for each scaled record.

Table 4.1b Damage of materials for records scaled to the AASHTO spectral acceleration at T=0.5s

COLUMN T = 0.5s DAMAGE OF MATERIALS AT MATCHING							
EQ	Failure type	Max. Displacement (m)	Time (s)	TOTAL OF FATIGUED BARS	Time (s)	Max. ε_c	Max. ε_s
Pisco,2007 (Perú)	$\varepsilon_c > \varepsilon_{cu}$ + LOW-CYCLE-FATIGUE	0.215	26.3	14	18.2 to 30.5	0.022	0.058
Caleta,1985 (México)	LOW-CYCLE-FATIGUE	0.138	21.6	8	21.7 to 23.17	0.016	0.047
Melipilla,1985 (Chile)	NO FAILURE	0.054	23.4	0	-	0.006	0.020

4.4.2. Results for 1.27 times the Pisco record acting on the *T* = 0.5 s column.

Figures 4.5 a and b show the hysteretic response and the time history displacement of the bridge column, respectively. At time t = 16 s the column reaches the displacement capacity of 13.8 cm; therefore, there is crushing of the concrete. Figure 4.5 c confirms this result, since at this time ε_c = 0.018 = ε_{cu}, according to Mander et al. (1988). The design would be unacceptable according to AASHTO. In addition, at ε_c = 0.018 buckling could be initiated.

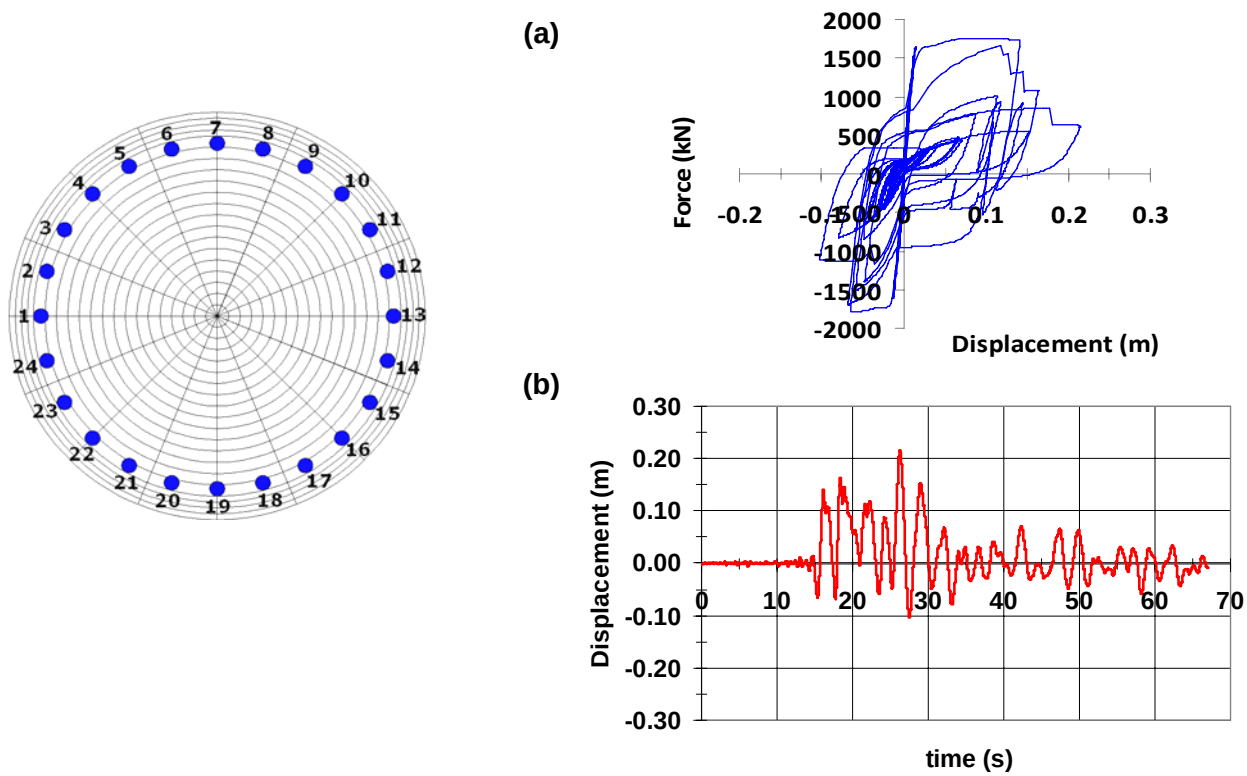

Figure 4.5 Response of the *T*=0.5 s column for 1.27 times the Pisco record and behavior of its materials

(c)

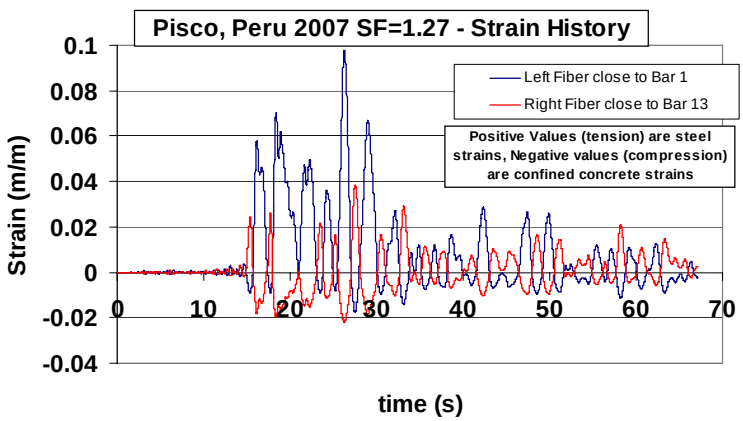

(d)

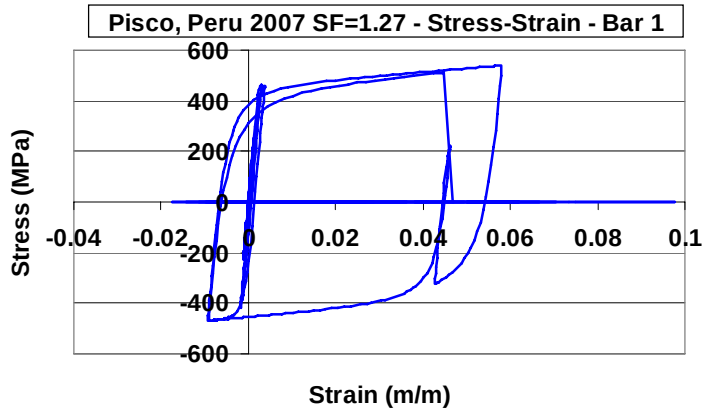

(e)

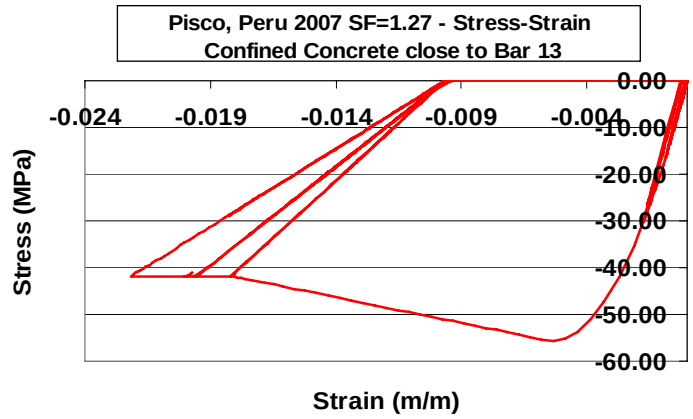

(f)

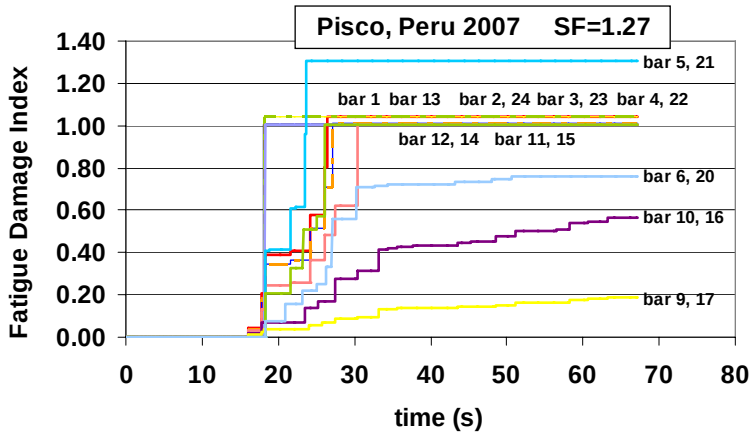

Figure 4.5 (cont.) Response of the *T*=0.5 s column for 1.27 times the Pisco record and behavior of its materials

Figures 4.5 c, d, e, and f allow observation of a complex situation for bar 1. The stress–strain curve in Figure 4.5 d shows that at $\varepsilon_s = 0.045$ bar 1 fractures and that from then on it does not take any more stresses. In Figure 4.5 c there is a tension strain peak in bar 1 that almost reaches 0.06 at $t = 15$ s. Because this strain is less than $\varepsilon_{su} = 0.09$, there is no fracture of this bar due to tension for this peak strain. However, as shown in Figure 4.5 f, at $t = 19$ s, 3 s after the column reached ε_{cu}, bar 1 fractures due to low-cycle fatigue during the second cycle at $\varepsilon_s = 0.045$ and $\varepsilon_{scycle} = 0.055$, where ε_{scycle} is the cyclic strain in bar 1. Figure 4.5 f shows that a total of 14 bars fracture between $t = 19$ s and $t = 29$ s. Clearly, it is not only the amplitude of the steel strain causing fatigue but also the number of cycles and the strain amplitude. In this case, crushing of the concrete could have initiated buckling of bar 1 and the fracture of the fatigued bar.

Going back to Figure 4.5 c, there are more measures of strains in bar 1 even though it already fractured. This is so because OpenSees continues capturing the strains at bar 1, but because of the fracture it does not continue measuring stresses for that bar, as seen in Figure 4.5 d.

Figure 4.5 e shows the continue measuring of stresses and strains in the confined concrete fiber close to bar 13 even though it crushed at $t = 16$ s. This is because in OpenSees it is possible to keep the residual stresses capacity as indicated by Mander et al. (1988), and for the FFEM it was chosen not to drop the confined concrete strength to zero after reaching ε_{cu} (Mander et al., 1988) but to let the concrete continue taking stresses through the residual strength, as seen in Figure 4.5 e. The maximum lateral displacement is 21.5 cm at $t = 26$ s. After that, there are a few more cycles that leave four more bars with fatigue life lost between 60% and 80%.

In Figure 4.5 a there are several decreases of strength in the form of stairs. These occur because of fractures of the bars due to low-cyclic fatigue, and the maximum lateral displacement of 22 cm is reached by the column because of the strength degradation induced by low-cyclic fatigue of the bars in the critical section. Notice that the final hysteresis reaches very low strengths (see Figure 4.5 a).

For $P = 2850$ kN, $\Delta_{max} = 21.5$ cm and $M_p = 4200$ kN m; the product $P\Delta$ is $0.13M_p$, less than $0.25M_p$.

The T = 0.5 s column does not meet, for this scaled record, the code requirement to limit the lateral displacement and avoid crushing of the concrete. In addition, the column loses 14 bars because of low-cyclic fatigue. However, the design meets all code requirements for the elastic modal analysis.

4.4.3. Results for 2.26 times the Caleta record acting on the T = 0.5 s column

Figures 4.6 a and b show the hysteretic response and the displacement time history response of the T = 0.5 s bridge column. The maximum lateral displacement is just 13.8 cm at t = 21.3 s, and Figure 4.6 c shows that the concrete strain reaches its maximum strain ε_c = 0.0155, which is less than ε_{cu} = 0.018. Therefore, the concrete does not crush.

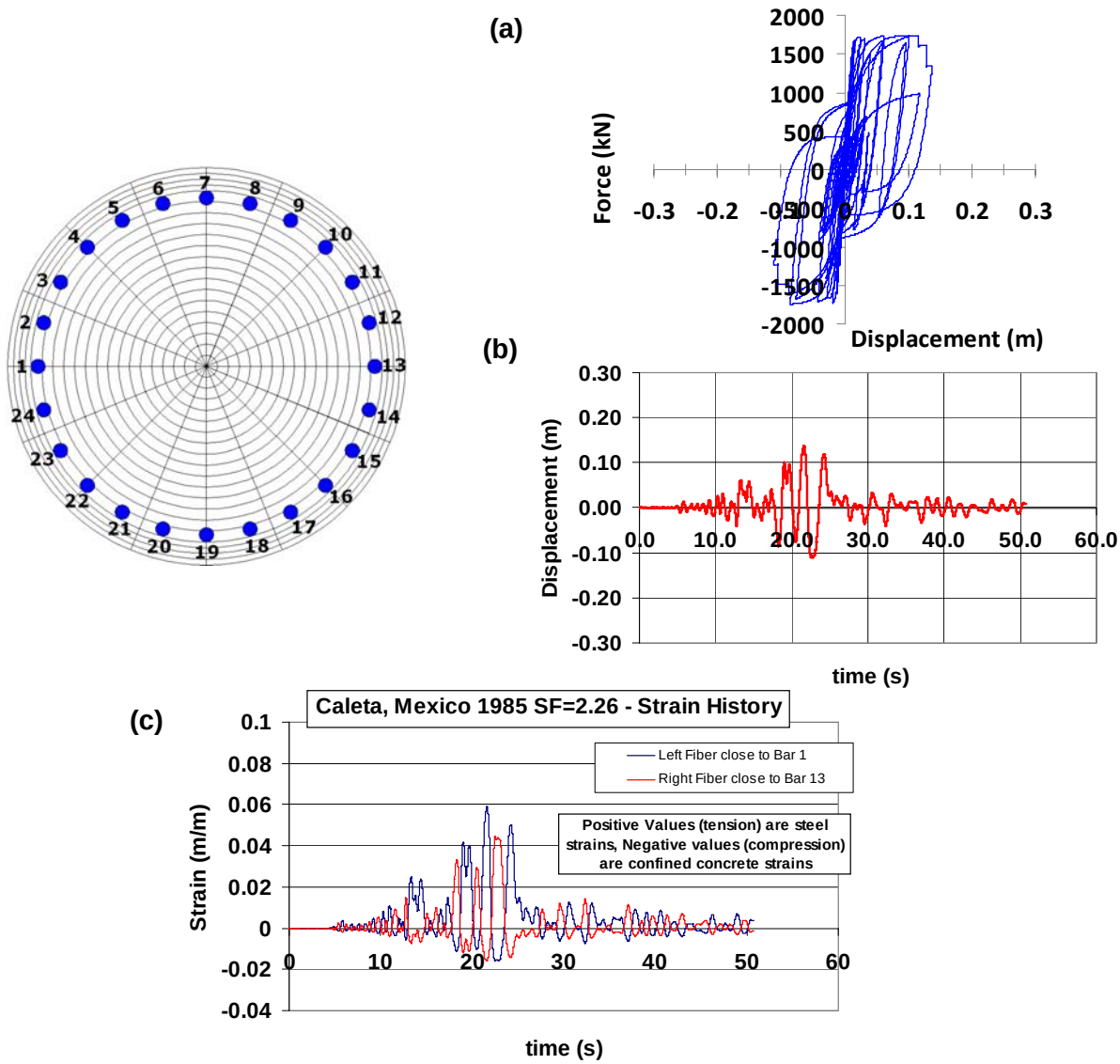

Figure 4.6 Response of the T=0.5 s column for 2.26 times the Caleta record and behavior of its materials

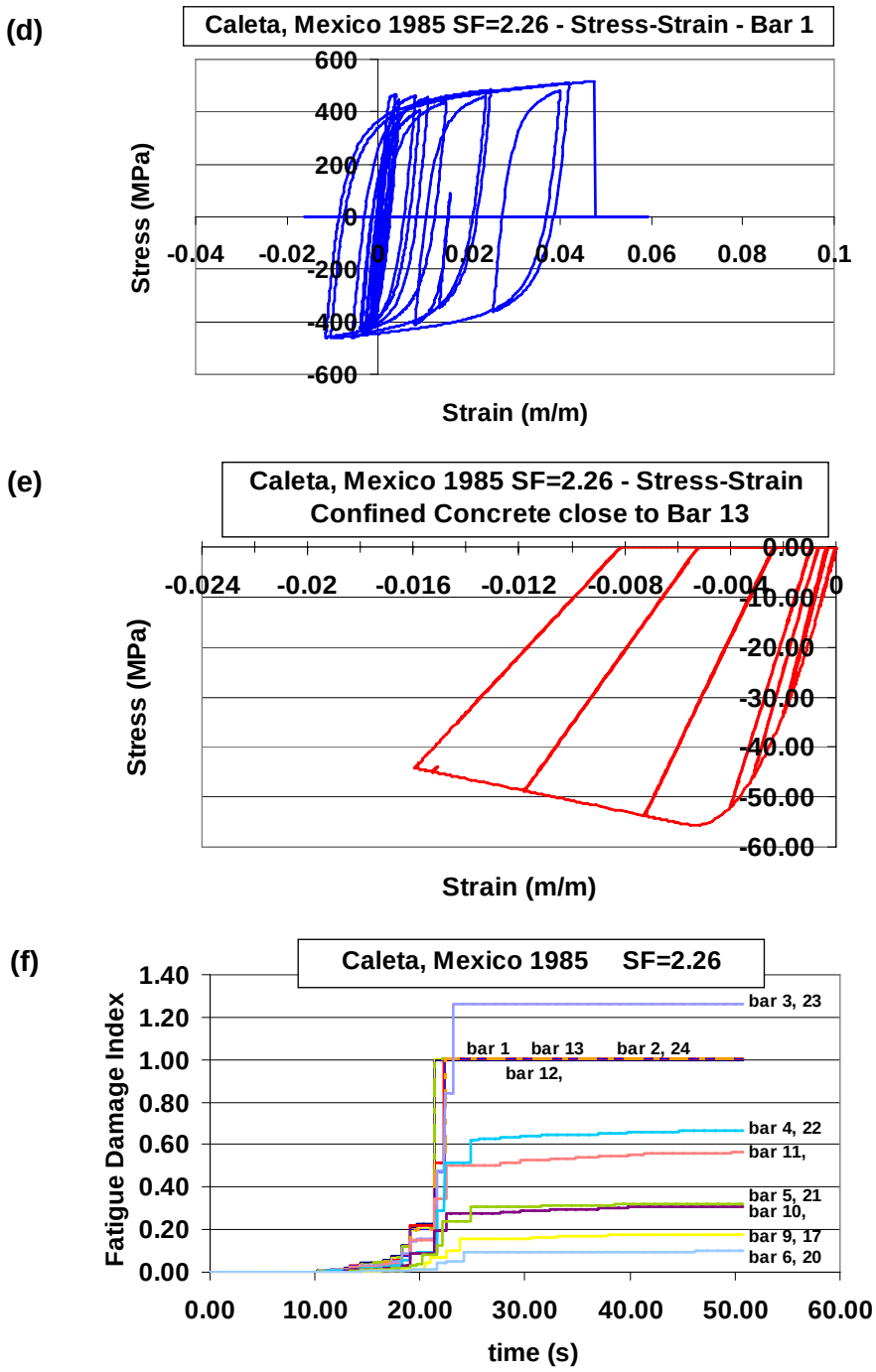

Figure 4.6 (cont.) Response of the *T*=0.5 s column for 2.26 times the Caleta record and behavior of its materials

Figure 4.6 f shows that at t = 21 s bars 1, 2, and 24 fracture because of low-cyclic fatigue and that at t = 23.5 s a total of eight bars fracture because of the same mechanism. Figure 4.6 a shows the strength deterioration of the column due to the fracture of the bars.

The P-Δ product is $0.09M_p$, which is less than $0.25M_p$.

For this ground motion scaled 2.26 times the original record to match the code spectrum, the design meets code requirements, although the proposed FFEM has been able to predict the fracture of eight bars due to low-cyclic fatigue.

4.4.4. Results for 0.79 times the Melipilla record acting on the T = 0.5 s column

Figure 4.7 shows the responses for the Melipilla record scaled 0.79 times to match the code design spectrum.

Figures 4.7 a and b show that the maximum lateral displacement reaches 5 cm, a value lower than the capacity. Figures 4.7 c and d show that the maximum tensile steel strain demand is 0.015, less than 0.09, and Figures 4.7 c and e give the maximum confined concrete strain demand that reaches 0.06, which is less than 0.018.

The product PΔ is $0.034M_p$; therefore, there is no $P\Delta$ effect.

Figure 4.7 f shows that for the scaled Melipilla record there is no fracture of the bars due to low-cyclic fatigue. The damage by fatigue in bar 13 is 6.5% and in bar 1 is 5%.

For this record, this column also meets code elastic modal analysis requirements, and the proposed FFEM demonstrated that there is small damage due to low-cyclic fatigue. Cracks due to tension in the unconfined cover concrete are due to tension strains of 0.02, as seen in Figure 4.7 c, and there is no other flexural failure mechanism. Therefore, the design is accepted.

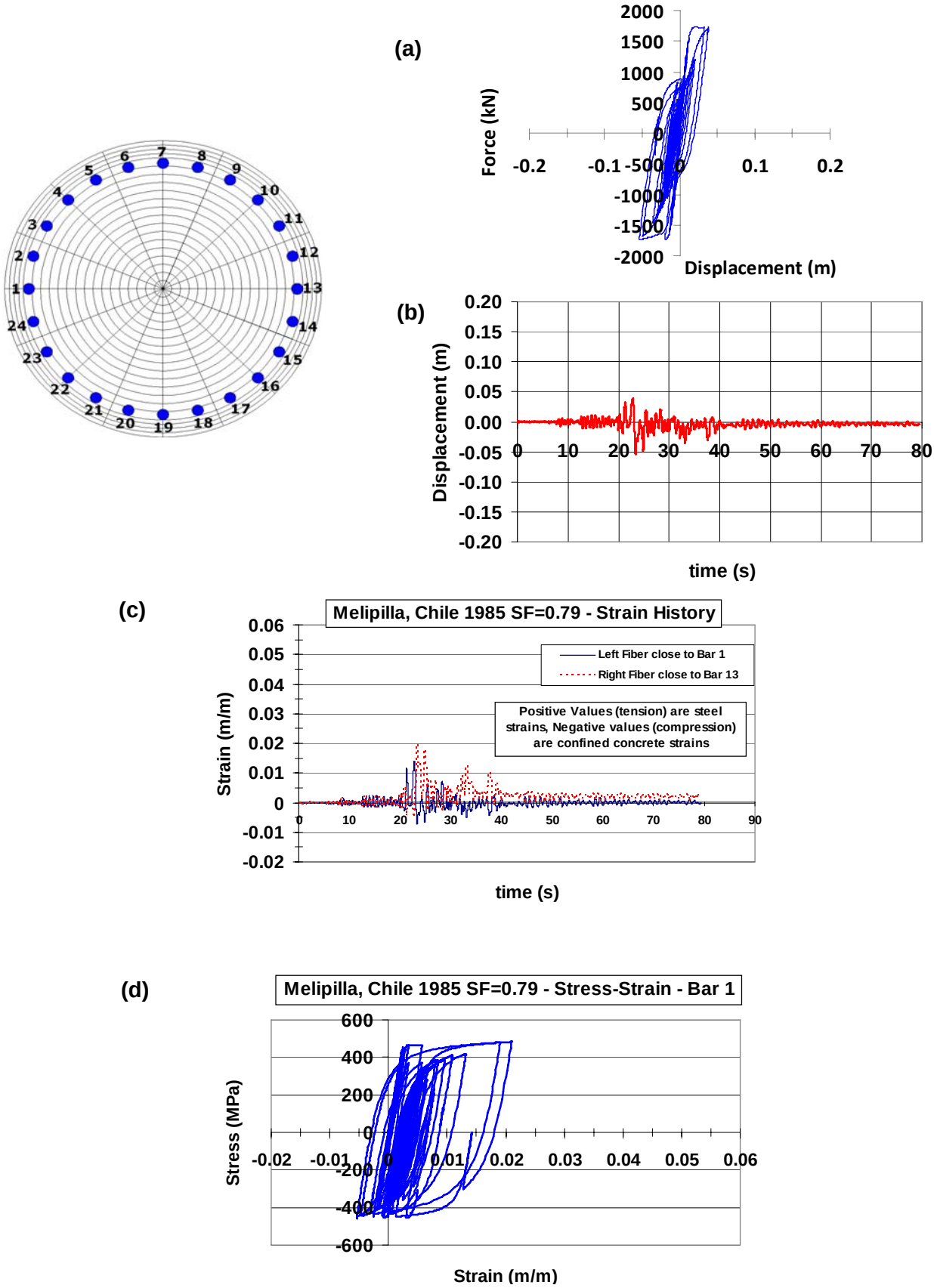

Figure 4.7 Response of the *T*=0.5 s column for 0.79 times the Melipilla record and behavior of its materials

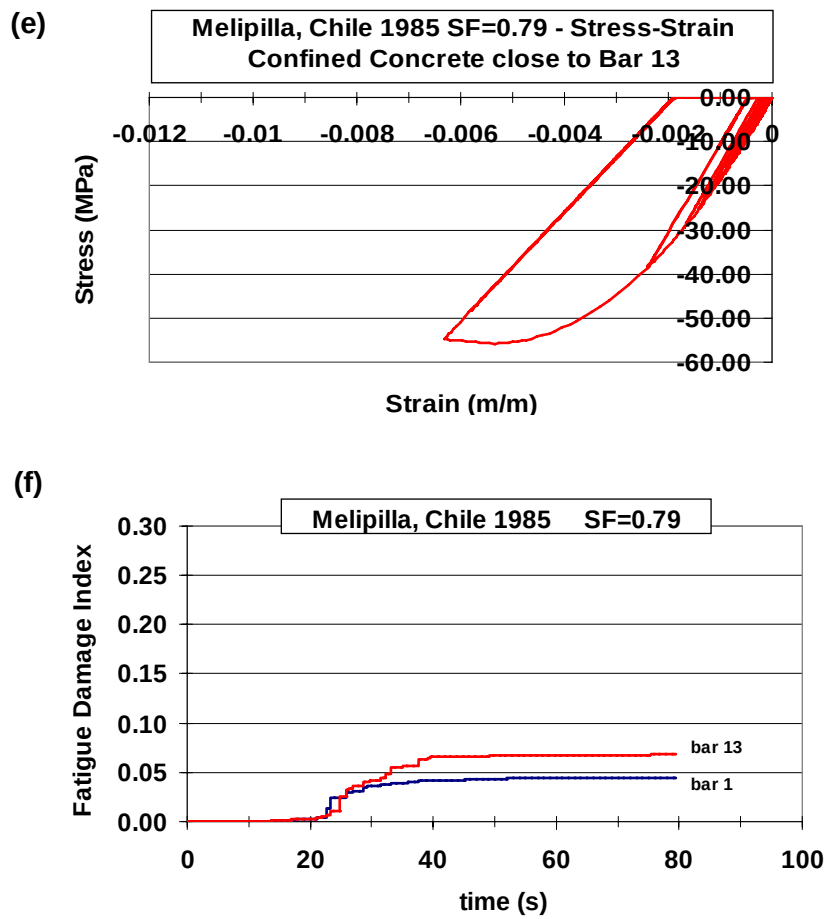

Figure 4.7 (cont.) Response of the *T*=0.5 s column for 0.79 times the Melipilla record and behavior of its materials

4.5. Performance of a bridge column with period *T* = 1.0 s

4.5.1 General results

According to Figure 4.2 c, for the T = 1.0 s column the displacement capacity and the yielding displacement are 24 and 2.4 cm, respectively. Table 4.2a shows the scaling factors to match the spectral code acceleration reaching 0.494g at T = 1.0 s for ξ = 5%. The factors are 0.95 for Pisco, 2.28 for Caleta, and 2.01 for Melipilla.

After the inelastic dynamic analysis the bridge column does not reach failure for the Pisco record, but it shows low-cyclic fatigue for the Caleta and Melipilla scaled records, as shown in Table 4.2b.

Table 4.1 a Analysis for records scaled to the AASHTO spectral acceleration at T=1.0s

COLUMN T = 1.0s SCALING FOR MATCHING WITH AASHTO SPECTRUM								
EQ	Duration (s)	PGA (%g)	Tg (s)	Scale Factor (SF) (for matching)	Sa (%g) for T=1.0s Spectral Acceleration (original record)	Matching Sa (%g) for T=1.0s Spectrum Acceleration	Enveloping Energy, Eucpe (kN-m)	Repeated Energy, Eucpr (kN-m)
Pisco,2007 (Perú)	67.00	0.300	0.82	0.95	0.520	0.494	307.14	804.93
Caleta,1985 (México)	50.63	0.154	1.05	2.28	0.217	0.494	493.00	618.44
Melipilla,1985 (Chile)	79.32	0.686	0.35	2.01	0.246	0.494	525.34	835.54

Table 4.2 b Damage of materials for records scaled to the AASHTO spectral acceleration at T=1.0s

COLUMN T = 1.0s DAMAGE OF MATERIALS AT MATCHING							
EQ	Failure type	Max. Displacement (m)	Time (s)	TOTAL OF FATIGUED BARS	Time (s)	Max. ε_c	Max. ε_s
Pisco,2007 (Perú)	NO FAILURE	0.149	26.3	0	-	0.014	0.048
Caleta,1985 (México)	LOW-CYCLE-FATIGUE	0.207	18.5	1	36.9	0.014	0.047
Melipilla,1985 (Chile)	LOW-CYCLE-FATIGUE	0.211	31.8	8	33.4 to 39.6	0.015	0.049

4.5.2 Results for 0.95 times the Pisco record acting on the *T* = 1.0 s column

Figures 4.8 a and b show the hysteretic response and the displacement time history of the designed column to the main shock of the Pisco record scaled 0.95 times to match the design spectra at T = 1.0 s. The response was obtained through the proposed FFEM. The maximum lateral displacement is 15 cm, less than the displacement capacity.

Figures 4.8 c and d show the steel strain time history and the stress–strain responses for bar 1. In Figure 4.8 c the maximum tensile strain is 0.035, lower than the maximum allowed by the code, which is equal to 0.09.

Figures 4.8 c and e show the confined concrete strain time history and the stress–strain curves. The strain reaches 0.01, less than ε_{cu} = 0.018; therefore, there is no crushing of the confined concrete. However, the concrete tension strain is 0.025, so there are cracks in the cover concrete.

Figure 4.6 e shows the stress–strain response of the confined concrete, showing some deterioration of strength when the strain reaches 0.0052.

For P = 2850 kN, Δ = 15 cm, and M_p = 4400 kN m, the product $P\Delta$ is $0.1M_p$, lower than $0.25M_p$. Up to this point, the design meets all requirements from AASHTO.

Figure 4.8 f shows that bars 1, 2, and 24 have reached a fatigue damage index of 0.5, whereas this index for bars 12, 13, and, 24 is in the order of 0.34.

There is no fatigue, and therefore the design of the column for the scaled Pisco main shock is accepted.

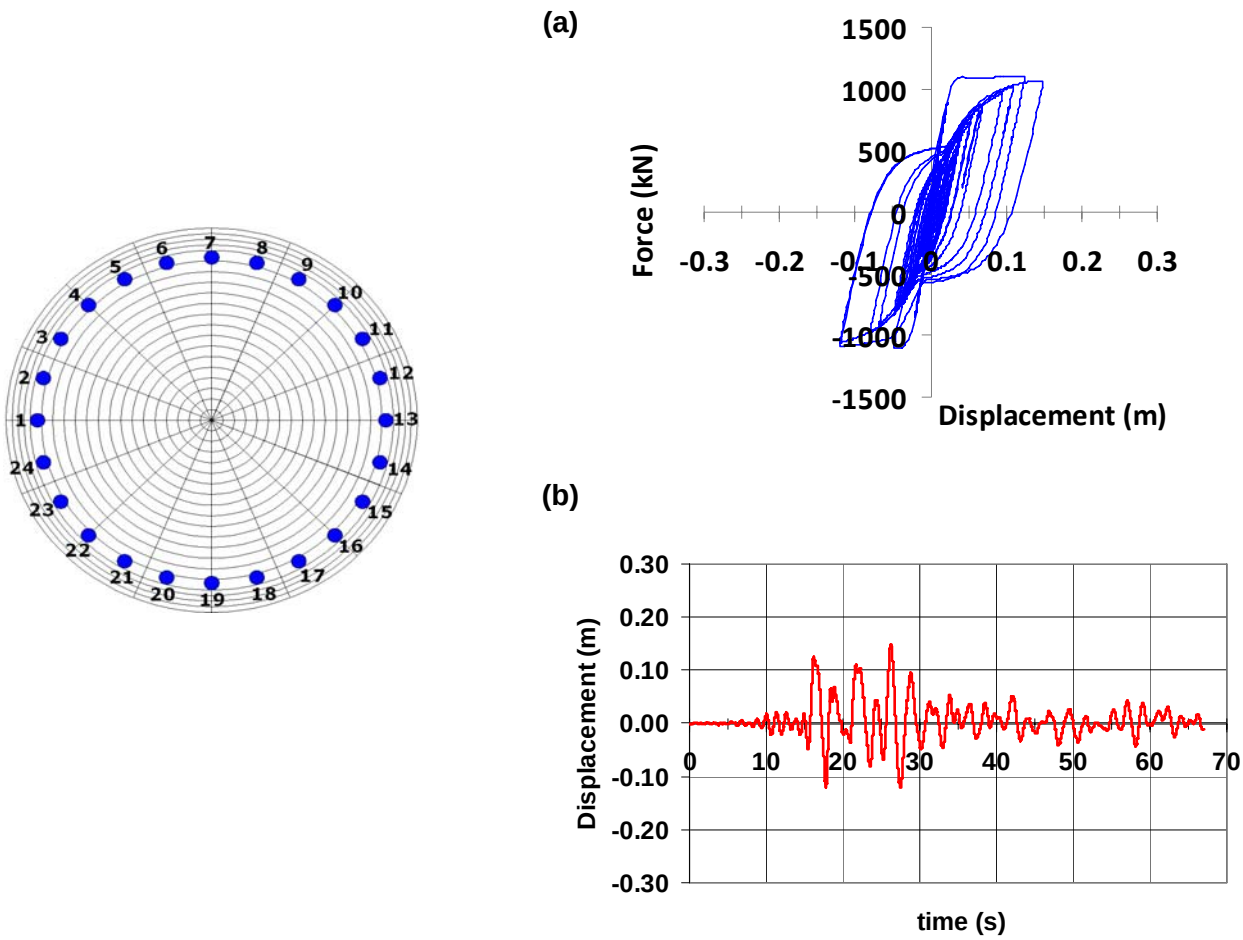

Figure 4.8 Response of the *T*=1.0 s column for 0.95 times the Pisco record and behavior of its materials

(c)

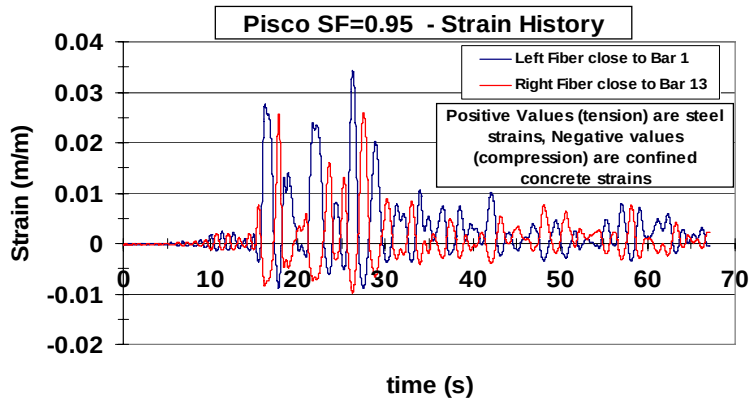

(d)

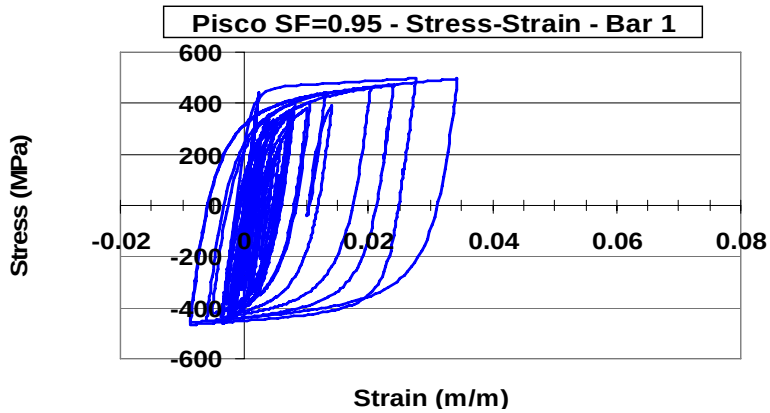

(e)

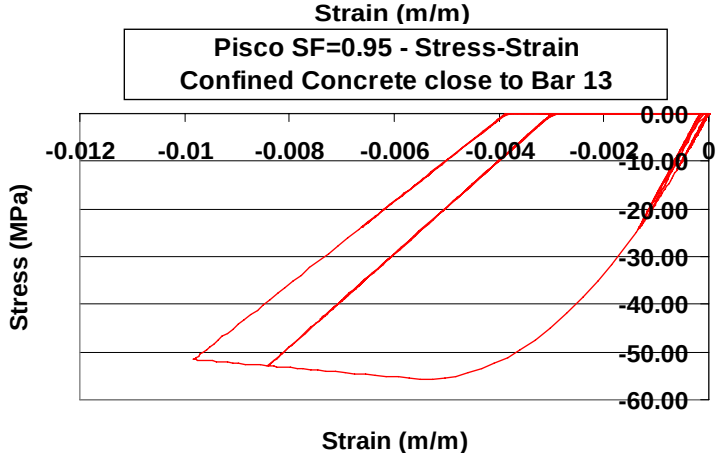

(f)

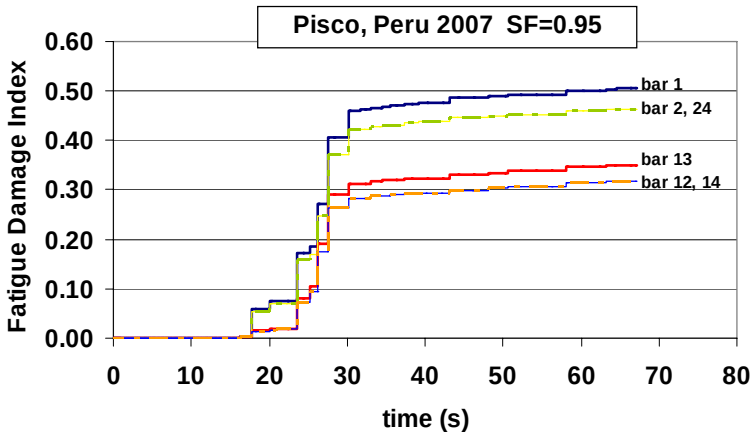

Figure 4.8 (cont.) Response of the *T*=1.0 s column for 0.95 times the Pisco record and behavior of its materials

4.5.3 Results for 2.28 times the Caleta record acting on the T = 1.0 s column

Figure 4.9 a shows the hysteretic response of the designed column to the Caleta record scaled 2.28 times to match the design spectrum. The maximum lateral displacement is 20 cm and is shown in Figure 4.9 b. This demand is lower than the capacity.

The maximum steel strain demand is 0.049, as shown in Figures 4.9 c and d, and the maximum confined concrete strain demand is 0.0135, as seen in Figures 4.9 c and e. Both strain demands are less than the ultimate 0.09 and 0.018, respectively, and so the steel does not fracture by flexure and the confined concrete does not crush. In addition, the product $P\Delta$ is $0.13M_p$: therefore, there is no $P\Delta$ effect.

The column for the Caleta record meets the code requirements. However, Figure 4.9 f shows that bar 13 fractures due to low-cyclic fatigue, making the design unacceptable. In addition, bars 12 and 14 have lost 60% of their fatigue life.

The damage captured by the FFEM could increase vulnerability for an aftershock or a future severe earthquake.

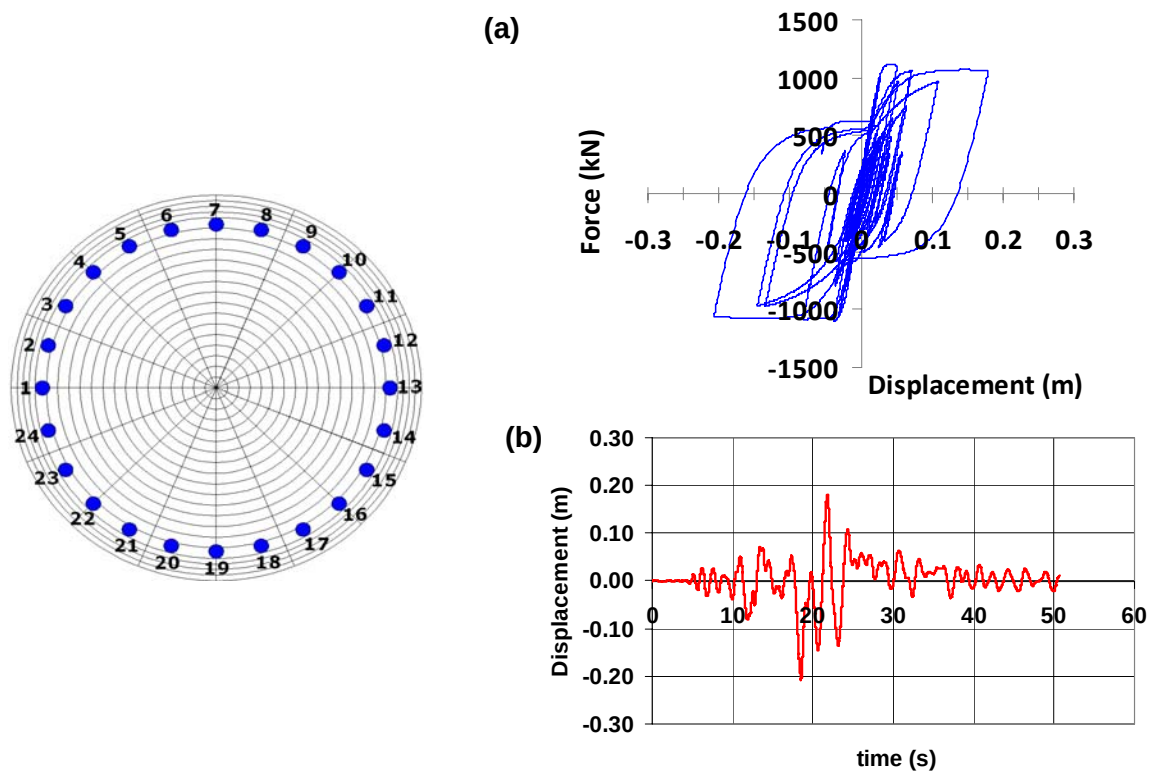

Figure 4.9 Response of the T=1.0 s column for 2.28 times the Caleta record and behavior of its materials

(c)

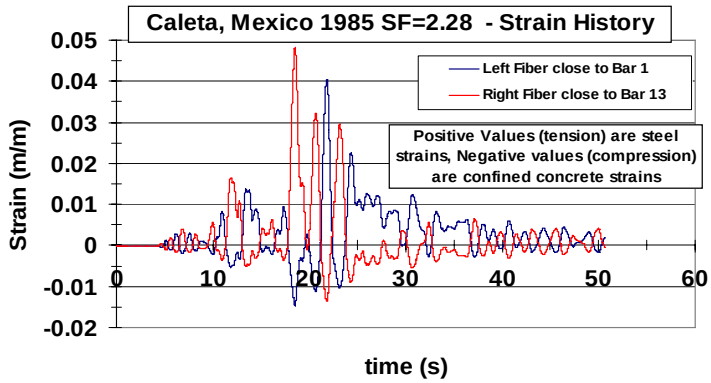

(d)

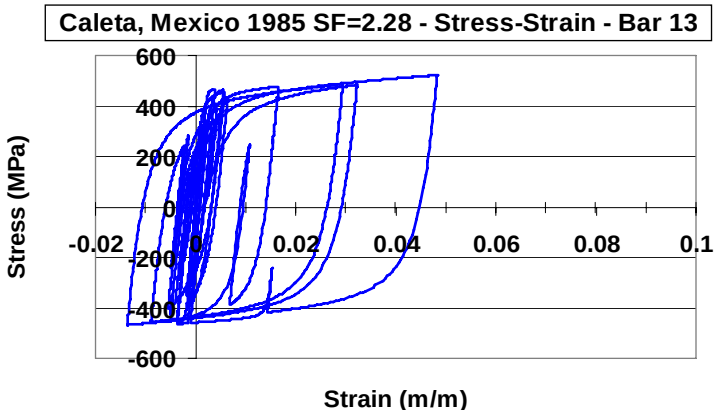

(e)

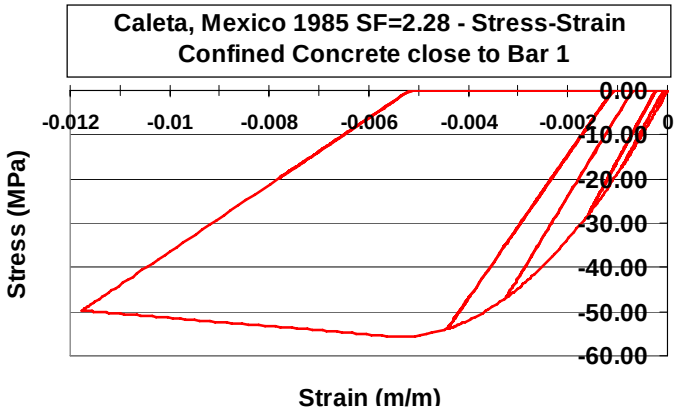

(f)

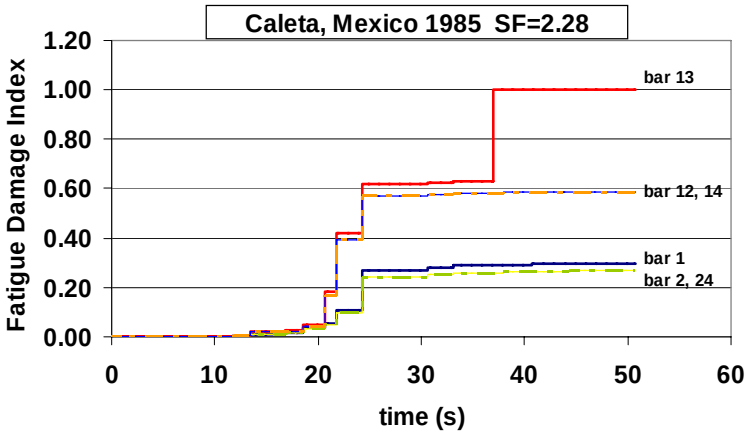

Figure 4.9 (cont.) Response of the *T*=1.0 s column for 2.28 times the Caleta record and behavior of its materials

4.5.4 Results for 2.01 times the Melipilla record acting on the T = 1.0 s column

Figure 4.10 shows the responses for the Melipilla record scaled 2.01 times to match the code design spectrum.

In Figures 4.10 a and b the maximum lateral displacement reaches 21 cm, a value lower than the capacity. Figures 4.10 c and d show that the maximum tensile steel strain demand is 0.05, less than 0.09, and Figures 4.10 c and e give the maximum confined concrete strain demand that reaches 0.014, less than 0.018. The product $P\Delta$ is $0.136M_p$; therefore, there is no $P\Delta$ effect.

Figure 4.10 f shows that for the Melipilla code scaled record there are eight bars that fracture between t = 31 s and t = 38 s due to low-cyclic fatigue and that four more bars have lost 50% of their fatigue life.

For this record this column also meets code requirements, but the FFEM demonstrated that there is fatigue in 8 of the 24 bars; therefore, the design is unacceptable.

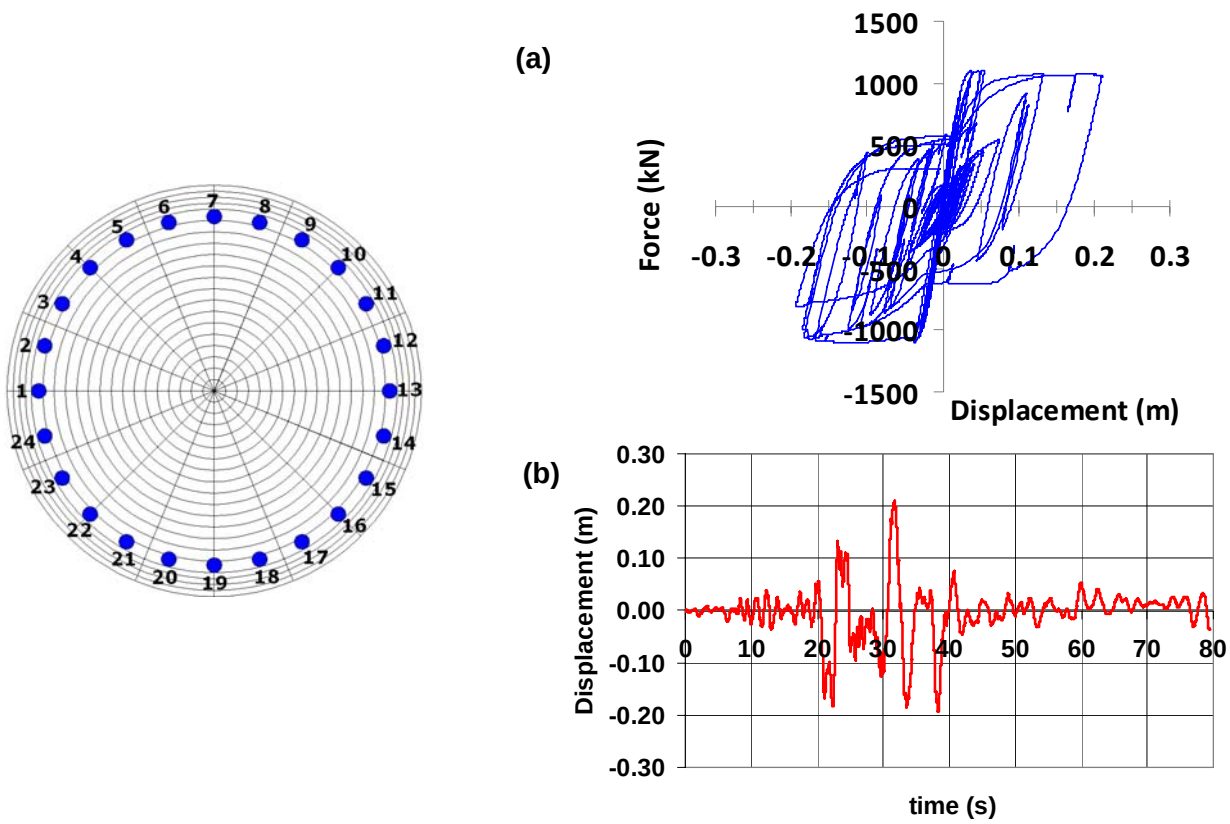

Figure 4.10 Response of the T=1.0 s column for 2.01 times the Melipilla record and behavior of its materials

(c)

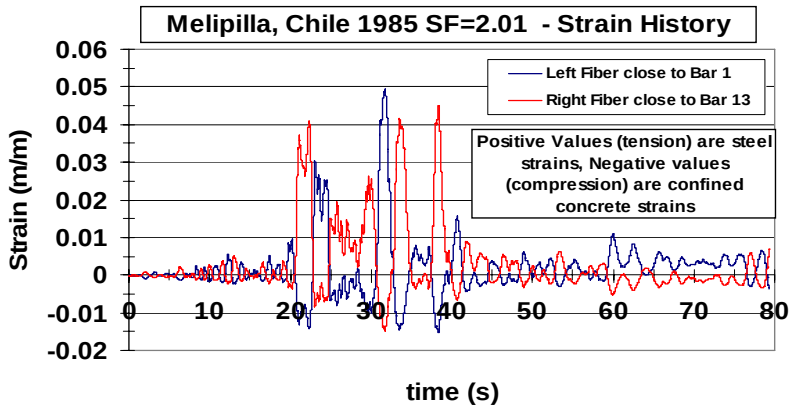

(d)

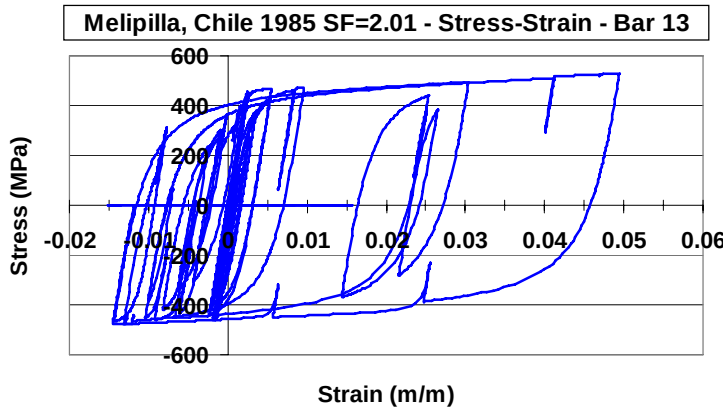

(e)

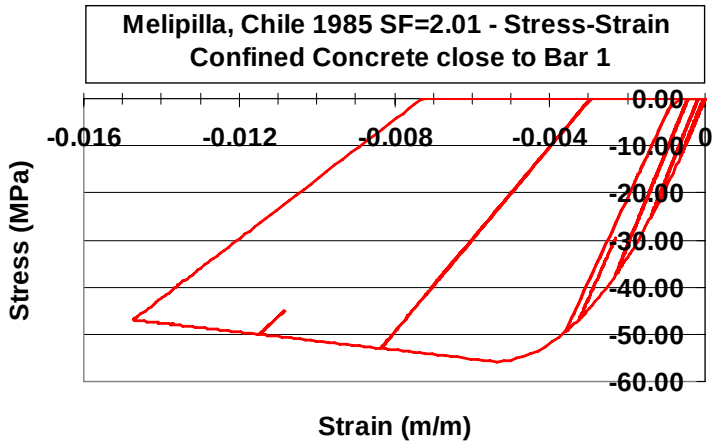

(f)

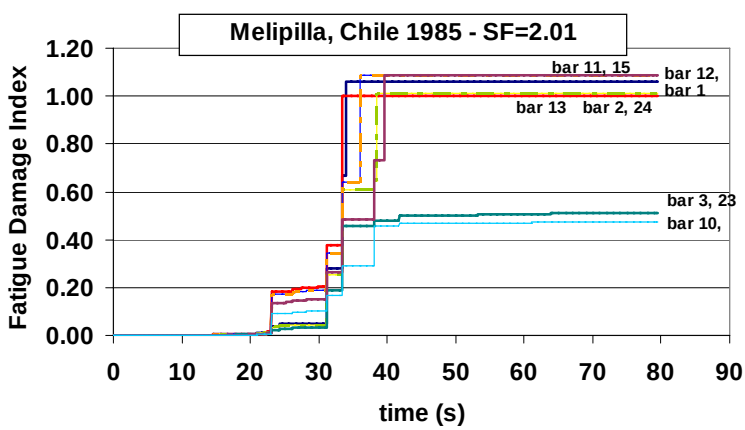

Figure 4.10 (cont.) **Response of the *T*=1.0 s column for 2.01 times the Melipilla record and behavior of its materials**

4.6. Performance of a bridge column with period *T* = 1.5 s

Table 4.3a Analysis for records scaled to the AASHTO spectral acceleration at T=1.5s

COLUMN T = 1.5s SCALING FOR MATCHING WITH AASHTO SPECTRUM								
EQ	Duration (s)	PGA (%g)	Tg (s)	Scale Factor (SF) (for matching)	Sa (%g) for T=1.5s Spectral Acceleration (original record)	Matching Sa (%g) for T=1.5s Spectrum Acceleration	Enveloping Energy, Eucpe (kN-m)	Repeated Energy, Eucpr (kN-m)
Pisco,2007 (Perú)	67.00	0.300	0.82	1.04	0.317	0.329	302.30	584.49
Caleta,1985 (México)	50.63	0.154	1.05	2.17	0.151	0.329	259.85	443.94
Melipilla,1985 (Chile)	79.32	0.686	0.35	1.16	0.283	0.329	251.77	217.55

Table 4.3b Damage of materials for records scaled to the AASHTO spectral acceleration at T=1.5s

COLUMN T = 1.5s DAMAGE OF MATERIALS AT MATCHING							
EQ	Failure type	Max. Displacement (m)	Time (s)	TOTAL OF FATIGUED BARS	Time (s)	Max. ε_c	Max. ε_s
Pisco,2007 (Perú)	NO FAILURE	0.221	26.4	0	-	0.009	0.032
Caleta,1985 (México)	NO FAILURE	0.207	21.9	0	-	0.009	0.030
Melipilla,1985 (Chile)	NO FAILURE	0.200	31.8	0	-	0.008	0.027

4.6.1. Results for 1.04 times the Pisco record acting on the *T* = 1.5 s column

Figures 4.11 a to f show that there is no damage for this *T* = 1.5 s column. Maximum lateral displacement is 22 cm less than the displacement capacity of 38 cm. Steel and concrete strains are 0.31 and 0.09 lower than 0.09 and 0.018 maximum values allowed by AASHTO (2007). Finally, there is no low-cyclic fatigue for any of the bars. The more fatigued bar is bar 1, which loses 28% of its fatigue life.

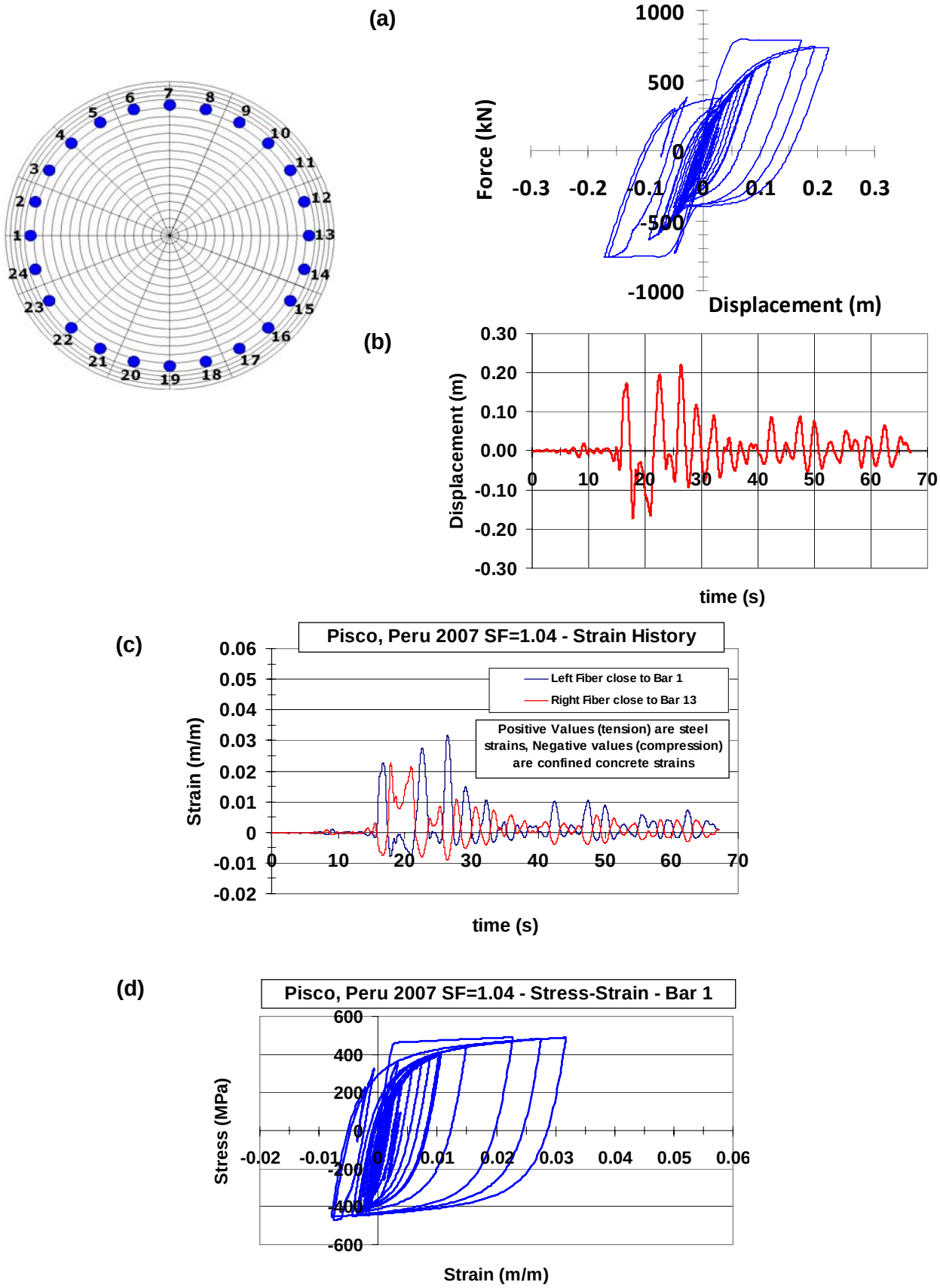

Figure 4.11 Response of the *T*=1.5 s column for 1.04 times the Pisco record and behavior of its materials

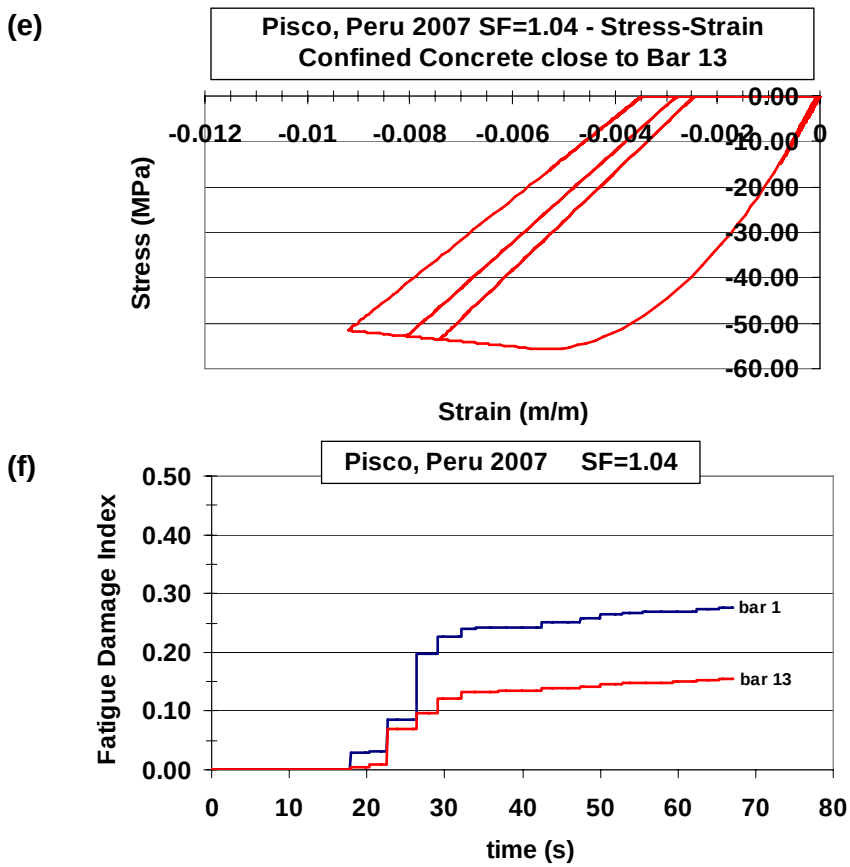

Figure 4.11 (cont.) Response of the *T*=1.5 s column for 1.04 times the Pisco record and behavior of its materials

4.6.2. Results for 2.17 times the Caleta record acting on the *T* = 1.5 s column

Figures 4.12 a to f show no damage for this column. Bar 1 loses 17% of its fatigue life.

4.6.3. Results for 1.16 times the Melipilla record acting on the *T* = 1.5 s column

For this scaled record Figures 4.13 a to f show no damage for the column. Bar 1 has lost 10% of its fatigue life.

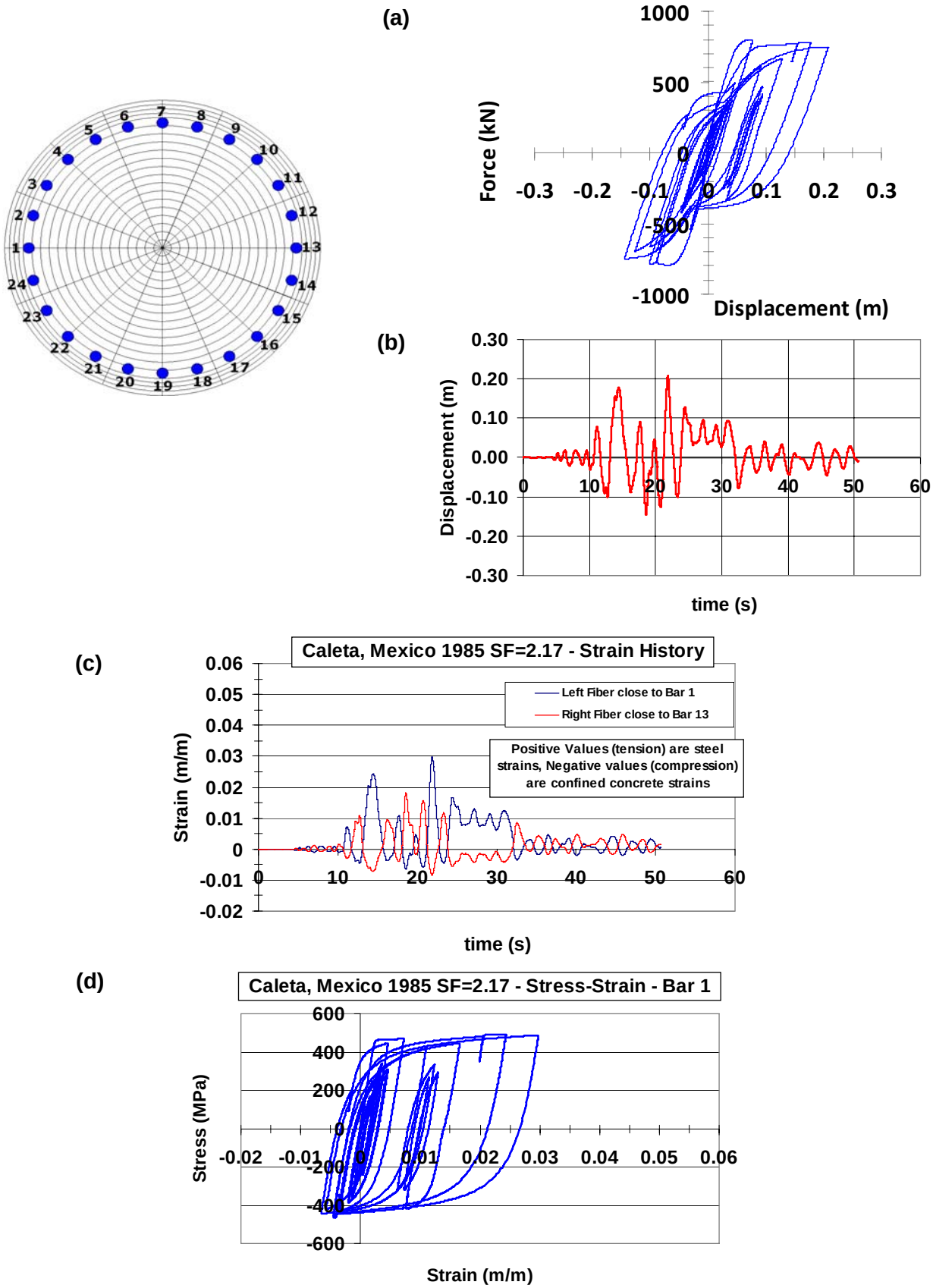

Figure 4.12 Response of the *T*=1.5 s column for 2.17 times the Caleta record and behavior of its materials

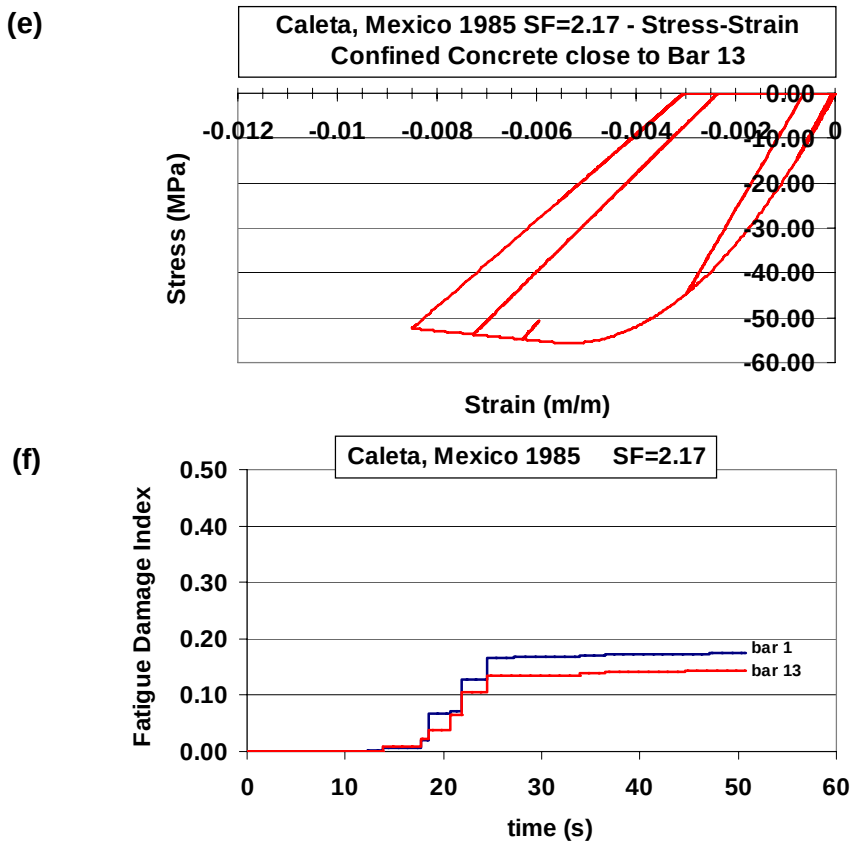

Figure 4.12 (cont.) Response of the *T*=1.5 s column for 2.17 times the Caleta record and behavior of its materials

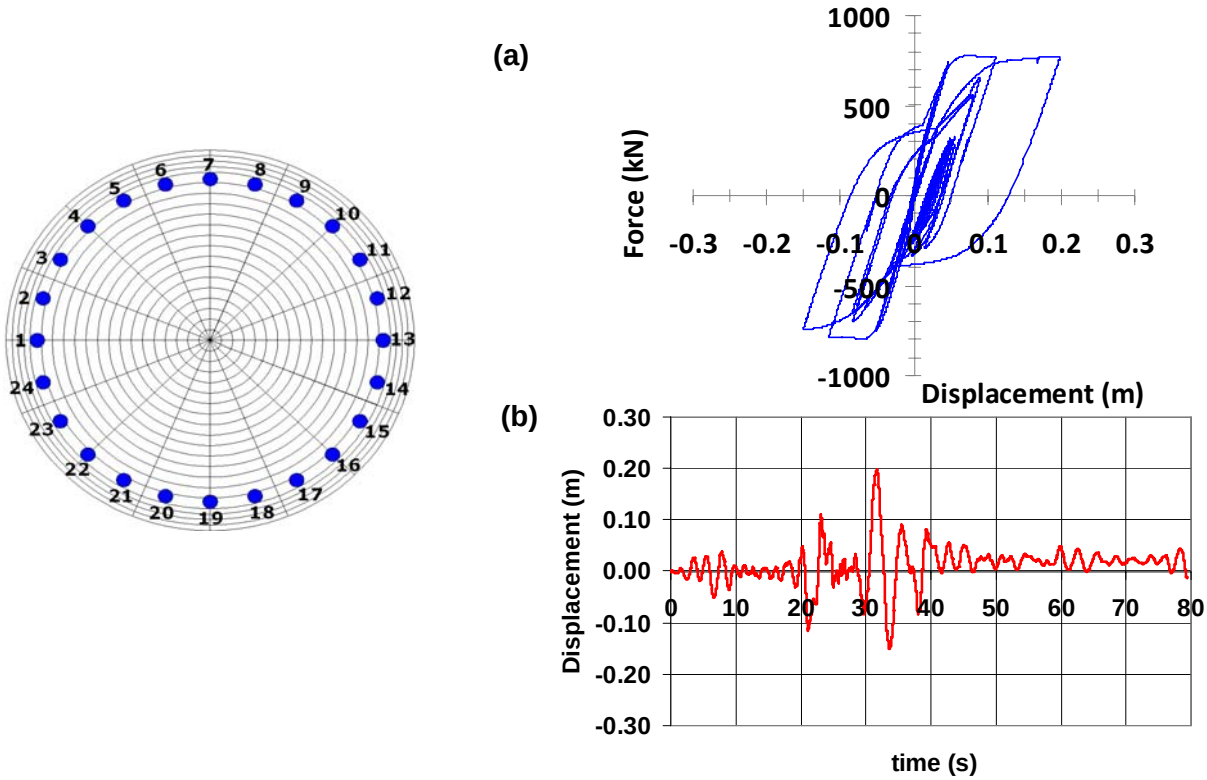

Figure 4.13. Response of the *T*=1.5 s column for 1.16 times the Melipilla record and behavior of its materials

(c)

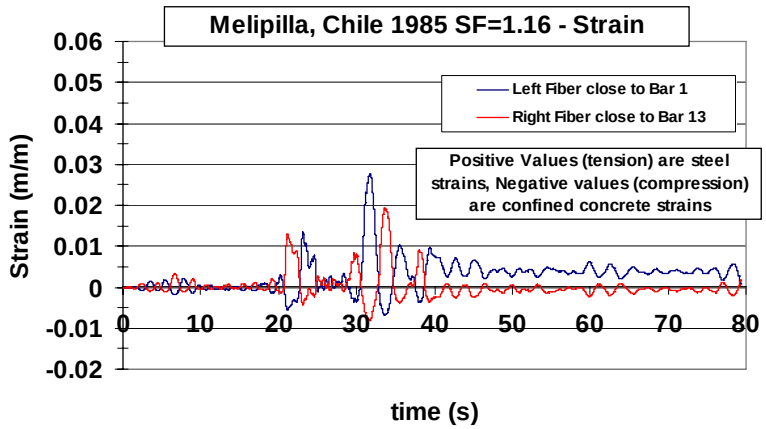

(d)

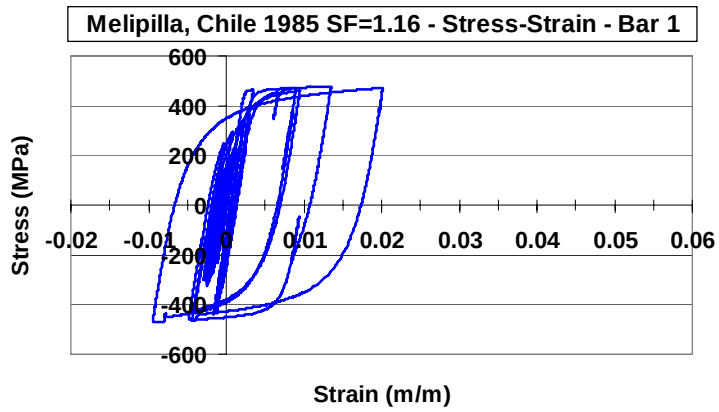

(e)

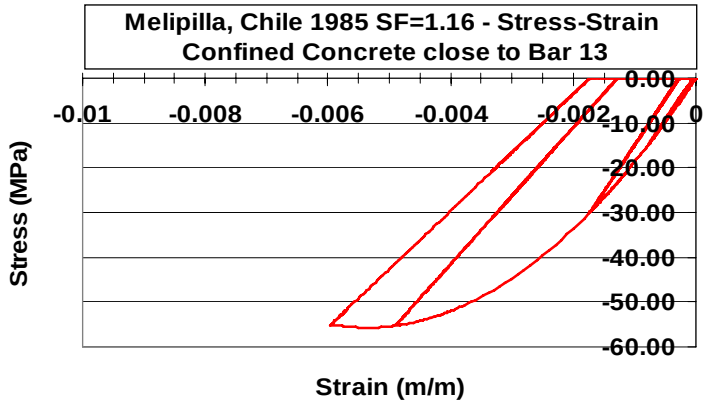

(f)

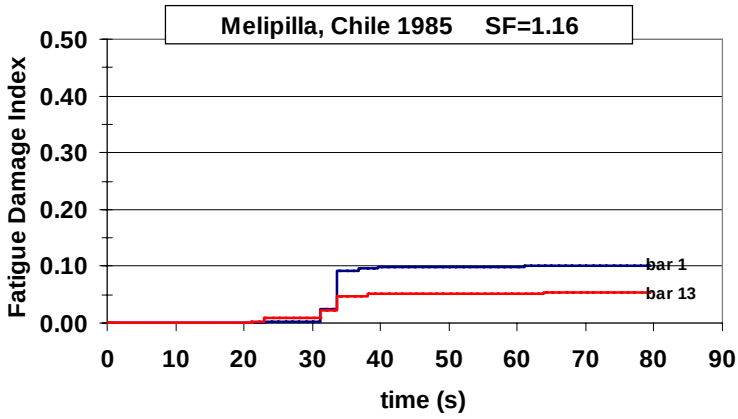

Figure 4.13 (cont.) Response of the *T*=1.5 s column for 1.16 times the Melipilla record and behavior of its materials

4.7 Effects of aftershocks on the code-designed bridge columns

The bridge columns well designed to code have suffered the consequences of the three code matching scaled severe earthquakes. The main damage in the code scaled records is the fracture of one or more bars because of low-cyclic fatigue and in one case crushing of the concrete followed immediately by fatigue of several longitudinal bars. In this condition, the bridge columns become vulnerable owing to accumulation of damage during the main shock; This damage will increase because of the aftershocks that make the columns irreparable or even lead them to a near collapse performance level.

To study the effects of aftershocks, the code spectral acceleration matching of the three records becomes the main shock that will be followed by an aftershock; the intensity is an increasing fraction of the code scaled main shock until additional damage occurs. The fraction begins at 40% and then increases each time up to 100% of the main shock, if necessary.

The aftershock is introduced 10 s after the main shock finishes so that the model keeps the memory of the response, but the aftershock time scale indicated in the following figures loses meaning.

If the aftershock scaled up to 100% of the main shock does not cause any additional damage, then a second aftershock is introduced 10 s after the first aftershock. The criteria for the intensity of the second aftershock are the same as before. That is, the percentage of the main shock is increased up to the occurrence of additional damage.

Table 4.4 shows the results of the effects of the aftershocks on the three bridge columns.

Comparing Tables 4.1 a and b, 4.2 a and b, and 4.3 a and b with Table 4.4 shows that in all cases except one, the maximum lateral displacement reached by the column is due to the first shock. The exception is the response of the T = 1.0 s Melipilla record followed by two aftershocks; this will be discussed later.

In what follows each of the code-designed columns is subjected to the main shock followed by aftershocks.

Table 4.4. Analysis for aftershocks

COLUMN T = 0.5s ADDITIONAL DAMAGE OF MATERIALS DUE TO AFTERSHOCKS								
EQ	Enveloping Energy, Eucpe (kN-m)	Repeated Energy, Eucpr (kN-m)	Max. Displacement (m)	Máx. FDI of a critical steel bar	MAIN SHOCK FRACT. BARS	AFTERSHOCK FRACT. BARS	Max. ε_c	Max. ε_s
1.27*Pisco + 0.6*(1.27*Pisco)	554.06	1326.83	0.215	1.00	14	4	0.022	0.058
2.26*Caleta + 0.6*(2.26*Caleta)	481.64	1395.75	0.138	1.00	8	4	0.016	0.047
0.79*Melipilla + 1.0*(0.79*Melipilla)	177.78	588.63	0.054	0.19	0	0	0.006	0.021
0.79*Melipilla + 1.0*(0.79*Melipilla) + 1.0*(0.79*Melipilla)	195.36	955.36	0.059	0.28	0	0	0.007	0.023

COLUMN T = 1.0s ADDITIONAL DAMAGE OF MATERIALS DUE TO AFTERSHOCKS								
EQ	Enveloping Energy, Eucpe (kN-m)	Repeated Energy, Eucpr (kN-m)	Max. Displacement (m)	Máx. FDI of a critical steel bar	MAIN SHOCK FRACT. BARS	AFTERSHOCK FRACT. BARS	Max. ε_c	Max. ε_s
0.95*Pisco + 0.9*(0.95*Pisco)	307.14	1694.78	0.149	1.00	0	3	0.014	0.048
2.28*Caleta + 0.6*(2.28*Caleta)	493.00	1033.54	0.207	1.00	1	2	0.014	0.047
2.28*Caleta + 0.8*(2.28*Caleta)	493.00	1249.65	0.207	1.00	1	7	0.014	0.047
2.01*Melipilla + 0.6*(2.01*Melipilla)	525.34	1258.22	0.211	1.00	8	4	0.015	0.049
2.01*Melipilla + 0.8*(2.01*Melipilla)	568.14	1416.13	0.254	1.00	8	6 + $\varepsilon_c > \varepsilon_{cu}$ (AFTER FATIGUE)	0.020	0.062

COLUMN T = 1.5s ADDITIONAL DAMAGE OF MATERIALS DUE TO AFTERSHOCKS								
EQ	Enveloping Energy, Eucpe (kN-m)	Repeated Energy, Eucpr (kN-m)	Max. Displacement (m)	Máx. FDI of a critical steel bar	MAIN SHOCK FRACT. BARS	AFTERSHOCK FRACT. BARS	Max. ε_c	Max. ε_s
1.04*Pisco + 1.0*(1.04*Pisco)	305.48	1414.41	0.223	0.77	0	0	0.009	0.032
1.04*Pisco + 1.0*(1.04*Pisco) + 1.0*(1.04*Pisco)	316.59	2069.95	0.230	1.00	0	5	0.009	0.035
2.17*Caleta + 1.0*(2.17*Caleta)	262.00	1092.39	0.209	0.44	0	0	0.009	0.030
2.17*Caleta + 1.0*(2.17*Caleta) + 1.0*(2.17*Caleta)	262.00	1741.56	0.209	0.71	0	0	0.009	0.030
1.16*Melipilla + 1.0*(1.16*Melipilla)	277.82	611.84	0.211	0.23	0	0	0.009	0.029
1.16*Melipilla + 1.0*(1.16*Melipilla) + 1.0*(1.16*Melipilla)	277.82	1031.17	0.213	0.38	0	0	0.009	0.029

4.7.1 Aftershocks on *T* = 0.5 s bridge column

For this column the Pisco and Caleta aftershocks with intensities of 60% of the main shocks induce the fracture of four additional bars, as seen in Table 4.4. The same table shows for the Melipilla record that one or two aftershocks of the same intensity as the main shock do not cause any damage.

The strength deterioration of the critical section due to the fracture of 14 bars for this bridge column subjected to the scaled main shock Pisco record is shown in Figure 4.14 a. The fatigue life loss is shown in Figure 4.14 d, where it is seen that the aftershock induces the fracture of four more bars.

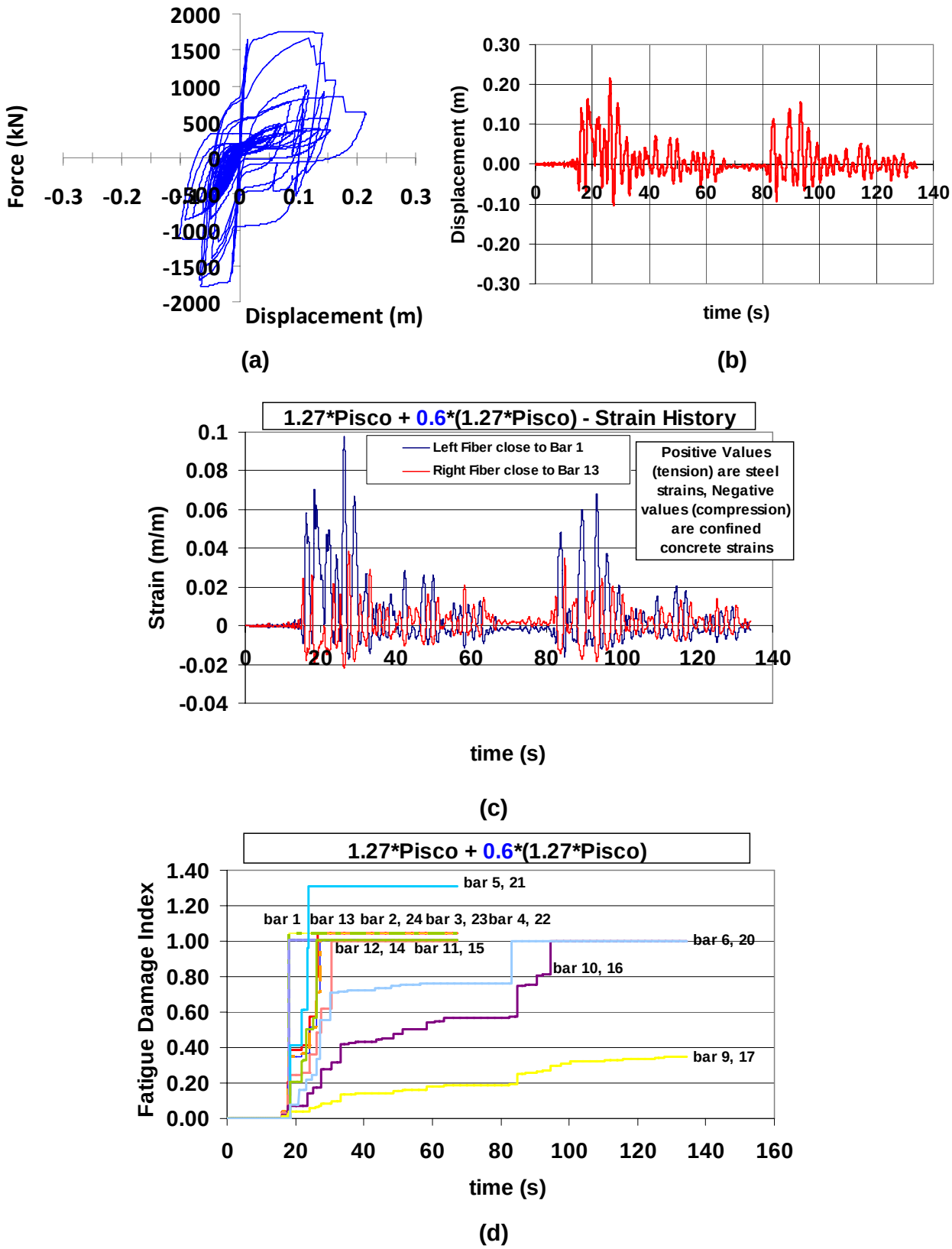

Figure 4.14 Response of the *T*=0.5 s column for 1.27 times the Pisco (main shock) record with an aftershock of 60% of intensity

Figure 4.14 b shows the maximum displacement time history of the column, demonstrating that the aftershock does not increase the maximum cyclic displacements but does increase the repeated ones.

Figure 4.14 c shows the strain time history for the steel and the confined concrete. Bar 1 already fractured because of low-cyclic fatigue during the main shock, but the fiber element continues capturing the strains in the location of bar 1.

Therefore, the design is unacceptable because of the fracture of additional bars for two of the three records followed by aftershocks. The exception, as mentioned above, is the response of the column to the Melipilla record followed by two aftershocks that did not induce any damage.

4.7.2 Aftershocks on *T* = 1.0 s bridge column

Table 4.4 shows that in all cases the aftershocks cause damage for this bridge column. For example, for 0.95 times the Pisco record there is no damage to this column, but for this main shock followed by an aftershock with intensity equal to 90% of the main shock, three bars fracture due to low-cyclic fatigue.

For the code scaled Caleta main shock one bar fractures owing to low-cyclic fatigue, and for the main shock followed by an aftershock with intensity of 80% times the main shock, seven more bars fracture by low-cyclic fatigue.

For the scaled Melipilla main shock eight bars fractured, and for an aftershock 60% of the main shock, four more bars fracture by low-cyclic fatigue. If the aftershock is 80% of the main shock six more bars fracture, and in addition the confined concrete crushes. Figure 4.15 a shows the strength deterioration due to fracture of the bars. Figure 4.15 b shows the increase in lateral displacements due to the aftershock that induces, in addition, crushing of the confined concrete.

Figure 4.15 c shows the steel and confined concrete strains, and Figure 4.13 d presents the fatigue of the longitudinal bars.

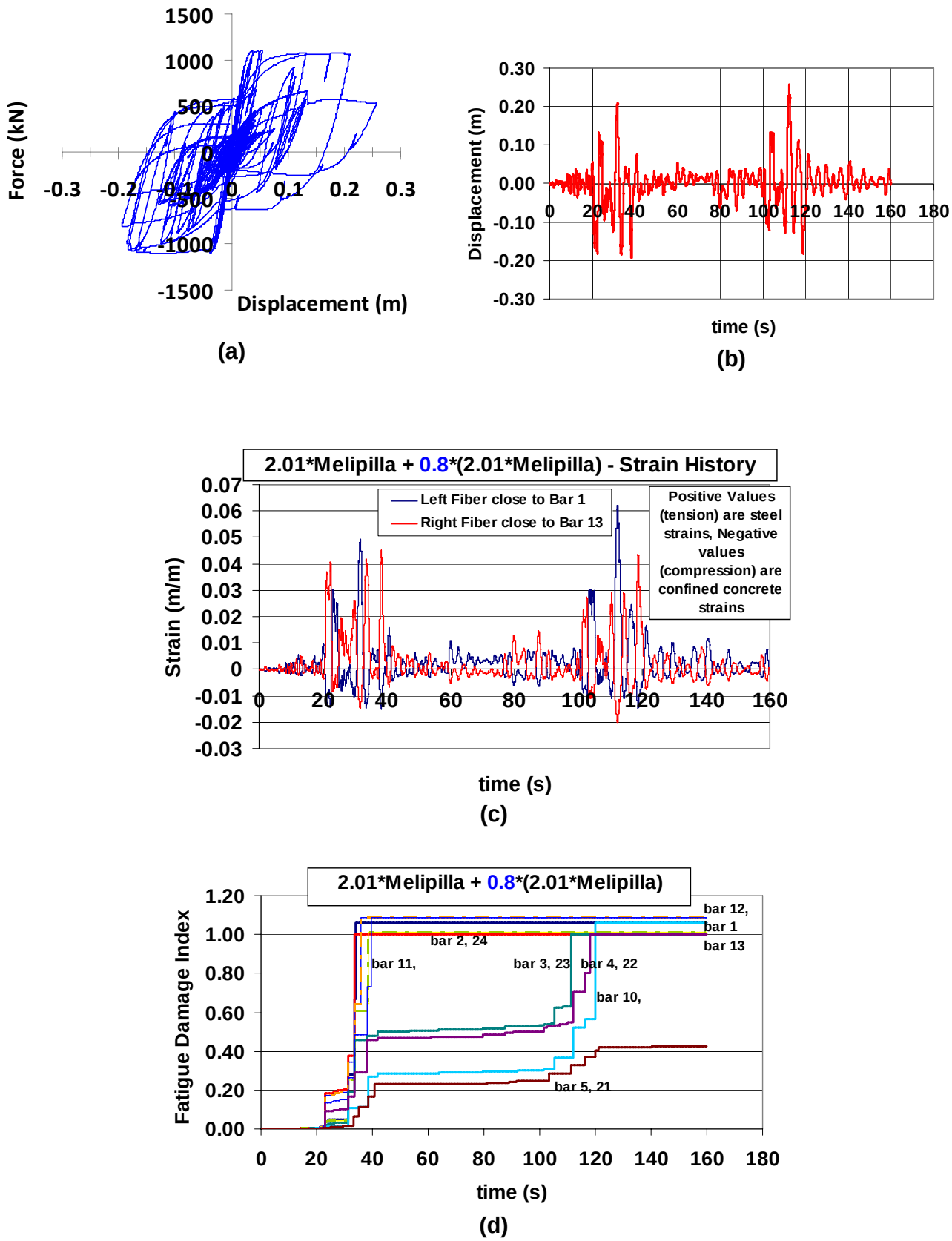

Figure 4.15 Response of the *T*=1.0 s column for 2.01 times the Melipilla (main shock) record with an aftershock of 80% of intensity

4.7.3 Aftershocks on T = 1.5 s bridge column

As seen in Table 4.4, for this bridge column only the scaled Pisco record followed by two aftershocks with intensity of 100% of the main shock induces the fracture of five bars due to low-cyclic fatigue. The other two records followed by one and two aftershocks induce damage, but the column does not reach the significant damage performance level.

Figure 4.16 shows the hysteretic and time history responses, the strain time histories, and the fatigue of the bars for the T = 1.5 s column for the Pisco records and two aftershocks.

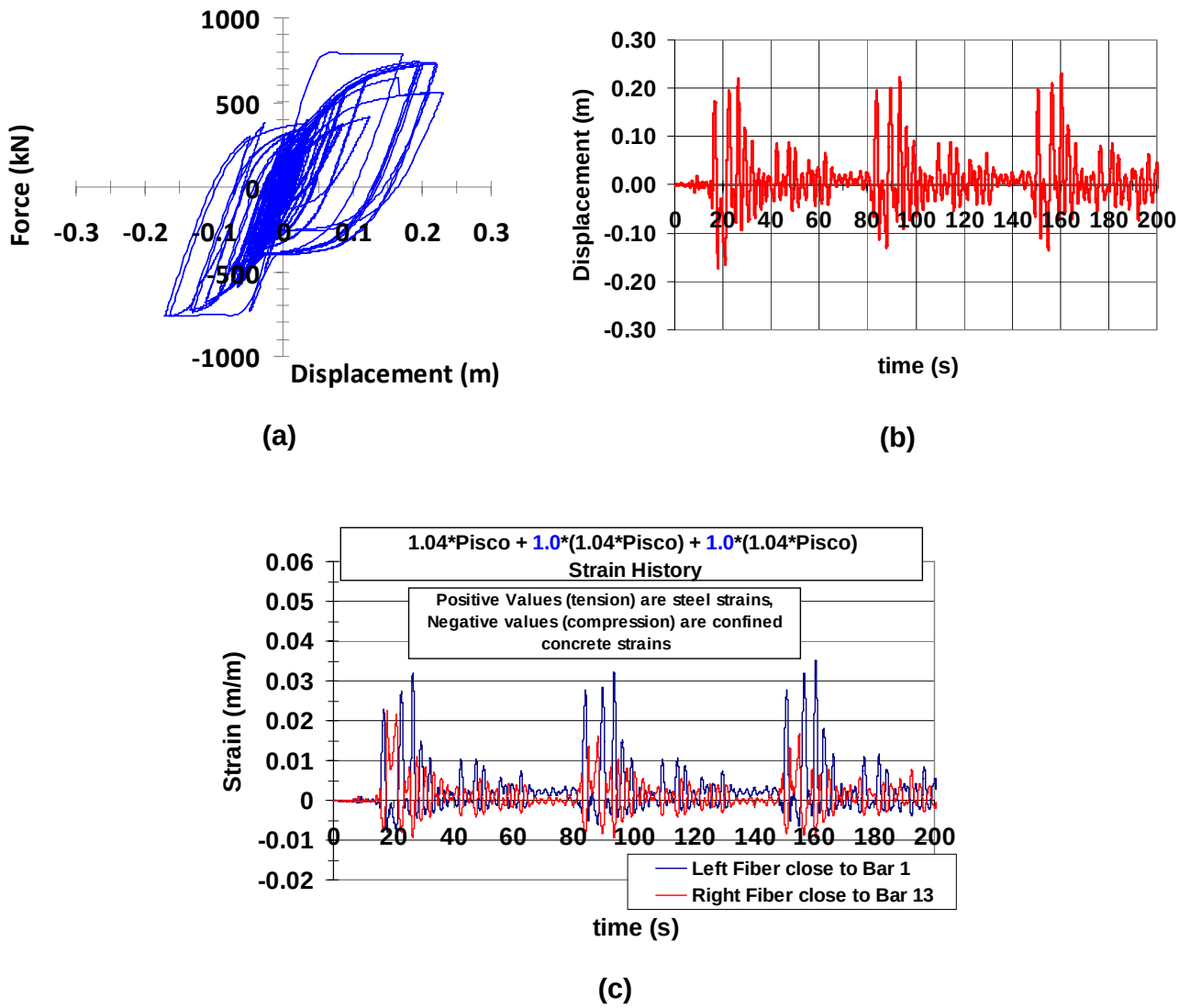

Figure 4.16. Response of the T=1.5 s column for 1.04 times the Pisco (main shock) record with two aftershocks of 100% of intensity

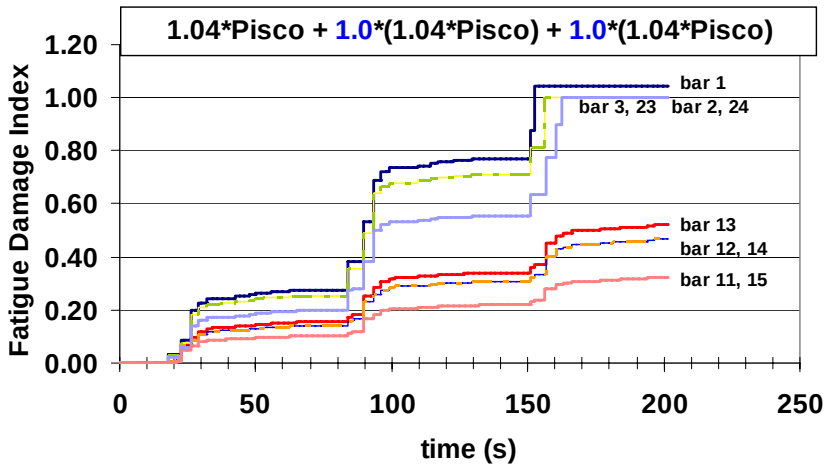

(d)

Figure 4.16 (cont.) Response of the *T*=1.5 s column for 1.04 times the Pisco (main shock) record with two aftershocks of 100% of intensity

4.8 Summary

1. New AASHTO and Caltrans code provisions for design of reinforced concrete bridge columns are based on controlling maximum lateral displacements. The procedure uses elastic dynamic analysis and linear elastic reduced spectra for different soil conditions.

2. In addition, codes also allow, for design or to check an elastic analysis, the use of three ground motions that should meet several code requirements to obtain inelastic responses. In this part of the investigation three requirements are considered: similar magnitudes to the one expected in the site, similar source mechanisms, and similar type of soil. The expected magnitude is 8, the source mechanism is subduction, and the soil is alluvium, type D, according to AASHTO.

3. Three bridge columns designed according to the elastic procedure of the codes are subjected to three different ground motions that meet the above codes requirements for dynamic inelastic analysis.

4. The ground motions used are Pisco and Melipilla records, products of the subduction of the Nazca plate under the South American plate, and the Caleta record, product of the subduction of the Cocos plate under the Caribbean plate.

5. The FFEM used in this chapter predicted damage by fracture of the longitudinal bars owing to low-cyclic fatigue in most of the columns studied subjected to the mentioned ground motions. In one case, the model-predicted crushing of the confined concrete followed after 3 s of fracture of bars due to low-cyclic fatigue.

6. The FFEM also predicted more damage due to low-cyclic fatigue induced by the aftershocks. All main shock records and aftershocks were scaled following AASHTO prescriptions. The exception is the T = 1.5 s because of the low spectral accelerations of the scaled records for this structure period.

4.9 Conclusions

1. Three bridge columns are designed according to AASHTO specifications under elastic conditions for the required elastic design spectra. The requirements are that the maximum lateral displacement demand be a value lower than the displacement corresponding to the ultimate confined concrete strain, to the ultimate tension strain, and that such demand times the vertical load should be less than 25% of maximum flexural capacity. In addition, AASHTO requires that the displacement ductility demand be less than 6.

   The design is then checked using AASHTO prescriptions for three earthquakes that show similar magnitude, source mechanism, and soil conditions. The selected earthquake records are: Melipilla from the Chile 1985 earthquake, Pisco from the Pisco 2007 earthquake, and Caleta from the Michoacan 1985 earthquake. The three of them have magnitudes in the order of Mw = 8, are subduction earthquakes, and were recorded in type D soil condition. The records are factored to meet the specified spectral acceleration at the structure period according to AASHTO prescriptions

   The results of the inelastic dynamic analysis using the FFEM show that the design meets the above code specifications.

   However, the results of the analysis show reduction of fatigue life and even fracture of some bars due to accumulation of damage for each earthquake. This damage due to low-cyclic fatigue is not considered as a flexural failure mechanism in the AASHTO design requirements. In addition, if the columns are subjected to aftershocks, these may cause an increase of the number of fractured bars and therefore more damage will be observed. The

aftershocks were introduced as percentages of the main shock factored according to AASHTO recommendations.

4.10 Remarks

1. The results of the analysis show that low-cyclic fatigue is a very common type of flexural failure in bridge columns subjected to severe earthquakes.

2. Actual prescriptions do not take into consideration the cyclic reversible characteristic of dynamic response; therefore, designs are still based only on lateral maximum displacements, but now limited to maximum strains of the confined concrete and the steel bars, maximum P-Δ moment and maximum displacement ductility ratio. The new specifications can be considered an improvement with respect to old requirements. However, AASHTO specifications are not enough since through the analysis it has been proved that the response to severe earthquakes can cause reduction of fatigue life.

3. The cyclic plastic reversible displacements and plastic strains are measured along the duration of the strong motion in the FFEM.

4. With only the stress–strain relation of the materials it is not possible to capture the strength deterioration of the column unless the concrete crushes and/or the longitudinal steel bar fractures due to tensional flexure. The incorporation of the fatigue model in the fiber finite element model allows capturing the deterioration of the strength that occurs any time a bar fractures due to low-cyclic fatigue along the duration of the strong motion.

5. Fatigue of the bars is indirectly related to the dissipated energy since fatigue is calculated through the measurement of the plastic strains and the corresponding number of cycles which constitute dissipation of energy.

6. Aftershocks introduced in the analysis are fractions of the main shocks or have amplitudes similar to the main shock therefore, the frequency content is preserved and only the amplitudes change. In this way according to the results of the analysis, the aftershocks induce an increase of the repeated dissipated energy without new plastic displacements therefore increasing the reduction of fatigue life in several other bars.

5. SIGNIFICANT DAMAGE PERFORMANCE LEVEL AND CYCLIC DAMAGE INDEX FOR SEISMIC DESIGN OF REINFORCED CONCRETE BRIDGE COLUMNS

5.1 Introduction

In this chapter, a cyclic damage index (CDI) is proposed to quantify numerically the damage above or below the significant damage performance level (SDPL). Recall that the SDPL corresponds to the occurrence of one or more of the four flexural failure mechanisms defined in Chapters 1 and 3 for any one of the records chosen for design as prescribed by AASHTO (2007). The SDPL can be associated with the life safety performance level that is not related to a particular damage state of the column, such as post-yielding or near collapse, but is between these two levels of performance. Therefore, the SDPL could help to define the level of damage at which the danger to life safety is triggered.

5.2 Damage indices

Appendix C.1 presents a brief summary of several damage indices, emphasizing the ones more closely related to the proposed CDI.

5.3 The proposed significant damage performance level and the cyclic damage index

5.3.1 General remarks

Non-cyclic ductility ratios and drifts have been widely used as measures of damage, although it has been demonstrated in Chapters 2 and 3 that none of these measure plastic displacements or plastic strains. Therefore, they cannot be considered as measures of damage. Damage indices are an important improvement in measurement of damage and are used by researchers and practitioners.

5.3.2 Basis for the proposed cyclic damage index

This chapter proposes the following expression to estimate the CDI:

$$\mathrm{CDI} = \frac{E_{\mathrm{ucpe}}}{E_{\mathrm{c}}} + \beta_{\mathrm{c}} \frac{E_{\mathrm{ucpr}}}{E_{\mathrm{c}}} \tag{5.1}$$

E_{ucpe} is the energy dissipated by the new cyclic plastic displacements, and E_{ucpr} is the energy dissipated by the repeated cyclic plastic displacements. Because both energies are based on cyclic reversible hysteretic response, this study proposes to normalize each one by the energy capacity of the bridge column, E_c.

E_c is the energy dissipated by the bridge column after reaching SDPL under one cyclic sine function limited by a maximum lateral positive and negative displacement, both of the same value. E_c is equal to the area enclosed by the envelope of the one cyclic plastic displacement response of the bridge column. The parameter β_c controls the importance of the energy dissipated by the repeated plastic displacements on the damage.

The rationality of the proposed CDI is based on the following analysis. When the response tends to be one sided, causing excessive lateral plastic displacement, as is the case of records containing large pulses, the response is controlled by E_{ucpe}, the participation of E_{ucpr} is minimal, the structure could reach incremental collapse, and CDI is controlled by the first term of equation (5.1). In the other extreme, when the response contains many repeated cycles of plastic displacements, E_{ucpr} is larger than E_{ucpe}, the structure could reach low-cycle fatigue, its performance is controlled by E_{ucpr}, and the second term of equation (5.1) controls CDI.

The proposed CDI is a simple tool to estimate structural damage due to earthquakes, similar to other successful proposed damage indices. The difference is that the one proposed here considers the cyclic plastic response.

5.3.3 The parameter β_c and the possible values for the CDI

The baseline for the proposed CDI is the SDPL; therefore, the first step to estimate the CDI is to carry the column to a SDPL. This is accomplished by scaling up or down the selected records until one or more than one flexural failure mechanism occurs for each of the ground motions. The fiber finite element model (FFEM) will provide the dissipated energies from the responses of the column. The energy capacity is calculated as indicated above.

Once the column reaches SDPL, in equation (5.1) CDI = 1 and the value of β_c is

$$\beta_c = \frac{E_c - E_{ucpe}}{E_{ucpr}} \tag{5.2}$$

For subduction and crustal earthquakes and for very soft soil records there will be many cycles during the response; therefore, E_{ucpr} is large and the parameter $\beta_c < 1.0$. In this case, β_c is a parameter that serves to regulate the importance of E_{ucpr} on the damage. Since β_c is a fixed value for the bridge column and for the record, any aftershock or future earthquake could increase E_{ucpr}, thereby increasing CDI to values larger than 1.0.

Near fault records present very different characteristics. Some of them show very large pulses and a small number of cycles, so that when the column reaches SDPL $\beta_c > 1.0$. In these cases β_c does not control the importance of E_{ucpr} because the response tends to be similar to the one obtained from a pushover.

In addition to the above reasoning, when $E_c = E_{ucpe}$, $\beta_c = 0$. In this case, the energy capacity is equal to the energy dissipated by the new plastic excursions. The response is one complete cycle, and the energy dissipated by the repeated plastic displacements is equal to E_{ucpe}. It is also possible for E_{ucpr} to be small, but since $E_c = E_{ucpe}$, $\beta_c = 0$. This can happen for near fault records when the enveloping plastic displacements are so large that $E_{ucpe} = E_c$.

When $E_c - E_{ucpe} = E_{ucpr}$, $\beta_c = 1$. This can happen when E_c is much larger than E_{ucpe} and there are many repeated cycles. No matter the difference between E_c and E_{ucpe}, as long as $E_{ucpr} > E_c - E_{ucpe}$, the value for β_c will be between 0 and 1. The results clearly show that β_c is a parameter that depends on the characteristics of the excitation and the column.

Since the SDPL is associated with CDI = 1.0, once the column is subjected to the ground motions scaled according to the codes, the values for the CDI will vary with respect to the SDPL. A CDI = 1.0 indicates that the damage for the code scaled record is equal to the SDPL. A CDI > 1.0 indicates that the damage due to the code scaled record is larger than the SDPL. A CDI < 1.0 indicates that the damage due to the code scaled record is less than the SDPL.

If in one or more bridge columns the CDI is equal or larger than 1.0 the vulnerability of the complete bridge structure increases. Therefore, the CDI can be considered not only as a local damage index but also as a global one.

Notice that another difference between the CDI and other damage indices is that the CDI can reach values as indicated above, whereas known damage indices are characterized by the limit values of 0 if the structure remains elastic or 1 if it reaches a potential state of collapse.

In this chapter, CDIs will be calculated for the main shock and aftershocks. The proposed CDI is calculated for the three bridge columns already designed in Chapter 4.

5.4 Cyclic damage index study of three code-designed bridge columns

5.4.1 General remarks

In Chapter 4, three bridge columns with different periods T were designed according to the new AASHTO (2007) and Caltrans (2006) codes. These columns are now studied to obtain the SDPL, the associated parameter β_c, and the CDI. The three columns will now be subjected to 28 records of severe earthquakes grouped in four different bins.

The four bins are subduction, soft soils, crustal, and near fault earthquake records. The first 21 records have long durations; therefore, there are many cycles of inelastic response, and β_c controls the importance of E_{ucpr} at SDPL < 1.0. The fourth bin containing near fault records will yield small values of E_{ucpr}, and therefore β_c values can become even larger than 1.0. For this reason the proposed CDI is not valid for near fault records with small E_{ucpr} because their response is of the pushover type. The results for these records are shown in Appendix C.2.

Once SDPL and β_c have been obtained, the records are applied to the columns with scale factor equal to 1.0. This scaling is not the one prescribed by the code, but it was chosen in this study to give a uniform way to compare the damage in the three columns due to the 28 records. In equation (5.1) the CDI is normalized by the energy capacity of the bridge column; therefore, in what follows the energy capacity E_c is calculated for each column.

5.4.2 Energy capacity for the T = 0.5 s bridge column

Figure 5.1 a shows the hysteretic response for the T = 0.5 s column. The maximum lateral displacement response due to the sine function is 12 cm, which is lower than the 13.8 cm capacity, as shown in Figure 4.2 b. Therefore, there should be no crushing of the confined concrete. Figure 5.1 b shows the time history displacement response of the column.

Figure 5.1 c shows the strain time history for the confined concrete at a location close to bar 13 and for steel bar 1. Both locations are for the more strained fiber in each column material. In all strain graphics the steel tension strains are read above the zero strain line and the confined concrete compression strains below the zero strain line. Figure 5.1 c shows that the maximum steel strain is 0.05, lower than ε_{su} = 0.09. Therefore, according to AASHTO (2007) there is no tensile fracture of the bar and the confined compressive concrete strain is 0.015, lower than ε_{cu} = 0.018, as given by Mander et al. (1988) and prescribed by AASHTO (2007). This proves that there is no crushing of the concrete. In Figure 5.1 c it is noted that the tensile strain in bar 1 reaches 0.05, but this bar is close to the unconfined concrete fiber. Therefore, the cover concrete has cracked. By a similar reasoning, the compressive strain in the confined concrete close to bar 13 is 0.015, and therefore, the cover concrete close to the location of this measure has crushed.

The axial force on the bridge column is 2850 kN, the moment capacity is 5020 kN m and the product P-Δ is $0.07M_p$, less than the $0.25M_p$ prescribed by AASHTO (2007). Therefore, there is no P-Δ effect.

Figure 5.1 d illustrates that bar 1 fractures because of low-cyclic fatigue. This is the only flexure failure mechanism that occurs because of the one cyclic sine displacement applied to the bridge column. Therefore, the column reached SDPL, and the energy calculated for the hysteretic response represents the energy capacity of the column under analysis. The area under the hysteretic response gives E_c = 521.2 kN m.

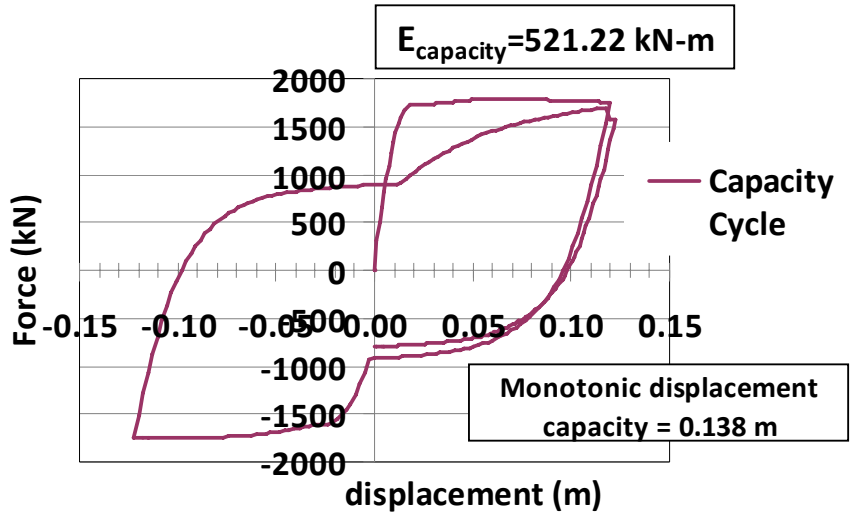

(a)

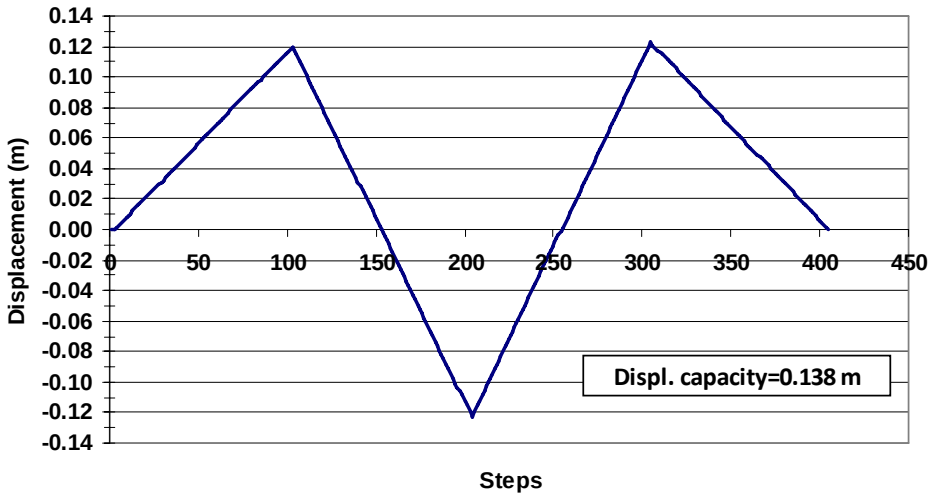

(b)

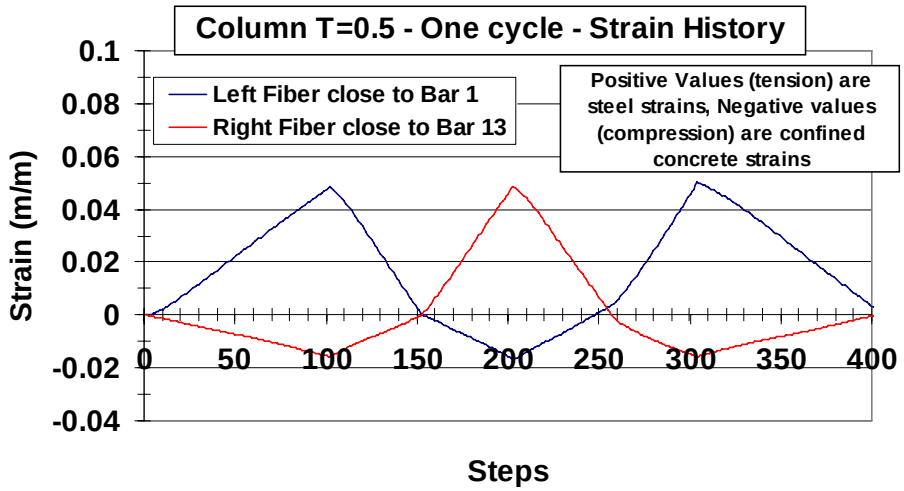

(c)

Figure 5.1 One cycle capacity analysis for *T*=0.5 s column

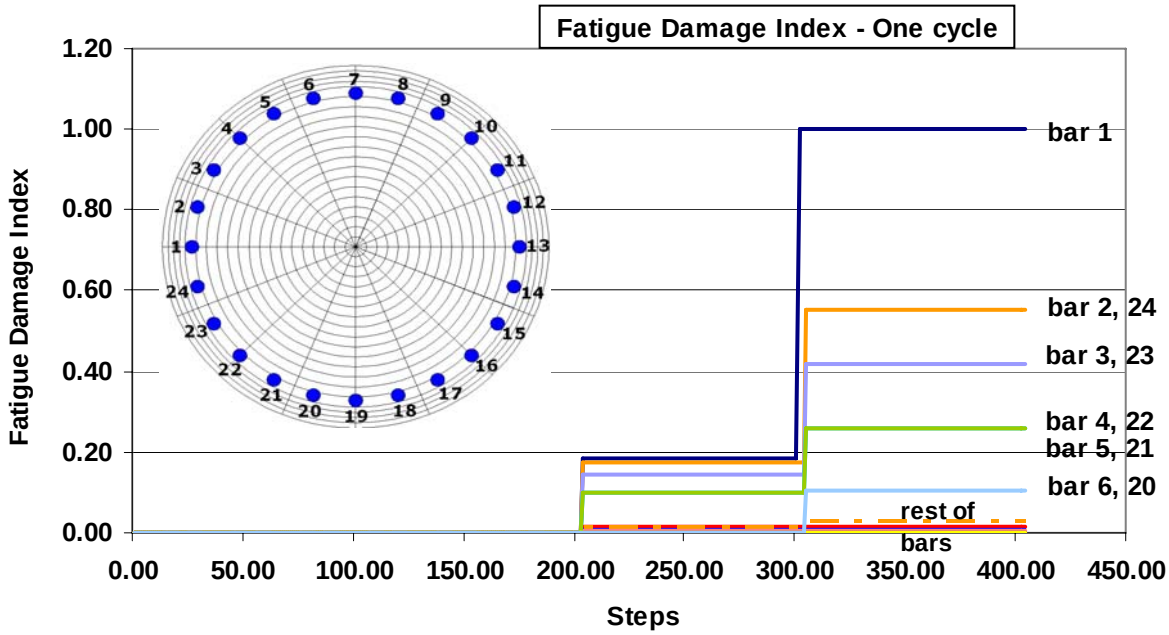

(d)

Figure 5.1 (cont.) One cycle capacity analysis for *T*=0.5 s column

5.4.3 Energy capacity for the *T* = 1.0 s bridge column

Figure 5.2 a shows the hysteretic response for the T = 1.0 s column. The maximum lateral displacement is 21 cm, which is less than the 24 cm displacement capacity, as seen in Figure 4.2 c. Figure 5.2 b shows the time history response for this column.

Figure 5.2 c shows that the maximum strain for the confined concrete at a location close to bar 13 is 0.016, less than ε_{cu} = 0.018, and that the maximum steel strain for bar 1 is 0.05, less than ε_{su} = 0.09. Both limits are imposed by AASHTO (2007), and the locations of the strains measured are for the more strained fiber in each material. The confined concrete does not crush, and the steel does not fracture due to flexural tension. The unconfined concrete cracks and crushes.

The axial force on the column is 2850 kN, and the moment capacity is 4080 kN m. The product P-Δ is 0.14M_p, lower than the 0.25M_p prescribed by AASHTO. Therefore, there is no P-Δ effect.

Figure 5.2 d illustrates that the only flexural failure occurs in bar 1 because of low-cyclic fatigue carrying the column to a SDPL. The area under the hysteretic response gives E_c = 548.8 kN m.

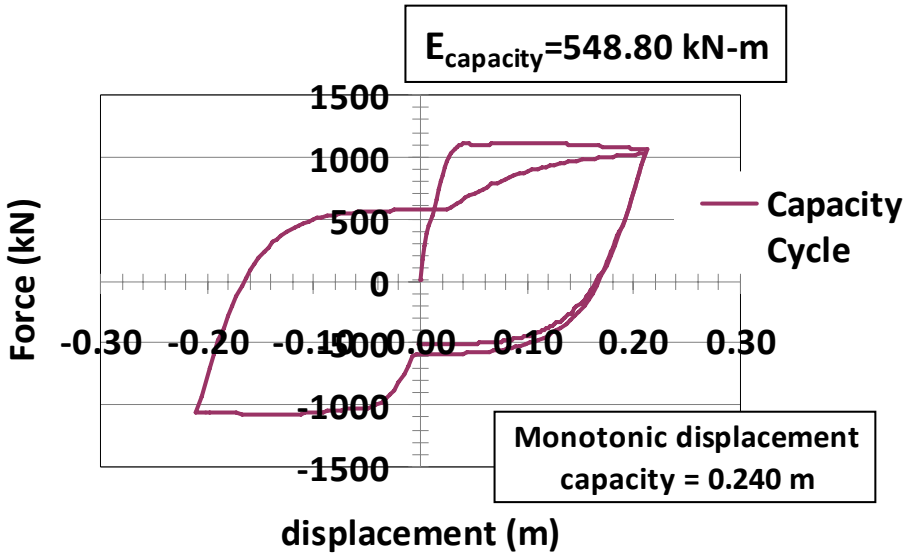

(a)

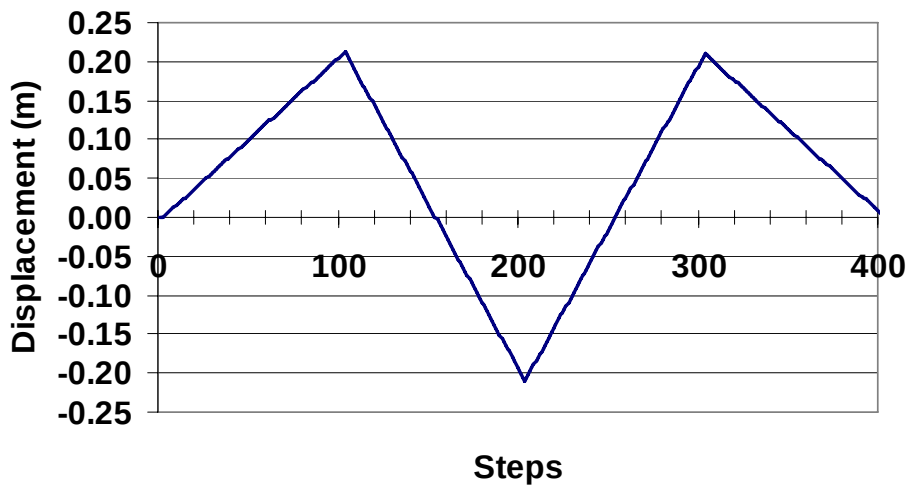

(b)

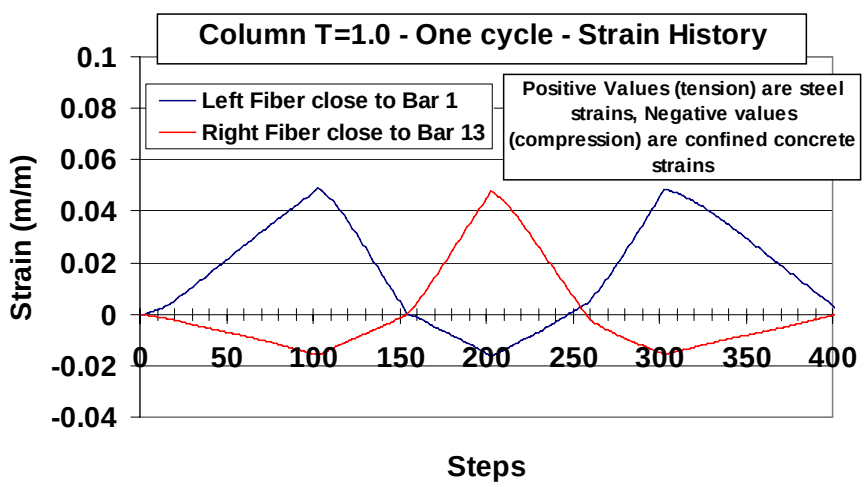

(c)

Figure 5.2 One cycle capacity analysis for *T*=1.0 s column

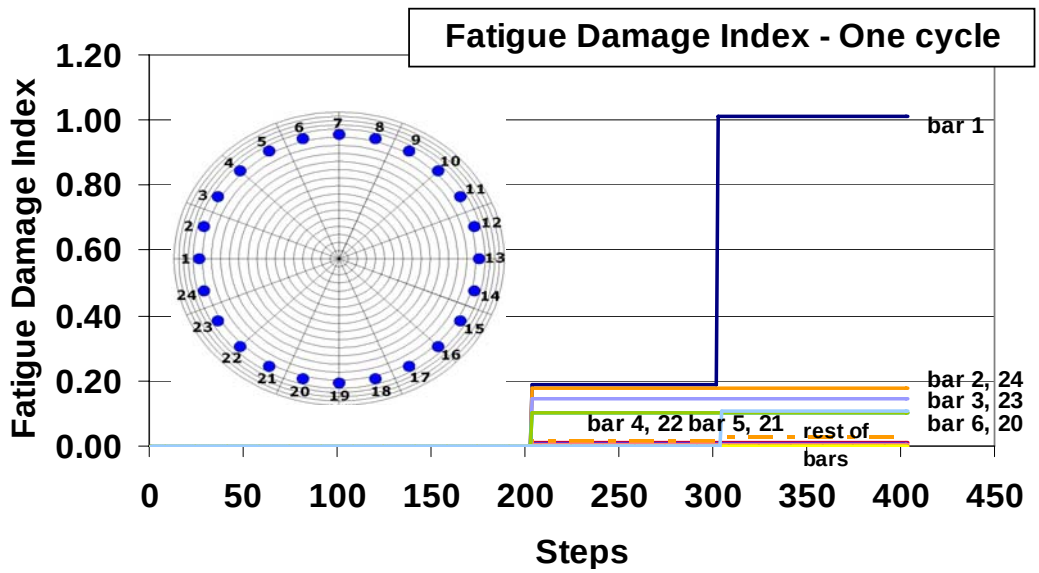

(d)

Figure 5.2 (cont.) One cycle capacity analysis for *T*=1.0 s column

5.4.4 Energy capacity for the *T* = 1.5 s bridge column

Figure 5.3 a shows the hysteretic response for this column. The maximum lateral displacement is 33 cm, and the displacement capacity calculated according to AASHTO (2007) is 38 cm (Figure 4.2 d). Figure 5.3 b shows the time history response of this column.

Figure 5.3 c shows that the maximum strain for the confined concrete at a location close to bar 13 is 0.016, lower than ε_{cu} = 0.018, and the maximum steel strain for bar 1 is 0.05, lower than ε_{su} = 0.09. The locations of the strains measured are for the more strained fiber in each material for the column. There is no crushing of the confined concrete, and the steel does not fracture due to flexural tension. These measures indicate that the unconfined cover concrete cracks and crushes.

The axial force on the column is 2850 kN, and the moment capacity is 3680 kN m. The product P-Δ is $0.25M_p$, equal to the $0.25M_p$ prescribed by AASHTO. Therefore, there is no P-Δ effect.

Figure 5.3 d illustrates that bar number 1 fractures owing to low-cyclic fatigue carrying the column to the SDPL. The area under the hysteretic response gives E_c = 631.9 kN m.

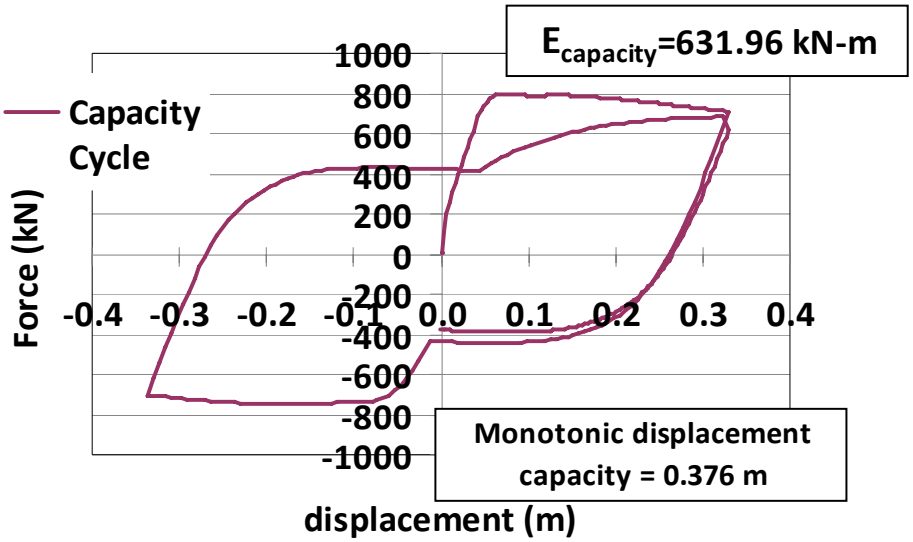

(a)

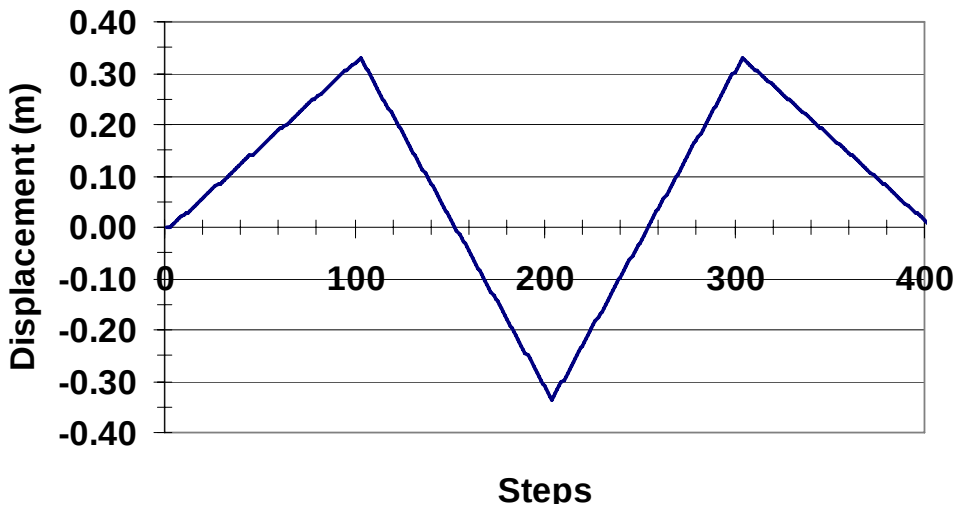

(b)

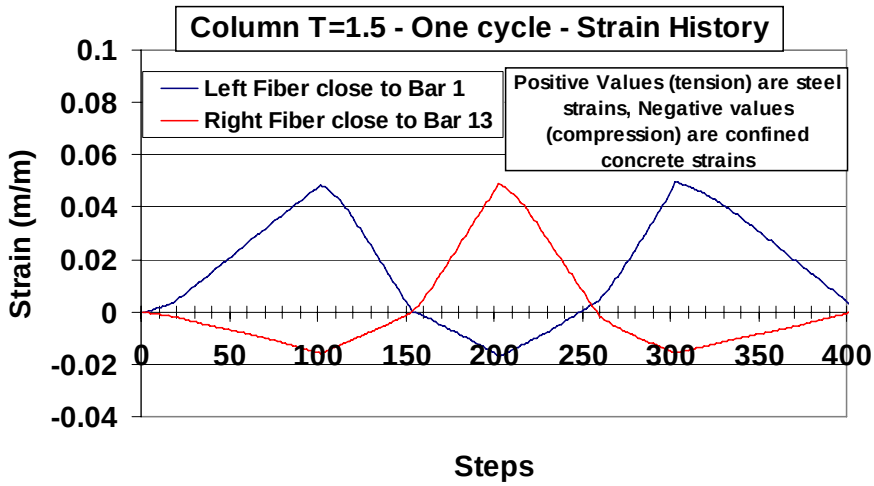

(c)

Figure 5.3 One cycle capacity analysis for *T*=1.5 s column

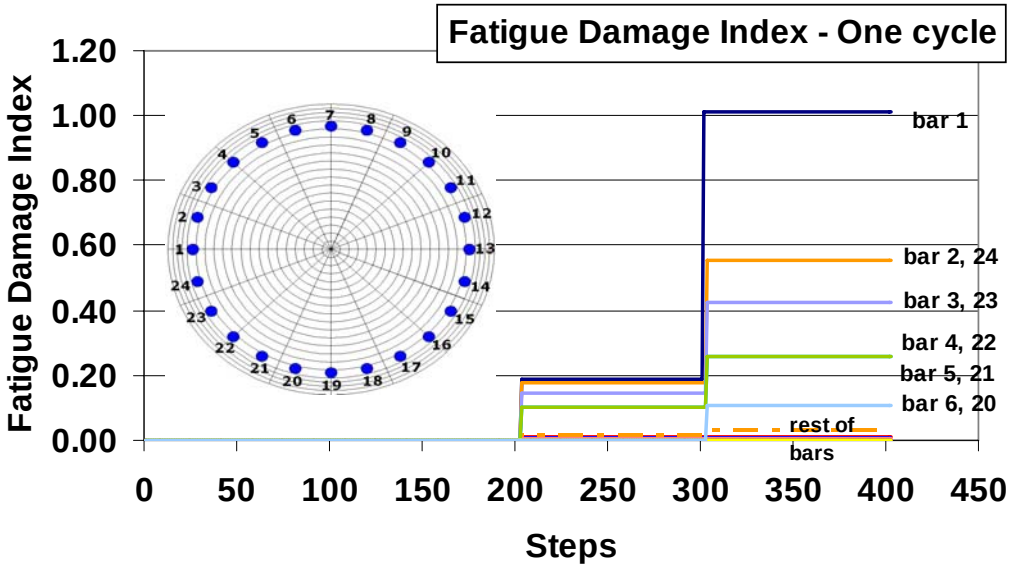

(d)

Figure 5.3 (cont.) One cycle capacity analysis for *T*=1.5 s column

5.4.5 Determination of β_c values once the column reaches SDPL

Tables 5.1, 5.2, and, 5.3 show, for each of the records and for each bridge column, the duration, the peak ground acceleration, the period of the record T_g, the scale factor applied to the record so the column reaches SDPL, the failure type, the number of fatigued bars, the time of failure, the maximum displacement at the time of failure, the energy capacity, the envelope, and the repeated energies and the calculated values of β_c for each record and for each of the bins, except the near fault bin records. In addition, the average value for β_c for each bin is also indicated.

The results of the three columns at SDPL for each one of the 21 records are discussed in Appendixes C.3, C.4, and C.5.

5.4.5.1 β_c values for the *T* = 0.5 s column

Table 5.1 shows that the SDPL for the *T* = 0.5 s column is reached for 20 scaled records by fracture of one bar due to low-cyclic fatigue. The exceptions are the following two cases: For the Melipilla record scaled 1.49 times its original amplitudes there is, first, crushing of the confined and unconfined concrete and, later, fracture of one bar due to low-cyclic fatigue. For the Tihuac Deportivo record scaled 1.05 times its original amplitudes there is crushing of the confined and unconfined concrete and no other failure mechanism. As seen in Appendix C.3, the scaled Tihuac Deportivo record induces damage in two steel bars that lost about 50% of their fatigue

life and in four more bars that lost about 18% of their fatigue life. Therefore, in addition to crushing the concrete, this record induced fatigue in some bars, damaging them but without reaching fracture due to low-cyclic fatigue.

The average β_c values for the T = 0.5 s column is 0.156 for the subduction scaled records, 0.16 for the scaled soft soil records, and 0.175 for the crustal scaled records.

5.4.5.2 β_c values for the T = 1.0 s column

Table 5.2 shows similar results to those in Table 5.1. The failure mechanism that carries the column to the SDPL for 20 subduction scaled records is the fracture of one bar due to low-cyclic fatigue except in one case. The Sismex Viveros record scaled 2.98 times its original accelerations induced the crushing of the confined and unconfined concrete and no other failure mechanism.

The average β_c values for this column are 0.108 for the scaled subduction records, 0.14 for the scaled soft soil records, and 0.175 for the scaled crustal records, as seen in Appendix C.4.

Table 5.1 β_c values for T = 0.5 s bridge column

Calculation of β_c - Circular Column T=0.5s																		
		EQ	Duration (s)	PGA (%g)	Tg (s)	Scale Factor (CDI=1)	Failure type	Number of fatigued bars	Time (failure)	Max. Displacement (m)	Energy Capacity, Ec (kN-m)	Enveloping Energy, Eucpe (kN-m)	Repeated Energy, Eucpr (kN-m)	Eucpe/Ec	Eucpr/Ec	β_c	β_c average
BIN 1 - SUBDUCTION	1	Valparaiso,1985 (Chile)	79.37	0.180	0.49	2.67	LOW-CYCLE-FATIGUE	1	57.34	0.109	521.22	345.59	1367.46	0.66	2.62	0.128	0.156
	2	Llolleo,1985 (Chile)	116.38	0.710	0.45	0.95	LOW-CYCLE-FATIGUE	1	50.98	0.092	521.22	337.81	1460.39	0.65	2.80	0.126	
	3	Llayllay,1985 (Chile)	62.45	0.460	0.69	0.97	LOW-CYCLE-FATIGUE	1	60.02	0.076	521.22	255.94	1835.14	0.49	3.52	0.145	
	4	Pisco, 2007 (Perú)	67.00	0.300	0.82	0.87	LOW-CYCLE-FATIGUE	1	35.73	0.128	521.22	366.78	618.55	0.70	1.19	0.250	
	5	Caleta,1985 (México)	50.63	0.154	1.05	1.88	LOW-CYCLE-FATIGUE	1	38.76	0.103	521.22	380.44	804.86	0.73	1.54	0.175	
	6	Viña del Mar,1985 (Chile)	112.59	0.363	0.69	1.10	LOW-CYCLE-FATIGUE	1	71.78	0.097	521.22	276.81	1799.48	0.53	3.45	0.136	
	7	Melipilla,1985 (Chile)	79.32	0.686	0.35	1.49	$\varepsilon_c > \varepsilon_{cu}$ + LOW CYCLE FATIGUE	1	23.00	0.140	521.22	414.43	801.09	0.80	1.54	0.133	
BIN 2 - SOFT SOIL	8	SCT1,1985 (Mexico)	164.00	0.163	2.00	0.63	LOW-CYCLE-FATIGUE	1	64.04	0.116	521.22	458.33	541.62	0.88	1.04	0.116	0.160
	9	CDAF,1985 (Mexico)	60.00	0.082	2.10	1.47	LOW-CYCLE-FATIGUE	1	53.34	0.118	521.22	409.42	863.33	0.79	1.66	0.130	
	10	CDAO,1985 (Mexico)	180.00	0.082	3.90	1.39	LOW-CYCLE-FATIGUE	1	110.80	0.116	521.22	427.34	1182.68	0.82	2.27	0.079	
	11	Tlhuac Bombas,1985 (Mexico)	150.00	0.106	3.70	0.90	LOW-CYCLE-FATIGUE	1	71.70	0.112	521.22	450.89	593.10	0.87	1.14	0.119	
	12	Tlhuac Deportivo,1985 (Mexico)	150.00	0.120	2.10	1.04	$\varepsilon_c > \varepsilon_{cu}$	0	60.93	0.140	521.22	383.07	332.45	0.73	0.64	0.416	
	13	Sismex Viveros,1985 (Mexico)	60.00	0.045	1.34	3.55	LOW-CYCLE-FATIGUE	1	48.10	0.105	521.22	351.26	1345.81	0.67	2.58	0.126	
	14	TXSO,1985 (Mexico)	214.05	0.105	2.00	0.97	LOW-CYCLE-FATIGUE	1	86.73	0.111	521.22	350.73	1243.26	0.67	2.39	0.137	
BIN 3 - CRUSTAL	15	El Centro,1940 (USA)	31.20	0.320	0.46	1.42	LOW-CYCLE-FATIGUE	1	26.46	0.118	521.22	356.53	596.48	0.68	1.14	0.276	0.166
	16	Loma Prieta - San Francisco Airport,1989 (USA)	39.96	0.235	0.90	2.76	LOW-CYCLE-FATIGUE	1	37.94	0.121	521.22	470.33	1003.50	0.90	1.93	0.051	
	17	Loma Prieta - Hollister City, 1989 (USA)	39.09	0.260	0.91	1.28	LOW-CYCLE-FATIGUE	1	26.33	0.111	521.22	455.30	654.95	0.87	1.26	0.101	
	18	Loma Prieta - Sunnyvale, 1989 (USA)	39.24	0.210	2.86	1.29	LOW-CYCLE-FATIGUE	1	23.79	0.100	521.22	399.49	782.96	0.77	1.50	0.155	
	19	San Fernando - Hollywood Sto., 1971 (USA)	79.46	0.170	2.00	3.30	LOW-CYCLE-FATIGUE	1	15.86	0.121	521.22	359.13	670.68	0.69	1.29	0.242	
	20	Northridge - St. Centinela, 1994 (USA)	44.00	0.330	0.87	1.81	LOW-CYCLE-FATIGUE	1	26.06	0.129	521.22	394.74	635.85	0.76	1.22	0.199	
	21	Coalinga - Parkfield, 1983 (USA)	59.98	0.135	0.63	5.67	LOW-CYCLE-FATIGUE	1	58.72	0.087	521.22	280.76	1781.14	0.54	3.42	0.135	

Table 5.2 β_c values for T = 1.0 s bridge column

Calculation of β_c - Circular Column T=1.0s																		
		EQ	Duration (s)	PGA (%g)	Tg (s)	Scale Factor (CDI=1)	Failure type	Number of fatigued bars	Time (failure)	Max. Displacement (m)	Energy Capacity, Ec (kN-m)	Enveloping Energy, Eucpe (kN-m)	Repeated Energy, Eucpr (kN-m)	Eucpe/Ec	Eucpr/Ec	β_c	β_c average
BIN 1 - SUBDUCTION	1	Valparaiso,1985 (Chile)	79.37	0.180	0.49	3.71	LOW-CYCLE-FATIGUE	1	72.71	0.222	548.80	420.78	1167.73	0.77	2.13	0.110	0.108
	2	Llolleo,1985 (Chile)	116.38	0.710	0.45	1.56	LOW-CYCLE-FATIGUE	1	49.99	0.170	548.80	419.76	1225.10	0.76	2.23	0.105	
	3	Llayllay,1985 (Chile)	62.45	0.460	0.69	1.75	LOW-CYCLE-FATIGUE	1	57.34	0.195	548.80	387.68	1507.55	0.71	2.75	0.107	
	4	Pisco, 2007 (Perú)	67.00	0.300	0.82	1.11	LOW-CYCLE-FATIGUE	1	52.93	0.172	548.80	407.93	1004.48	0.74	1.83	0.140	
	5	Caleta,1985 (México)	50.63	0.154	1.05	2.28	LOW-CYCLE-FATIGUE	1	36.95	0.207	548.80	492.37	618.70	0.90	1.13	0.091	
	6	Viña del Mar,1985 (Chile)	112.59	0.363	0.69	2.32	LOW-CYCLE-FATIGUE	2	60.61	0.165	548.80	385.36	1985.66	0.70	3.62	0.082	
	7	Melipilla,1985 (Chile)	79.32	0.686	0.35	1.79	LOW-CYCLE-FATIGUE	1	60.82	0.191	548.80	462.47	715.89	0.84	1.30	0.121	
BIN 2 - SOFT SOIL	8	SCT1,1985 (Mexico)	164.00	0.163	2.00	0.50	LOW-CYCLE-FATIGUE	1	74.38	0.185	548.80	384.30	1276.91	0.70	2.33	0.129	0.140
	9	CDAF,1985 (Mexico)	60.00	0.082	2.10	0.96	LOW-CYCLE-FATIGUE	1	53.48	0.155	548.80	320.37	1325.63	0.58	2.42	0.172	
	10	CDAO,1985 (Mexico)	180.00	0.082	3.90	0.88	LOW-CYCLE-FATIGUE	1	114.90	0.165	548.80	336.53	1548.07	0.61	2.82	0.137	
	11	Tlhuac Bombas,1985 (Mexico)	150.00	0.106	3.70	0.59	LOW-CYCLE-FATIGUE	1	72.69	0.183	548.80	424.24	876.88	0.77	1.60	0.142	
	12	Tlhuac Deportivo,1985 (Mexico)	150.00	0.120	2.10	1.02	LOW-CYCLE-FATIGUE	1	80.07	0.207	548.80	399.44	1105.84	0.73	2.02	0.135	
	13	Sismex Viveros,1985 (Mexico)	60.00	0.045	1.34	2.98	$\varepsilon_c > \varepsilon_{cu}$	0	27.40	0.246	548.80	430.17	787.40	0.78	1.43	0.151	
	14	TXSO,1985 (Mexico)	214.05	0.105	2.00	1.00	LOW-CYCLE-FATIGUE	1	147.87	0.162	548.80	338.70	1799.81	0.62	3.28	0.117	
BIN 3 - CRUSTAL	15	El Centro,1940 (USA)	31.20	0.320	0.46	1.72	LOW-CYCLE-FATIGUE	1	25.52	0.202	548.80	422.69	518.67	0.77	0.95	0.243	0.175
	16	Loma Prieta - San Francisco Airport,1989 (USA)	39.96	0.235	0.90	4.00	LOW-CYCLE-FATIGUE	1	36.68	0.184	548.80	404.32	772.99	0.74	1.41	0.187	
	17	Loma Prieta - Hollister City, 1989 (USA)	39.09	0.260	0.91	1.64	LOW-CYCLE-FATIGUE	1	38.13	0.230	548.80	519.47	716.70	0.95	1.31	0.041	
	18	Loma Prieta - Sunnyvale, 1989 (USA)	39.24	0.210	2.86	1.00	LOW-CYCLE-FATIGUE	1	36.35	0.173	548.80	415.60	824.28	0.76	1.50	0.162	
	19	San Fernando - Hollywood Sto., 1971 (USA)	79.46	0.170	2.00	3.24	LOW-CYCLE-FATIGUE	1	26.02	0.236	548.80	356.72	536.16	0.65	0.98	0.358	
	20	Northridge - St. Centinela, 1994 (USA)	44.00	0.330	0.87	2.55	LOW-CYCLE-FATIGUE	1	43.38	0.182	548.80	453.58	956.40	0.83	1.74	0.100	
	21	Coalinga - Parkfield, 1983 (USA)	59.98	0.135	0.63	9.41	LOW-CYCLE-FATIGUE	1	56.38	0.161	548.80	304.64	1772.03	0.56	3.23	0.138	

5.4.5.3 β_c values for the T = 1.5 s column

A similar situation as for the T = 0.5 s and the T = 1.0 s columns is observed for the T = 1.5 s column, as shown in Table 5.3. For 20 of the 21 crustal scaled records the T = 1.5 s column suffers fracture of one bar due to low-cyclic fatigue when it reaches SDPL. The exception is for the San Fernando – Hollywood Storage record that carries the column to crushing of the confined and unconfined concrete and no other failure mechanism. This record is scaled 3.18 times. With respect to fatigue, this record induced 20% fatigue life loss in bar 1 and 4% fatigue life loss in bar 13, as seen in Appendix C.5.

Table 5.3 β_c values for T = 1.5 s bridge column

Calculation of β_c - Circular Column T=1.5s																		
		EQ	Duration (s)	PGA (%g)	Tg (s)	Scale Factor (CDI=1)	Failure type	Number of fatigued bars	Time (failure)	Max. Displacement (m)	Energy Capacity, Ec (kN-m)	Enveloping Energy, Eucpe (kN-m)	Repeated Energy, Eucpr (kN-m)	Eucpe/Ec	Eucpr/Ec	β_c	β_c average
BIN 1 - SUBDUCTION	1	Valparaiso,1985 (Chile)	79.37	0.180	0.49	5.58	LOW-CYCLE-FATIGUE	1	75.55	0.260	631.96	416.48	1594.92	0.66	2.52	0.135	0.163
	2	Llolleo,1985 (Chile)	116.38	0.710	0.45	2.54	LOW-CYCLE-FATIGUE	1	98.45	0.323	631.96	491.49	1500.24	0.78	2.37	0.094	
	3	Llayllay,1985 (Chile)	62.45	0.460	0.69	2.74	LOW-CYCLE-FATIGUE	1	53.68	0.281	631.96	466.78	1416.06	0.74	2.24	0.117	
	4	Pisco, 2007 (Perú)	67.00	0.300	0.82	1.42	LOW-CYCLE-FATIGUE	1	55.46	0.296	631.96	362.90	944.62	0.57	1.49	0.285	
	5	Caleta,1985 (México)	50.63	0.154	1.05	3.40	LOW-CYCLE-FATIGUE	1	41.79	0.306	631.96	466.55	811.51	0.74	1.28	0.204	
	6	Viña del Mar,1985 (Chile)	112.59	0.363	0.69	3.54	LOW-CYCLE-FATIGUE	1	69.48	0.282	631.96	399.83	1932.58	0.63	3.06	0.120	
	7	Melipilla,1985 (Chile)	79.32	0.686	0.35	1.99	LOW-CYCLE-FATIGUE	3	38.69	0.380	631.96	516.89	610.02	0.82	0.97	0.189	
BIN 2 - SOFT SOIL	8	SCT1,1985 (Mexico)	164.00	0.163	2.00	0.78	LOW-CYCLE-FATIGUE	1	126.64	0.251	631.96	417.82	1466.18	0.66	2.32	0.146	0.154
	9	CDAF,1985 (Mexico)	60.00	0.082	2.10	1.31	LOW-CYCLE-FATIGUE	1	56.52	0.256	631.96	404.80	1651.79	0.64	2.61	0.138	
	10	CDAO,1985 (Mexico)	180.00	0.082	3.90	0.65	LOW-CYCLE-FATIGUE	1	165.08	0.213	631.96	328.12	2163.90	0.52	3.42	0.140	
	11	Tlhuac Bombas,1985 (Mexico)	150.00	0.106	3.70	0.53	LOW-CYCLE-FATIGUE	1	76.80	0.353	631.96	440.16	847.37	0.70	1.34	0.226	
	12	Tlhuac Deportivo,1985 (Mexico)	150.00	0.120	2.10	1.14	LOW-CYCLE-FATIGUE	1	145.26	0.275	631.96	316.28	1177.81	0.50	1.86	0.268	
	13	Sismex Viveros,1985 (Mexico)	60.00	0.045	1.34	3.78	LOW-CYCLE-FATIGUE	1	46.10	0.339	631.96	596.56	925.79	0.94	1.46	0.038	
	14	TXSO,1985 (Mexico)	214.05	0.105	2.00	1.57	LOW-CYCLE-FATIGUE	1	178.77	0.223	631.96	341.74	2414.19	0.54	3.82	0.120	
BIN 3 - CRUSTAL	15	El Centro,1940 (USA)	31.20	0.320	0.46	2.37	LOW-CYCLE-FATIGUE	1	20.38	0.362	631.96	616.15	532.58	0.97	0.84	0.030	0.222
	16	Loma Prieta - San Francisco Airport,1989 (USA)	39.96	0.235	0.90	6.02	LOW-CYCLE-FATIGUE	1	34.94	0.368	631.96	491.61	657.15	0.78	1.04	0.214	
	17	Loma Prieta - Hollister City, 1989 (USA)	39.09	0.260	0.91	2.61	LOW-CYCLE-FATIGUE	1	32.96	0.294	631.96	493.47	1083.02	0.78	1.71	0.128	
	18	Loma Prieta - Sunnyvale, 1989 (USA)	39.24	0.210	2.86	1.37	LOW-CYCLE-FATIGUE	1	36.56	0.264	631.96	420.43	1079.46	0.67	1.71	0.196	
	19	San Fernando - Hollywood Sto., 1971 (USA)	79.46	0.170	2.00	3.18	$\varepsilon_c > \varepsilon_{cu}$	0	12.40	0.381	631.96	401.07	314.52	0.63	0.50	0.734	
	20	Northridge - St. Centinela, 1994 (USA)	44.00	0.330	0.87	3.38	LOW-CYCLE-FATIGUE	1	40.14	0.335	631.96	535.26	824.17	0.85	1.30	0.117	
	21	Coalinga - Parkfield, 1983 (USA)	59.98	0.135	0.63	13.70	LOW-CYCLE-FATIGUE	1	42.40	0.273	631.96	422.13	1538.74	0.67	2.43	0.136	

The average values for the parameter β_c for the T = 1.5 s column are 0.163 for the scaled subduction records, 0.153 for the scaled soft soil records, and 0.222 for the scaled crustal earthquake records.

5.5 Estimation of damage through the cyclic damage index

5.5.1 Introduction

Once the SDPL has been determined for each of the three code-designed columns subjected to the 21 scaled records and the values for β_c have been obtained, it is necessary to estimate the damage of the bridge columns for the same records but with a different scale factor. In order to

compare results it was decided not to follow code recommendations in regard to scaling of the records for design and use the 21 records but without scaling them.

The near fault records are not considered, since the large pulses induce a response with small dissipation of energy. Therefore, β_c does not control the effect of the repeated plastic displacements in the damage of the column. .

It should be recalled that, once determined, β_c is an invariant for the bridge column and the SDPL, so it will be used to calculate the CDI. In addition, the energy capacity E_c is also an invariant for the column.

5.5.2 CDI for the *T* = 0.5 s bridge column

Tables 5.4, 5.5, and 5.6 show the name of the record, the scale factor that is equal to 1.0 for all of them, the energy capacity, the envelope and the repeated energies, the β_c values copied for convenience, the calculated CDI of the column for each record, the failure type, the maximum displacement, and the relation between the number of fatigued bars and the fatigue life lost during the response of the column. The fatigue life lost is equivalent to the fatigue damage index (FDI). The discussion of the results is presented in Appendix C.6.

Table 5.4 shows that for most of the records there is no failure mechanism in this column. However, the unscaled records induce damage in the steel bars, making them lose a percentage of their fatigue life. With respect to the few flexural failures shown in Table 5.4 for the Pisco, the SCT-1, and the Tihuac Bombas unscaled records, there is crushing of the confined and unconfined concrete and, later during the same run, fracture of the longitudinal bars due to low-cyclic fatigue. The unscaled Pisco record induces the fracture of seven bars, the SCT-1 unscaled record fractures 20 bars, and the unscaled Tihuac Bombas record fractures all 24 bars. For the Llolleo, Llayllay, and TXSO unscaled records there is fracture due to low-cyclic fatigue in three, one, and five bars, respectively. The CDIs larger than 1.0, showing that there is damage above the SDPL, are 1.04 for the Llolleo and Llayllay records, 1.34 for Pisco, 1.6 for SCT-1, 1.79 for Tihuac Bombas, and, 1.14 for the TXSO record.

Table 5.4 CDI for the T = 0.5 s bridge column

Circular Column T=0.5s			CDI values for records with Scale Factor (SF) = 1								
		EQ	Scale factor	Energy Capacity, Ec (kN-m)	Enveloping Energy, Eucpe (kN-m)	Repeated Energy, Eucpr (kN-m)	β_c	CDI	Failure type	Max. Displacement (m)	Number of fatigued bars / FDI of critical bar
BIN 1 - SUBDUCTION	1	Valparaiso,1985 (Chile)	1.00	521.22	51.07	218.75	0.128	0.15	NO FAILURE	0.026	0 / 0.05
	2	Llolleo,1985 (Chile)	1.00	521.22	346.71	1570.10	0.126	1.04	LOW-CYCLE-FATIGUE	0.092	3 / 1.00
	3	Llayllay,1985 (Chile)	1.00	521.22	265.02	1916.53	0.145	1.04	LOW-CYCLE-FATIGUE	0.079	1 / 1.00
	4	Pisco, 2007 (Perú)	1.00	521.22	493.83	827.90	0.250	1.34	$\varepsilon_c > \varepsilon_{cu}$ + LOW-CYCLE-FATIGUE	0.154	7 / 1.00
	5	Caleta,1985 (México)	1.00	521.22	71.20	209.98	0.175	0.21	NO FAILURE	0.030	0 / 0.05
	6	Viña del Mar,1985 (Chile)	1.00	521.22	250.11	1554.41	0.136	0.88	NO FAILURE	0.083	0 / 0.65
	7	Melipilla,1985 (Chile)	1.00	521.22	201.06	408.35	0.133	0.49	NO FAILURE	0.075	0 / 0.16
BIN 2 - SOFT SOIL	8	SCT1,1985 (Mexico)	1.00	521.22	738.38	831.14	0.116	1.60	$\varepsilon_c > \varepsilon_{cu}$ + LOW-CYCLE-FATIGUE	0.248	20 / 1.00
	9	CDAF,1985 (Mexico)	1.00	521.22	54.04	80.90	0.130	0.12	NO FAILURE	0.029	0 / 0.02
	10	CDAO,1985 (Mexico)	1.00	521.22	70.88	185.75	0.079	0.16	NO FAILURE	0.034	0 / 0.04
	11	Tlhuac Bombas,1985 (Mexico)	1.00	521.22	845.73	723.55	0.119	1.79	$\varepsilon_c > \varepsilon_{cu}$ + LOW-CYCLE-FATIGUE	0.348	24 / 1.00
	12	Tlhuac Deportivo,1985 (Mexico)	1.00	521.22	333.04	249.87	0.416	0.84	NO FAILURE	0.125	0 / 0.34
	13	Sismex Viveros,1985 (Mexico)	1.00	521.22	29.35	16.51	0.126	0.06	NO FAILURE	0.021	0 / 0.01
	14	TXSO,1985 (Mexico)	1.00	521.22	394.72	1459.29	0.137	1.14	LOW-CYCLE-FATIGUE	0.120	5 / 1.00
BIN 3 - CRUSTAL	15	El Centro,1940 (USA)	1.00	521.22	202.99	342.55	0.276	0.57	NO FAILURE	0.073	0 / 0.22
	16	Loma Prieta - San Francisco Airport,1989 (USA)	1.00	521.22	162.10	176.02	0.051	0.33	NO FAILURE	0.063	0 / 0.06
	17	Loma Prieta - Hollister City, 1989 (USA)	1.00	521.22	324.71	410.55	0.101	0.70	NO FAILURE	0.091	0 / 0.20
	18	Loma Prieta - Sunnyvale, 1989 (USA)	1.00	521.22	219.66	375.51	0.155	0.53	NO FAILURE	0.069	0 / 0.22
	19	San Fernando - Hollywood Sto., 1971 (USA)	1.00	521.22	61.92	27.54	0.242	0.13	NO FAILURE	0.030	0 / 0.01
	20	Northridge - St. Centinela, 1994 (USA)	1.00	521.22	185.55	181.14	0.199	0.43	NO FAILURE	0.073	0 / 0.10
	21	Coalinga - Parkfield, 1983 (USA)	1.00	521.22	42.58	73.30	0.135	0.10	NO FAILURE	0.027	0 / 0.02

5.5.3 CDI for the T = 1.0 s bridge column

As seen in Table 5.5, only six unscaled records induce a flexural failure mechanism in the T = 1.0 s column. The SCT-1 unscaled record fractures 16 longitudinal bars and later crushes the confined and unconfined concrete owing to a large displacement of 28 cm that induces concrete

strain larger than the ultimate. The Tihuac Bombas unscaled record crushes the confined and unconfined concrete owing to the large 32.2 cm displacement and later fracture of 17 longitudinal bars. Due to the strength deterioration induced by these two failures, the column is not able to continue supporting the ground motion; thus the run ends at t = 56 s. The other records induce damage due to fatigue in several percentages, as seen in Table 5.5. The discussion of the results is presented in Appendix C.7.

Table 5.5 CDI for T = 1.0 s bridge column

Circular Column T=1.0s			CDI values for records with Scale Factor (SF) = 1								
		EQ	Scale factor	Energy Capacity, Ec (kN-m)	Enveloping Energy, Eucpe (kN-m)	Repeated Energy, Eucpr (kN-m)	β_c	CDI	Failure type	Max. Displacement (m)	Number of fatigued bars / FDI of critical bar
BIN 1 - SUBDUCTION	1	Valparaiso,1985 (Chile)	1.00	548.80	79.71	138.40	0.1096	0.17	NO FAILURE	0.067	0 / 0.04
	2	Llolleo,1985 (Chile)	1.00	548.80	220.20	543.53	0.1053	0.51	NO FAILURE	0.110	0 / 0.19
	3	Llayllay,1985 (Chile)	1.00	548.80	169.03	624.15	0.1069	0.43	NO FAILURE	0.098	0 / 0.18
	4	Pisco, 2007 (Perú)	1.00	548.80	338.25	867.56	0.1402	0.84	NO FAILURE	0.157	0 / 0.48
	5	Caleta,1985 (México)	1.00	548.80	164.43	132.80	0.0912	0.32	NO FAILURE	0.097	0 / 0.07
	6	Viña del Mar,1985 (Chile)	1.00	548.80	191.76	399.97	0.0823	0.41	NO FAILURE	0.133	0 / 0.12
	7	Melipilla,1985 (Chile)	1.00	548.80	134.37	200.94	0.1206	0.29	NO FAILURE	0.090	0 / 0.05
BIN 2 - SOFT SOIL	8	SCT1,1985 (Mexico)	1.00	548.80	567.05	1281.94	0.1288	1.33	LOW-CYCLE-FATIGUE + $\varepsilon_c > \varepsilon_{cu}$	0.281	16 / 1.00
	9	CDAF,1985 (Mexico)	1.00	548.80	339.39	1419.31	0.1723	1.06	LOW-CYCLE-FATIGUE	0.162	3 / 1.00
	10	CDAO,1985 (Mexico)	1.00	548.80	562.80	1808.90	0.1371	1.48	LOW-CYCLE-FATIGUE	0.235	16 / 1.00
	11	Tlhuac Bombas,1985 (Mexico)	1.00	548.80	542.00	396.00	0.1420	1.09	$\varepsilon_c > \varepsilon_{cu}$ (Run ends at 56 seconds)	0.322	17 / 1.00
	12	Tlhuac Deportivo,1985 (Mexico)	1.00	548.80	389.81	1047.09	0.1351	0.97	NO FAILURE	0.203	0 / 0.55
	13	Sismex Viveros,1985 (Mexico)	1.00	548.80	42.29	63.33	0.1507	0.09	NO FAILURE	0.044	0 / 0.02
	14	TXSO,1985 (Mexico)	1.00	548.80	338.70	1799.81	0.1167	1.00	LOW-CYCLE-FATIGUE	0.162	1 / 1.00
BIN 3 - CRUSTAL	15	El Centro,1940 (USA)	1.00	548.80	157.03	172.31	0.2431	0.36	NO FAILURE	0.112	0 / 0.07
	16	Loma Prieta - San Francisco Airport,1989 (USA)	1.00	548.80	87.09	68.12	0.1869	0.18	NO FAILURE	0.085	0 / 0.02
	17	Loma Prieta - Hollister City, 1989 (USA)	1.00	548.80	299.22	322.16	0.0409	0.57	NO FAILURE	0.156	0 / 0.16
	18	Loma Prieta - Sunnyvale, 1989 (USA)	1.00	548.80	415.60	824.28	0.1616	1.00	LOW-CYCLE-FATIGUE	0.173	1 / 1.00
	19	San Fernando - Hollywood Sto., 1971 (USA)	1.00	548.80	22.20	3.13	0.3582	0.04	NO FAILURE	0.039	0 / 0.00
	20	Northridge - St. Centinela, 1994 (USA)	1.00	548.80	112.32	170.87	0.0996	0.24	NO FAILURE	0.082	0 / 0.07
	21	Coalinga - Parkfield, 1983 (USA)	1.00	548.80	3.46	0.00	0.1378	0.01	NO FAILURE	0.023	0 / 0.00

The Central de Abastos (Frigorifico) (CDAF), Central de Abastos (Oficina) (CDAO), Texcoco Lake (Sosa) (TXSO), and the Loma Prieta – Sunnyvale records fracture longitudinal bars owing to low-cyclic fatigue in the T = 1.0 s column. The number of bars fractured is 3, 16, 1, and 1 for each record, respectively. The CDI larger than 1.0 are 1.06 for SCT-1 record, 1.06 for CDAF, 1.48 for CDAO, and 1.09 for Tihuac Bombas. For Loma Prieta – Sunnyvale, CDI = 1.0, meaning that the damage is the same as that for SDPL.

Table 5.6 CDI for T = 1.5 s bridge column

Circular Column T=1.5s			CDI values for records with Scale Factor (SF) = 1								
		EQ	Scale factor	Energy Capacity, Ec (kN-m)	Enveloping Energy, Eucpe (kN-m)	Repeated Energy, Eucpr (kN-m)	β_c	CDI	Failure type	Max. Displacement (m)	Number of fatigued bars / FDI of critical bar
BIN 1 - SUBDUCTION	1	Valparaiso,1985 (Chile)	1.00	631.96	23.46	16.92	0.1351	0.04	NO FAILURE	0.067	0 / 0.01
	2	Llolleo,1985 (Chile)	1.00	631.96	147.28	277.03	0.0936	0.27	NO FAILURE	0.140	0 / 0.06
	3	Llayllay,1985 (Chile)	1.00	631.96	89.04	146.41	0.1166	0.17	NO FAILURE	0.098	0 / 0.03
	4	Pisco, 2007 (Perú)	1.00	631.96	295.91	546.94	0.2848	0.71	NO FAILURE	0.210	0 / 0.24
	5	Caleta,1985 (México)	1.00	631.96	82.74	130.97	0.2038	0.17	NO FAILURE	0.098	0 / 0.03
	6	Viña del Mar,1985 (Chile)	1.00	631.96	92.75	79.93	0.1201	0.16	NO FAILURE	0.122	0 / 0.03
	7	Melipilla,1985 (Chile)	1.00	631.96	204.86	145.33	0.1886	0.37	NO FAILURE	0.156	0 / 0.05
BIN 2 - SOFT SOIL	8	SCT1,1985 (Mexico)	1.00	631.96	515.68	1509.35	0.1461	1.16	LOW-CYCLE-FATIGUE	0.326	7 / 1.00
	9	CDAF,1985 (Mexico)	1.00	631.96	248.56	1247.17	0.1375	0.66	NO FAILURE	0.190	0 / 0.50
	10	CDAO,1985 (Mexico)	1.00	631.96	608.85	1574.05	0.1404	1.31	$\varepsilon_c > \varepsilon_{cu}$ + LOW-CYCLE-FATIGUE	0.437	14 / 1.00
	11	Tlhuac Bombas,1985 (Mexico)	1.00	631.96	540.00	500.00	0.2264	1.03	LOW-CYCLE-FATIGUE + $\varepsilon_c > \varepsilon_{cu}$	0.379	13 / 1.00
	12	Tlhuac Deportivo,1985 (Mexico)	1.00	631.96	266.70	911.66	0.2680	0.81	NO FAILURE	0.241	0 / 0.36
	13	Sismex Viveros,1985 (Mexico)	1.00	631.96	33.13	56.43	0.0382	0.06	NO FAILURE	0.073	0 / 0.01
	14	TXSO,1985 (Mexico)	1.00	631.96	218.14	1169.00	0.1202	0.57	NO FAILURE	0.172	0 / 0.33
BIN 3 - CRUSTAL	15	El Centro,1940 (USA)	1.00	631.96	175.97	142.71	0.0297	0.29	NO FAILURE	0.146	0 / 0.05
	16	Loma Prieta - San Francisco Airport,1989 (USA)	1.00	631.96	38.23	0.00	0.2136	0.06	NO FAILURE	0.071	0 / 0.00
	17	Loma Prieta - Hollister City, 1989 (USA)	1.00	631.96	227.29	210.62	0.1279	0.40	NO FAILURE	0.171	0 / 0.06
	18	Loma Prieta - Sunnyvale, 1989 (USA)	1.00	631.96	277.96	783.26	0.1960	0.68	NO FAILURE	0.226	0 / 0.42
	19	San Fernando - Hollywood Sto., 1971 (USA)	1.00	631.96	70.80	38.69	0.7341	0.16	NO FAILURE	0.102	0 / 0.01
	20	Northridge - St. Centinela, 1994 (USA)	1.00	631.96	109.84	113.48	0.1173	0.19	NO FAILURE	0.115	0 / 0.02
	21	Coalinga - Parkfield, 1983 (USA)	1.00	631.96	0.98	0.19	0.1364	0.00	NO FAILURE	0.023	0 / 0.00

5.5.4 CDI for the T = 1.5 s bridge column

Only three of the 21 records induce flexural failure mechanisms in this column, as seen in Table 5.6. The SCT-1 unscaled record fractures seven longitudinal bars due to low-cyclic fatigue. The CDAO unscaled record crushes the confined and unconfined concrete because of a large displacement that reaches 43.7 cm. Later, the same run fractures 14 bars owing to low-cyclic fatigue. The Tihuac Bombas unscaled record fractures 13 bars owing to low-cyclic fatigue and after that induces crushing of the confined and unconfined concrete because the column suffers a large displacement reaching 37.9 cm. The other records do not cause flexural failure mechanisms, although they induce damage in the steel bars due to the loss of different percentages of their fatigue life. The CDIs are 1.16 for the SCT-1 record, 1.31 for the CDAO, and 1.03 for Tihuac Bombas. These values indicate that the damage for each of these records is larger than the SDPL. The discussion of the results is presented in Appendix C.8.

5.6 Effects of aftershocks

5.6.1 Introduction

Some of the unscaled records already damaged the bridge columns, and it was decided to determine if aftershocks could induce even more damage in those columns or damage those other columns that suffered percentages of fatigue life lost but not any failure mechanism. The additional damages are shown in Tables 5.7, 5.8, and 5.9. The procedure followed is that the original unscaled record is considered to be main shock, and after a few seconds of zero amplitude ground motion a fraction of the main shock is applied to the column as a aftershock. The discussion of the results is presented in Appendix C.9.

5.6.2 Effects of aftershocks in the T = 0.5 s column

For the T = 0.5 s column, in addition to the damage shown in Table 5.4, Table 5.7 shows the damage caused by the main shock and the aftershock. The Pisco unscaled record crushes the confined and unconfined concrete and fractures seven bars because of low-cyclic fatigue. The aftershock induces the fracture of one more bar. The CDI increases to 1.56. The Viña del Mar unscaled record did not cause any failure mechanism, but the aftershock fractures six bars because of low-cyclic fatigue. The CDI is 1.25. The unscaled Tihuac Deportivo record did not induce any failure mechanism, but the aftershock fractures 10 bars because of low-cyclic fatigue and later crushes the confined and unconfined concrete because of a large displacement that carries the confined concrete strain to 0.02, a value larger than the ultimate value of 0.018. The

Loma Prieta unscaled record followed by a similar ground motion as aftershock does not cause any failure mechanism. However, an additional aftershock or a future event with the same characteristics as the main shock induces the fracture of six bars because of low-cyclic fatigue, and the CDI increases to 1.96.

Table 5.7 Additional damage due to aftershocks in the *T* = 0.5 s column

COLUMN T = 0.5s CDI AND ADDITIONAL DAMAGE OF MATERIALS DUE TO AFTERSHOCKS											
EQ	Energy Capacity, Ec (kN-m)	Enveloping Energy, Eucpe (kN-m)	Repeated Energy, Eucpr (kN-m)	β_c	CDI	Max. Displacement (m)	Failure type	MAIN SHOCK FRACT. BARS	AFTERSHOCK FRACT. BARS	Max. ε_c	Max. ε_s
Pisco + 0.6*(Pisco)	521.22	499.12	1255.25	0.25	1.56	0.154	$\varepsilon_c > \varepsilon_{cu}$ + LOW-CYCLE-FATIGUE	7	1	0.020	0.063
Viña + 1.0*(Viña)	521.22	262.00	2880.00	0.14	1.25	0.090	LOW-CYCLE-FATIGUE (at aftershock)	0	6	0.011	0.037
Tlhuac Dep. + 1.0*(Tlhuac Dep.)	521.22	485.57	1284.90	0.42	1.96	0.174	LOW-CYCLE-FATIGUE + $\varepsilon_c > \varepsilon_{cu}$ (at aftershock)	0	10	0.020	0.075
Loma Prieta HCHA + 1.0*(Loma Prieta HCHA)	521.22	339.34	1082.95	0.10	0.86	0.091	NO FAILURE	0	0	0.011	0.042
Loma Prieta HCHA + 1.0*(Loma Prieta HCHA) + 1.0*(Loma Prieta HCHA)	521.22	355.73	1727.55	0.10	1.02	0.097	LOW-CYCLE-FATIGUE (at 2nd aftershock)	0	6	0.011	0.038

5.6.3 Effects of aftershocks in the *T* = 1.0 s column

The main unscaled Pisco and Tihuac Deportivo unscaled records did not cause any failure mechanism for this column; however, their aftershocks cause fracture of one and three bars owing to low-cyclic fatigue, respectively, as shown in Table 5.8. If the aftershock was 0.8 times the main shock, Table 5.8 shows that five bars would fracture because of low-cyclic fatigue. The CDIs are 1.03 and 1.13, respectively.

With 0.8 times the main shock acting as aftershock, the CDI increases to 1.2. The TXSO and the Loma Prieta – Sunnyvale unscaled records each induce the fracture of one bar owing to low-cyclic fatigue in this column. The aftershocks fracture five and three more bars owing to low-cyclic fatigue, respectively. The CDIs are 1.17 and 1.14. All the values of CDI are larger than 1.0; therefore, the damage is above the SDPL.

Table 5.8 Additional damage due to aftershocks in the *T* = 1.0 s bridge column

COLUMN T = 1.0s CDI AND ADDITIONAL DAMAGE OF MATERIALS DUE TO AFTERSHOCKS											
EQ	Energy Capacity, Ec (kN-m)	Enveloping Energy, Eucpe (kN-m)	Repeated Energy, Eucpr (kN-m)	β_c	CDI	Max. Displacement (m)	Failure type	MAIN SHOCK FRACT. BARS	AFTERSHOCK FRACT. BARS	Max. ε_c	Max. ε_s
Pisco + 0.8*(Pisco)	548.80	338.25	1639.51	0.14	1.03	0.157	LOW-CYCLE-FATIGUE (at aftershock)	0	1	0.010	0.036
Tlhuac Dep. + 0.6*(Tlhuac Dep.)	548.80	389.81	1686.17	0.14	1.13	0.203	LOW-CYCLE-FATIGUE (at aftershock)	0	3	0.014	0.048
Tlhuac Dep. + 0.8*(Tlhuac Dep.)	548.80	389.81	1987.14	0.14	1.20	0.203	LOW-CYCLE-FATIGUE (at aftershock)	0	5	0.014	0.048
TXSO + 0.6*(TXSO)	548.80	338.70	2590.43	0.12	1.17	0.163	LOW-CYCLE-FATIGUE	1	5	0.011	0.037
Loma Prieta Sunnyvale + 0.6*(Loma Prieta Sunnyvale)	548.80	415.60	1306.75	0.16	1.14	0.173	LOW-CYCLE-FATIGUE	1	3	0.012	0.040

5.6.4 Effects of aftershocks in the *T* = 1.5 s column

For this column the Pisco, CDAF, and Sunnyvale unscaled records do not cause any failure mechanism for the main shock, but the second aftershocks for the Pisco and CDAF records and the first aftershock for the Sunnyvale record induce fracture of three longitudinal bars due to low-cyclic fatigue for each one. The SCT-1 main shock induced the fracture of seven bars due to low-cyclic fatigue and the aftershock the fracture of one more bar due to this failure mechanism.

Table 5.9 Additional damage due to aftershocks in the *T* = 1.5 s bridge column

COLUMN T = 1.5s CDI AND ADDITIONAL DAMAGE OF MATERIALS DUE TO AFTERSHOCKS											
EQ	Energy Capacity, Ec (kN-m)	Enveloping Energy, Eucpe (kN-m)	Repeated Energy, Eucpr (kN-m)	β_c	CDI	Max. Displacement (m)	Failure type	MAIN SHOCK FRACT. BARS	AFTERSHOCK FRACT. BARS	Max. ε_c	Max. ε_s
Pisco + 1.0*(Pisco) + 1.0*(Pisco) + 1.0*(Pisco)	631.96	310.76	2011.43	0.28	1.40	0.224	LOW-CYCLE-FATIGUE (at 2nd aftershock)	0	3	0.009	0.034
SCT + 0.6*(SCT)	631.96	515.68	2046.35	0.15	1.29	0.326	LOW-CYCLE-FATIGUE	7	1	0.015	0.049
CDAF + 1.0*(CDAF)	631.96	270.30	2572.94	0.14	1.00	0.193	LOW-CYCLE-FATIGUE (at 2nd aftershock)	0	3	0.007	0.027
Sunnyvale + 1.0*(Sunnyvale)	631.96	307.92	1693.16	0.20	1.01	0.226	LOW-CYCLE-FATIGUE (at aftershock)	0	3	0.009	0.032

The CDIs are 1.4, 1.29, 1.00, and 1.01 for the Pisco, the SCT, the CDAF, and the Loma Prieta Sunnyvale main shocks and aftershocks, as seen in Table 5.9. This values for the CDIs indicate that the damage is above the SDPL.

5.7 Summary

1. A CDI is proposed to quantify the damage in reinforced concrete bridge columns.

2. The methodology is based on finding the SDPL using the FFEM that identifies the first flexural failure mechanism that occurs in the column. To reach this failure the records chosen for design of the column must be scaled up or down.

3. Once the SDPL is found, using equation (5.1) with CDI = 1.0 gives the parameter β_c. This parameter, associated with SDPL, also controls the importance of E_{ucpr} in the response.

4. The damage can be fracture of a longitudinal bar due to tension, crushing of the confined concrete, reduction of the moment capacity because of the increase of the external moment P-Δ, or fracture of a longitudinal bar due to low-cyclic fatigue.

5. Three bins with seven records each are used on the three bridge columns designed in Chapter 4, according to AASHTO and Caltrans. As explained above, the records are scaled to obtain β_c.

6. It was decided not to scale the records to calculate the CDI for the column and for each record. Some of the unscaled records induce damage in the bridge columns.

7. Aftershocks increase the damage induced by the unscaled records.

8. A CDI is proposed to quantify the damage in reinforced concrete bridge columns.

5.8 Conclusions

1. The results of this investigation show that when crushing of the confined concrete occurs, almost immediately there is fracture of bars due to low cyclic fatigue.
2. The results for the near fault records show that in most of the cases the equation for the damage index needs to be reviewed and improved. It is suggested that the damage index for these records should be based on the new plastic displacements of the few cycles of response.
3. The CDI is later calculated for the unfactored records and the results show that there is reduction of fatigue life for most the ground motions. In few cases, crushing of the confined concrete occurs first but then after a few seconds fracture of several bars occurs.

4. The CDI calculations show that the subduction and the soft soil records induce more damage due to low-cyclic fatigue than the crustal earthquakes and that the close to the fault records, with few exceptions, induce damage due to crushing of the confined concrete.
5. Aftershocks induce an increase of the reduction of fatigue life and in some cases, crushing of the confined concrete.

5.9 Remarks

1. Life safety performance level covers an ample range from yielding to near collapse. The SDPL is associated to one of the four flexural mechanisms so it will allow the designer to know how close is the design to the near collapse limit state.

2. In general, the additional damage due to aftershocks is due to the increase in number of repeated cycles of plastic strain that will increment the repeated dissipated energy, E_{ucpr} and therefore the CDI.

6. DESIGNING FOR STRONG MOTION DURATION AND CYCLIC PLASTIC DUCTILITY DEMANDS

6.1 Introduction

In order to observe the effects of the strong duration of the ground motion in bridge columns this chapter presents a comparison with and without the fatigue model included in the FFEM. Also, the FFEM is used in this chapter to demonstrate that the strength required to take into account the cyclic reversible displacements is larger than that demanded when only lateral displacements are considered for design.

6.2 Effects of strong motion duration on code-designed bridge columns

6.2.1 General remarks

As Krawinkler et al. (1983) pointed out, materials have a memory of the plastic reversible strains and in the steel bars this memory keeps adding the effects of plastic cyclic strains along the duration of the strong part of the motion. The effect of the accumulation of damage is the continuous decrease of the fatigue life of the bars until fracture occurs. The fracture can happen during a main shock or later owing to an aftershock. The measure and accumulation of the plastic strains leads to low-cyclic fatigue that causes fracture of the bars, as explained in Chapter 5.

6.2.2 Damage due to the CDAO record on the T = 1.0 s bridge column, fatigue model included

Figures 6.1 a and b show the hysteretic and the displacement time history responses of the T = 1.0 s bridge column subjected to the unscaled CDAO station record of the 1985 Mexico earthquake. The fatigue model is activated for this example.

At t = 53 s the bridge column reaches its maximum lateral displacement of 20.5 cm, which is less than the 24 cm lateral displacement capacity of this column, according to the codes,. Figure 6.1 c shows that the corresponding maximum concrete compressive strain in a confined concrete fiber located close to bar 1 is 0.016, a value that is also smaller than ε_{cu} = 0.018. Therefore, the 20.5 cm lateral displacement does not induce crushing of the confined concrete. However, at t =

40 s the unconfined concrete close to bar 1 cracks, and it crushes at t = 80 s inducing more deterioration of the strength and stiffness of the column.

At t = 59 s, 12 longitudinal bars fracture because of low-cyclic fatigue, as seen in Figure 6.1 f. These fractures immediately deteriorate the stiffness and strength of the bridge column, as shown by the deteriorated loop that reaches 20 cm of lateral displacement (Figure 6.1 a).

As explained in Chapter 4, OpenSees continues measuring the strains in the fiber located at the fractured bar, although the bar does not take any more stresses, as shown in Figure 6.1 d for bar 1.

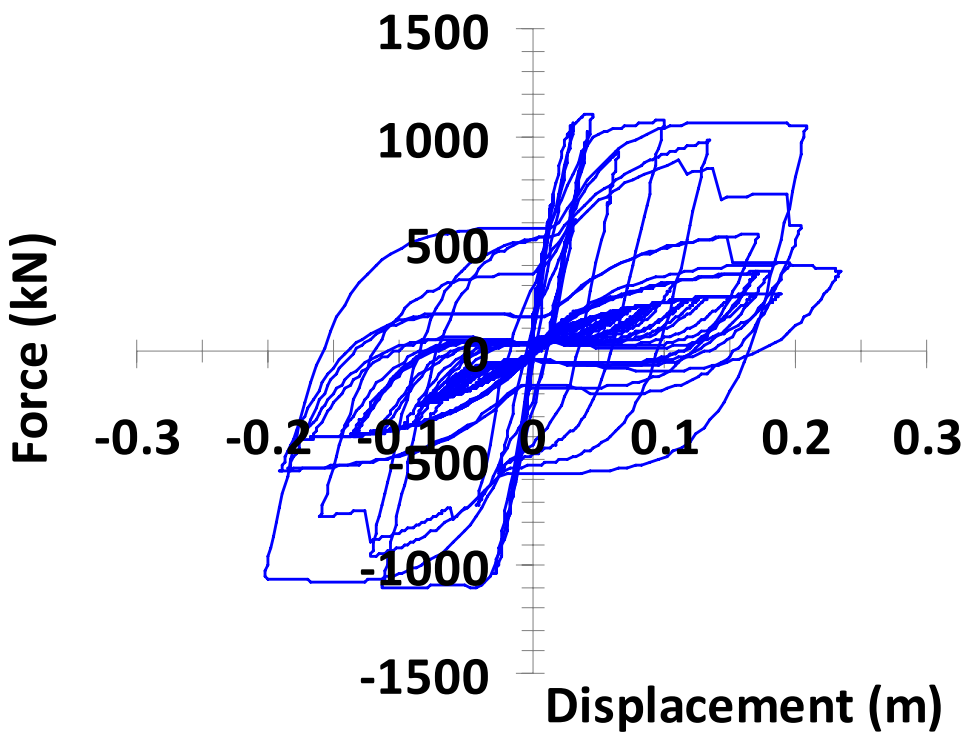

(a)

Figure 6.1 Column *T*=1.0 s, damage for CDAO Mexico record SF=1.00, fatigue model included

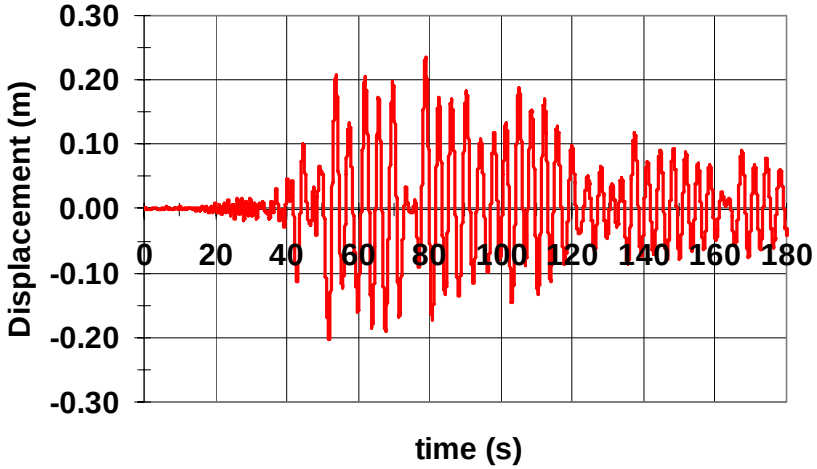

(b)

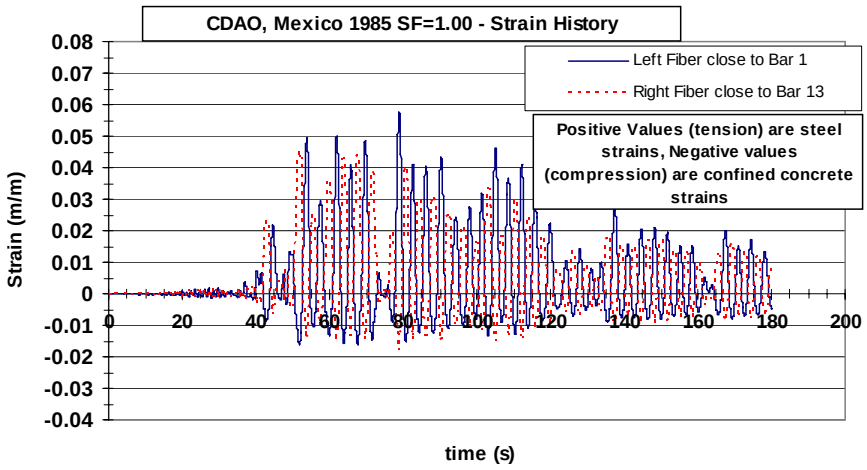

(c)

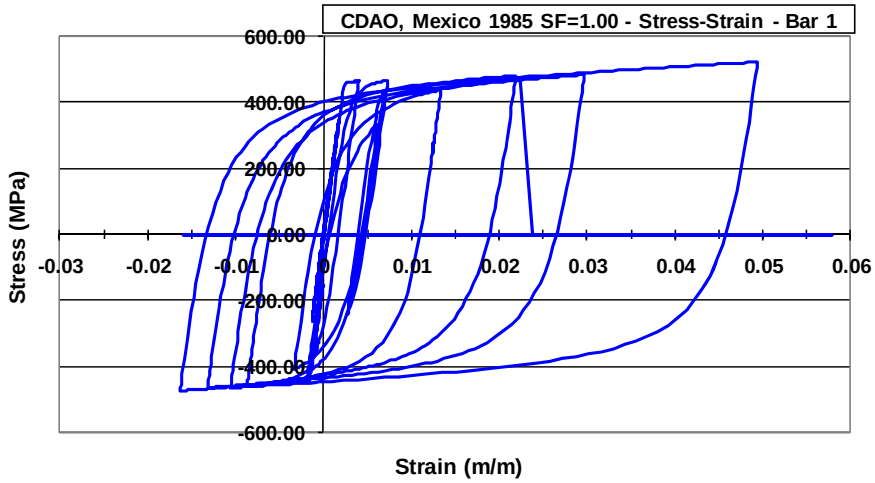

(d)

Figure 6.1 (cont.) Column *T*=1.0 s, damage for CDAO Mexico record SF=1.00, fatigue model included

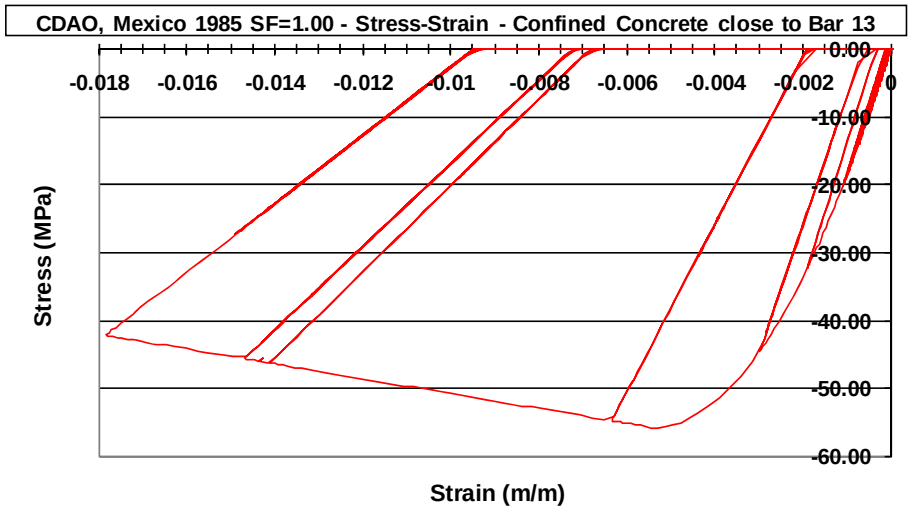

(e)

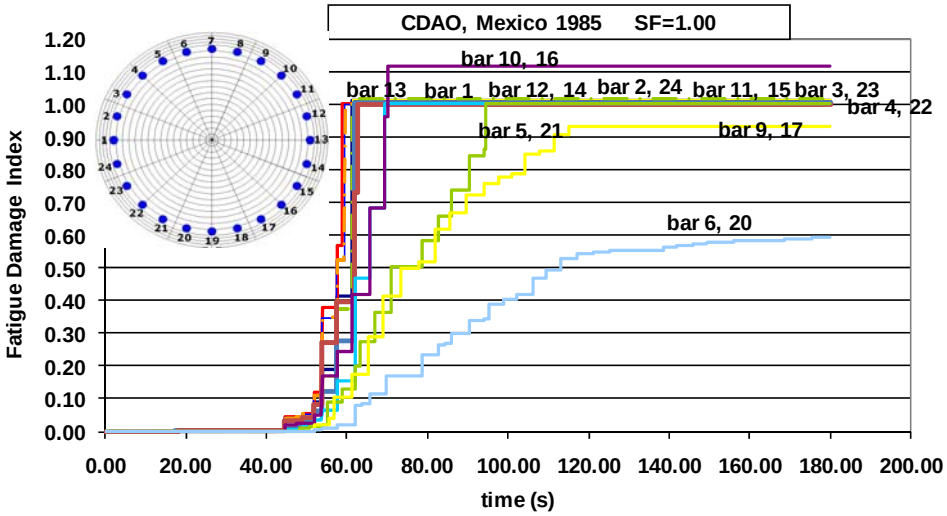

(f)

Figure 6.1 (cont.) Column *T*=1.0 s, damage for CDAO Mexico record SF=1.00, fatigue model included

At t = 67 s bars 10 and 16 also fracture owing to low-cyclic fatigue, and bars 9 and 17 have lost 50% of their fatigue life. The deterioration of the critical section of the bridge column increases, as seen in Figure 6.1 a, and the column reaches a maximum lateral displacement close to 24 cm at t = 79.5 s. The confined concrete strain fiber located close to bar 13 reaches almost 0.018; the concrete has reduced its strength from 55 to 41 MPa and is near crushing. Finally, at t = 92 s bars 5 and 21 fracture owing to low-cyclic fatigue and bars 9 and 17 have lost 75% of their fatigue life. At t = 104 s these bars have lost 92% of their fatigue life.

At time t = 104 s a total of 16 bars have fractured owing to low-cyclic fatigue, which can be considered a total loss of the bridge column, as shown in the hysteretic response where the strength of the deteriorated column reaches about 25% of its maximum capacity and the stiffness is about 2.5% of the initial stiffness.

6.2.3 Damage due to the CDAO record on the T = 1.0 s bridge column, fatigue model not included

Figures 6.2 a, and b show the responses of the T = 1.0 s bridge column subjected to the same unscaled CDAO record but with the fatigue model suppressed from the FFEM.

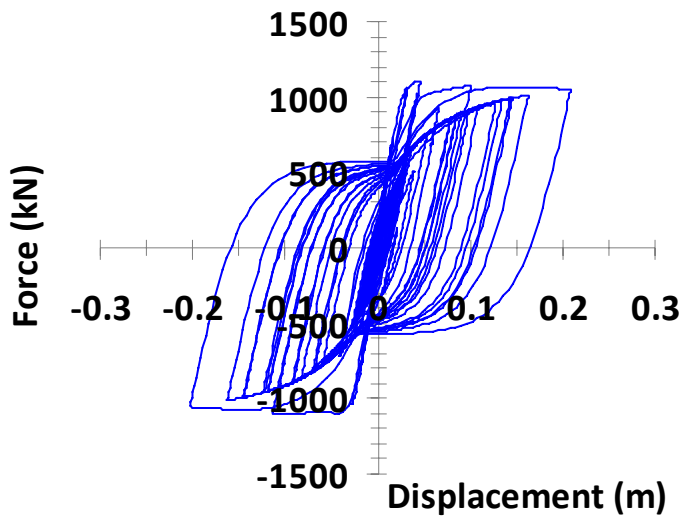

(a)

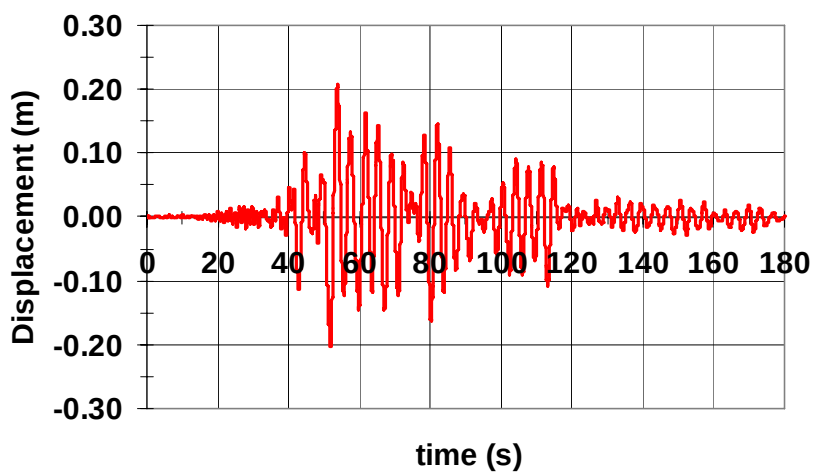

(b)

Figure 6.2 Column T=1.0 s, damage for CDAO Mexico record SF=1.00, fatigue model not included

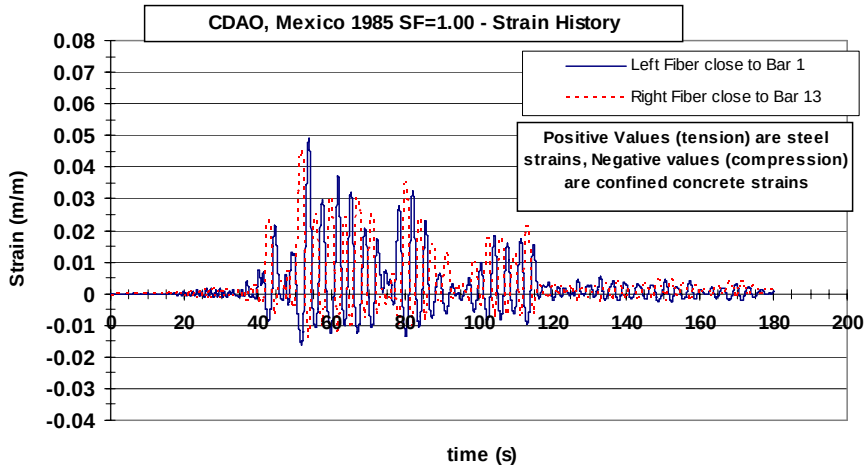

(c)

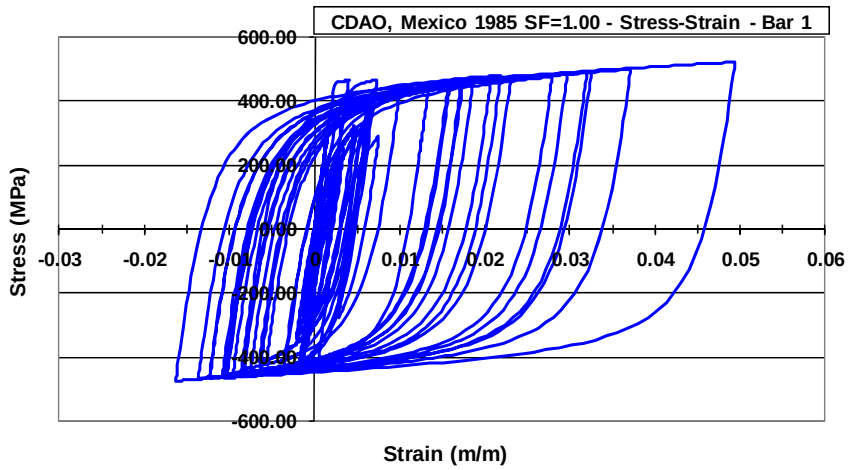

(d)

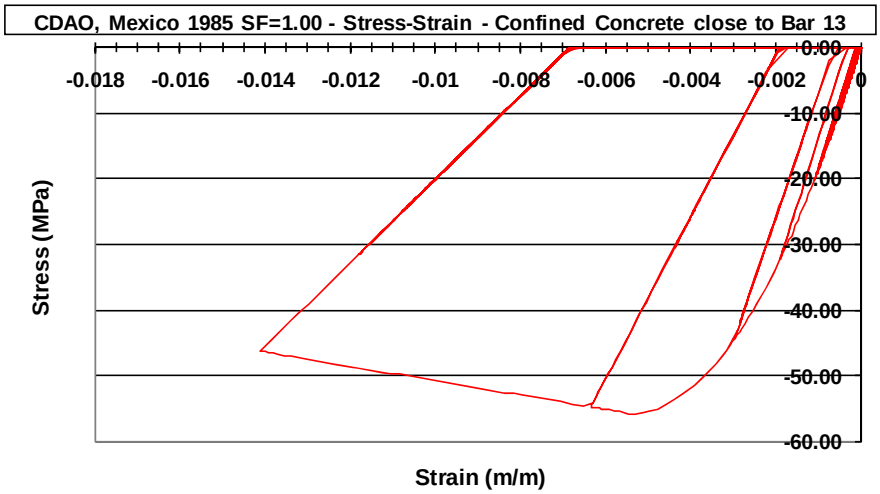

(e)

Figure 6.2 (cont.) Column *T*=1.0 s, damage for CDAO Mexico record SF=1.00, fatigue model not included

The maximum lateral displacement occurs at the same time as the FFEM that includes fatigue and reaches the same value of 20.5 cm (Figures 6.1 a, and 6.2 a). The corresponding maximum compression strain in a location close to bar 1 is 0.016 as before, and the compression strain close to bar 13 is 0.014, as shown in Figures 6.1 c and e and 6.2 c and e.

Since the fatigue model is not activated in this example, only the Bauschinger effect causes a deterioration of the stiffness of the column, and there is a slight loss of strength because the compressive strain is 0.014 in the fiber close to bar 13 and 0.016 in the fiber close to bar 1. Both strains are less than 0.018, which is the ultimate confined concrete strain. Therefore, there is no crushing. The unconfined cover concrete close to bar 1 cracks at t = 40 s and crushes at t= 42 s.

In this example the total unscaled time history of the CDAO record shakes the FFEM of the bridge column, but the effect of the strong motion duration of the record is not taken into account.

The consequences are clear. There is no fatigue of the longitudinal bars and the strength deterioration is minimal because there is no crushing of the confined concrete.

6.3 Effects of cyclic plastic displacements

6.3.1 General remarks

In Chapter 2 it was demonstrated that the large cyclic reversible plastic displacements occurring in structural systems because of severe earthquakes demand larger strengths than those demanded by only the plastic lateral displacement, as prescribed in the new codes.

This last demonstration implied that strength reduction factors used for design should be variable and smaller for cyclic response and that the use of large constant reduction factors increases the vulnerability of structures because a lower strength will increase the damage potential.

In what follows, one bridge column designed according to the new codes that suffered fracture of six bars due to low-cyclic fatigue is redesigned to avoid this flexural failure mechanism, at least for the main shock.

6.3.2 Response of the T = 1.5 s due to the unscaled SCT-1 record

In Table 5.6 the response of the T = 1.5 s bridge column under the SCT-1 record indicates that for this unscaled record there is fracture of seven longitudinal bars owing to low-cyclic fatigue. In addition to cracking and crushing of the unconfined cover concrete, low-cyclic fatigue is the only other failure mechanism because there is no crushing of the confined concrete, no P-Δ effects, and no fracture of any bar due to tension.

The design of the T = 1.5 s bridge column meets all new AASHTO (2007) and Caltrans (2006) prescriptions; however, the fracture of seven bars induced by the unscaled SCT-1 record is a damage that could require a complex and costly retrofit or even a demolition.

6.3.3 Redesign of the T = 1.5 s bridge column for SCT-1

In Chapter 4, Section 4.2.2, it is established that the elastic shear demand on the bridge column is 6620 kN and that the strength reduction factor that results after meeting the lateral displacement code prescriptions is 8.

Because of the damage observed for the main shock, it is decided to redesign the bridge column in order to avoid the damage caused by the accumulation of cyclic plastic reversible strains in the longitudinal steel bars. The height of the column, the mass, and the axial force are the same.

After several trials reducing the strength reduction factor, it will be seen that the new design is not affected by low-cyclic fatigue. Figure 6.3 shows the column diameter changing from 1.0 to 1.6 m and the reinforcement increasing from 24 longitudinal steel bars to 52 bars of 32 mm diameter. The transverse reinforcement changes diameter and spacing to 24 and 90 mm, respectively. The steel and confined and unconfined concrete strengths remain the same.

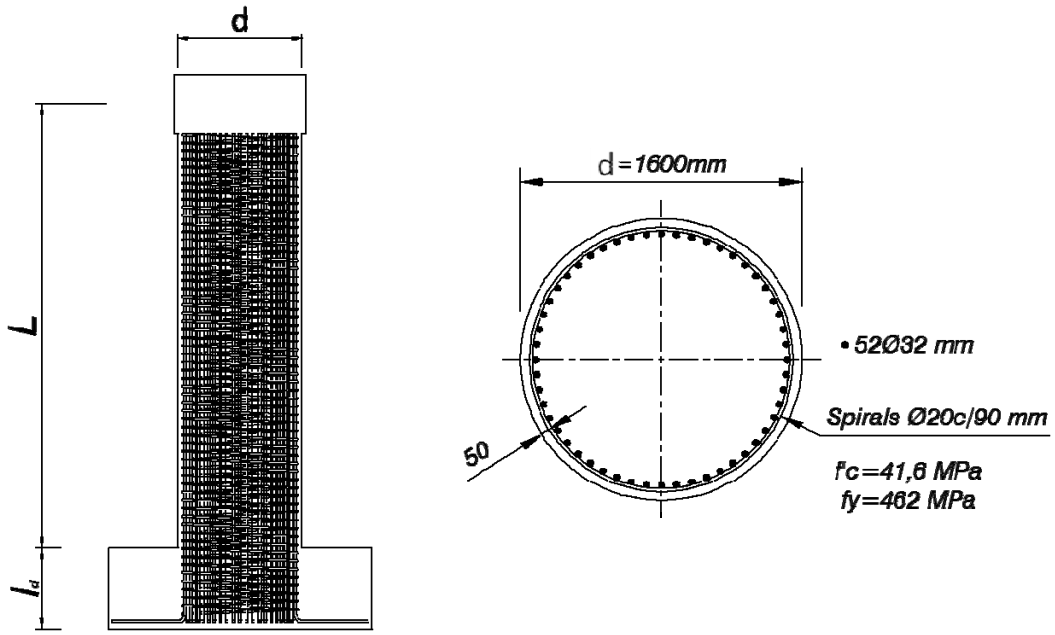

Figure 6.3 Column redesign

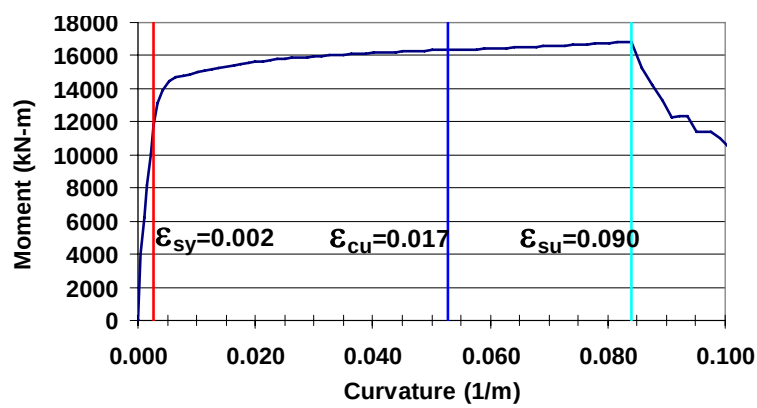

(a)

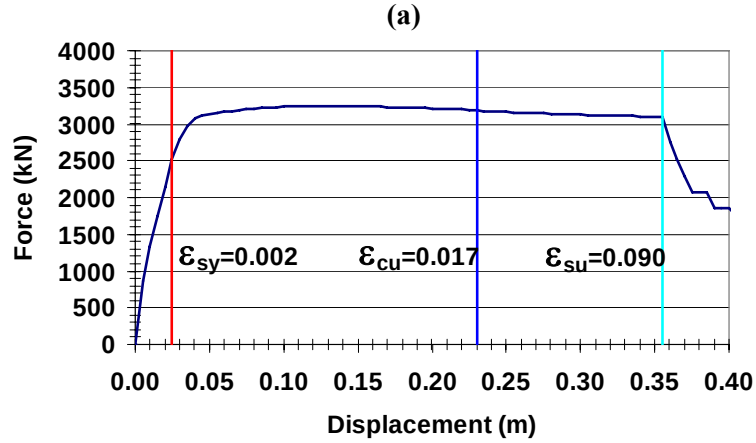

(b)

Figure 6.4 Moment–curvature relationship for the column redesign

Figure 6.4 a shows the moment–curvature relationship for the new design. The ultimate confined concrete strain as calculated by Mander et al. (1988) is $\varepsilon_{cu} = 0.017$, and the corresponding lateral displacement capacity for the bridge column is 23 cm, as seen in Figure 6.4 b. This figure also shows that the yield displacement is 2.5 cm. For the same mass acting on top of the column the period becomes $T = 0.58$ s.

6.3.4 Energy capacity for the redesigned bridge column

A sine function displacement inducing a complete cyclic displacement response seen in Figure 6.5 a indicates that the displacement capacity of the bridge column is 19.5 cm and that the SDPL for this applied displacement is the fracture of one bar due to low-cyclic fatigue, as seen in Figure 6.5 b. This failure mechanism occurs after cracking and crushing of the unconfined cover concrete but before crushing of the confined concrete or reduction of the flexural moment capacity or fracture of bars caused by tension.

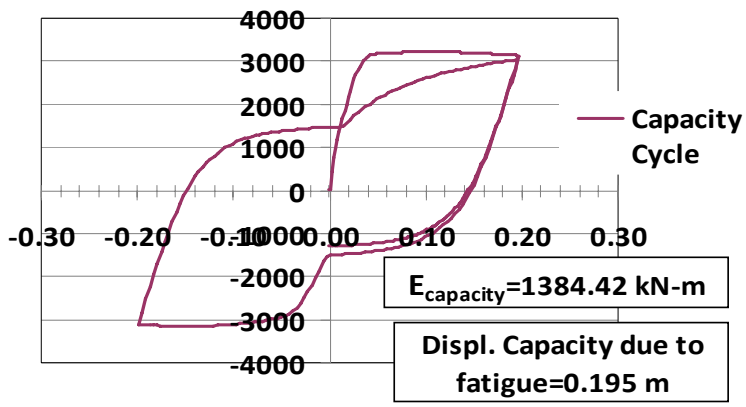

(a)

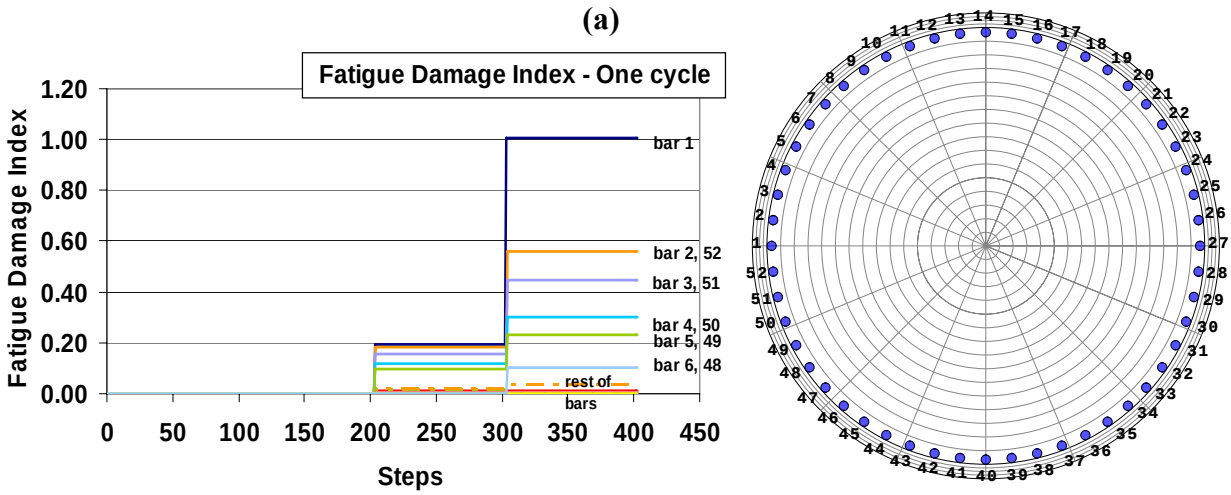

(b)

Figure 6.5 One cycle capacity analysis for redesigned column

6.3.5 Significant damage performance level and calculation of the parameter β_c for the redesigned column

A scale factor of 1.04 is applied to the SCT-1 record to cause SDPL in the T = 0.58s bridge column (see Table 6.1). This scaled record induces SDPL in the form of the fracture of one bar due to low-cyclic fatigue. Once SDPL is reached, CDI = 1.0; therefore, the value for β_c for this bridge column is 0.125.

Table 6.1 β_c value of redesigned column for 1.04SCT-1 record

Calculation of β_c - Circular Column														
EQ	Duration (s)	PGA (%g)	Tg (s)	Scale Factor (CDI=1)	Failure type	Number of fatigued bars	Time (failure)	Max. Displacement (m)	Energy Capacity, Ec (kN-m)	Enveloping Energy, Eucpe (kN-m)	Repeated Energy, Eucpr (kN-m)	Eucpe/Ec	Eucpr/Ec	β_c
SCT1,1985 (Mexico)	164.00	0.163	2.00	1.04	LOW-CYCLE-FATIGUE	1	65.58	0.180	1384.42	1191.17	1541.84	0.86	1.11	0.125

6.3.6 Cyclic damage index for the redesigned column under the SCT-1 unscaled record

Figure 6.6 shows the responses of the T = 0.58 s bridge column subjected to the SCT-1 unscaled record. Notice that the scale factor of 1.0 used to determine the CDI is lower than the one used to calculate SDPL and the value of β_c. This value of the scale factor is chosen using the assumption that the code prescribes such scaling for the record in order to match the prescribed code spectrum.

Figure 6.6 a shows the hysteretic response with deterioration of stiffness due to the Bauschinger effect and a very small deterioration of strength due to cracking and crushing of the unconfined concrete cover, as seen in the strain time history shown in Figure 6.6 c, which shows the strain levels at fibers close to bars 1 and 27. Figure 6.6 b shows that the maximum lateral displacement demand is 15 cm, a value that is less than the displacement capacity of 23 cm.

In Figure 6.6 c the maximum confined concrete compressive strain is 0.011, less than ε_{cu} = 0.017. The maximum compression strain in the steel is 0.011. These strains are larger than the cracking and crushing strains of the unconfined concrete. The maximum tensile strain is 0.035; both values are lower than the maximum values for cyclic strain ε_{su} = 0.09 given by AASHTO (2007).

Figures 6.6 d and e show the stress–strain relationship of the steel and the concrete, respectively. The fatigue time history of the steel bars is shown in Figure 6.6 f. Clearly, there is no fracture of any bar due to low-cyclic fatigue, but bars 1 and 27 lost 45% of their fatigue life and all the other bars have lost between 11% and 38% of their fatigue life.

According to Table 6.2 the CDI for the unscaled record is 0.78, a value lower than CDI = 1.0, which corresponds to the SDPL. Therefore, the damage of the column under the unscaled record is less than the SDPL.

The redesign of the bridge column meets all code prescriptions, and in addition it has allowed the designer to avoid fracture of the longitudinal bars due to low-cyclic fatigue, although there is already damage in the longitudinal bars that has decreased their fatigue life and the strength of the column, as seen in Figure 6.6 a.

.

Table 6.2 CDI values of redesigned column for SCT record and aftershocks

CDI value									
EQ	Scale factor	Energy Capacity, Ec (kN-m)	Enveloping Energy, Eucpe (kN-m)	Repeated Energy, Eucpr (kN-m)	β_c	CDI	Failure type	Max. Displacement (m)	Number of fatigued bars / FDI of critical bar
SCT1,1985 (Mexico)	1.00	1384.42	923.02	1211.75	0.125	0.78	NO FAILURE	0.150	0 / 0.45
SCT + 0.6*SCT		1384.42	923.02	1789.21	0.125	0.83	NO FAILURE	0.150	0 / 0.51
SCT + 0.8*SCT		1384.42	978.56	3934.10	0.125	1.06	LOW-CYCLE-FATIGUE	0.152	22 / 1.00

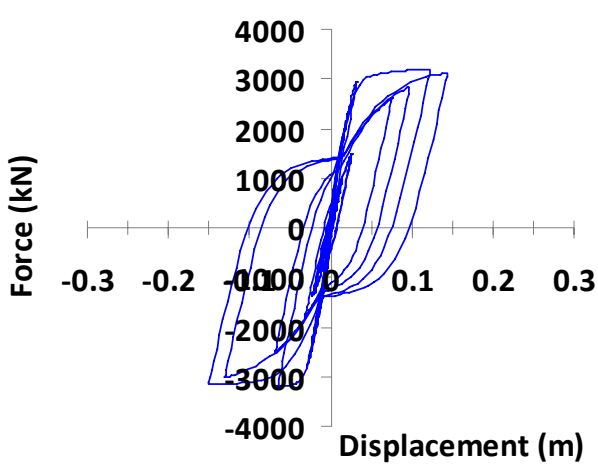

(a)

Figure 6.6 Response of the redesigned *T* = 0.58 s bridge column subjected to the SCT-1 unscaled record

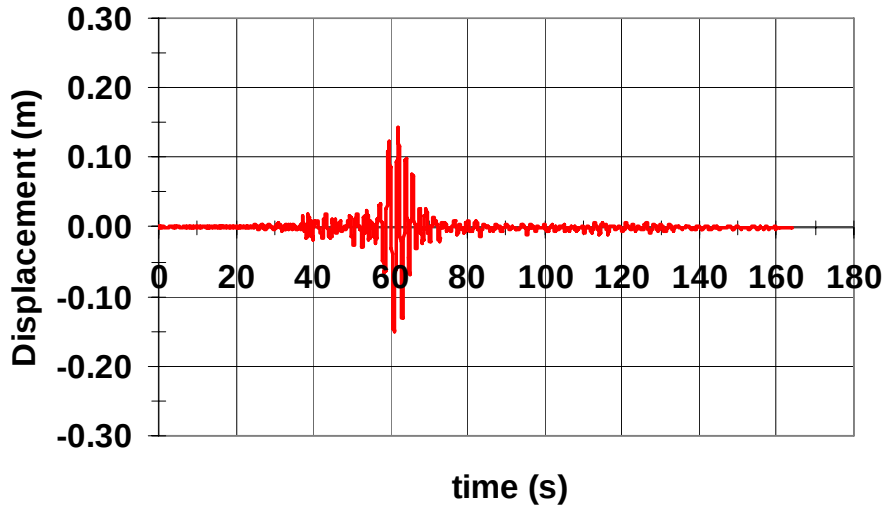

(b)

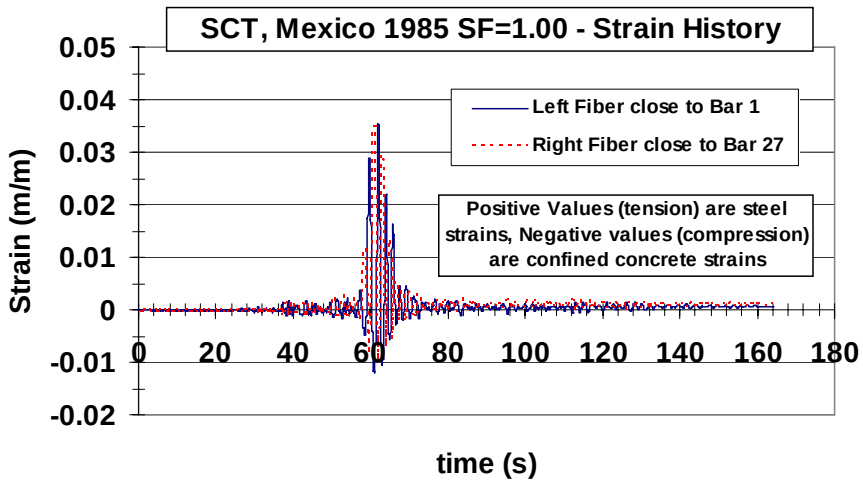

(c)

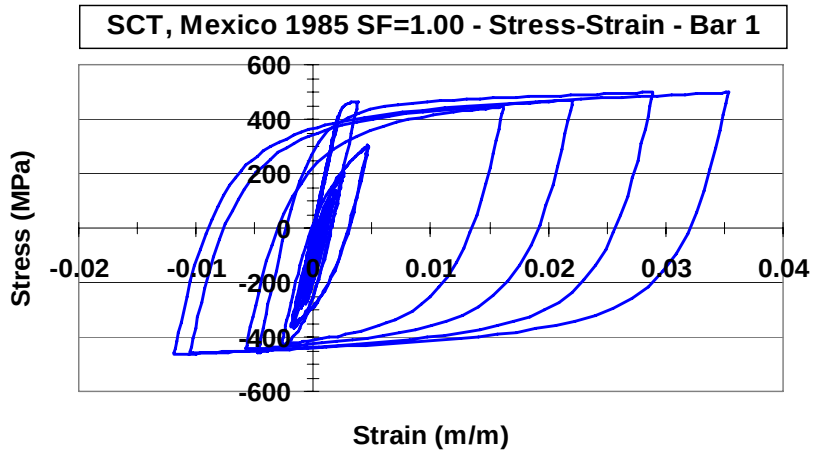

(d)

Figure 6.6 (cont.) Response of the redesigned T = 0.58 s bridge column subjected to the SCT-1 unscaled record

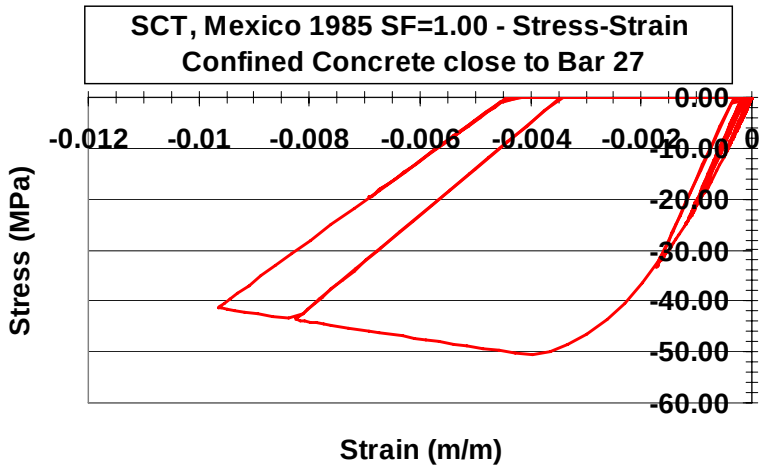

(e)

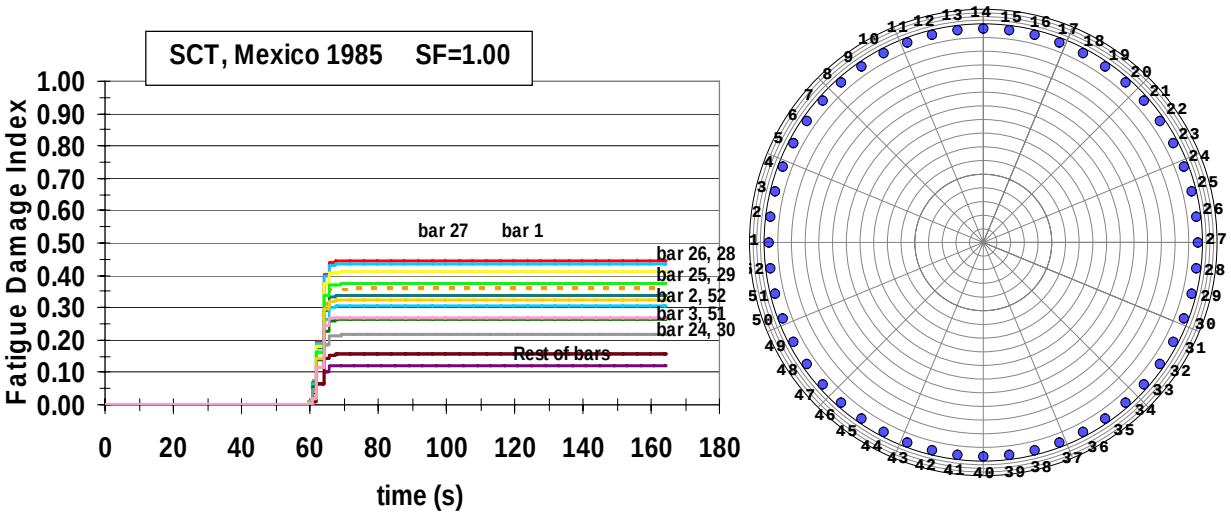

(f)

Figure 6.6 (cont.) Response of the redesigned *T* = 0.58 s bridge column subjected to the SCT-1 unscaled record

In Figure 6.4 b the shear resistance provided to the redesigned bridge column is 3200 kN. Since the elastic shear demand is 6620 kN, the reduction factor is now 2.1. This value is almost 4 times lower than the reduction factor used for the original design of the bridge column; therefore, it meets new code requirements that ignore cyclic response inducing low-cyclic fatigue.

This is one of the important conclusions from Chapter 2, where it was demonstrated that if the designer considers that the real seismic response is cyclic and reversible during the strong part of the motion, the strength demanded to sustain such large plastic displacements is larger than the one required to sustain only the plastic lateral displacement as the codes prescribe.

It should be mentioned that the new codes have omitted the use of constant reduction factors as they were prescribed in several codes in the past. However, the designer must use a strength reduction factor in order to avoid an elastic design; this factor now depends indirectly on the period of the column under analysis. This is so because design is now based on the maximum lateral displacement, which depends on the stiffness and strength of the bridge column, and both parameters intervene in the calculation of the column period *T*. Although this new prescription is a significant advance it is not enough, since lateral displacements ignore the cyclic characteristic of earthquake response inducing low-cyclic fatigue of the steel bars.

The cyclic response expressed in terms of the demanded new plastic displacements and the demanded repeated ones requires a large strength, as now confirmed with the FFEM.

6.3.7 Response of the redesigned column to the SCT-1 main shock and aftershocks

In what follows the response of the redesigned bridge column due to the unscaled SCT-1 record, considered now as a main shock, followed by an aftershock with 80% of the intensity of the main shock, is studied.

Figures 6.7 a and b show the hysteretic and displacement time history responses of the redesigned T = 0.58 s bridge column. In Figure 6.7 a there are clear signs of strength deterioration due to fatigue of 22 bars and of course of stiffness deterioration due to both the Bauschinger effect and the fatigue of the bars.

Figure 6.7 b shows a small increase of the lateral displacements due to the aftershock, but the 15 cm lateral displacement is less than the displacement capacity of the column.

Figures 6.7 c, d, and, e, show that the steel and confined concrete strain has lower values than the maximum values prescribed by AASHTO (2007), although the strains in the unconfined cover concrete close to bars 1 and 27 cause cracking and crushing of the unconfined cover concrete.

Figure 6.7 f shows that 22 bars fracture due to low-cyclic fatigue and that the rest of the bars have lost between 51% and 87% of their fatigue life.

The CDI is now 1.06, as seen in Table 6.2. Since this value is larger than 1.0 the damage expected is larger than the SDPL associated with $\beta_c = 0.125$.

The observed damage indicates that the redesign is not enough to avoid serious damage, such as the loss of 22 bars for an aftershock intensity equal to 80% of the main shock.

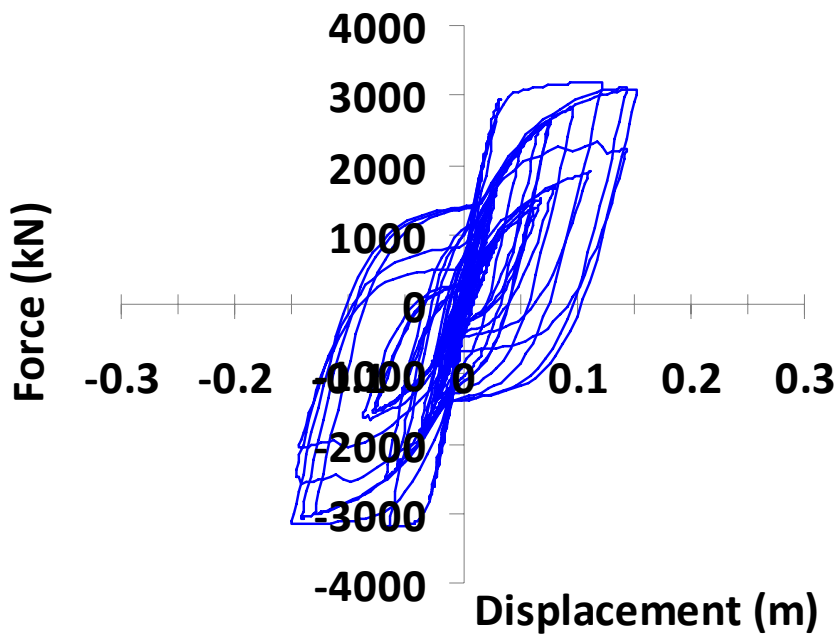

(a)

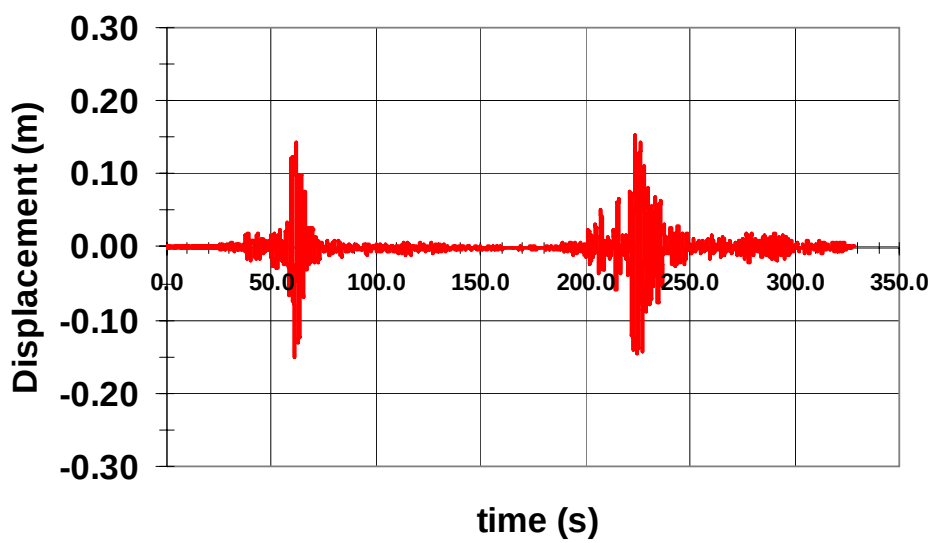

(b)

Figure 6.7 Response of the redesigned column to the SCT-1 main shock and a 80% aftershock

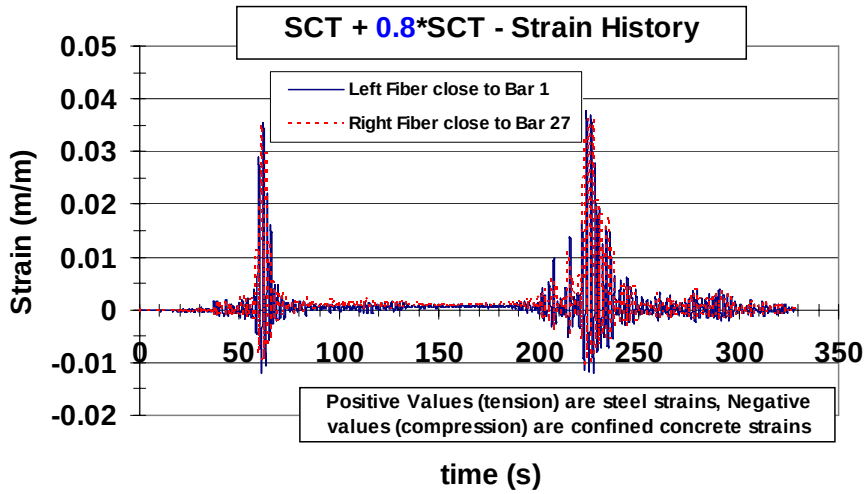

(c)

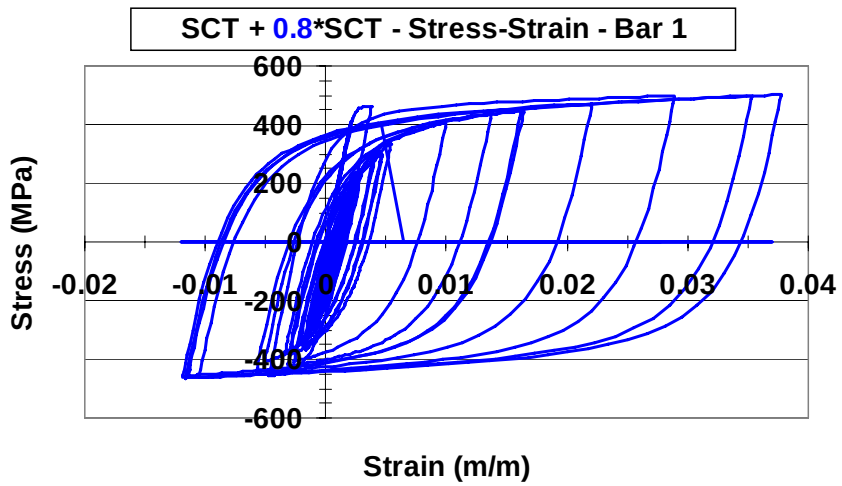

(d)

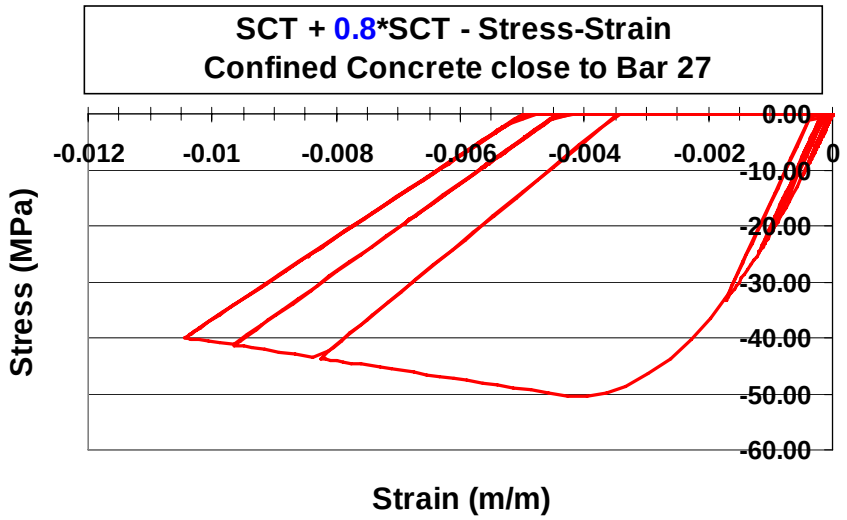

(e)

Figure 6.7 (cont.) Response of the redesigned column to the SCT-1 main shock and a 80% aftershock

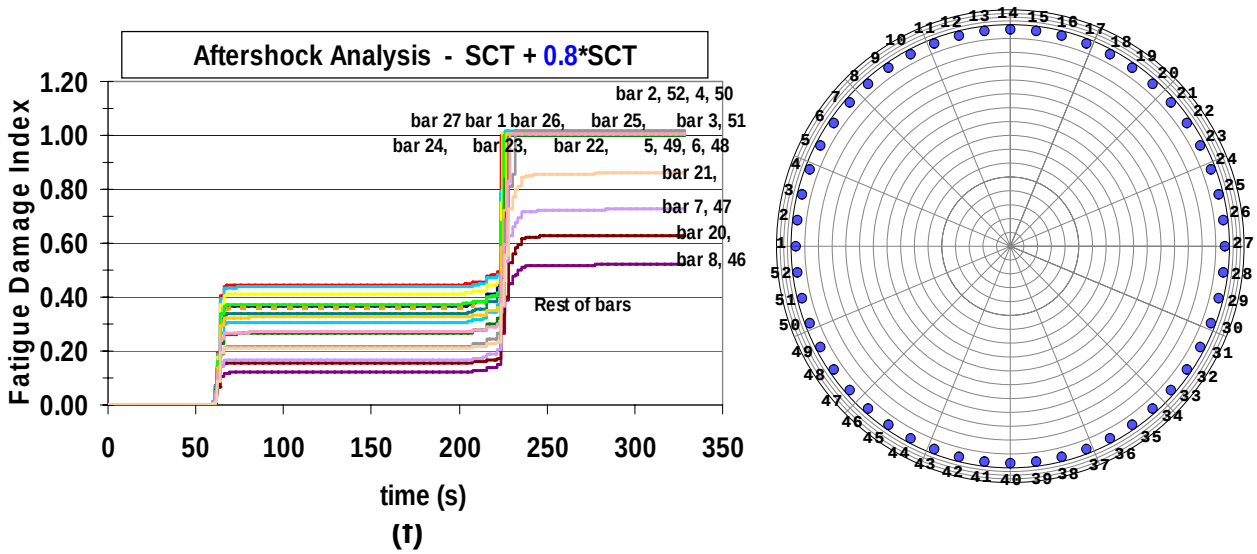

Figure 6.7 (cont.) Response of the redesigned column to the SCT-1 main shock and a 80% aftershock

6.4 Summary

1. In this chapter the effects of the strong duration of the ground motion has been demonstrated. The method used was to subject one of the already designed bridge columns to severe earthquakes to obtaining the seismic response by using the FFEM, activating and deactivating the fatigue model.

2. Also in this chapter the demonstration given in Chapter 2 has been corroborated in regard to the necessary increase in strength of the bridge column to be able to sustain the large cyclic plastic and reversible plastic displacements. The bridge columns were designed according to the new seismic codes prescriptions, but the design failed because of the fracture of one or more longitudinal bars due to the accumulation of plastic strains.

6.5 Conclusions

1. One of the columns with period T = 1.0 s designed according to the AASHTO specifications was subjected to the unscaled CDAO record of the Michoacán, Mexico earthquake. That column is well designed for code requirements but suffered fracture of several bars due to low-cyclic fatigue at t = 59 s and crushing of the confined concrete at about 80 s. The loss of stiffness and strength due to the fracture of bars and later due to the crushing of the confined concrete is very large as seen in Figure 6.1.

2. The same column but without the fatigue model included in the FFEM, subjected to the same factored record shows small reductions in strength and stiffness due to the post-elastic strains of the materials and since there is no fatigue there are no drastic reductions of stiffness and strength. Clearly, the fatigue model allows identifying the accumulation of damage the record induces on the column giving a more realistic response of the column to the unscaled CDAO, Mexico 1985 earthquake.

3. The redesign of a column to increase the strength and stiffness by selecting a larger diameter section to reduce the cyclic plastic strains on the steel bars resulted in a good solution for the design earthquake. However, in the event of aftershock equal to 0.80 times the main shock, 22 bars fracture due to low-cycle fatigue.

4. The previous redesign is not a final solution to decrease the amplitude of the plastic strains to avoid low-cyclic fatigue. It appears that another solution must be sought like the use of dampers, isolators, or energy dissipation devices.

6.6 Remarks

1. Reduction of the fatigue life of the longitudinal steel bars while they are experiencing numerous cycles with large plastic strains during an earthquake is a common flexural failure mechanism. This failure mechanism occurs by fracture of the bars after accumulation of cyclic reversible plastic strains. Once the bar fractures the fatigue model incorporated in the FFEM retires the bar from the section reducing the strength of the bridge column and also its stiffness. Fatigue can be seen as the effect of the duration of the strong part of the ground motion.

2. It can be clearly observed in the examples that when the fatigue model is deactivated from the FFEM there is almost no reduction of the strength, only that corresponding to the crushing of the unconfined concrete cover and that due to decreasing of the confined concrete capacity for large strains as long as they are lower than the ultimate. In addition, the Bauschinger effect deteriorates the stiffness of the column.

3. The fiber finite elements are based on the stress–strain relationship of the confined and unconfined concrete and the steel materials. These relationships are independent of the

duration of the ground motion. Therefore, there is no strength deterioration except that mentioned above.

4. New codes do not prescribe any actions to avoid low-cyclic fatigue.

5. Recognition of the severity of the problem caused by low-cyclic fatigue in code-designed bridge columns highlights the necessity to look for solutions. One possible solution to avoid low-cyclic fatigue could be to reduce the size of the plastic strains so that the cycles can cause some fatigue but the bars do not reach fracture. In Chapter 6 a bridge column was redesigned to avoid fracture of bars due to low-cyclic fatigue. The results show that the re-design fails for the chosen ground motion followed by an aftershock equal to 0.8 times the ground motion

7. DISCUSSION, FINAL REMARKS AND RECOMMENDATIONS

7.1 Discussion

In this section a number of issues related to this research are discussed.

Energy dissipation to measure cumulative damage: It has been demonstrated that the equation of motion can be transformed into the energy equation and that the hysteretic force-displacement response is energy dissipated through heat developed during plastic response. Therefore, the hysteretic energy represents damage in the form of energy dissipated so its use as a measure of damage is conceptually justified. In addition, it is a practical approach to use the hysteretic response since it is possible to use the force-displacement relationship to measure the damage using a single parameter.

Justification of using EPP hysteretic responses for several examples in Chapter 2: The purpose of the examples using EPP systems is to better understand the problem of cyclic response since the demands of strength are directly related to plastic displacement demands. The examples demonstrate that the strength reduction factors and drifts, which are the basis of the force design method specified by many codes, are not enough to obtain safe seismic designs. This is because the strength necessary to satisfy the maximum lateral plastic displacement is not enough to resist the large cyclic plastic displacement demands.

Why not use buckling as a damage indicator? In this dissertation four flexural failure mechanism are used to determine the Significant Damage Performance Level, SDPL. However, buckling has not been used as a damage trigger more important than fracture due to fatigue for the following reasons.

In this dissertation four flexural failure mechanisms inducing damage are considered: crushing of the confined concrete, fracture of bars due to tension, instability of the column due to the P-Delta effect, and reduction of the fatigue life and eventual fracture of bars due to low-cyclic fatigue. The first three are considered as failure mechanisms by AASHTO (2007) so bridge designs must meet such requirements. Fatigue is presented as a fourth mechanism proposed in this dissertation after observing the large cyclic plastic displacements demands and plastic strains demands

during an earthquake. The results of experimental investigations show that those demands induce reduction of the fatigue life and even fracture of the bars.

The model for buckling is not considered in the FFEM. The dissertation is concerned with low-cyclic fatigue and its effects on stiffness and strength degradation of the columns. The FFEM measures strains in every fiber so the analyst knows when the three flexural failures for which bridges are designed according to AASHTO, are reached in a column under strong motion. If crushing of the confined concrete occurs, the analyst will be able to know that in addition to this failure, triggering of buckling could occur in the bars.

From the tests studied by the author, and from the report by Brown and Kunnath (2004), it is clear that reduction of fatigue life begins with the first cyclic plastic strain, and such reduction increases with every additional cyclic plastic strain. If there are enough cycles and the amplitudes of the plastic strains are large, one or more bars can fracture due to low-cyclic fatigue. In order to trigger buckling it is necessary that the confined concrete strain reaches the ultimate confined concrete strain capacity. Then, buckling could occur as long as those very strained bars have not fractured due to low-cyclic fatigue.

Is fatigue a life safety issue? The author considers that the reduction of fatigue life is a safety issue since the bars are weakened by the amount of reduction of fatigue life during the main shock. Further reduction can happen due to a severe aftershock or a future severe ground motion. The fatigue mechanism becomes even more important as a life safety issue if the main shock fractures one or more bars and the aftershock, or a future earthquake, increases the number of fractured bars and reduce even more the fatigue life of the other bars.

The relationship between SDPL and Performance Based Design: In the overall philosophy of performance based design the ranges between performance levels are sometimes very difficult to define. Collapse and life safety performance levels are perhaps the most difficult levels to associate with traditional design parameters. The SDPL can be used to develop a better understanding of the state of a column immediately after the main shock, and how that column will approach the near-collapse level after subsequent aftershocks or future earthquakes.

Are spalling and fracture due to fatigue at the same level of performance? Spalling is not at the same level of performance than fracture of bars due to low-cyclic fatigue. Spalling is related to a minor damage that could trigger other important phenomena. When spalling of the cover concrete occurs, spirals and longitudinal bars support is lost, and cracking of the confined concrete can develop. This could initiate bond slip at the plastic hinge region. In contrast, fracture of bars due to low-cyclic fatigue is related to reduction of strength and stiffness and, therefore, directly related to life safety.

Limitations of fiber elements: In traditional modeling assumptions such as plane sections remain plane, simplified bar pullout, disregard for deformations related to buckling, no bond slip along plastic hinge, etc, are generally made by the analyst. The models used in this research incorporated these assumptions and it is recognized that the quality of results is limited by these assumptions. However, through judicious calibration of several parameters the results from the FFEM simulations matched in a very satisfactory manner the experimental results, both for static and dynamic experiments. The author recognizes that more studies can be performed in the future to overcome the limitations of the fiber elements used for this study.

P-Delta effects: It is recognized that P-Delta effects can be and may likely be a problem as that associated to rebar fracture. In this study the design of the columns studied was done in accordance to the AASHTO provisions which require that P-Delta be less than 25% of the flexural moment capacity. The numerical analyses conducted by the author include P-Delta effects and the results showed no failures related to P-Delta effects. This is why it has been stated that P-Delta was not a controlling factor. Further studies could be conducted in the future for columns where P-Delta is a failure mechanism.

Effect of bar fracture on displacement time history: The results in Chapter 6 show that the peak displacements are similar whether or not fatigue is included in the model. But a closer look at the traces of the time histories shows that they are very different.

Is the relation between fatigue and energy dissipation causal or indirect? The relationship between energy dissipation and fatigue is indirect. The damage due to fatigue is measured using the amplitude of every plastic strain and the number of cycles associated to such strain. The energy dissipation is measured using the demanded lateral strength and the cyclic displacement.

Doubling the strength does not necessarily halve fatigue. The problem is non-linear but the increase in strength will increase the stiffness and for the same energy dissipated there will be less reduction of fatigue life in the steel bars. For instance, in Chapter 6 the column that suffered the fracture of several bars due to low-cyclic fatigue during the main shock did not show fracture but reduction of fatigue life in several bars after re-designing it. The re-design increased the stiffness and strength of the column changing its period. However, an aftershock induced the fracture of even more bars than for the original design.

Relevance of the onset of first damage: The onset of first damage is relevant because it defines at what acceleration level of the design earthquake one of the flexural failure mechanisms occurs. This damage has been defined as the Significant Damage Performance Level which allows the designer to know what is the mechanism inducing such performance level for the factored design earthquake.

Damage index based on the most heavily damaged bar: It would be interesting to consider the fatigue life remaining of the most heavily damaged bar, or the average fatigue life remaining, as the damage index. But one would have to keep in mind that the fatigue damage index measures the reduction of fatigue life of the bars and does not consider the other three mechanisms. Therefore, this index would not be able to capture all of the other possible mechanisms that have been considered in this study.

7.2 Final remarks

In this dissertation there is a set of conclusions at the end of each chapter; therefore, in what follows a set of final remarks and recommendations for future research are presented.

This investigation focuses on the flexural seismic resistant design of bridge columns, considering the effects of cyclic response such as plastic strains leading to the accumulation of damage and deterioration of strength and stiffness of the columns during seismic response.

New seismic bridge design codes do not consider the effect of cyclic plastic displacements and base the design procedures on the displacement capacity of the column calculated when the confined concrete reaches its ultimate strain (given by Mander et al., 1988) or when the P-Δ product reaches a value equal to or larger than 0.25 times the flexural moment capacity as

limited by the new seismic bridge codes. However, the peak lateral displacement as a measure of damage becomes insufficient because it does not measure the accumulation of damage.

The fiber finite element model (FFEM) developed in this investigation was calibrated to simulate the response of columns under cyclic reversible and increasing displacements and later recalibrated to simulate scaled earthquake response of columns tested in a shake table. Therefore, the FFEM can perform acceptable simulations of earthquake response of bridge columns that allow observation of the deterioration of stiffness and strength.

The FFEM contains fiber finite elements with the material characteristics for the steel and the confined and unconfined concrete. These characteristics allow the FFEM to capture the strain levels so that the cracking and crushing of the concrete or fracture of the bars due to tension can be detected. The effect of the confinement given by the spirals is introduced in the FFEM using the equations given by Mander et al. (1988) so that if crushing of the confined concrete occurred the longitudinal bar could have buckled. In addition, the FFEM contains column characteristics like P-Δ effect and low-cyclic fatigue of the longitudinal steel bars.

The proposed FFEM was used in a blind prediction contest organized by the Pacific Earthquake Engineering Research Center to predict the response of a bridge column shake table tested at the University of California, San Diego. The results were sufficiently satisfactory and were awarded a prize of excellence.

Fatigue related damage of the steel bars begins with the first plastic strain, and it increases owing to the accumulation of damage induced by each of the repeated cyclic plastic strains. The continuous damage of the bar during the strong part of the motion could induce its fracture because of low-cyclic fatigue if the strains in the confined concrete are not close to the ultimate confined concrete strain value. If the confined concrete strains are close to the ultimate value, the accumulation of damage in the bar can facilitate its buckling, since the bar has lost its lateral support owing to the crushing of the confined concrete and the enlargement of the spiral.

The vertical component of the earthquake and the transverse horizontal component not considered in this investigation could worsen the damage in the spirals, the steel bars, and the confined concrete.

Following the findings by Mahin and Bertero (1973), in this investigation the cyclic plastic response has been separated into two parts: the new cyclic plastic displacements, each causing major structural damage, and the repeated cyclic plastic displacements, each causing less damage. However, the summation of the repeated displacements could induce fracture of the longitudinal bars due to low-cyclic fatigue.

Results of this investigation show that near fault records with large pulses and few cycles of repeated plastic displacements induce large positive and negative lateral displacements. These form very early in the response envelope of cyclic plastic displacements where the new plastic displacements are located. The large lateral cyclic plastic displacements crack and crush the unconfined concrete and crush the confined concrete, inducing a flexural failure mechanism that is recognized by the new codes; it is the basis for design mentioned above.

The majority of the studies performed in the investigation show that for subduction, crustal, and soft soil records there are several cycles of repeated plastic displacements. Each one causes some amount of damage that is less than that caused by the new plastic displacements, but their accumulation could lead in some cases to fracture of the steel bars due to low-cyclic fatigue during a severe earthquake. Since the materials have a memory, an aftershock or a future severe earthquake can increase the accumulated damage, fracturing several additional bars.

The dissipated energy is the damage induced by the ground motion in a bridge column, and according to the above mentioned findings the total energy can also be separated into that due to all the new plastic displacements and that due to all the repeated ones. Each of these energies is normalized by the energy capacity of the bridge column, and the repeated energy is multiplied by a parameter β_c, which measures the importance of the repeated plastic displacements in the total damage. Adding both fractions and equating them to a cyclic damage index (CDI) allows damage to the bridge column to be estimated.

To estimate β_c a significant damage performance level (SDPL) is proposed. The SDPL corresponds to the occurrence of one of the following flexural failure mechanisms: crushing of the confined concrete, P-Δ effects, fracture of longitudinal bars due to tension, and fracture of

those bars due to low-cyclic fatigue. All of these mechanisms, which are included in the FFEM, can induce damage that could require a costly and difficult retrofit.

In this investigation it is proposed that the SDPL corresponds to a CDI =1.0. Since energies are known from the response, the value for β_c is calculated and results are less than 1.0 for subduction, crustal, and soft soil records. For near fault records with few repeated cycles, β_c can have values larger than 1.0; therefore, β_c does not measure the importance of the repeated cyclic plastic displacements, since the large pulses induce a response of a pushover type. In addition, the SDPL could be used as a way to define the life safety performance level.

The CDI should be estimated not only for the selected ground motions scaled according to the prescriptions of the new codes but also for aftershocks that generally occur after the main shock. The materials have a memory that keeps the damage intact until another earthquake increases it.

Another important feature of this investigation is the comparison of results of code-designed columns under the same earthquake ground motions with and without the low-cyclic fatigue model incorporated into the FFEM.

Without the low-cyclic fatigue model the deterioration of the strength of the column is small, compatible with strains that are large but not close to the ultimate, and the deterioration of the stiffness is due to the Bauschinger effect.

With the fatigue model included, if there is fracture of bars the deterioration of strength and stiffness is quite important because, in addition to the Bauschinger effect, the fracture of the bars decreases the stiffness of the column.

Since the original stress–strain curves of the materials introduced into the fiber finite elements do not change with the duration of the ground motions, it appears that the only way to capture the deterioration of the critical sections of the columns is to include the low-cyclic fatigue model. In this investigation the counting method proposed by Uriz and Mahin (2008) is incorporated in the FFEM.

To avoid the occurrence of low-cyclic fatigue the redesign of columns that suffered fracture of several bars due to this flexural failure mechanism could be based on making the column more rigid, for example, decreasing the limit value of the ultimate confined concrete strain given by the new codes but considering the effect on an aftershock.

Also, the use of external equipment like vibration isolators, energy dissipaters, or dampers could represent a better solution to avoid low-cyclic fatigue.

The redesign of the column shows that in order to consider the effect of cyclic response the strength must be larger than when only the maximum peak lateral displacement is considered for design.

Inelastic structural dynamic analysis for seismic design is needed in order to estimate the cyclic response. As has been pointed out several times, earthquake response is cyclic, and the number of cycles and the amplitude of plastic strains are determining factors in the establishment of the flexural failure mechanism of fracture of steel bars due to low-cyclic fatigue.

Displacement based design (Priestley et al., 2007) is the basis for new code recommendations. It can be used as a pre-design method that should be refined using inelastic dynamic analysis and cyclic response.

Design for low-cyclic fatigue should be included in code recommendations.

7.3 Recommendations

Since the finite fiber element model proposed in Chapter 3 is three dimensional, a program to continue this research is suggested.

A study of the vertical component of the ground motion acting simultaneously with one of the horizontal components of the same ground motion should be considered. The vertical component could add more tension and compression strains to the steel and to the confined concrete.

During this research, it was assumed that the bridge column is fixed only at the lower extreme end and free at the upper one. Any other configuration can be added to the model to consider different support conditions at both ends.

OpenSees contains a model for considering the interaction effects between the foundation and the soil, and it is easy to include the head piles, the piles, and the column. The dynamic soil-structure model can be added to the FFEM proposed in this investigation to study those effects. As well, the kinematic soil and structure interaction can be added to the FFEM.

OpenSees has a drawback. The shear model is independent of the flexural model. This means that the shear model is able to capture the shear response of any fiber representing the confined or unconfined concrete of the bridge column, but there is no relation to the flexural response of the same fiber.

Another extension of this research would be to write the computer model for shear response interacting with the flexural model and incorporate it in OpenSees.

Another drawback in OpenSees is that there is no model to consider the strain penetration in the steel bar into the foundation. This computer model can also be written and incorporated into OpenSees. The writing of this computer model would be another extension of this study. It should be mentioned that in the proposed FFEM a beam-column element of length equal to the strain penetration length was used to simulate this effect and two lateral hinges supports were added in the plane to allow the rotation of the column. The results of the simulations were satisfactory.

Near fault records are recognized by the large pulses inducing large lateral responses; thus, these responses resemble a pushover more than the typical cyclic response. In such cases the energy dissipated by the repeated cyclic plastic displacements is very low and causes little damage. A pushover type of analysis such as the one used in displacement based design would suffice. However, it will always be necessary to check the performance of the inelastic dynamic analysis because in some cases the near fault records contain several repeated plastic displacements so that repeated energy becomes important. This is the case for the Takatory record of the Kobe 1995 earthquake, as can be observed in Appendix C.2.

Therefore, another extension to this investigation would be to separate near fault records into those that induce cyclic response so the parameter $\beta_c < 1.0$ and those with large pulses and almost no cyclic response where $\beta_c > 1.0$ and the response resembles a pushover.

Possibly, near fault records with cyclic response can be treated as all other ground motions studied. Also, when near fault records do not generate cyclic response, the CDI should be based on the pulse response normalized by the pushover capacity.

REFERENCES

American Association of State Highway and Transportation Officials. 2007. Proposed AASHTO Guide Specifications for LRFD Seismic Bridge Design. Subcommittee for Seismic Effects on Bridges T-3. Washington, D.C.

American Society of Testing Materials (ASTM). 2003. “ASTM E 1049 - 85: Standard Practices for Cycle Counting in Fatigue Analysis”. West Conshohocken, PA.California Department of Transportation. 2006.

Banon, H. and D. Veneziano. 1982. “Seismic Safety of Reinforced Concrete Members and Structures". Earthquake Engineering and Structural Dynamics, 10, 179-193.

Berry, M., Parish, M., and Eberhard, M. O., 2004. PEER Structural Performance Database. Pacific Earthquake Research Center. University of California, Berkeley, CA.

Bertero, V.V. Private Communication. 2009.

Bertero, V.V., McClure, G. and Popov, E. 1962. Behavior of Reinforced Concrete frames subjected to repeated reversible loads. Series 100, issue 18. Structures and materials research.

Bozorgnia, Y. and Bertero, V.V. 2004. “Earthquake Engineering. From Engineering Seismology to Performance-Based Engineering”. International Code Council. CRC Press LLC, Boca Raton-Florida.

Brown, J., Kunnath, S.K. 2000. “Low Cycle Fatigue Behavior of Longitudinal Reinforcement in Reinforced Concrete Bridge Columns”. Report No. MCEER-00-0007, Multidisciplinary Center for Earthquake Engineering Research, Buffalo, N.Y.

Brown, J., Kunnath, S.K. 2004. “Low-Cycle Fatigue Behavior of Reinforcing Steel Bars”. ACI Materials Journal, Vol.101, No.6, 457-466.

Calderone, A. J., Lehman, D. E., and Moehle, J. P., 2001. “Behavior of Reinforced Concrete Bridge Columns Having Varying Aspect Ratios and Varying Lengths of Confinement”. Report No. PEER-2000/08. Pacific Earthquake Research Center. University of California, Berkeley, CA.

California Department of Transportation. Cal Trans, 2006. Seismic Design Criteria. Version 1.4. Sacramento, C.A.

Chai, Y., Priestley, M., and Seible, F. 1991. "Seismic Retrofit of Circular Bridge Columns for Enhanced Flexural Performance." ACI Struct. J., 88(5), 572-584.

Chai, Y. H., Priestley, M. J. N. and Seible, F. 1994. "Analytical Model for Steel-Jacketed RC Circular Bridge Columns ", Journal of Structural Engineering, ASCE, Vol. 120, No. 8, pp. 2358-2376.

Chai, Y. H., Romstad, K. M., and Bird, S. 1995. "Energy Based Linear Damage Model for High-Intensity Seismic Loading." Journal of Structural Engineering, ASCE, Vol. 121, No. 5, pp. 857-864.

Cheok, G.S., and Stone, W. C. 1986. “Behavior of 1/6-Scale Model Bridge Columns Subjected to Cycle Inelastic Loading.” NBSIR 86-3494, U.S. National Institute of Standards and Technology, Gaithersburg, Maryland.

Christopoulos, C. and Filiatrault, A. 2006. Principles of Passive Supplemental Damping and Seismic Isolation. IUSS PRESS, Pavia – Italy.

Chung, Y. S., Meyer, C., Shinozuka, M. 1987 . “Seismic damage assessment of reinforced concrete members”. NCEER-87-0022, National Center for Earthquake Engineering Research. Buffalo N. Y.

Clough, R.W., and Penzien, J. 1975. “Dynamics of Structures”. 1st Edition, McGraw-Hill, New York, USA.

Coffin, L. F. Jr. 1954. “A study on the effects of cyclic thermal stresses on a ductile metal”. Transactions of the American Society of Mechanicals Engineers. New York, N. Y., 76, pages 931-950.

Cosenza, E., Manfredi, G. Ramasco, R. 1993. “The use of damage functionals in earthquake engineering: a comparison between different methods”. Earthquake Engineering and structural Dynamics, 22, 10, pages 855-868.

Ecuadorian Society for Earthquake Engineering, 2005. Seismic Design Code for the City of Guayaquil.

Fajfar, P (1992), “Equivalent ductility factors taking into account low-cycle fatigue”, Earthquake Engineering and Structural Dynamics, Vol. 21, pp. 837-848.

Federal Emergency Management Agency. [FEMA]. Recommended seismic design criteria for new steel moment-frame buildings. Report No.FEMA-350, SAC Joint Venture, Washington DC, 2000.

Filippou, F. C., D’ Ambrisi, A., and Issa, A. 1992. “Nonlinear Static and Dynamic Analysis of Reinforced Concrete Subassemblages”. Report No. UCB/EERC-92/08. Earthquake Engineering Research Center. University of California, Berkeley, CA.

Filippou, F. C., Popov, E. and, Bertero, V. V. 1983. “Effects of Bond Deterioration on Hysteretic Behavior of Reinforced Concrete Joints”. Report No. UCB/EERC-83/19. Earthquake Engineering Research Center. University of California, Berkeley, CA.

Giuffre, A. and Pinto, P.E. 1970. “Il Comportamento del Cemento Armato per Sollecitazioni Cicliche di Forte Intensità”. Giornale del Genio Civile.

Hachem, M. M., Mahin, S. A., and Moehle, J. P. 2003. “Performance of Circular Concrete Bridge Columns under Bidirectional Earthquake Loading”. Report No. PEER-2003/06. Pacific Earthquake Research Center. University of California, Berkeley, CA.

Hamilton, C.H., Pardoen, G.C., Kazanjy, R.P. 2002 "Experimental Testing of Bridge Columns Subjected to Reversed-Cyclic and Pulse-type Loading Histories," Report 2001-03, Civil Engineering Technical Report Series, University of California, Irvine.

Haselton, C.B., A.B. Liel, S. Taylor Lange, and G.G. Deierlein. 2008. Beam-Column Element Model Calibrated for Predicting Flexural Response Leading to Global Collapse of RC Frame Buildings, PEER Report 2007/03, Pacific Engineering Research Center, University of California, Berkeley, CA.

Henry, L., and Mahin, S. A. 1999. “Study of Buckling of Longitudinal Bars in Reinforced Concrete Bridge Columns.” Report to the California Department of Transportation.

Hernando, T. Bernal, I. Salas, H. 2007. Informe Preliminar: el sismo de Pisco del 15 de agosto, 2007 (7.9 Mw.). Instituto Geofísico del Perú (IGP).

Hindi, R. A. 2001. “A proposed damage model for R/C bridge elements under cyclic loading”. Ph.D. Thesis, University of British Columbia, Canada.

Hose, Y.D., Seible, F. and Priestley, M.J.N. 1997. Strategic Relocation of Plastic Hinges in Bridge Columns, Structural Systems Research Project, 97/05, University of California, San Diego.

Housner, G.W. 1956. Limit Design of Structures to Resist Earthquakes. Proceedings of First World Conference on Earthquake Engineering, Berkeley, CA. Part 5: 1-13.

Ibarra, L. F., Medina, R. A., and Krawinkler, H. 2005. “Hysteretic models that incorporate strength and stiffness deterioration”. Earthquake Engineering and Structural Dynamics, Vol 34, pp. 1489-1511.

International Building Code, 2006. International Code Council.

Kent, D. C., Park, R. 1971. “Flexural Members with confined concrete”. Journal of the Structural Division, ST-7, ASCE.

Kratzig, W. B. and Meskouris, M. 1987. “Nonlinear seismic analysis of reinforced concrete frames”. Earthquake Prognostics. Vogel and Brandes (editors), Berlag Friedr, Vieweg and Sohn, Braunschweig, 453-462.

Krawinkler, H. 1996. “Cyclic Loading Histories for Seismic Experimentation on Structural Components”. Earthquake Spectra, Vol. 12, No. 1.

Krawinkler, H., Bertero, V.V. and Popov, E.P. 1971. Inelastic Behavior of Steel Beam-to-column Subassemblages. Report No. EERC 71-7, University of California, Berkeley, Calif.

Krawinkler, H., Zohrei, M., Lashkari-Irvani, B., Cofie, N., and Hadidi-Tamjed, H. 1983. “Recommendations for experimental studies on the seismic behaviour of steel components and materials”. Report No. 61, The John A. Blume Earthquake Engineering Center. Stanford University, CA.

Kunnath, S. K., El-Bahy, A., Taylor, A. W. and Stone, W. C. 1997. “Cumulative Seismic Damage of Reinforced Concrete Bridge Piers”. National Institute of Standards and Technology (NIST), Report No 6075.

Kunnath, S. K., Reinhorn, A. M., Lobo, R. F. 1992. “IDARC version 3.0: a program for the inelastic damage analysis of reinforced concrete structures ”. NCEER-92-0022, National Center for Earthquake Engineering Research, Buffalo N.Y.

Lara, O. and Bertero, V.V. 2003. Estudio de los factores de reducción del manual de diseño de estructuras sismo resistentes para Guayaquil y del Uniform Building Code. 12th Congreso Iberoamericano de Ingeniería Sísmica. Mendoza, Argentina.

Lara, O., Bertero, V.V., Ventura, C. and Centeno, J. 2007. Importance of Cyclic Physical Ductility and Cyclic Strength Demand Spectra in Analysis and Design of Earthquake Resistant Structures. Ninth Canadian Conference on earthquake Engineering. Ottawa, Ontario, Canada, 26-29 June 2007.

Lara, O. and Centeno, J. 2007. El sismo de Pisco, Perú de Agosto 17, 2007. Reporte de la Sociedad Ecuatoriana de Ingeniería Sísmica (SEIS). Noviembre, 2007.

Lara, O., Parodi, R., Centeno, J. and Bertero, V.V. 2004. Physical Ductility Demand Spectra for Earthquake Ground Motions Containing Severe Pulses. 13th world conference on Earthquake Engineering. Vancouver, Canada.

Lara O., Ventura, C. and Centeno, J. 2008. The Need for Improving the Reliability of Reduction Factors and Deformations used in the Practice of Seismic Analysis and Design of Structures. 14th world Conference on Earthquake Engineering. October 12-17, 2008, Beijing, China.

Lehman, D.E., and Moehle, J.P. 2000. "Seismic Performance of Well-Confined Concrete Bridge Columns." Pacific Earthquake Engineering Research Center Report 1998/01, University of California, Berkeley, CA.

Lignos, D.G. Krawinkler H. and Whittaker, A. S. 2008. Shaking table collapse tests of two scale models of a 4-story moment resisting steel frame. 14th world Conference on Earthquake Engineering. October 12-17, 2008, Beijing, China.

Lim, K. Y., McLean, D. I., and Henley, E. H. (1991). "Moment-Reducing Hinge Details for the Bases of Bridge Columns." Transportation Research Record, No. 1275, Transportation Research Board, Washington, D.C.

Mahin, S.A. and Bertero, V.V. 1972. “Rate of Loading Effects on Uncracked and Repaired Reinforced Concrete Members”. Report No. EERC 72-9. Earthquake Engineering Research Center. College of Engineering. University of California, Berkeley, CA.

Mahin, S.A. and Bertero, V.V. 1981. An Evaluation of Inelastic Seismic Design Spectra. Journal of the Structural Division. Proceedings of the American Society of Civil Engineers. ASCE. 107: ST9.

Mander, J. B., Panthaki, F. D., and Kasalanti, A. 1985. “Low Cycle Fatigue Behavior of Reinforcing Steel,” Journal of Materials in Civil Engineering, ASCE, V. 6, No. 4.

Mander, J. B., Priestley, M. J. N., and Park, R. 1988. “Theoretical Stress-Strain Model for Confined Concrete”. Journal of Structural Engineering, Vol. 114, Nº 8, ASCE.

Manson, S. S. 1953. “Behavior of materials under conditions of thermal stress”. Heat Transfer Symposium, University of Michigan Engineering Research Institute, Ann Arbor, Michigan, pages 9-75.

Mazzoni, S., McKenna, F., Fenves G. L. and el Al. 2006. “Open System for Earthquake Engineering Simulation User Manual”. *www.opensees.berkeley.edu*.

McKenna Frank. 1997. “Object-Oriented Finite Element Programming: Frameworks for Analysis. Algorithms and Parallel Computing”. PhD Thesis, University of California, Berkeley, CA.

Menegotto, M. and Pinto, P.E. 1973. “Method of Analysis for Cyclically Loaded Reinforced Concrete Plane Frames Including Changes in Geometry and Non-Elastic Behavior of Elements under Combined Normal Force and Bending”. Proceedings, IABSE Symposium on Resistance and Ultimate Deformability of Structures Acted on by Well Defined Repeated Loads. Lisbon, pp. 15-22.

Miner, M. A. 1945. “Cumulative Damage in fatigue”. Journal of Applied Mechanics, Vol. 12, pages A-159.

Miranda, E. and Bertero, V.V. 1994. Evaluation of Strength Reduction Factors for Earthquake Resistant Design. Earthquake Spectra, Vol. 10, No. 2.

Moyer, M., and Kowalsky, M. (2001). “Influence of Tension Strain on Buckling of Reinforcement in RC Bridge Columns.” Department of Civil Engineering, North Carolina State University, Raleigh, North Carolina.

National Building Code of Canada, 2005. National Research Council, Ottawa.

National Geophysical Data Center, NGDC website, 2008.

Newmark, N.M. 1959. A Method of Computation for Structural Dynamics. Journal of the Engineering Mechanics Division, ASCE, 85: 67-94.

Ng K. H., Priestley, M.J.N., and Park, R. 1978. “Seismic Behaviour of Circular Reinforced Concrete Bridge Piers.” Report 78-14, Department of Civil Engineering, University of Canterbury, Christchurch, New Zealand.

Park, Y.J., Ang, A. H-S. 1985. “Mechanistic seismic damage model for reinforced concrete”. Journal of Structural Engineering, 111, 4.

Park, Y.J., Ang, A. H-S. and Wen, Y.K. 1987. Damage-limiting aseismic design of buildings. Earthquake Spectra, 3(1) 1987.

Pontangaroa, R.T., Priestley, M.J.N., and Park, R. 1979. “Ductility of Spirally Reinforced Concrete Columns Under Seismic Loading.” Report 79-8, Department of Civil Engineering, University of Canterbury, Christchurch, New Zealand.

Powell, G H y R Allahabadi (1988), “Seismic damage prediction by deterministic methods: concepts and procedures”, Earthquake Engineering and Structural Dynamics, Vol. 16, 719-734.

Priestley, M. J. N., Calvi, G.M., Kowalsky M. J. 2007. “Displacement-Based Seismic Design of Structures”. IUSS Press, Pavia, Italy.

Priestley, M. J. N., Seible., F., and Calvi, G.M. 1996. “Seismic Design and Retrofit of Bridges”. John Wiley and Sons, New York, USA.

Roeder C., Soderstom, and Graph 2001. "Seismic Performance of Pile-Wharf Connections", Pacific Earthquake Engineering Research Center, PEER.

Saatcioglu, M. 1991. “Modelling Hysteretic Force-Deformation Relationships for Reinforced Concrete Elements”. ACI Special Publication SP-127.

Sasani, M., Bertero, V.V., Anderson, J.C. 1999. Rehabilitation of nonductile RC frame building using encasement plates and energy-dissipating devices. Report No. PEER-1999/12. Pacific Earthquake Research Center. University of California, Berkeley, CA.

Scott, B. D., Park, R. and Priestley, M. J. N. 1982. “Stress-Strain Behavior of Concrete Confined by Overlapping Hoops at Low and High Strain Rates”. ACI Journal, Vol. 79, Nº 1, pp. 13-27.

SEAOC. 1995. Vision 2000 – Performance Based Seismic Engineering of Buildings. Structural Engineering Association of California, Sacramento, CA.

SEAOC. 2003. "Revised Interim Guidelines Performance-Based Seismic Engineering / Force-Displacement Approach for Performance-Based Seismic Engineering". Blue Book. Revised

Sritharan, S., Priestley, M.J.N., Seible F. 1996. "Seismic Response of Column/Cap Beam Tee Connections with Cap Beam Prestressing." Structural Systems Research Project, Report No. ssrp-96/09, University of California, San Diego.

Taucer, F., Spacone, E., and Filippou, F. C. 1991. “A fiber beam-column element for seismic response analysis of reinforced concrete structures”. Report No. UBC/EERC-91/17. Earthquake Engineering Research Center. University of California, Berkeley, CA.

Uriz, P., Mahin, S. 2008. “Toward Earthquake-Resistant Design of Concentrically Braced Steel-Frame Structures”. Report No. PEER-2008/08. Pacific Earthquake Research Center. University of California, Berkeley, CA.

Villemure Isabel. 1995. “Damage indices for reinforced concrete frames: Evaluation and Correlation”. Master’s Thesis, University of British Columbia, Canada.

Williams, M. S., Villemure, I., and Sexsmith, R. G. 1997. “Evaluation of seismic damage indices for concrete elements loaded in combined shear and flexure”. ACI Structural Journal, 94, (3), May-June, 315-322.

Wong, Y.L., Paulay, T., and Priestley, M.J.N. 1990. “Squat Circular Bridge Piers Under Multi-Directional Seismic Attack.” Report 90-4, Department of Civil Engineering, University of Canterbury, Christchurch, New Zealand.

APPENDIX A

Cyclic and non-cyclic strength and plastic displacements demand spectra

A.1 Strength spectra and spectral comparison of cyclic and non-cyclic displacements in terms of strength reduction factors

Strength spectra C_y for several values of R are shown in Figure A.1 a. The ordinate C_y is the seismic coefficient, S_a is the spectral acceleration and W is the weight of the structure.

The importance of R in strength and displacement demands is demonstrated in the following example. In Figure A.1 a for a T = 2.0s structure and R = 4 the demanded strength is C_y = 0.24g.

Figures A.1 b to e show the spectral comparison between the cyclic plastic envelope response u_{cpe} and the non-cyclic lateral plastic response u_{ncp} for several values of R. The results agree with the values shown in Figures 2.4 and 2.5.

For the example, for the T = 2.0s structure and R = 4 in Figure A.1 c there are two values of displacement. For non-cyclic response the displacement demand is u_{ncp} = 20cm while for cyclic response the cyclic plastic envelope demand is u_{cpe} = 60cm.

The question is, will be the structure designed with C_y = 0.24g able to sustain u_{cpe}?

The answer is yes. C_y = 0.24g will sustain u_{cpe} and u_{ncp} but it is questionable whether this resistance will be enough to sustain the fraction of the accumulated u_{cpr} that also causes damage. However, the nature of the EPP system does not allow having an estimation of the level of damage caused by u_{ncp} or by u_{cpe} and the fraction of u_{cpr}. EPP systems do not have limits. It is possible to use any value for R and the resulting cyclic and non-cyclic displacement demands are unlimited, they can be any value.

Since seismic response must be limited by controlling the damage, building codes prescribe fixed values for R_c and for drifts. The fixed R_c reduce the elastic strength demands to be applied

on an elastic model of the structure being designed and the fixed drifts limit only the peak lateral non-cyclic displacements of the structure.

Unfortunately, drifts prescriptions ignore the cyclic reversible response characteristic of structures during earthquakes that demand large values of cyclic ductility. In addition, constant code reduction factors R_c are not related to the ductility demanded by the earthquake on an inelastic structure. This last statement will be demonstrated later in this Appendix.

Notice that according to the building codes, $C_y = 0.24g$ sustains $u_{ncp} = 20cm$, as long as the drift prescription is met. According to the new bridge codes $u_{ncp} = 20cm$ can be acceptable as long this lateral displacement added to the yielding displacement is lower or equal than the displacement capacity. In both cases cyclic response is unknown.

The above analysis also shows that $C_y = 0.24g$ will be able to sustain $u_{cpe} = 60cm$ as mentioned but this strength might not be enough to sustain the fraction of the accumulated u_{cpr} that has not been estimated in the example. The repeated plastic displacements will add vulnerability to the structure particularly if there are several cycles of plastic repeated response therefore the accumulated u_{cpr} must be taking into account using more reliable models to obtain hysteretic responses.

Notice in Figures A.1 b to e that for most of the periods and for any R u_{cpe} is considerably larger than u_{ncp} associated to the same value of R.

This explains clearly that because of the cyclic characteristic of seismic response it is necessary to calculate the energies dissipated by u_{cpe} and by u_{cpr} instead of only u_{ncp} in order to have a more reliable estimation of the potential damage.

Ductility ratios along with drifts still used by buildings codes are not measures of plastic displacements however; the main role of ductility ratios is to limit maximum cyclic or non-cyclic displacements. In what follows cyclic enveloping μ_{cpe} and non-cyclic μ_{nc} ductility ratios are used to limit the corresponding displacements and to prescribe the corresponding strength.

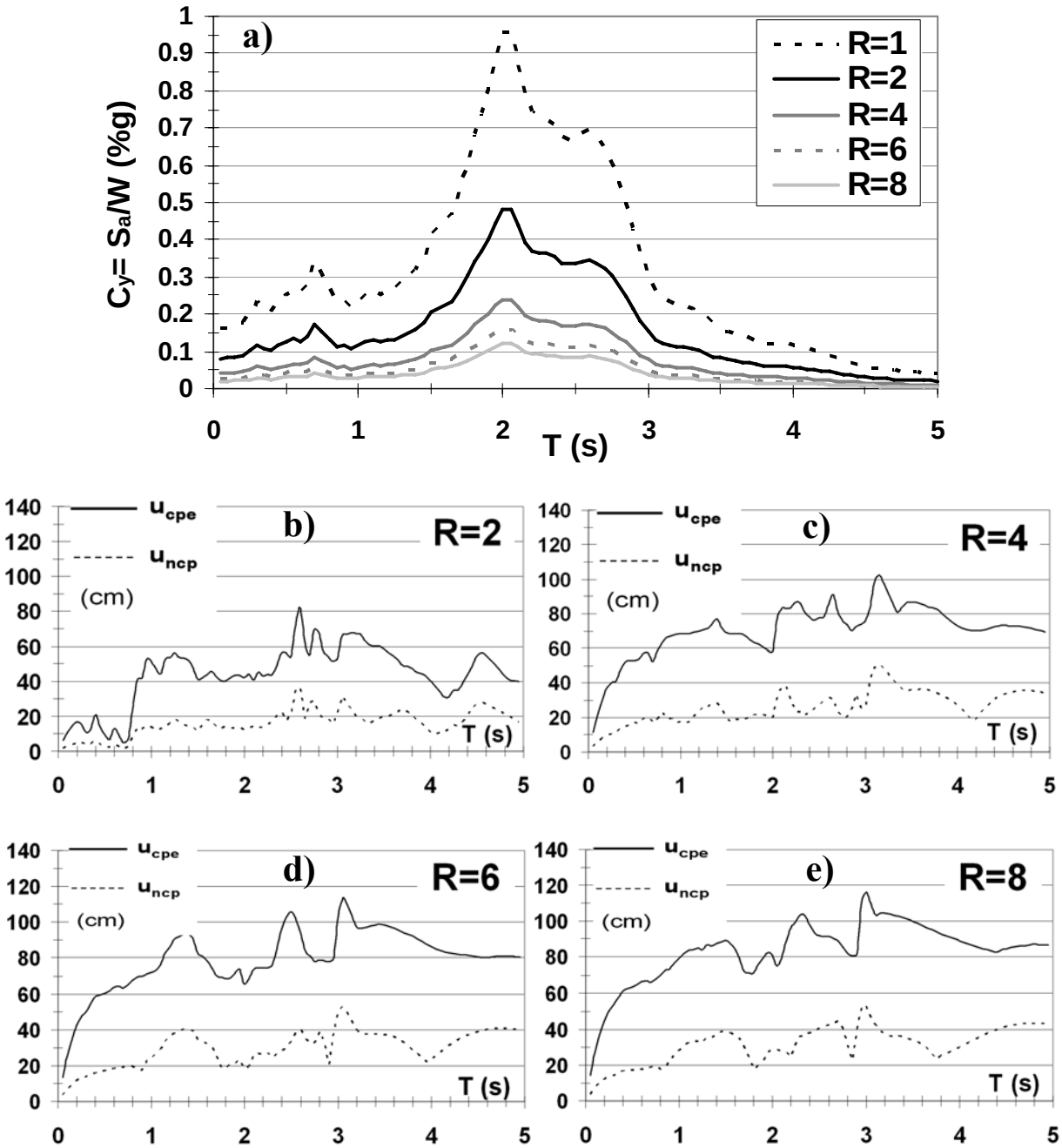

Figure A.1 u_{ncp} **vs.** u_{cpe} **plastic displacements for different values of R. SCT-1 record (ξ = 5%)**

A.2 Cyclic and non-cyclic strength demand spectra for target ductility ratios for the Michoacan 1985 earthquake

To evaluate the effect on strength demand of the limited cyclic envelope response, u_{cpe}, and of the limited peak lateral non-cyclic response, $|u_m| = u_{nc}$, strength spectra for targeted $\mu_{cpe} = \mu_{nc} = 4$ are computed for $\xi = 5\%$ for the SCT-1, CDAO, and CDAF records of the 1985 Michoacán,

Mexico EQ (National Geophysical Data Center – NGDC website, 2008). These are shown in Figures A.2 a, to c. Notice that in what follows u_{nc} is used for the lateral peak response as indicated in the definitions and μ_{nc} is the traditional non-cyclic ductility ratio also indicated in the definitions.

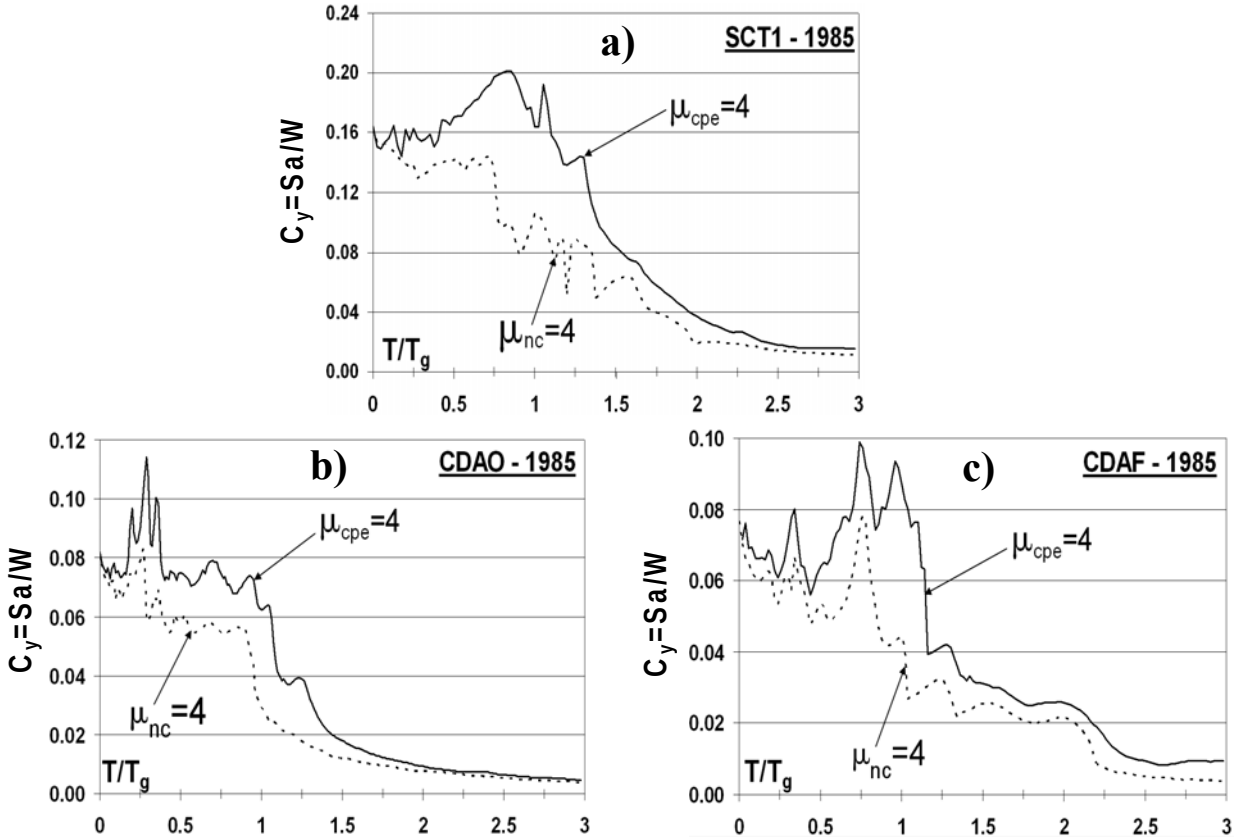

Figure A.2 Cycle envelope and Non Cyclic Strength Demand Spectra for three records of the Michoacán, México 1985 earthquake (ξ = 5%).

The abscissa of these plots represents the ratio between the structure period T and the dominant period of the record T_g that is the period of the soil at the site of the record. This ratio identifies at what T occurs a maximum response and how close it is with respect to T_g, which in the lake bed zone of Mexico City is a value equal or larger than two seconds. The ordinates C_y represent the seismic coefficient or seismic resistance.

According to Miranda and Bertero (1994) the SCT-1 record was recorded on a soil with T_g = 2.0s.

Consider now the following example. In Figure A.2 a for T = 2.0s, T/T_g = 1.0 and μ_{cpe} = 4, the required strength is C_y = 0.162g while for μ_{nc} = 4 this strength is C_y = 0.1g.

Observing Figures A.2 a, to c, the strength ordinates for the μ_{cpe} spectra are considerably larger than the μ_{nc} spectra for almost all period ratios. This means that R for cyclic response is lower than for non-cyclic response, therefore, strengths to sustain u_{cpe} will be larger than those to sustain u_{nc}.

A.3 Physical ductility demand spectra for target ductility ratios for the Michoacan 1985 earthquake

The displacement spectra for u_{cpe} and u_{nc} limited by the target values of μ_{cpe} and μ_{nc} = 4 for SCT-1, CDAO and, CDAF records are shown in Figures A.3 a, to c.

Following with the latest example, for the SCT-1 record, and T/T_g = 1.0 for μ_{cpe} = 4.0, the demanded u_{cpe} = 65 cm and for μ_{nc} = 4.0, u_{nc} = 40 cm as shown in Figure A.3 a.

The meaning of these results is that providing the structure with a strength C_y = 0.162g the structure should be able to sustain the envelope cyclic plastic displacement demand u_{cpe} = 65cm while if the structure is designed for C_y = 0.1g it should be capable to sustain the non-cyclic displacement demand u_{nc} = 40cm. Since the response is cyclic designing for C_y = 0.1g could leave the structure without the necessary strength to sustain u_{cpe} = 65cm therefore the potential damage increases

These results demonstrate that the use of strength reduction factors without the limits imposed by chosen ductility ratios is misleading. In the example shown in Figures A.1, for the T = 2.0s structure and R = 4 the strength demand is C_y = 0.24g to sustain either u_{cpe} = 60cm or u_{ncp} = 20cm. However using the spectra shown in Figures A.2 and A.3 if μ_{cpe} = 4 is used to limit the cyclic envelope response the strength demand is C_y = 0.162g to sustain u_{cpe} = 65cm and if μ_{ncp} = 4 is used the demanded strength C_y = 0.1 is able to sustain only u_{nc} = 40cm. As above indicated the 25cm difference may increase the potential damage. However, it should be kept in mind that

u_{cpr} has not been calculated for the EPP system so none of the strengths might be able to sustain the additional accumulated plastic repeated displacements.

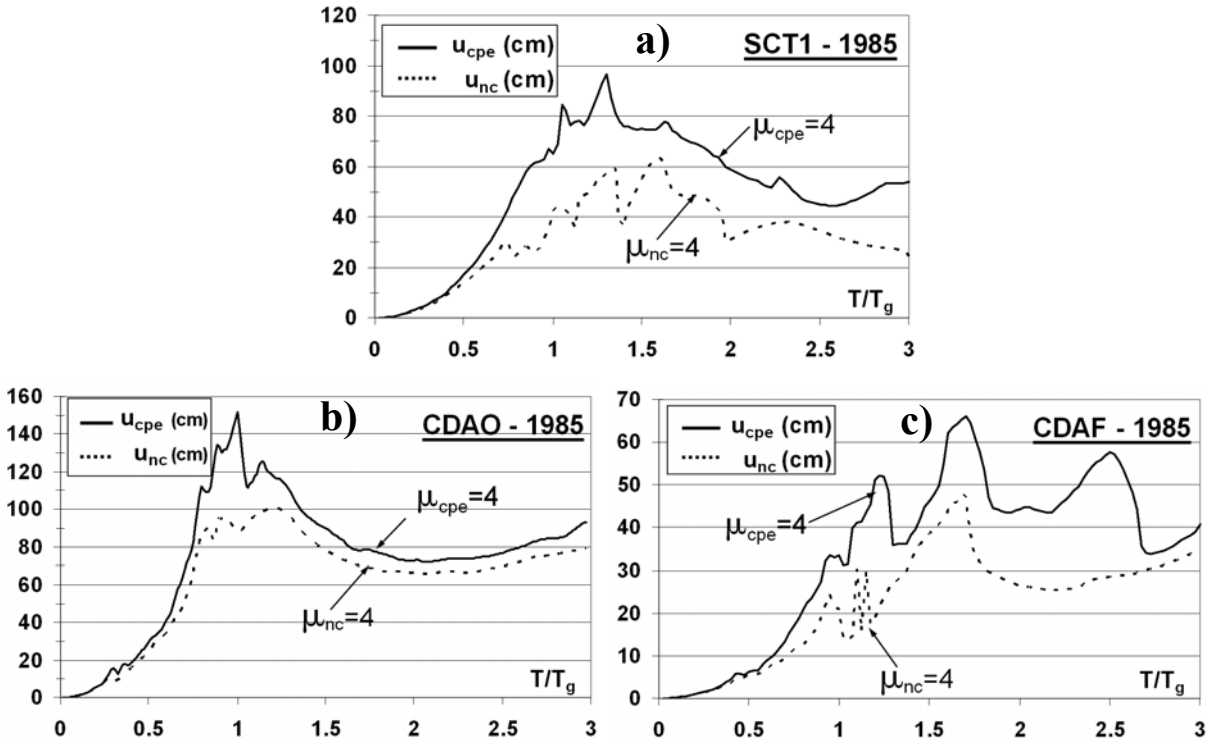

Figure A.3. Cyclic and non cyclic displacement demand spectra for $\mu_{cpe}=\mu_{nc}=4$

By limiting R_c and using drifts, building codes also attempt to limit displacements but drifts are not enough since as above mentioned drifts are independent of the cyclic nature of earthquake response and code reduction factors are not related to the cyclic ductility demand.

New bridge codes limit maximum lateral displacements demands to the lateral displacement capacity but still they do not recognize the cyclic plastic response.

A.3.1 Strength reduction factors for target ductility ratios for the SCT-1 record of the Michoacan 1985 earthquake

Following with the example, Figure A.4 shows the strength reduction factors R required in the T = 2.0s structure to limit u_{cpe} to 65cm and u_{ncp} to 40cm.

For T/T_g = 1.0 and μ_{nc} = 4.0 the value of R = 9.5 as seen in Figure A.4 and in Figure A.2a. This value for R results from Figure A.1 a that shows that F_0 = 0.95g and from Figure A.2 a showing that for μ_{nc} = 4.0, C_y = 0.1g. This large reduction in strength means large potential damage since C_y = 0.1g is able to sustain u_{ncp} = 40cm while u_{cpe} = 65cm.

On the other hand, if cyclic response is recognized for T/T_g = 1.0 and μ_{cpe} = 4.0 the value of R = 5.9 as shown in Figure A.4 and C_y = 0.162g from Figure A.2 a. The value of F_0 does not change and it is still 0.95g. The lower reduction means a larger strength but it is necessary to sustain the large cyclic envelope displacement u_{cpe} = 65cm demanded by the earthquake so the damage due to u_{cpe} can be controlled.

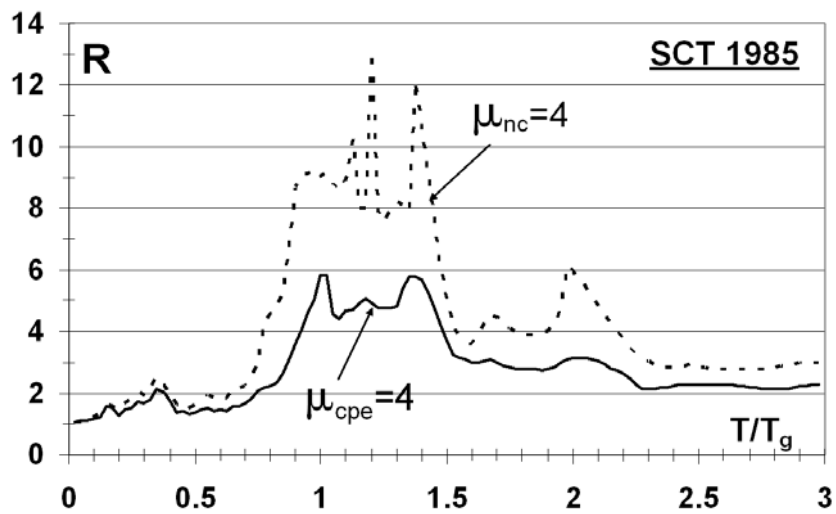

Figure A.4. Variation of strength reduction factor with period for $\mu_{cpe} = \mu_{nc} = 4$

A.4 Cyclic and non-cyclic strength demand spectra for target ductility ratios for firm soil records

Figure A.5 shows the strength spectra for u_{cpe} and u_{ncp} limited by μ_{cpe} and μ_{nc} = 6 and for four subduction earthquakes records. The Caleta record was recorded on rock during the Mexico, 1985 EQ and the others are Chilean records recorded on alluvium during the Valparaiso, 1985 EQ. Again, μ_{cpe} spectra show larger values than μ_{nc} in a wide range of periods. Therefore, strength for u_{cpe} response is equal or larger than that for u_{ncp} response, so R for cyclic response will be equal or lower than R for non-cyclic response.

Notice in Figures A.2 and A.5 the sudden decreases in ordinates for μ_{nc} that do not have a physical explanation but occur due to the numerical procedure involved in choosing the absolute maximum displacement between maximum positive and maximum negative displacements. These sudden decreases create uncertainties in the evaluation of the response (see A.7). The μ_{cpe} spectra are smoother than μ_{nc} spectra but still ordinates present few sudden decreases.

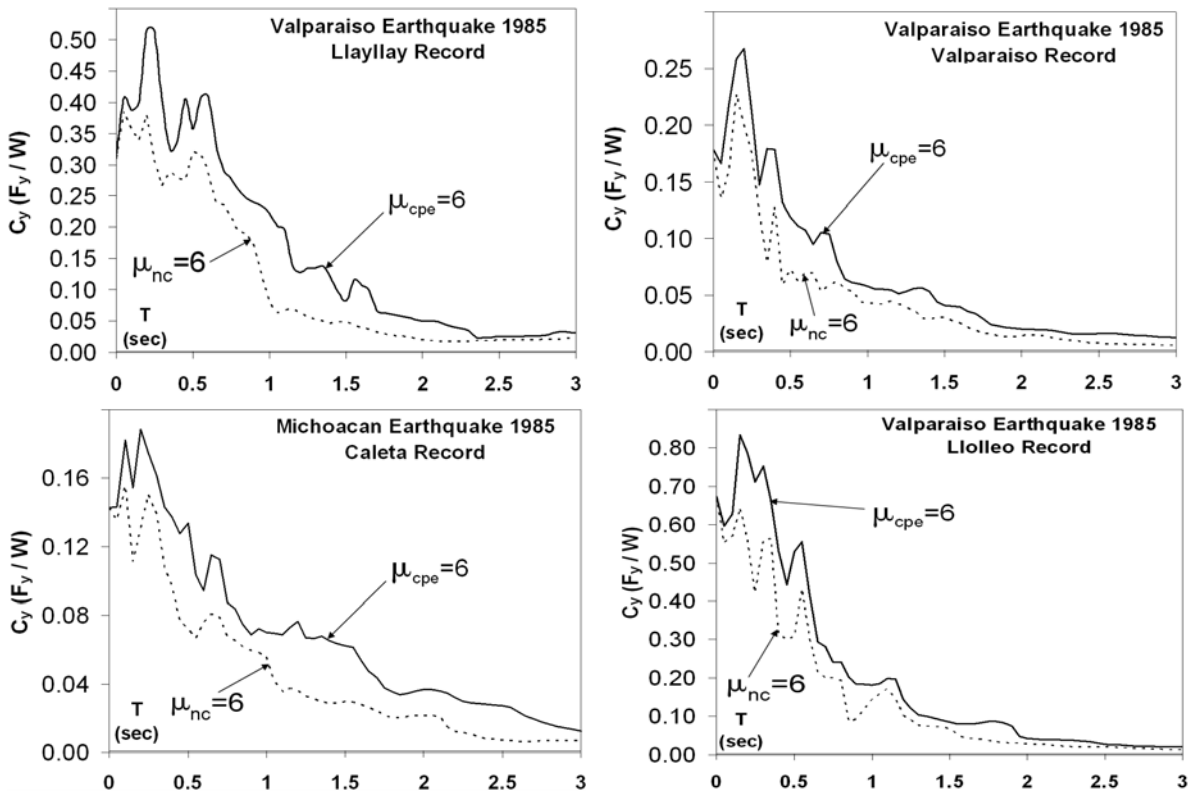

Figure A.5 Cyclic and Non Cyclic Strength Demand Spectra for $\mu_{cpe} = \mu_{nc} = 6$. $\xi = 5\%$

A.4.1 Strength reduction factors for target ductility ratios for firm soil records

Figure A.6 shows the hysteretic responses of a T = 1.0s structure subjected to the Llayllay record for $\mu_{nc} = \mu_{cpe} = 6$. The diagrams in Figure A.6 clearly show how the response is affected by the cyclic or non-cyclic ductility ratio selected. In addition, they show the role of the correspondent values of R as indicated by Lara, Ventura and Centeno (2008).

a)

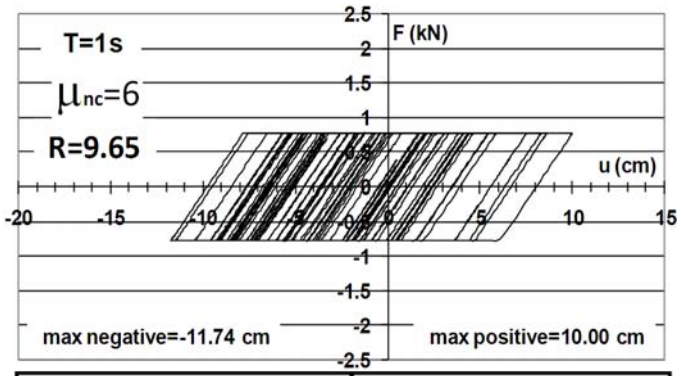

F_o= 7.58 kN	u_y= 1.98 cm
u_o= 19.07 cm	u_m= 11.74 cm
F_y= 0.79 kN	u_{ncp}= 9.76 cm

b)

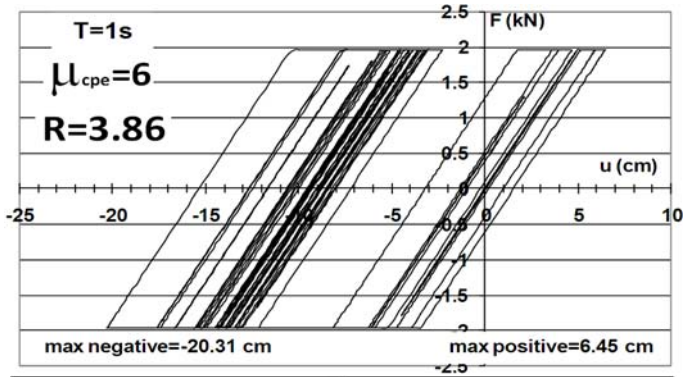

F_o= 7.58 kN	u_y= 4.94 cm
u_o= 19.07 cm	u_{cp}= 16.88 cm
F_y= 1.96 kN	u_{cpe}= 29.64 cm

Figure A.6. Hysteretic Responses for SDF systems with T=1.00s subjected to the Llayllay Record of the Valparaiso 1985 EQ, for (a) μ_{nc} = 6 and (b) μ_{cpe} = 6.

In the example, the elastic strength demand, F_0, is 7.58kN. For the target μ_{nc} = 6, Figure A.5 a shows that for T = 1.0s, R is 9.65 and F_y = 0.79kN while for the target μ_{cpe} = 6 and T = 1.0s, Figure A.6 b shows that R = 3.9 and F_y = 1.96kN. Assume that the designer chooses the traditional solution of μ_{nc}, then R = 9.65. Apparently, his/her selection leads to a more economical design. In this case, F_y = 0.79kN is the strength the structure needs to deform plastically u_{ncp} = 9.8cm as seen in Figure A.6 a.

If the designer is aware of cyclic response, Figure A.6 b indicates that for T = 1.0s and μ_{cpe} = 6, F_y = 1.96kN is the strength required by the structure to deform plastically in both directions the demanded u_{cpe} = 29.6cm. This cyclic plastic envelope displacement includes reversals of plastic displacements Thus, designing for F_y = 0.79kN will necessarily induce a larger potential damage. In addition, it should be kept in mind that cyclic plastic repeated displacements are not considered in any of these examples.

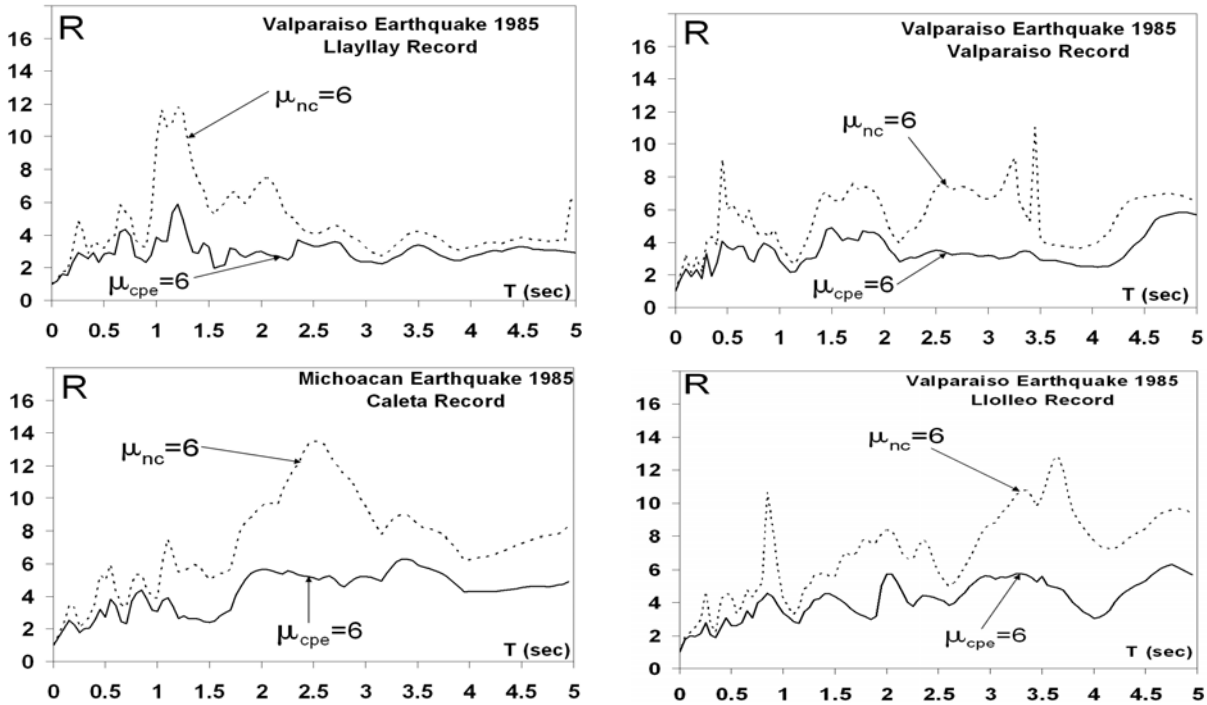

Figure A.7. Cyclic and non cyclic strength reduction factor demand spectra for $\mu_{nc} = \mu_{cpe} = 6$ and ξ=5%

Figure A.7 shows the variation of R with respect to T for $\mu_{nc} = \mu_{cpe}$ = 6 for four records. The differences between the values of R for μ_{cpe} and μ_{nc} are small for T ≤ 0.2s and become more important for longer values of T. The largest differences occur in different period ranges, i.e. for the Mexican Caleta record at T = 2.5s, for μ_{nc} = 6, R = 13.5 and for μ_{cpe} = 6, R = 5. Notice that the ordinates not only vary with the periods but also with the excitation and with the cyclic or non-cyclic response previously chosen for design. Therefore, reduction factors are not constants. These calculated variable R's are directly related to the expected ductility capacities to be provided to the structure through design. They are not code values.

At this point, it results clear that code R_c values are not necessarily related to the ductility demanded by the earthquake on the structure.

These results have two implications. First, if the designer chooses the traditional μ_{nc} the corresponding R is larger than the R he/she will obtain choosing $\mu_{cpe.}$. Second, the reduced strength for μ_{nc} might not be enough to restrict the potential damage induced by u_{cpe}.

Since plastic displacement is damage, the lower the F_y the larger the u_{cpe} and the larger the potential damage. Notice that this analysis is based only on u_{cpe} while the unknown fraction of the accumulated u_{cpr} that will add damage to the structure has not been considered for the reasons above mentioned.

A.4.2 Physical ductility demand spectra and energy demands for target ductility ratios for firm soil records

The comparisons between u_{cpe} and u_{ncp} for different values of R are shown in spectral form in Figure A.1 where it was already proven that u_{cpe} is larger than u_{ncp} for all the range of periods shown.

It was also proven above that maximum lateral or cyclic envelope displacements must be limited by ductility ratios therefore, in what follows the variations of u_{cpe} and u_{ncp} for constant selected values of μ_{cpe} and μ_{nc} is studied. The variations are studied for the four subduction ground motions above mentioned and a value of six is chosen for both ductility ratios.

Observing Figure A.8, u_{cpe} demands are considerably larger than u_{ncp} demands for all records, all periods and for both ductility ratios.

Recalling that potential damage is related to the energy dissipated, Figure A.9 shows the total dissipation of energy demanded by the ground motion. Figure A.9 a shows the hysteretic response and the demanded dissipation of energy for μ_{cpe} = 6 of a T = 1.0s structure subjected to the Llolleo record. Here, E_H = 108.4kN-cm; E_{ucpe} = 47.6kN-cm and E_{ucpr} = 60.8kN-cm. This result would indicate the importance of the repeated cyclic plastic displacements that could cause

low-cyclic fatigue during the response of the structure as it will be seen in the Chapters. The Figure also shows that the required strength to permit the demand of u_{cpe} = 29.8cm is F_y = 1.78kN and the calculated R is 3.4.

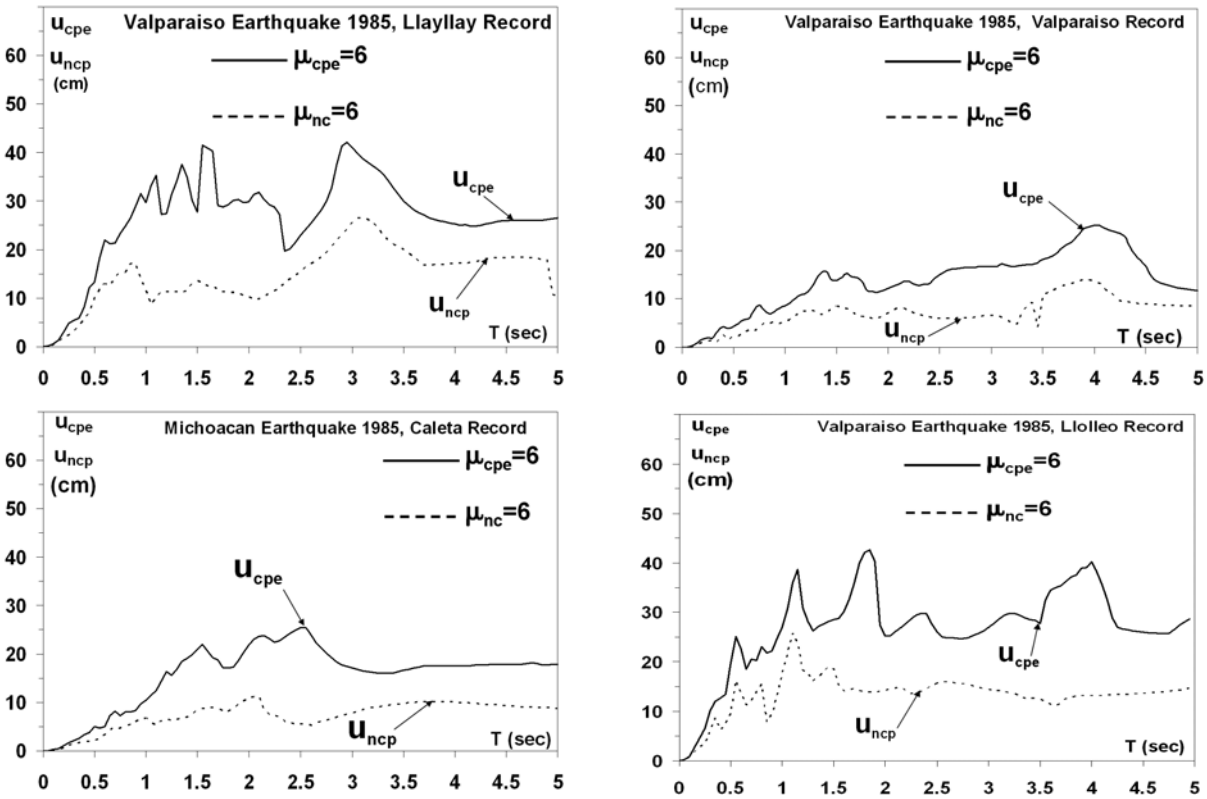

Figure A.8. u_{cpe} and u_{ncp} vs. $\mu_{cpe} = \mu_{nc}$ = 6 and ξ=5%.

For the same structure and same record, Figure A.3 b shows the hysteretic response for μ_{nc} = 6. In this example, E_H = 116.1kN-cm, E_{ucpe} = 56.0kN, and E_{ucpr} = 60.1kN. If μ_{nc} is chosen for design, the energy dissipated by the new plastic excursions is a close value to the one provoking low-cyclic fatigue so the non-cyclic result can mislead the designer. In addition, F_y = 1.4kN corresponding to R = 4.2 is required for the structure to displace laterally the demanded u_{ncp} = 21cm.

For this example, the demand of energy dissipation for cyclic plastic displacements is slightly lower than that when only lateral non-cyclic response is considered, but the required strength to cover u_{cpe} is larger than the one to cover u_{ncp}.

a)

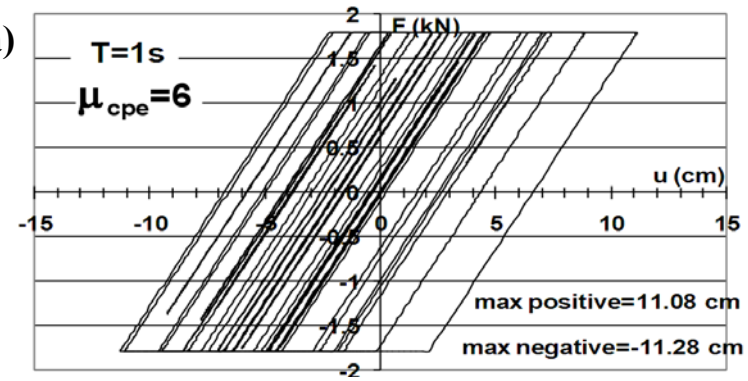

F_o= 5.99 kN	u_y= 4.50 cm	E_H= 108.41 kN-cm
u_o= 15.12 cm	u_{cpe}= 26.76 cm	E_{ucpe}= 47.63 kN-cm
F_y= 1.78 kN	R= 3.36	E_{ucpr}= 60.78 kN-cm

b)

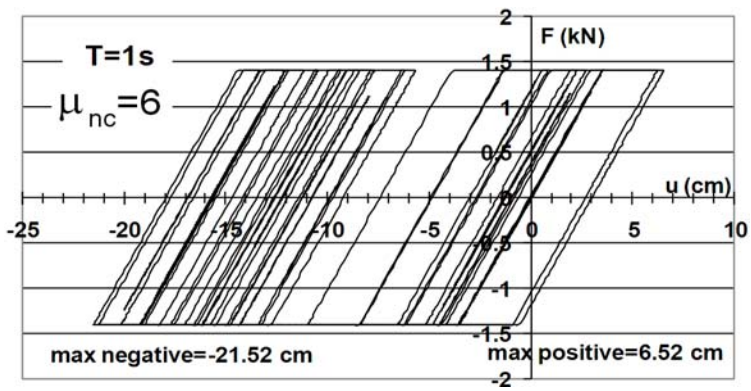

F_o= 5.99 kN	u_y= 3.54 cm	E_H= 116.14 kN-cm
u_o= 15.12 cm	u_{ncp}= 21.00 cm	E_{ucpe}= 56.00 kN-cm
F_y= 1.40 kN	R= 4.27	E_{ucpr}= 60.14 kN-cm

Figure A.9 Hysteretic responses of Llolleo 1985 record for T=1s and (a) μ_{cpe}=6; (b) μ_{nc} =6 and ξ=5%

A.5 Relationship between μ_{cpe} / μ_{nc} and R vs. T

Ductility ratios are not measures of damage, however as explained cyclic and non-cyclic ductility ratios limit the lateral and cyclic envelope displacements and in addition codes assume that R = $\mu_{nc.}$ Therefore, the sensitivity of μ_{nc} and μ_{cpe} to values of T for different R's is studied.

The procedure used is: (1) choose μ_{nc} or μ_{cpe}; (2) solve equation 2.12 for several values of R until the selected values of μ_{nc} and μ_{cpe} are met; (3) select the absolute maximum values for μ_{nc} and μ_{cpe} and draw the corresponding spectra.

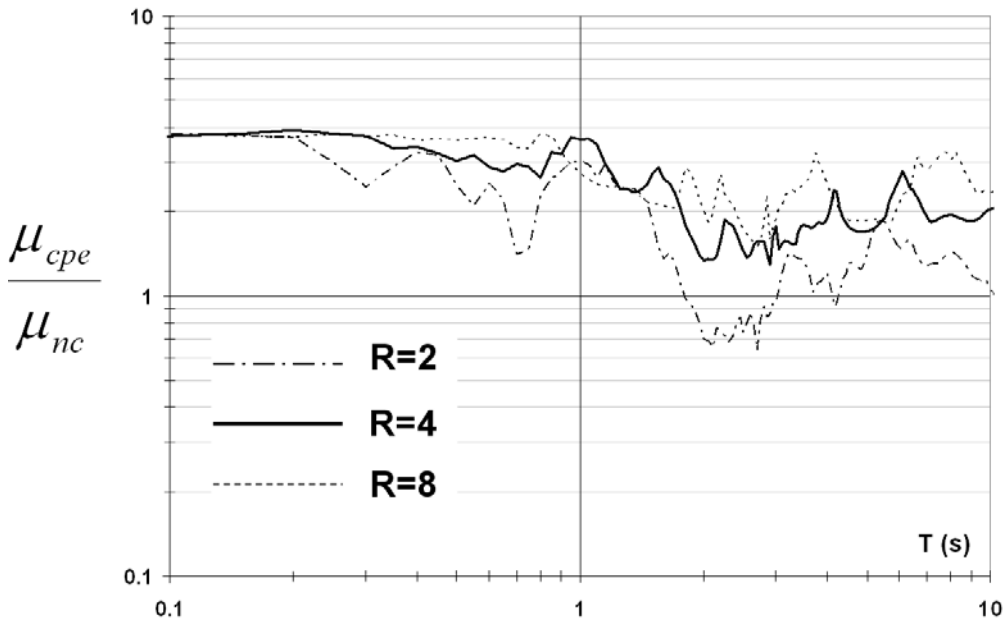

Figure A.10 μ_{cpe} / μ_{nc} ductility ratios vs. T for different values of R. SCT-1 record, ξ = 5%

Figure A.10 shows for the SCT-1 record that for any value of R, μ_{cpe} values are larger than μ_{nc} in almost all regions of the spectra except for R = 2 in the range of periods between T = 2s and 3s and that ductility ratios are not equal to strength reduction factors, R.

The Figure A.10 also shows that for R = 4 and T $\leq$ 2.0s, μ_{cpe} demands vary between 2 and 4 times μ_{nc} demands.

A.6 Effects of aftershocks on the cyclic response

Figure A.11 shows the acceleration record registered at the ICA Pisco E-W station during the August 17, 2007, Pisco, Peru earthquake, Hernando, Bernal, and Salas (2007), where it can be observed that there are two events. The first shock duration is 67s, Lara and Centeno, (2007) and immediately the aftershock triggers for a total duration of 220s for the acceleration record. The earthquake caused total collapse of adobe houses, heavy damage in some reinforced concrete buildings and sinking of small reinforced concrete houses due to liquefaction, Lara and Centeno (2007).

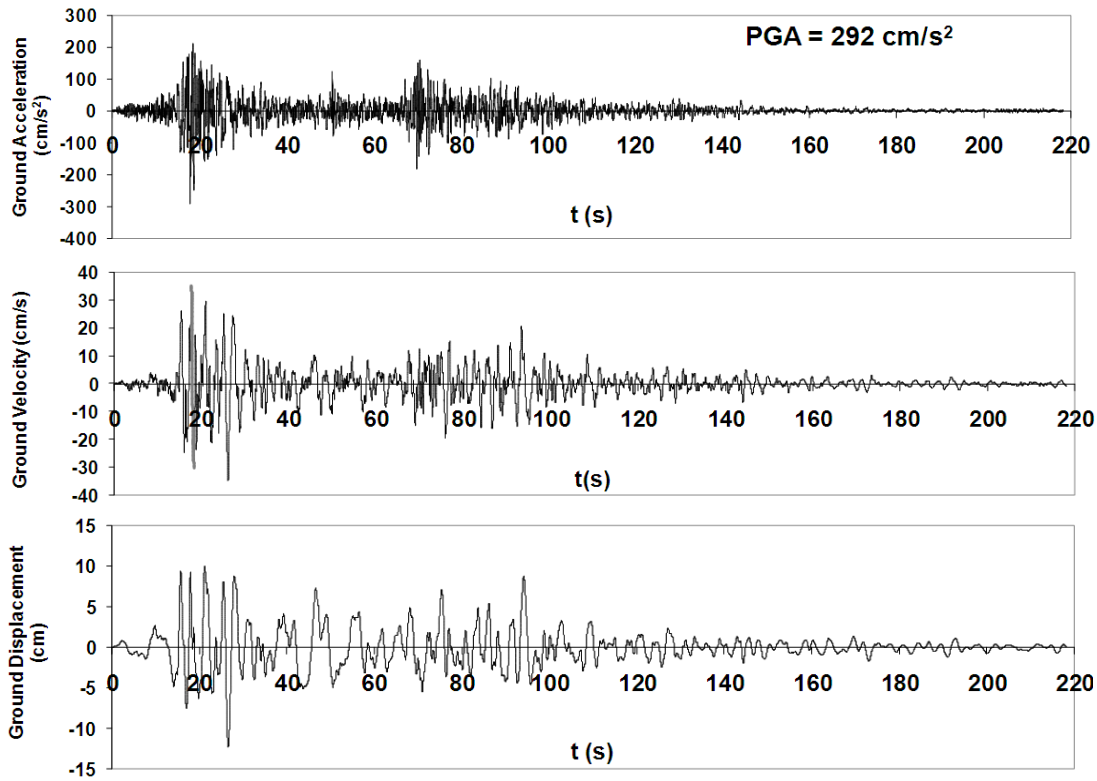

Figure A.11 Pisco (EW) record of the 2007 Peru Earthquake.

In order to observe the effect of the aftershock on the response, a T = 1.0s EPP, SDOF structure is subjected to the record of the first shock and its responses for R = 4 and 8 are shown in Figure A.12.

When R = 4, Figure A.12 a, at t = 17.6s the system reaches its maximum negative displacement of 19.4cm being an almost one sided response. There is only one maximum positive displacement reaching 4.1cm and after that, all displacements become negative since there is not a single crossing for zero displacement that would displace the structure in the positive direction. At the end, the total residual displacement would have been 10.7cm, and the plastic residual displacement would have been 7.5cm since u_y = 3.2cm, if the aftershock had not occurred.

The demanded E_H is 56.5kN-cm, E_{ucpe} = 34.9kN-cm and E_{ucpr} = 21.6kN-cm as seen in Figure A.13 a. The importance of the new plastic displacements is seen in the tendency of the structure to displace in one direction, which could lead to an incremental collapse type of failure for the EPP model.

For R = 8 as seen in Figure A.12 b, the maximum negative displacement reaches 33.01cm while the maximum lateral positive displacement is 6.0cm. After a positive cycle, the response is again one sided thus the new plastic excursions would lead the structure to a large lateral displacement. For R = 8, E_H = 64.1kN-cm, E_{ucpe} = 38.2kN-cm and E_{ucpr} = 25.9kN-cm, Figure A.13 b.

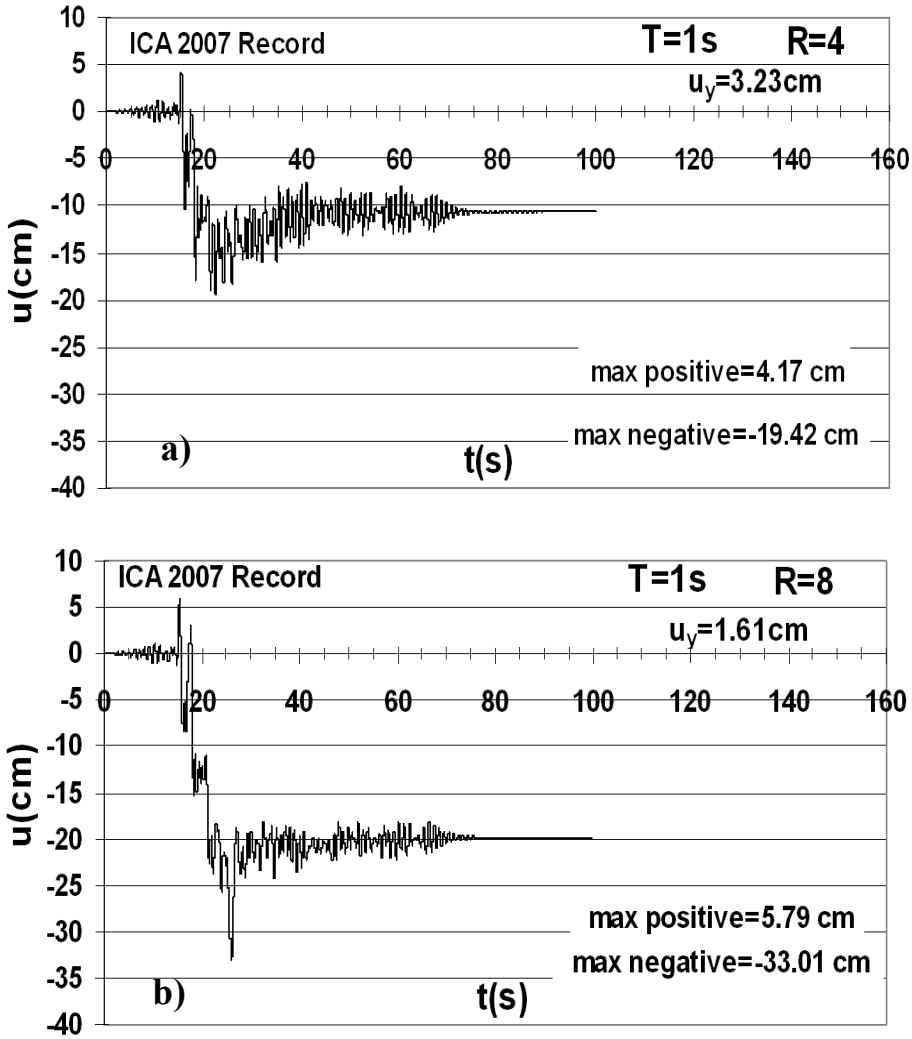

Figure A.12 Response of a T = 1.0s structure to the first shock: (a) R = 4; (b) R = 8.

The residual displacement would have been 20cm, and the plastic residual displacement would have been 18.4cm since u_y = 1.6cm, if the aftershock had not occurred.

Figures A.14 a, and b show the time history responses of the same structure to the complete record. For the same values of R, the demanded cyclic plastic envelope displacements are about the same because most of the plasticity takes place during the first shake and the response is mainly one sided.

a)

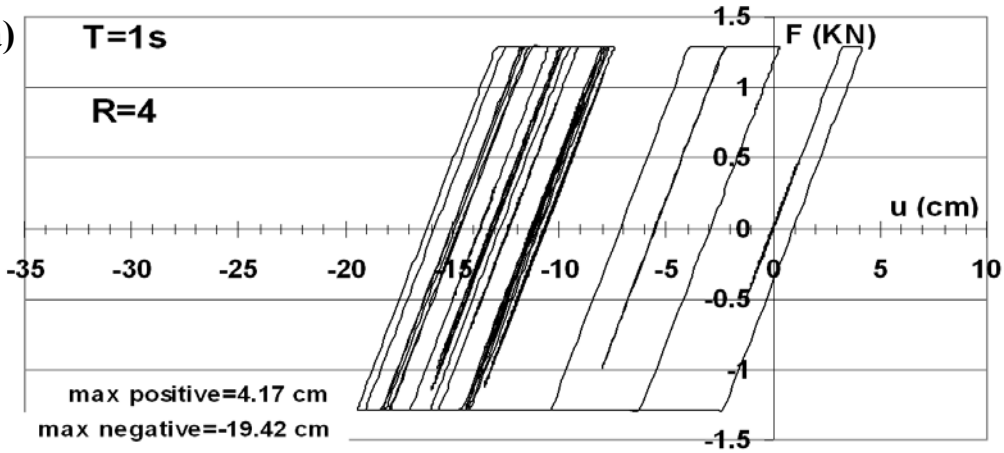

F_o=	5.12 KN	u_{cpe}=	27.26 cm
u_o=	12.92 cm	E_H=	56.46 kN-cm
F_y=	1.28 KN	E_{ucpe}=	34.89 kN-cm
u_y=	3.23 cm	E_{ucpr}=	21.57 kN-cm

b)

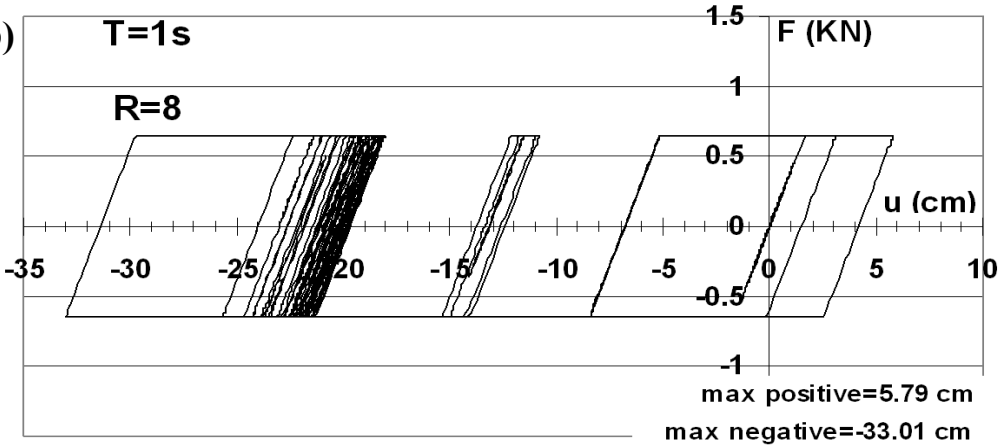

F_o=	5.12 KN	u_{cpe}=	59.66 cm
u_o=	12.92 cm	E_H=	64.08 kN-cm
F_y=	0.64 KN	E_{ucpe}=	38.18 kN-cm
u_y=	1.61 cm	E_{ucpr}=	25.90 kN-cm

Figure A.13 Hysteretic response to the first shock

The residual displacement for R = 4 is 14.6cm, 37% larger than the one left by the main shock and the plastic residual displacement is 11.4cm since u_y = 3.2cm. For R = 8 the residual

displacement is 25cm, an increase of 26% from that of the main shock and the plastic residual displacement is 23.4cm since u_y = 1.6cm.

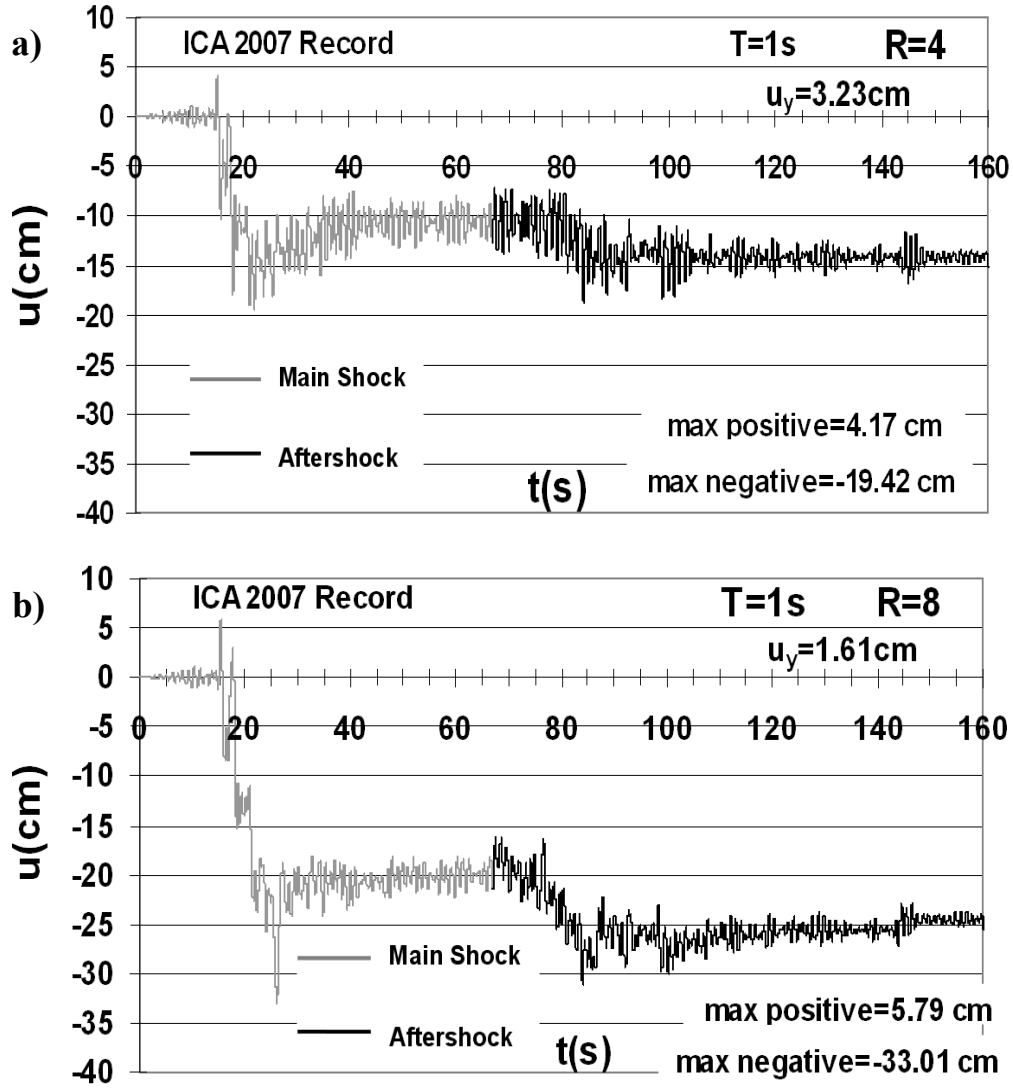

Figure A.14 Time History responses for T=1s, R=4 and 8 of the Pisco complete record.

The aftershock increases the number of cycles for both R values. For example, when R = 8, Figure A.15 b, E_H = 100.6kN-cm, value 56% higher than for the first shock. E_{ucpe} = 39.5kN-m, just 3% higher than for the first shock, and E_{ucpr} = 61.1kN-cm that is 235% higher. In Figure A.15 b the results indicate that for the complete record low-cyclic fatigue could lead the structure to a high level of damage.

a)

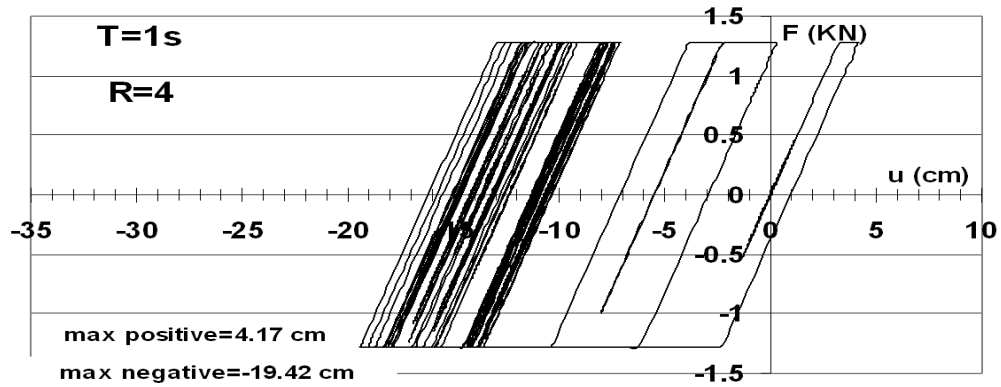

F_o=	5.12 KN	u_{cpe}=	28.10 cm
u_o=	12.92 cm	E_H=	75.62 kN-cm
F_y=	1.28 KN	E_{ucpe}=	35.97 kN-cm
u_y=	3.23 cm	E_{ucpr}=	39.65 kN-cm

b)

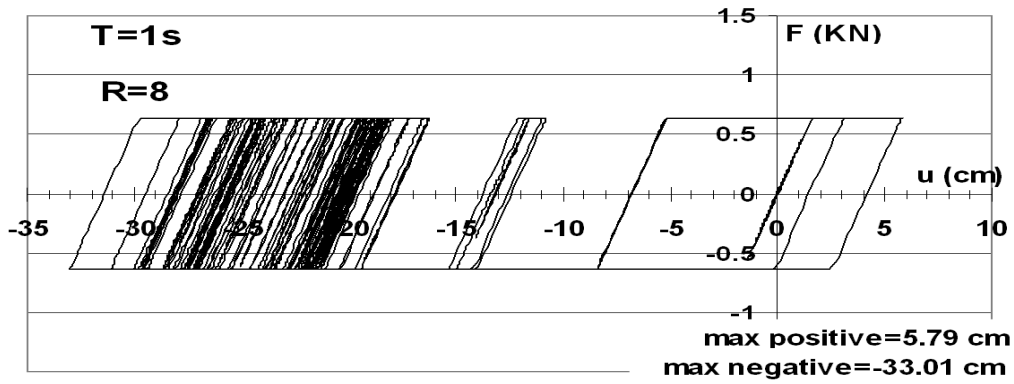

F_o=	5.12 KN	u_{cpe}=	61.66 cm
u_o=	12.92 cm	E_H=	100.56 kN-cm
F_y=	0.64 KN	E_{ucpe}=	39.46 kN-cm
u_y=	1.61 cm	E_{ucpr}=	61.10 kN-cm

Figure A.15 Hysteretic responses for T=1s, R=4 and 8 of the Pisco complete record.

A.7 Sudden variations of the μ_{nc} spectra

The inelastic μ_{nc} spectra generally show several sudden abrupt changes of their ordinates (Sasani, Bertero, Anderson, 1999) and it is of interest to determine the reason for these changes. Consider the inelastic response of two structures characterized by T = 1.0 and T = 1.05s and μ_{nc} = 8 (Figures A.16 and A.17) to the Takatori 1995 ground motion. For structures with close periods, there is no apparent reason to have a large difference between their responses. However,

Figures A.16b, A.17b, show the contrary. For T = 1.0s, u_m = + 71.33cm, and u_y = 8.92cm (Figure A.16b) while for T = 1.05s, u_m = - 49.24cm, and u_y = 6.18cm (Figure A.17b). Figures A.18a and A.18b show the respective time histories. In addition, from Figures A.16b and A.17b, for T = 1.0s, R associated to μ_{nc} is 4.5 while for T = 1.05s, R associated to μ_{nc} = 7.2 meaning that in just 0.05s increase in period there is a sudden decrease in strength of 60%.

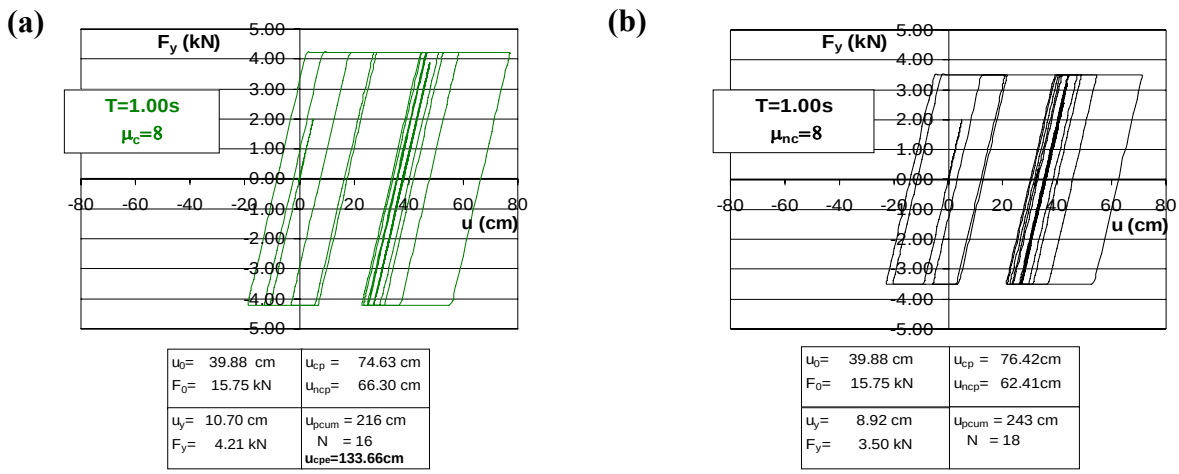

Figure A.16. Hysteretic Response for SDFS with T=1.00s to the Takatori Record from Kobe 1995 Earthquake ; (a) μ_c =8; and (b) μ_{nc} =8

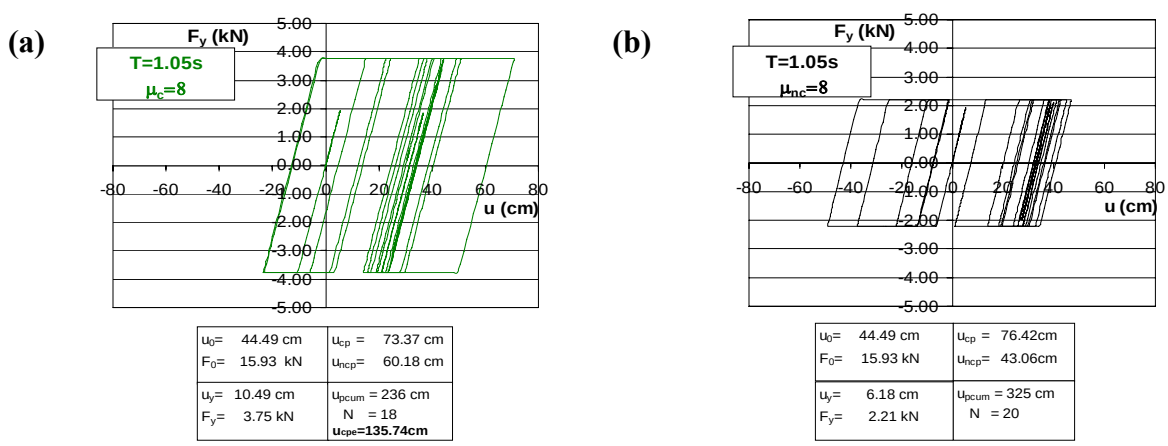

Figure A.17. Hysteretic Response for SDFS with T=1.05s to The Takatori Record from Kobe 1995 Earthquake: (a) μ_c =8; and (b) μ_{nc} =8

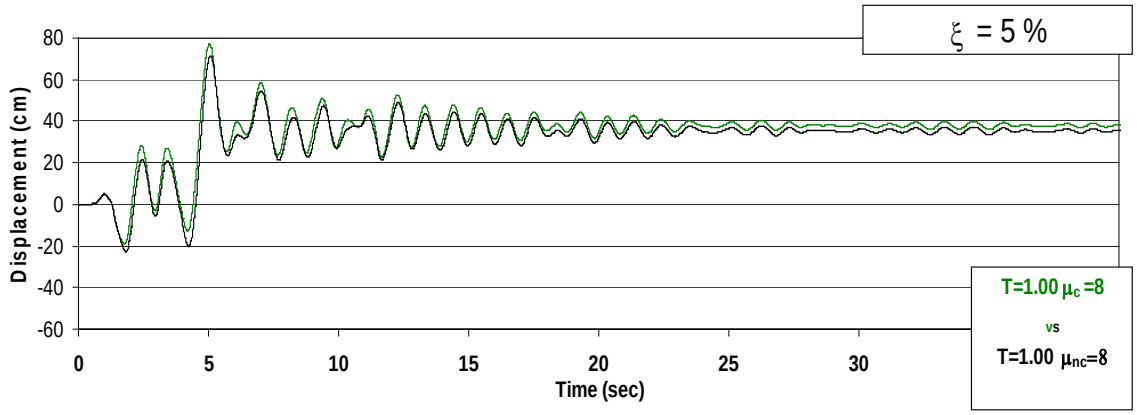

Figure A.18a. Time History Response for SDFS with T=1.00s and $\mu_c = \mu_{nc}$ =8 to the Takato Record from Kobe 1995 Earthquake

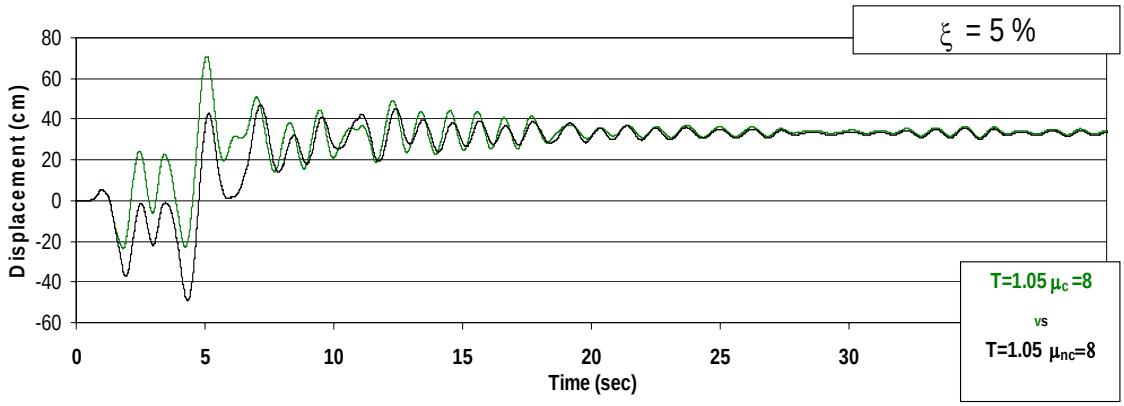

Figure A.18b. Time History Response for SDFS with T=1.05s and $\mu_c = \mu_{nc}$ = 8 to the Takatori Record from Kobe 1995 Earthquake.

Figure A.19a shows that for T = 1.0s there are two values of R: 4.5 and 7.1 that would allow a dynamic response limited by the target μ_{nc} = 8. The lowest value, R = 4.5, will provide the maximum yielding strength and therefore is chosen as the strength reduction. In effect, for this μ_{nc}, F_0 = 15.75kN and F_y = 3.5kN. Notice that R = 4.5 for μ_{nc} is associated to negative values of u_m, while R = 7.1 for μ_{nc} is related to positive values of u_m and that both deformations cross at R = 7.5 and μ_{nc} = 9.0.

Figure A.19b shows that to meet the target μ_{nc} = 8 for the T = 1.05s structure there are also two values of R associated to μ_{nc}: 7.2 and 7.5. The first is associated to positive values of u_m and the

second to negative values of u_m. Again, the lowest value of R, equal to 7.2, is chosen as the strength reduction to obtain a response limited by $\mu_{nc} = 8$ for this structure. Both deformations cross each other at R = 7.0 and $\mu_{nc} = 6.8$. The reason for these changes is the use of u_m that does not account for the previous plastic deformation. When cyclic deformations are used to calculate the response limited by target cyclic ductility ratios, the above mentioned incongruence does not occur. In Figure A.19a there is a one to one relation between $R_{\mu c}$ and μ_c. For T = 1.0s and $\mu_c = 8$, R = 3.75. Thus, for F_0 = 15.75kN, F_y = 4.21kN. In Figure A.19b there is also a one to one relation between R and μ_c. For $\mu_c = 8$, R = 4.2 thus F_0 = 15.93kN and F_y = 3.75kN. This means that for this small increase of T the difference in strength reductions is only 10%, which is compatible with the difference in the values of F_0.

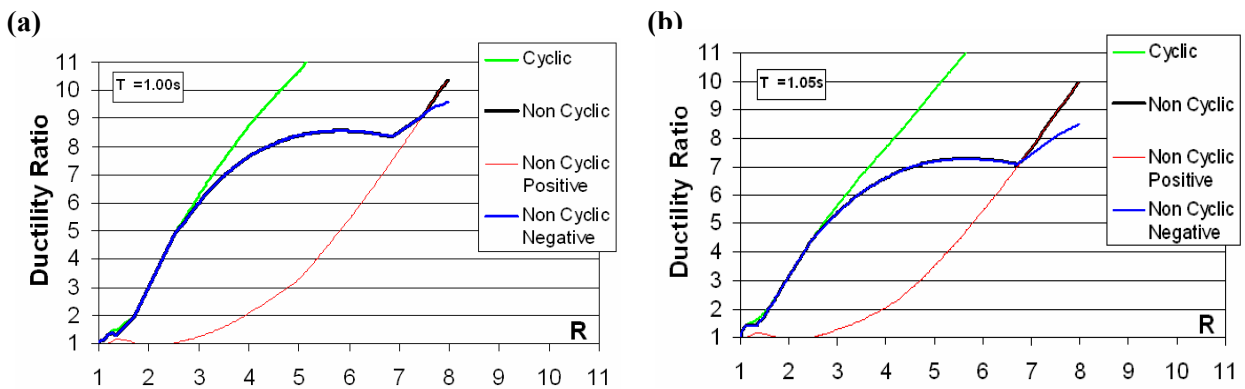

Figures A.19 Cyclic and non-cyclic ductility ratio vs. strength reduction factors

APPENDIX B

FFEM parameters calibration

B.1 Calibration of number of section fibers

Table B.1. Comparison of Energy calculated with different combinations of section fiber subdivisions.

	COLUMN		# Transverse Subdivisions	# Core Radial Subdivisions	# Cover Radial Subdivisions	TEST COLUMN DISSIPATED ENERGY (kN-m)			SIMULATED COLUMN DISSIPATED ENERGY (kN-m)			ERROR		
	COD.	AUTHOR				HYSTERETIC	ENVELOPE	REPEATED	HYSTERETIC	ENVELOPE	REPEATED	HYSTERETIC	ENVELOPE	REPEATED
1	328	Calderone et al. 2000	16	16	4	921.30	163.67	757.64	938.44	153.78	784.66	1.86%	-6.04%	3.57%
2	328	Calderone et al. 2000	20	10	1	921.30	163.67	757.64	920.68	151.32	769.37	-0.07%	-7.54%	1.55%
3	328	Calderone et al. 2000	20	10	2	921.30	163.67	757.64	922.96	151.86	771.10	0.18%	-7.22%	1.78%
4	328	Calderone et al. 2000	24	16	1	921.30	163.67	757.64	950.06	154.33	795.73	3.12%	-5.71%	5.03%
5	328	Calderone et al. 2000	24	16	4	921.30	163.67	757.64	942.26	152.78	789.48	2.27%	-6.65%	4.20%
6	328	Calderone et al. 2000	24	10	1	921.30	163.67	757.64	938.29	153.31	784.98	1.84%	-6.33%	3.61%
7	328	Calderone et al. 2000	24	10	4	921.30	163.67	757.64	940.53	152.62	787.91	2.09%	-6.75%	4.00%
8	328	Calderone et al. 2000	20	16	1	921.30	163.67	757.64	923.72	151.74	771.98	0.26%	-7.29%	1.89%
9	328	Calderone et al. 2000	20	16	4	921.30	163.67	757.64	919.52	151.72	767.80	-0.19%	-7.30%	1.34%
10	328	Calderone et al. 2000	16	10	1	921.30	163.67	757.64	934.49	152.01	782.47	1.43%	-7.12%	3.28%
11	328	Calderone et al. 2000	16	10	4	921.30	163.67	757.64	942.54	154.74	787.79	2.30%	-5.45%	3.98%
12	328	Calderone et al. 2000	12	10	1	921.30	163.67	757.64	937.89	152.40	785.50	1.80%	-6.89%	3.68%
13	328	Calderone et al. 2000	10	10	1	921.30	163.67	757.64	924.79	150.20	774.59	0.38%	-8.23%	2.24%
14	328	Calderone et al. 2000	10	16	4	921.30	163.67	757.64	928.94	149.82	779.12	0.83%	-8.46%	2.84%
15	328	Calderone et al. 2000	8	8	4	921.30	163.67	757.64	944.62	152.48	792.14	2.53%	-6.84%	4.55%

There is not a large difference on the dissipated energies between tested and simulated column if the number of fibers is changed. However, it is recommendable to use one of the first three combinations to avoid convergence errors in the simulation. In the present work the selected combination is number 1.

B.2 Calibration of hysteretic parameters for steel bars

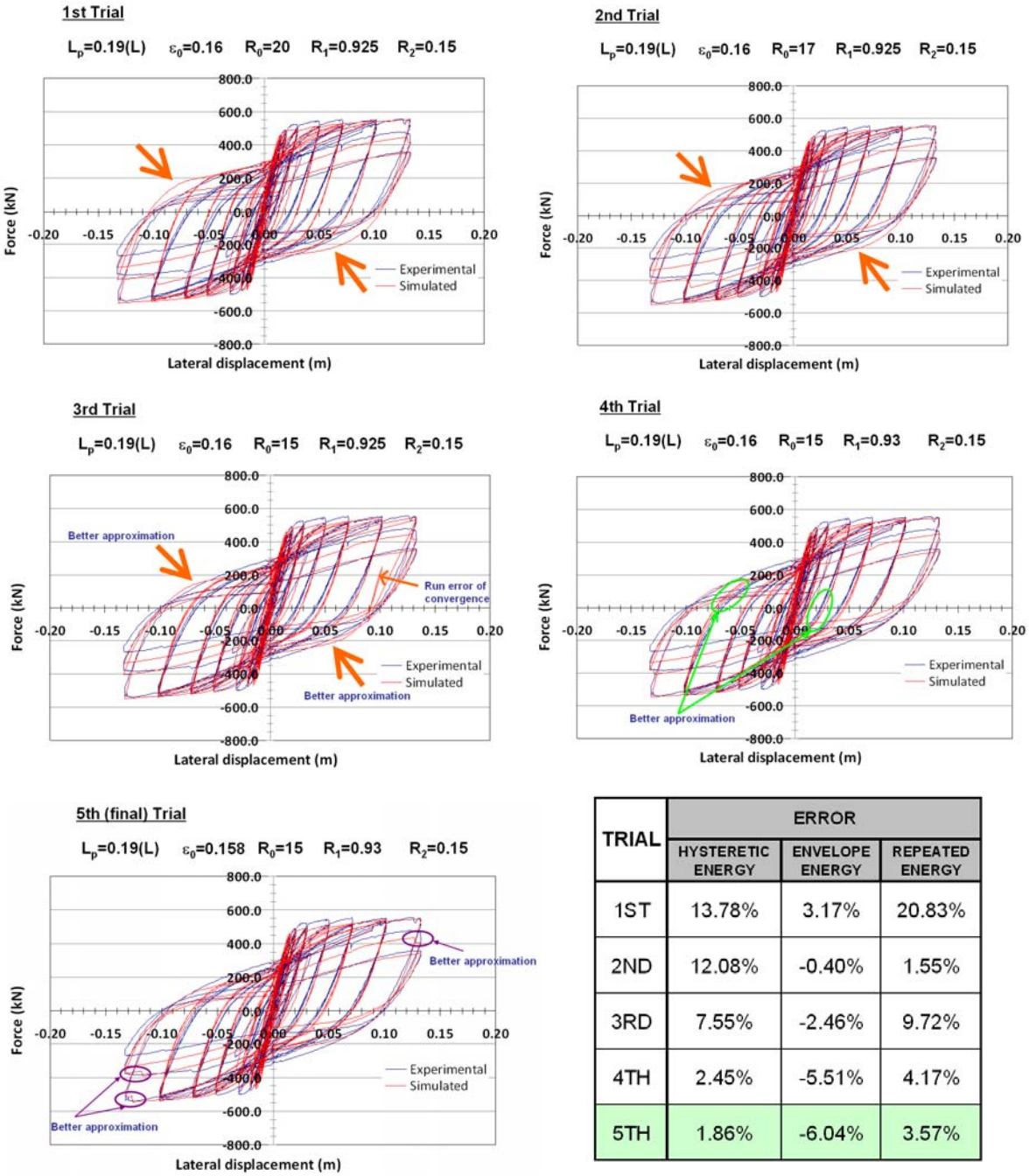

TRIAL	ERROR		
	HYSTERETIC ENERGY	ENVELOPE ENERGY	REPEATED ENERGY
1ST	13.78%	3.17%	20.83%
2ND	12.08%	-0.40%	1.55%
3RD	7.55%	-2.46%	9.72%
4TH	2.45%	-5.51%	4.17%
5TH	1.86%	-6.04%	3.57%

Figure B.1. Column 328 calibration.

First group of parameters (1st Trial) were adopted from the recommendations of previous works. L_p from Eq. (3.3) Priestley, Seible and Calvi (1996); ε_0 from Table 3.7 Brown and Kunnath (2000); R_0, R_1 and R_2 from Filippou, Popov and Bertero (1983). Then it was calibrated in order to obtain the best approximation compared with the Test response.

APPENDIX C

Damage indices summary and time history analysis for different cases in order to calculate the cyclic damage index of reinforced concrete bridge columns

C.1 Damage indices

A damage index to measure structural damage induced by earthquakes is a considerable improvement with respect to strength reduction factors, maximum lateral displacements, drifts, non-cyclic and cyclic envelope ductility ratios.

Damage indices vary between 0.0 for an essentially elastic response meaning that there is no damage and 1.0 that indicates a potential state of collapse for the column. At any other state of the structure such as operational or life safety the known damage indices will acquire values that vary between those two limits.

Damage indices can be identified into two types, non-cumulative and cumulative. The non-cumulative relate damage to some peak structural response while the cumulative types relate damage to the energy dissipated at the end of the ground motion.

The critical reviews by Chung, Meyer and, Shinozuka (1987), Isabel de Villemure (1995), Williams, Villemure and, Sexsmith (1997) and Hindi (2001) present important summaries of the existing damage indices so in this study just the ones more related to the proposed CDI will be briefly analyzed.

Some damage indices like the ones by Mander, Panthaki and, Kasalanti (1985) and Kunnath et Al. (1997) predict low-cyclic fatigue of the bridge columns or their materials using Coffin (1954), Manson (1953) and Miner (1945) rules.
According to Krawinkler (1996), Bozorgnia and Bertero (2004), the damage index presented by Park and Ang (1985) has been the most used to estimate damage in reinforced concrete structures.

Park and Ang (1985) developed their damage index based on the response of 261 reinforced concrete beams and columns tested in laboratory under cyclic load and expressed it “as a linear

combination of the damage caused by excessive deformation" and damage caused by hysteretic behavior. The "excessive deformation" refers to the maximum lateral displacement.

Krawinkler (1996) suggests that to evaluate structural performance through the cumulative plastic displacements the model proposed by Park et al. (1985) should be used. The objective of the model is to limit the potential damage of structures to a tolerable level. The tolerable degree of damage was calibrated on bases of observed damage during past earthquakes.

The Structural Damage Index defined by Park is expressed as:

$$D = \frac{\delta_m}{\delta_u} + \frac{\beta}{Q_y \delta_u} \int dE \qquad \text{(C5.1)}$$

In equation (C5.1), D is the Damage index. D ≥1 indicates excessive damage or collapse and D = 0 means no damage.

δm is the maximum lateral displacement response during the ground motion and δu is the ultimate displacement capacity under monotonic static load. Qy is the calculated yield strength from the monotonic force-displacement relationship and dE is the differential of the dissipated hysteretic energy.

The ∫dE is the dissipated hysteretic energy and β is a parameter to account for cycling loading and structural effects.

Tracing up the load-deformation curves of 261 laboratory cyclic tested beams and columns up to the point of failure, Park et al. (1985) determined the value of β which was later correlated to structural parameters such as shear span ratio, normalized axial stress, longitudinal steel ratio, confinement ratio and a constant value, equation (C5.2).

$$\beta = \left(-0.447 + 0.073\frac{L}{D} + 0.24\frac{P}{A_g f_c^{'}} + 0.314\rho_l \right) 0.7^{\rho_{sp}} \qquad \text{(C5.2)}$$

The value of the parameter β can vary between zero and 1. For instance, ground motions recorded close to the fault containing severe pulses, particularly those with forward directivity,

will show a low dissipation of energy and a large lateral displacement thus β will have a low value. On the contrary ground motions recorded far from the fault show large dissipation of energy and small lateral displacements thus β will have a large value close to one. The damage index by Park et al (1985) has been calibrated against experiments and structural behavior observations after earthquakes performed by Park, Ang and, Wen (1987) and a damage index between 0.4 and 0.5 is considered as the maximum tolerable value to assure reparability of the structural system damaged by a ground motion.

Park et al. (1987) point out that the covariance of β values for the 261 tested columns is only 60% after comparing β calculated from the experiments and β calculated from equation (C5.2). Several authors like Chai, Pristley and, Seible (1994), Kunnath, Reinhorn and, Lobo (1992) and, Park et al. (1987) coincide that the appropriate values for β vary from 0.05 to 0.15.

Continuing the discussion about the value of β, Cosenza, Manfredi and, Ramasco (1993) determined experimentally a median of 0.15. According to Bozorgnia and Bertero (2004) the value for β = 0.15 allows the damage index to correlate well with other damage indices like those proposed by Banon and Veneziano (1982) and Krawinkler and Zohrei (1983).

Several authors have pointed out two drawbacks on the damage index given by Park et al. 1985. First, looking at equation (C5.1), if the dynamic response is elastic the index should be zero. However, even though the hysteretic energy is zero the first term can still give a value larger than zero. Second, for monotonic load, once the value of δu has been reached the index should be equal to one meaning a potential failure however; the equation will provide a value larger than one.

Chai, Romstad and Bird (1995) modified equation (C5.1) to correct the second drawback.

Other damage indices like the Powell and Allahabadi (1988) are based on plastic displacements only.

$$D = (u_m - u_y) / (u_{mon} - u_y) = (\mu - 1) / (\mu_{mon} - 1) \qquad \text{(C5.3)}$$

u_m is the absolute maximum non-cyclic lateral displacement and u_y is the yielding displacement response. u_{mon} is the maximum lateral monotonic displacement. μ_{mon} is the monotonic ductility ratio equal to u_{mon} / u_y while μ is the non-cyclic ductility ratio equal to u_m / u_y.

As explained in chapter 2, the non-cyclic physical ductility $u_{ncp} = |u_m| - u_y$ does not account for the cyclic characteristic of the dynamic response and does not give any information regarding the number of cycles or the plastic displacements of those cycles. According to Mahin and Bertero (1981), u_{ncp} does not give any information on the cumulative effects of the cycles or on the dissipated energy.

Kratzig and Meskouris (1987) have indicated that u_{ncp} is not an appropriate measure to describe structural damage.

Mahin and Bertero (1981) defined the normalized hysteretic energy ductility ratio, μ_H. This equation is based on the dissipated hysteretic energy, E_H, normalized by the static energy.

$$\mu_H = [E_H / F_y\, u_y] + 1 \qquad \text{(C5.4)}$$

Where F_y and u_y are the yielding strength and yielding deformation respectively.
Fajfar (1992) and Cosenza, Manfredi and, Ramasco (1993) have presented a damage index based on hysteretic energy for elastic perfectly plastic systems.

$$D = [E_H / F_y\, u_y] / (\mu_{mon} - 1) \qquad \text{(C5.5)}$$

Hachem, Mahin and, Moehle (2003) indicate that the major problems with the damage index given by Park are the difficulties to estimate β and the estimation of the maximum monotonic displacement. The first one due to the absence of experimental data and the second due to the lack of consensus on the definition of maximum monotonic displacement. In addition, Hachem et al. (2003) point out that low-cyclic fatigue is not predicted by this type of damage indices.

In Chapter 2 it was pointed out that the maximum lateral non cyclic displacement, $|u_m|$, contains only the non-cyclic physical ductility, u_{ncp}, which results from the difference between $|u_m|$ and the yielding displacement, u_y. u_{ncp} appears as the lower limit measure of the total plastic displacement inducing damage and therefore it could be a non conservative measure to be used for design. In fact, the first term of the damage index given by Park and Ang (1985), equation (C5.1), misses a large part of the hysteretic enveloping cyclic plastic response, u_{cpe}, causing

major damage as explained in Chapter 2. The second term in equation (C5.1) contains all the hysteretic response even though part of it is already in the first term.

This form of equation (C5.1) creates some inconsistencies solved by Bozorgnia and Bertero (2004) who presented the following damage index

$$DI_1 = [(1 - \alpha_1)(\mu_c - \mu e) / (\mu_{mon} - 1)] + \alpha_1 (E_H / E_{H\,mon}) \qquad \text{(C5.6)}$$

$\mu = u_m / u_y$ is the traditional non-cyclic ductility ratio and $\mu_e = u_0 / u_y$ is the maximum elastic portion of displacement divided by u_y. In addition, $\mu_e = 1$ for inelastic response and $\mu_e \leq 1$ for elastic response. μ_{mon} is the monotonic ductility ratio capacity and E_H is the hysteretic energy demanded by the ground motion. E_{Hmon} is the hysteretic energy capacity under monotonically increasing lateral displacement.

α_1 gives an idea of the importance of the accumulation of damage, $0 \leq \alpha_1 \leq 1$ and measures the dissipation of energy in the hysteretic response. The value of α_1 is very large if the dissipation of energy is large. If there is small dissipation of energy even if there is a large number of cycles, there is no accumulation of damage therefore the value of α_1 is small.

The two drawbacks of Park and Ang (1985) damage index are solved by Bozorgnia and Bertero (2001a and b), by introducing a multiplier $(1 - \alpha_1)$ to the first term in equation (C5.6).
If a ground motion containing just a large pulse which for the structure is similar to a pushover for all practical purposes α_1 is zero so the damage is concentrated in the first term of the equation and $(1 - \alpha_1)$ is equal to 1. On the contrary assume a ground motion inducing a dynamic response with a great number of cycles and reversals of plastic deformations. In this case α_1 will be very large, close to a value of 1, therefore $(1 - \alpha_1)$ will be close to zero, which means that the damage is concentrated in the second term which measures the accumulation of plastic deformation or accumulation of damage.

According to Hindi (2001) damage indices can help structural designers to establish seismic design criteria, to estimate the extent of damage in a bridge and to assess vulnerability to aftershocks or future severe earthquakes helping authorities to decide if the bridge can be kept open to the traffic after a main shock.

C.2 Results for the second bin of 7 near fault records on T = 0.5s bridge column

This appendix show the variations of β_c for near fault records and for the T = 0.5s bridge column and the response of the column to the unscaled records.

As it will be seen the large pulses in the records and the small energy dissipated through the repeated cyclic plastic displacements will not allow to count with a parameter β_c that meets one of the objectives above indicated. These objectives are: control the importance of E_{ucpr} and to be the value associated to Significant Damage.

For these records the parameter β_c does not control the importance of E_{ucpr} on the damage.
For this bin all the records are scaled down to capture the first failure mechanism so CDI = 1.0 and the value for β_c is calculated as shown in Table C.1.

The characteristic of these records is the large pulses pushing the column to one side response thus the enveloping cyclic displacements are large. For three of the records the β_c values are larger than 1.0 therefore they do not control the influence of the repeated plastic displacements represented by E_{ucpr}. The repeated plastic displacements energy are to low, just 13% of the total dissipated energy. On the contrary, E_{ucpe} is about 87% of the total dissipated energy. For this three scaled records the failure is due to crushing of the confined concrete since the strain demanded ε_c is larger than ε_{cu}.

For the other four records the β_c values are lower than 1.0. However, for $\beta_c = 0.26$ and $\beta_c = 0.38$ there is crushing of the confined concrete. This is because E_{ucpr} although is larger than the above mentioned cases is still lower than E_{ucpe}. For $\beta_c = 0.26$ E_{ucpr} is 46% of the total dissipated energy and for $\beta_c = 0.38$ E_{ucpr} is only 22% of the total dissipated energy.

The last two records with β_c values lower than 1.0 show E_{ucpr} values larger than $E_{ucpe.}$ These records are the Kobe JMA and the Northridge NH records. For $\beta_c = 0.48$ and for $\beta_c = 0.18$ E_{ucpr} is 62% of the total dissipated energy. The reason for the difference in the values of β_c is in the total dissipated energy. For $\beta_c = 0.48$ the total dissipated energy is 764.4kn-m while for $\beta_c = 0.18$ it is 1049.3kN-m. The E_{ucpe} for Kobe is 293kN-m and for Northridge E_{ucpe} is 405kN-m. This means that the Kobe JMA record demands less dissipation of energy than the Northridge NH record

although these dissipations are small and also means that in both cases there are several cycles of plastic reversible response in addition to the large pulses.

Only for these two records the first failure mechanism leading to the Significant Damage Performance Level is low-cyclic fatigue.

Looking at Table C.1 it is not possible to attempt to find an average for β_c since the variability is too high due to the above mentioned reasons.

Table C.2 shows the results for scale factor = 1.0. For all cases the maximum lateral displacements are larger than the capacity that is 13.8cm therefore, crushing of the confined concrete occurs. For Northridge OV, Northridge NH and Morgan Hill-Coyote unscaled records after crushing of the concrete there is low cyclic fatigue of a large number of bars.

Figure C.1 shows the responses of the T = 0.5s column to the unscaled Erzincan and Imperial Valley A06 records.

Looking at the Erzincan response for the first quarter cycle there is already crushing of the concrete and for the third quarter the displacement demand is so large that whole concrete section crushes causing instability in the computer program that stops running.

For the Imperial Valley A06 record in the third quarter the concrete crushes due to large displacement and later in the first quarter the displacement is again so large that the complete section crushes and there is instability in the computer program.

Notice that for these two records and for the Kobe Takatori and the Kobe JMA records E_{ucpr} = 0.0, meaning that there are not repeated plastic cyclic displacements.

The E_{ucpr} for the Northridge OV and the Morgan Hill-Coyote are small compared to the large values shown by subduction, soft soil or crustal earthquakes just 6 and 12% of the total dissipated energy. The Northridge NH record dissipates through the repeated cyclic plastic displacements about 33% of the total energy dissipated.

It can be concluded that the Cyclic Damage Index as has been developed in this investigation is not able to give reliable information about the damage since the Index is based partially in the energy dissipated through the cyclic plastic repeated displacements.

Table C.1.- Calculation of β_c for Near Fault Records. T=0.5s

Calculation of β_c - Circular Column T=0.5s																
		EQ	Duration (s)	PGA (%g)	Tg (s)	Scale Factor (CDI=1)	Failure type	Number of fatigued bars	Time (failure)	Max. Displacement (m)	Energy Capacity, Ec (kN-m)	Enveloping Energy, Eucpe (kN-m)	Repeated Energy, Eucpr (kN-m)	Eucpe/Ec	Eucpr/Ec	β_c
BIN - NEAR FAULT (forward directivity)	1	Erzican,1992 (Turkey)	20.78	0.432	2.24	0.41	$\varepsilon_c > \varepsilon_{cu}$	0	3.65	0.144	521.22	338.49	47.07	0.65	0.09	3.882
	2	Imperial Valley A06,1979 (USA)	39.10	0.432	3.93	0.56	$\varepsilon_c > \varepsilon_{cu}$	0	6.55	0.139	521.22	349.74	41.48	0.67	0.08	4.134
	3	Kobe Takatori,1995 (Japan)	40.10	0.786	1.21	0.21	$\varepsilon_c > \varepsilon_{cu}$	0	4.97	0.147	521.22	421.98	372.10	0.81	0.71	0.267
	4	Kobe JMA,1995 (Japan)	60.00	1.087	0.84	0.29	LOW-CYCLE-FATIGUE	1	11.96	0.117	521.22	292.92	471.43	0.56	0.90	0.484
	5	Northridge OV,1994 (USA)	60.00	0.732	2.33	0.45	$\varepsilon_c > \varepsilon_{cu}$	0	4.72	0.144	521.22	469.21	133.68	0.90	0.26	0.389
	6	Northridge NH,1994 (USA)	60.00	0.723	1.37	0.63	LOW-CYCLE-FATIGUE	3	9.38	0.108	521.22	405.30	643.89	0.78	1.24	0.180
	7	Morgan Hill - Coyote,1984 (USA)	60.00	1.159	0.70	0.66	$\varepsilon_c > \varepsilon_{cu}$	0	3.70	0.138	521.22	315.77	76.51	0.61	0.15	2.685

Table. C.2- Calculation of CDI for Near Fault Records at SF=1. T=0.5s

Circular Column T=0.5s			CDI values for records with Scale Factor (SF) = 1								
		EQ	Scale factor	Energy Capacity, Ec (kN-m)	Enveloping Energy, Eucpe (kN-m)	Repeated Energy, Eucpr (kN-m)	β_c	CDI	Failure type	Max. Displacement (m)	Number of fatigued bars
BIN - NEAR FAULT (forward directivity)	1	Erzican,1992 (Turkey)	1.00	521.22	550.00	0.00	3.882	1.06	$\varepsilon_c > \varepsilon_{cu}$ (Run ends at 4.8 seconds)	0.220	0
	2	Imperial Valley A06,1979 (USA)	1.00	521.22	525.00	0.00	4.134	1.01	$\varepsilon_c > \varepsilon_{cu}$ (Run ends at 6.4 seconds)	0.186	0
	3	Kobe Takatori,1995 (Japan)	1.00	521.22	375.00	0.00	0.267	0.72	$\varepsilon_c > \varepsilon_{cu}$ (Run ends at 1.7 seconds)	0.240	0
	4	Kobe JMA,1995 (Japan)	1.00	521.22	655.00	0.00	0.484	1.26	$\varepsilon_c > \varepsilon_{cu}$ (Run ends at 8.7 seconds)	0.180	0
	5	Northridge OV,1994 (USA)	1.00	521.22	861.33	48.11	0.389	1.69	$\varepsilon_c > \varepsilon_{cu}$ + LOW-CYCLE-FATIGUE	0.380	18
	6	Northridge NH,1994 (USA)	1.00	521.22	722.00	333.04	0.180	1.50	$\varepsilon_c > \varepsilon_{cu}$ + LOW-CYCLE-FATIGUE	0.285	16
	7	Morgan Hill - Coyote,1984 (USA)	1.00	521.22	497.37	62.10	2.685	1.27	$\varepsilon_c > \varepsilon_{cu}$ + LOW-CYCLE-FATIGUE	0.221	7

Erzincan T=0.5 SF=1

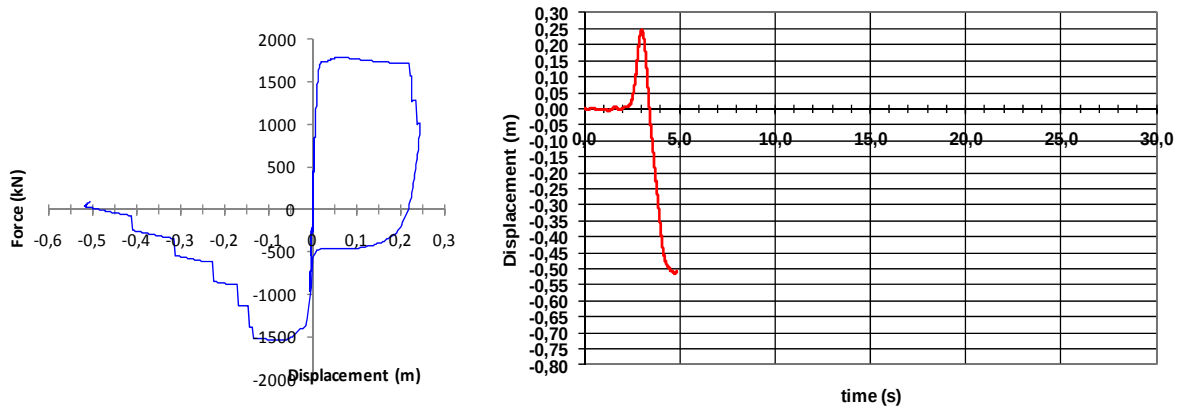

Imperial Valley A06 T=0.5 SF=1

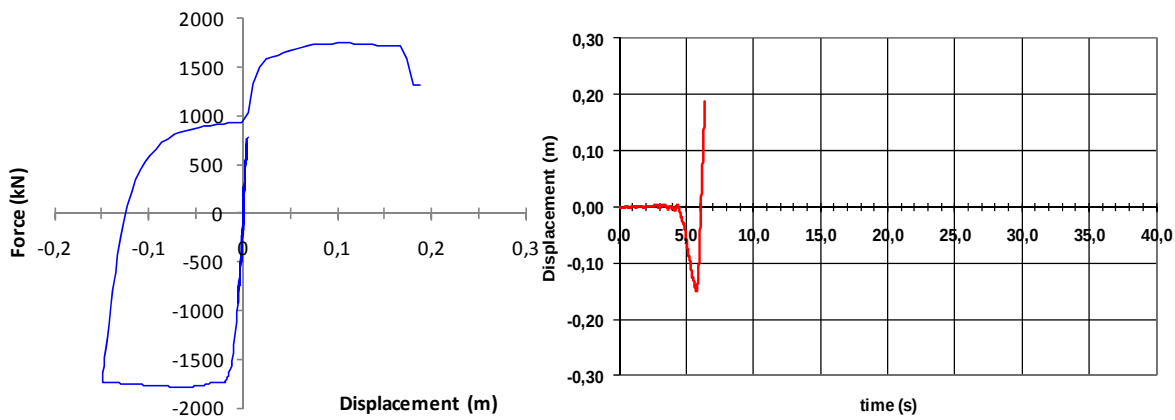

Figure C.1: Near Fault earthquake response examples

C.3 β_c values for the T = 0.5s bridge column.

C.3.1 β_c values for subduction records and T = 0.5 s.

As seen in Table 5.1 and Figures C.2 a and b, at t = 23s the maximum lateral displacement of the column for the scaled Melipilla record is 14cm while the displacement capacity according to Figure 4.2 b is 13.8cm. The 14cm displacement induces at t = 23s a compressive strain in the confined concrete of 0.019 larger than ε_{cu} = 0.018, Figure 4.2 a, causing crushing of the unconfined and confined concrete. The unconfined concrete suffered before tension cracks due to tensile strains of 0.0055. Later during the same run at t = 40s, bar number 1 fractures due to low-cyclic fatigue, Figure C.2 d. Therefore, for this record the column suffers two flexural

failure mechanisms leading it to reach SDPL so the CDI = 1.0. Introducing the energies shown in Table 5.1 into equation (5.2), β_c = 0.133 shown in Table 5.1.

In regard to the other six scaled records, every one of them induces fracture due to low-cyclic fatigue in one of the steel bars of the column. This failure becomes the SDPL of the column for each record so the CDI = 1.0. Using equation (5.2) and the dissipated energies, the values for β_c are calculated and shown in Table 5.1. This Table also shows that the lateral displacements of the column for each scaled record are lower than the displacement capacity shown in Figure 4.2 b so the confined concrete of this column does not crush for any of the 6 records. In addition, there is neither fracture of bars due to tension nor fracture due to low-cyclic fatigue for any of the six scaled records.

The average β_c value for the T = 0.5s bridge column under subduction records is 0.156. The minimum is 0.126 corresponding to a large E_{ucpr} that is 82% of the total dissipated energy. The maximum is 0.249 corresponding to the smallest E_{ucpr} that is 63% of the total dissipated energy. For both cases the values of E_{ucpe} are close. The largest E_{ucpr} is for the Llayllay record and represents 88% of the total dissipated energy. For this ground motion β_c = 0.145.

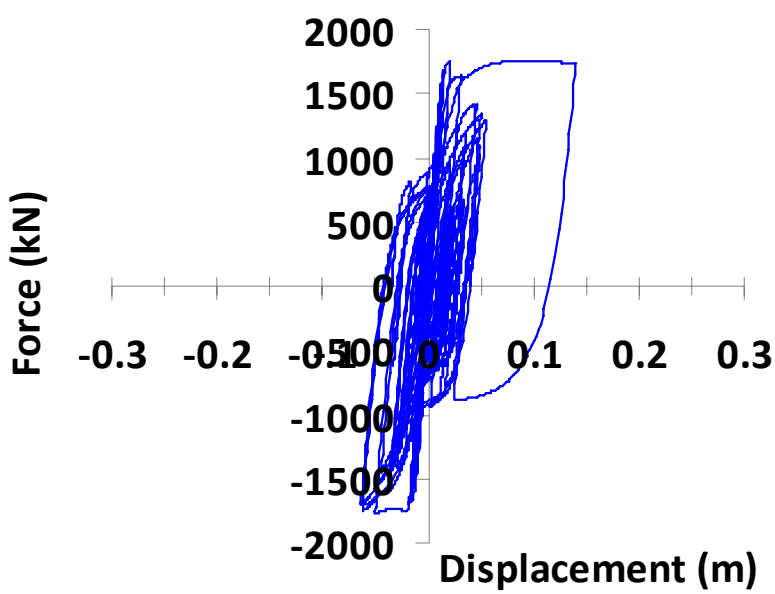

(a)

Figure C.2 Bridge Column T=0.5 s β_c for Melipilla Record. SF=1.49

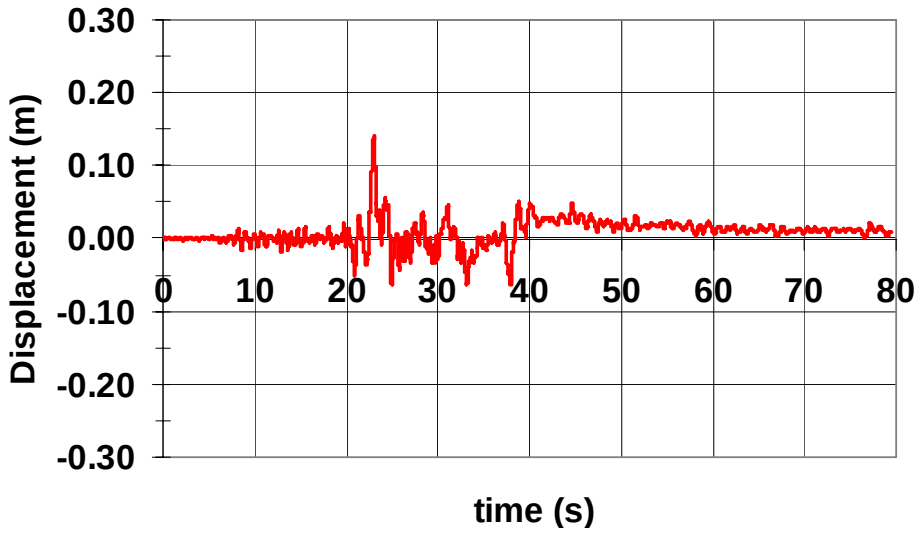

(b)

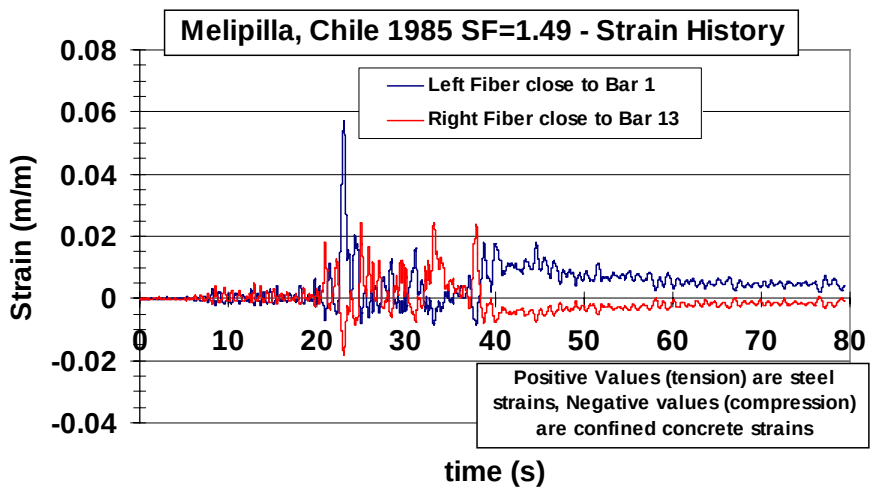

(c)

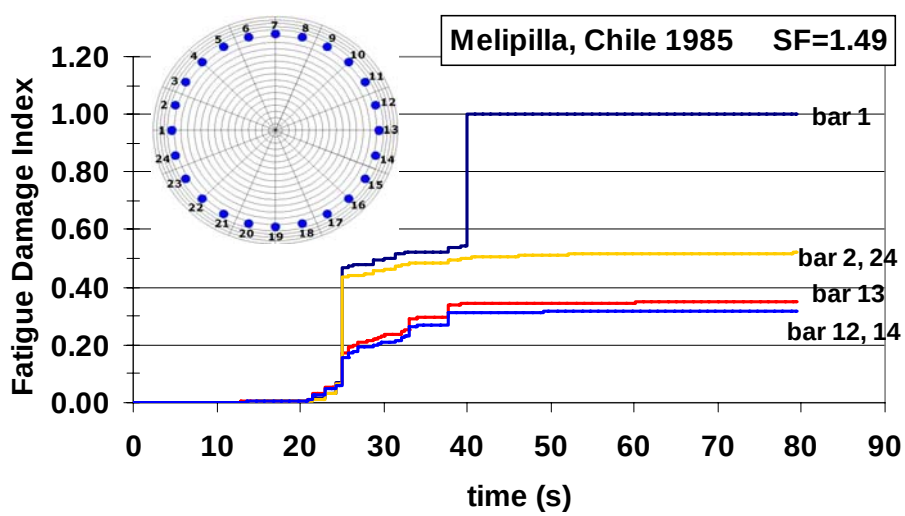

(d)

Figure C.2 (cont.) Bridge Column T=0.5 s β_c for Melipilla Record. SF=1.49

C.3.2 β_c values for soft soil records and T = 0.5s.

Figures C.3 a, and b and Table 5.1 show the hysteretic and time-history responses of the T = 0.5s column subjected to the scaled Tihuac Deportivo record. At t = 61s, the lateral displacement reaches 14cm value that is larger than the 13.8cm displacement capacity and ε_c = 0.02, Figure C.3 c, therefore the confined and unconfined concrete crushed. Before, the tensile concrete strain reached 0.0054 thus the cover concrete cracked. As seen in Figure C.3 d, there is no fatigue on any of the bars of the column and there is no fracture of any bar due to tension. For this record the SDPL is related only to $\varepsilon_c > \varepsilon_{cu}$ since there is no additional damage.

The other six records induce fracture of one bar of the column so for these records this is the only failure mechanism for the column causing SDPL.

The average value for β_c is 0.16. The maximum β_c for the Tihuac Deportivo record which has the lowest E_{ucpr} is 0.41 and the minimum β_c is 0.08 for the CDAO record where E_{ucpr} is 74% of the total dissipated energy.

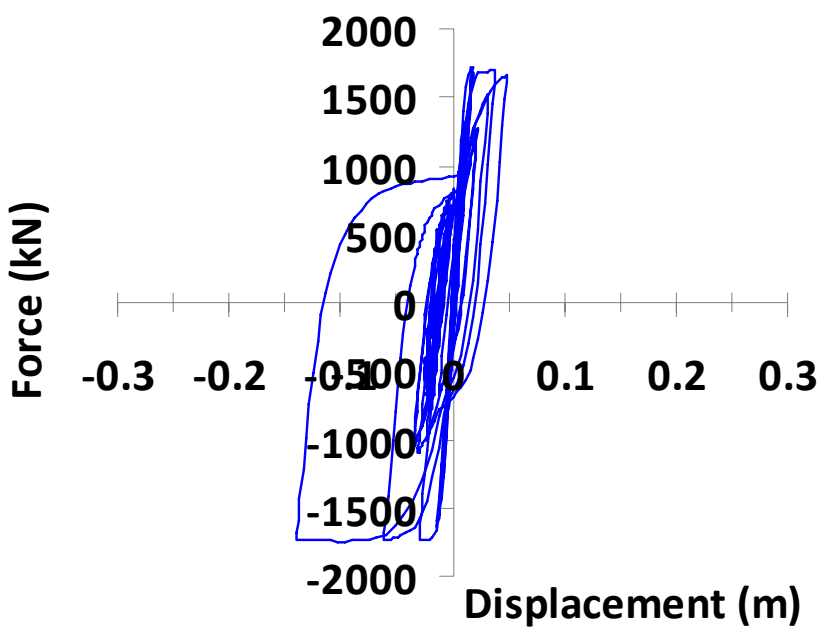

(a)

Figure C.3 Column T=0.5 s β_c for Tihuac Deportivo Record. SF=1.04

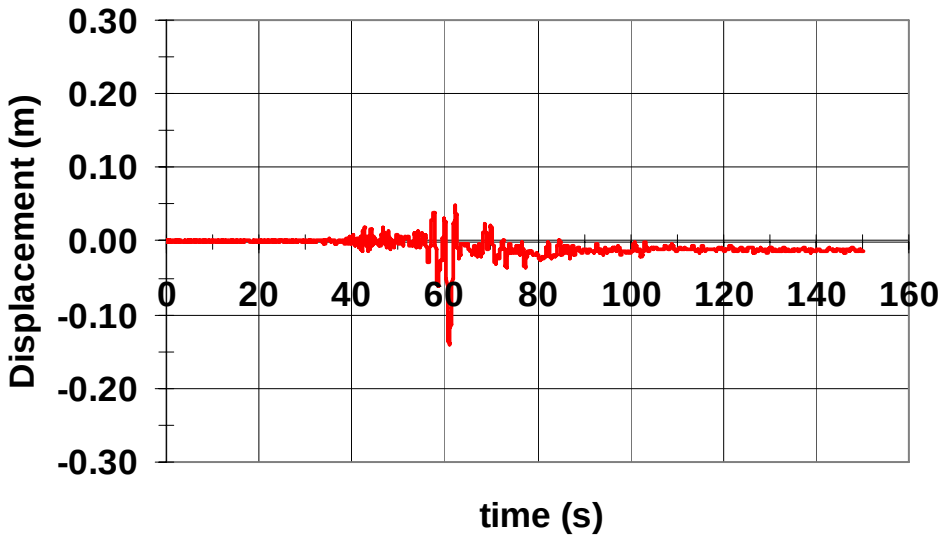

(b)

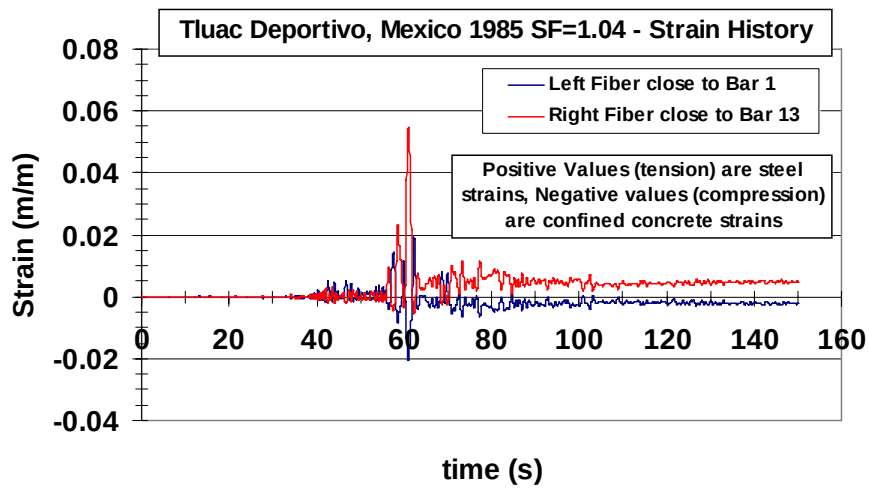

(c)

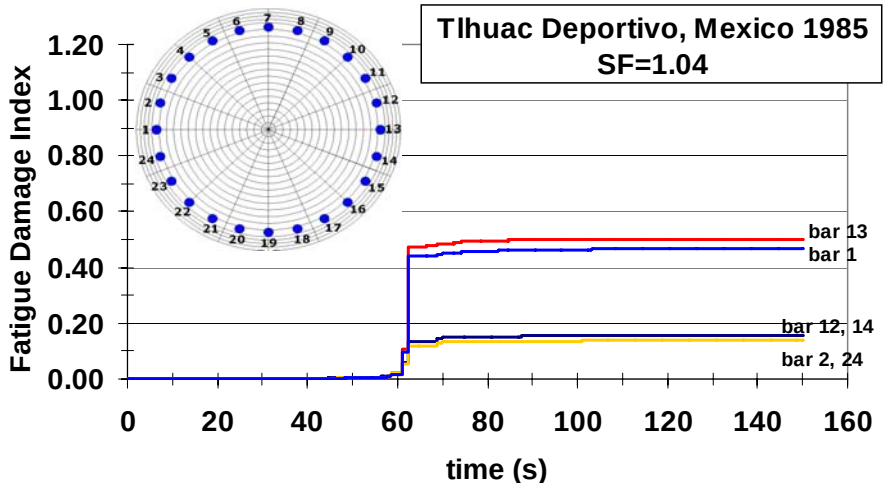

(d)

Figure C.3 (cont.) Column T=0.5 s β_c for Tihuac Deportivo Record. SF=1.04

C.3.3 β_c values for crustal records and T = 0.5 s.

For this bin all bridge columns reach SDPL due to fracture of bars by low-cyclic fatigue.

Figures C.4 a and b and Table 5.1 show the hysteretic and time-history responses of the T = 0.5s column due to the San Fernando-Hollywood record scaled 3.3 times the original record to find the SDPL. Figure C.4 c shows that the strains in the compressive confined and unconfined concrete are lower than ε_{cu} = 0.018. The concrete tensile strains reach 0.005 so the cover concrete cracked. Figure C.4 d shows that bar number 1 fractures due to low cyclic fatigue for the scaled record. The average β_c is 0.175.

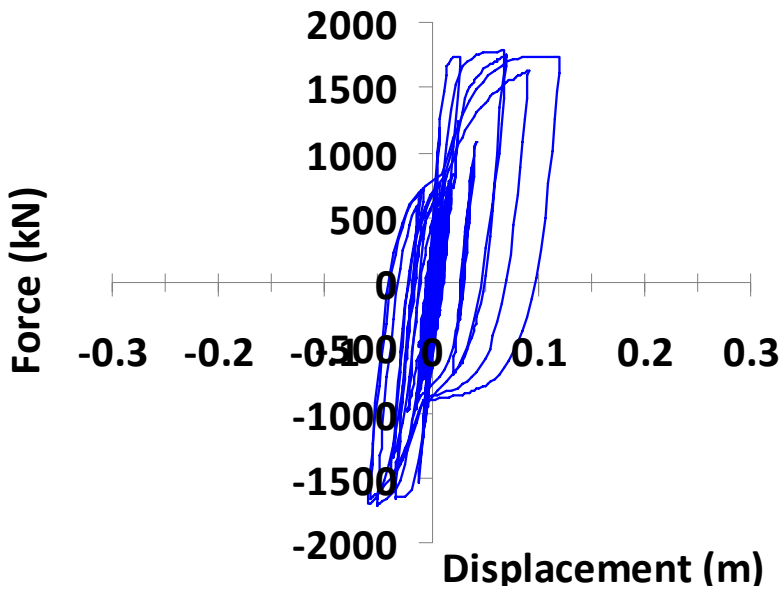

(a)

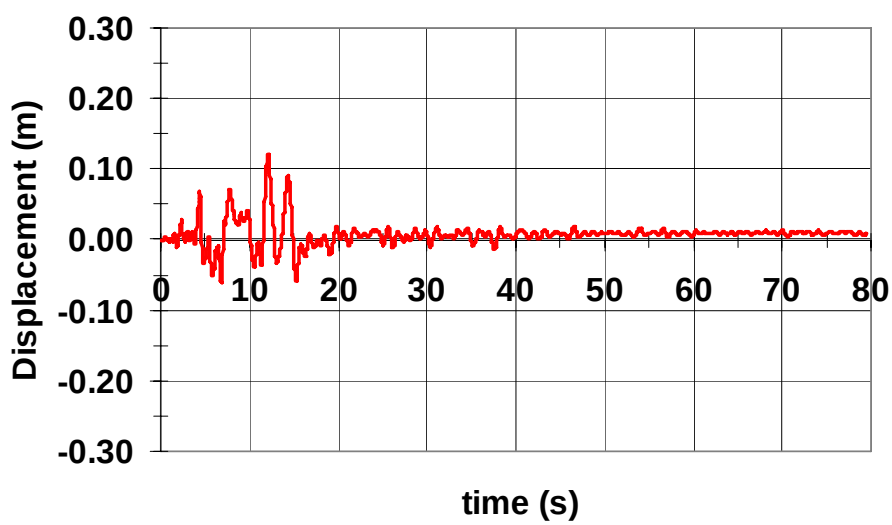

(b)

Figure C.4 Column T=0.5 s β_c for San Fernando Hollywood Record. SF= 3.30

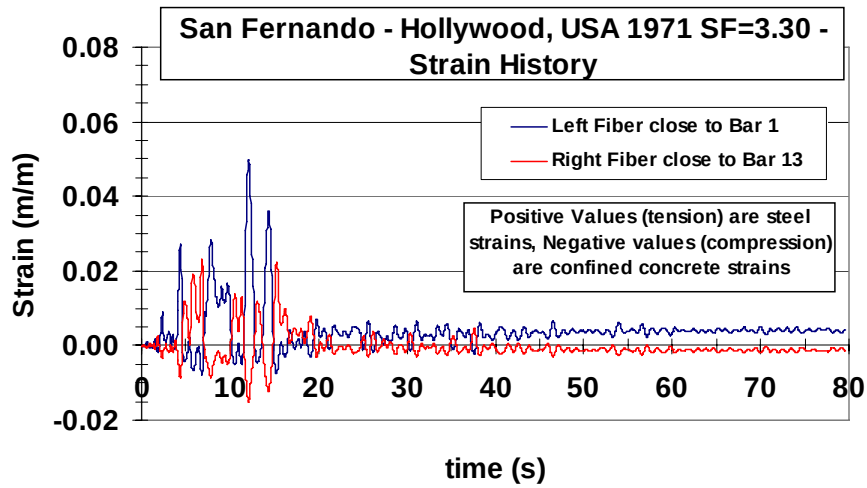

(c)

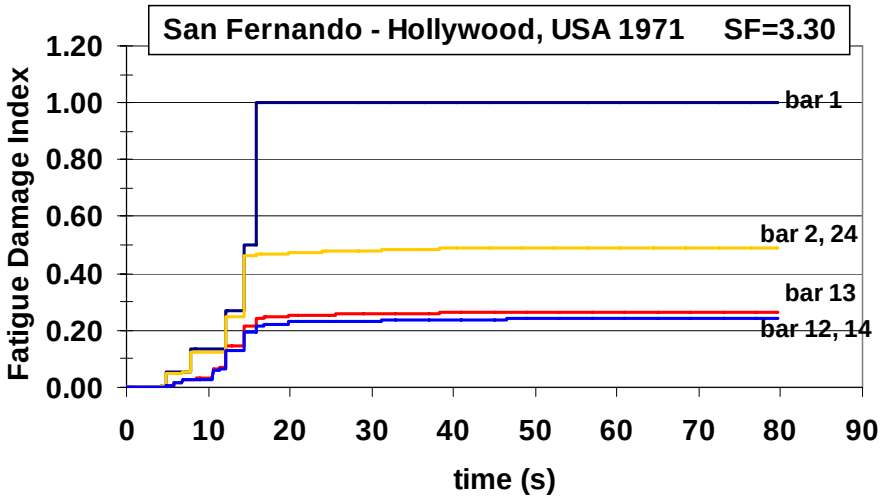

(d)

Figure C.4 (cont.) Column T=0.5s β_c for San Fernando Hollywood Record. SF= 3.30

C.4 β_c values for the T = 1.0 s bridge column.

C.4.1 β_c values for subduction records and T = 1.0 s.

Table 5.2 shows that for the scaled subduction records the T = 1.0s column reaches SDPL for all seven records due to low-cyclic fatigue that fractures the longitudinal bars.

Figure C.5 a, and b show the hysteretic and time history responses of the T = 1.0s column due to the scaled Viña del Mar subduction record and Figure C.5 c the strain time histories of the concrete and the steel bars. For Viña del Mar record the only flexural failure mechanism inducing SDPL is fracture of two bars due to low-cyclic fatigue.

The maximum β_c is 0.14 in this bin is for the Pisco scaled record and the minimum is 0.082 for the Viña del Mar scaled record. The average value for β_c is 0.10.

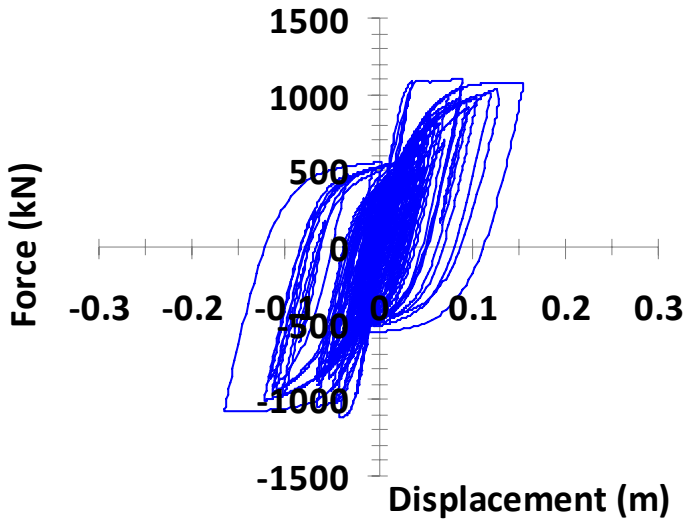

(a)

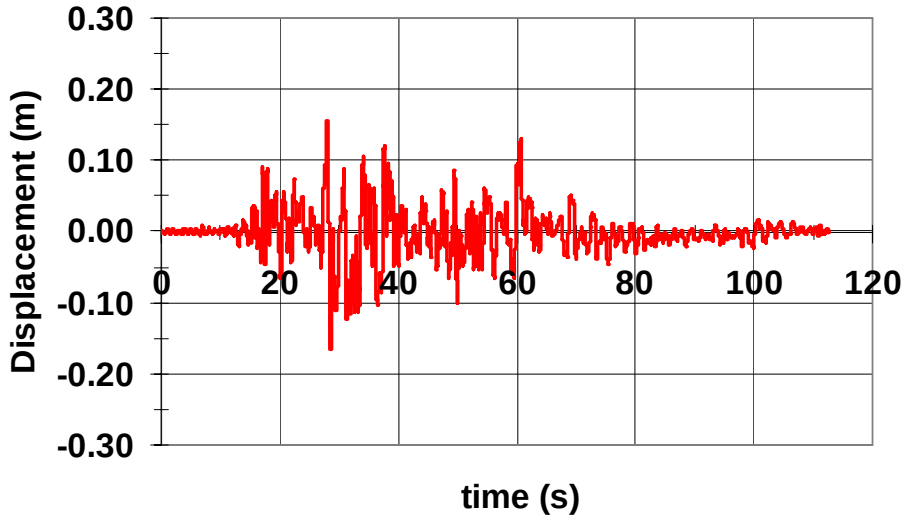

(b)

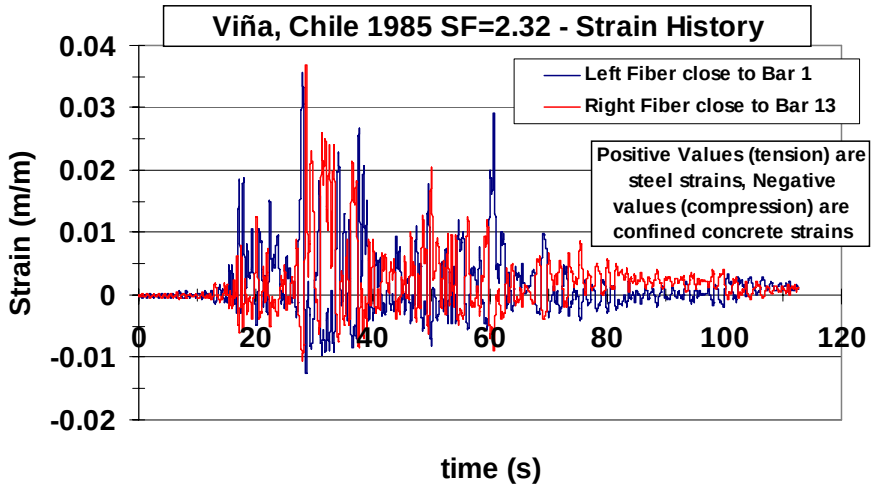

(c)

Figure C.5 Column T=1.0 s β_c for Viña del Mar Record. SF= 2.32

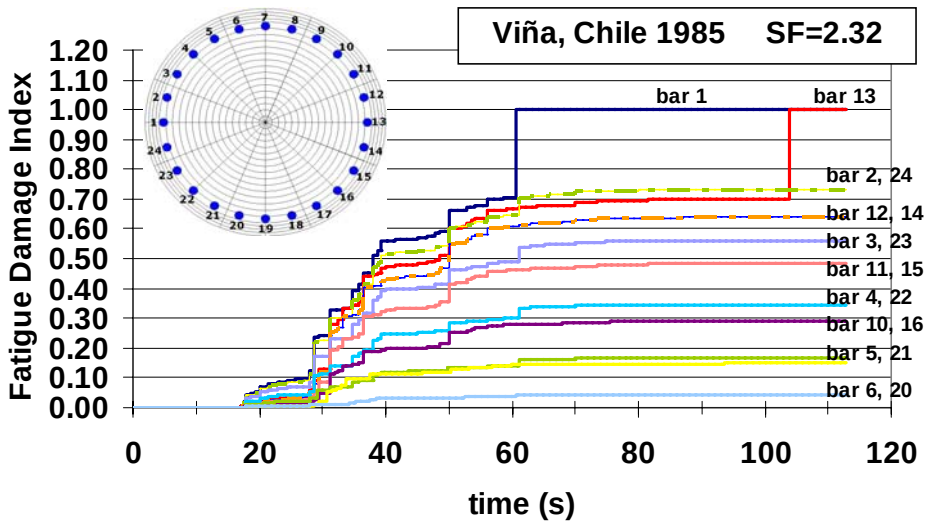

(d)

Figure C.5 (cont.) Column T=1.0s β_c for Viña del Mar Record. SF= 2.32

C.4.2 β_c values for soft soil records and T = 1.0 s.

For six of the seven soft soil scaled records the SDPL is due to fracture of one bar induced by low-cyclic fatigue.

For the Sismex Viveros soft soil scaled record, Figures C.6 a, and b show the hysteretic and time history responses of the T = 1.0s bridge column. The lateral displacement is 25cm larger than the 24cm capacity. The strain in the confined and unconfined concrete reaches 0.018, Figure C.6 c, therefore the unconfined and confined concrete crushes being this failure the one causing SDPL.

The average value for β_c is 0.14 being the maximum 0.17 for the scaled CDAF and the minimum 0.11 for TXSO record that contains the largest E_{ucpr}.

C.4.3 β_c values for crustal records and T = 1.0s.

For all seven scaled records of this bin there is flexural failure by fracture of the longitudinal bars due to low-cyclic fatigue. Figure C.7 a, and b show the responses for the T = 1.0s column subjected to the scaled Loma Prieta Sunnyvale earthquake record. The only failure mechanism inducing SDPL is fracture of one bar due to low-cyclic fatigue.

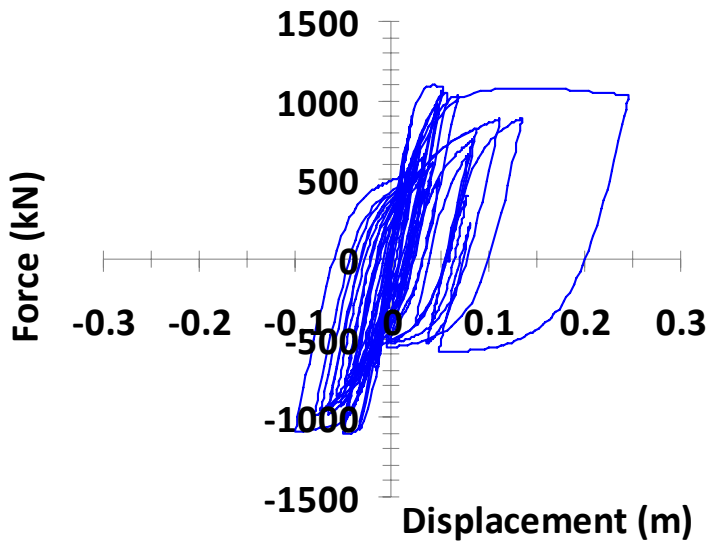

(a)

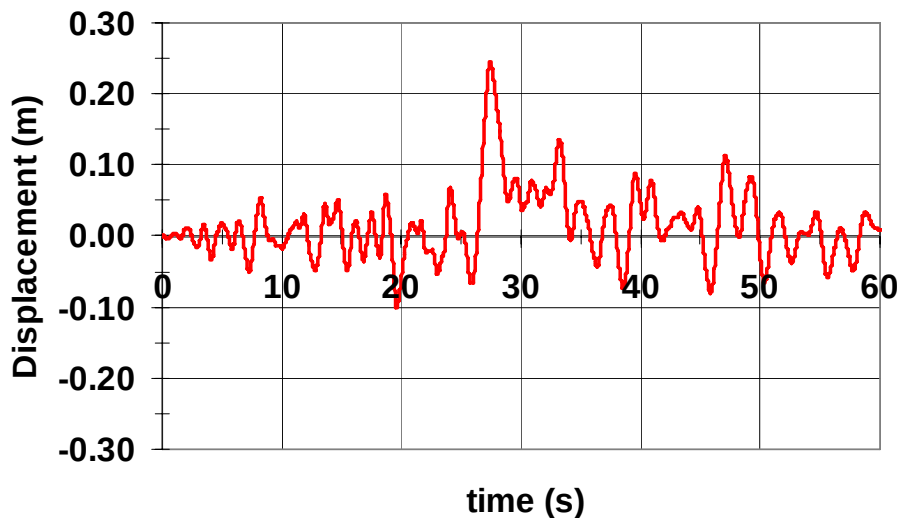

(b)

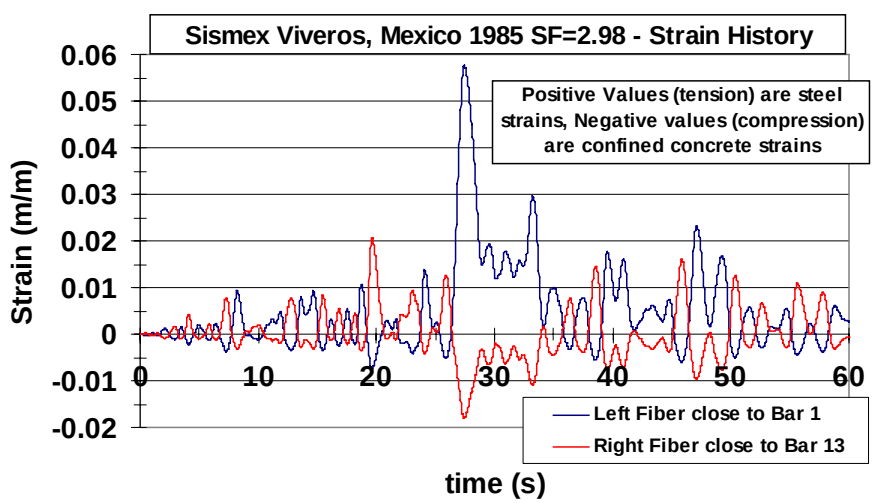

(c)

Figure C.6 Column T=1.0s β_c for Sismex Viveros Record SF= 2.98

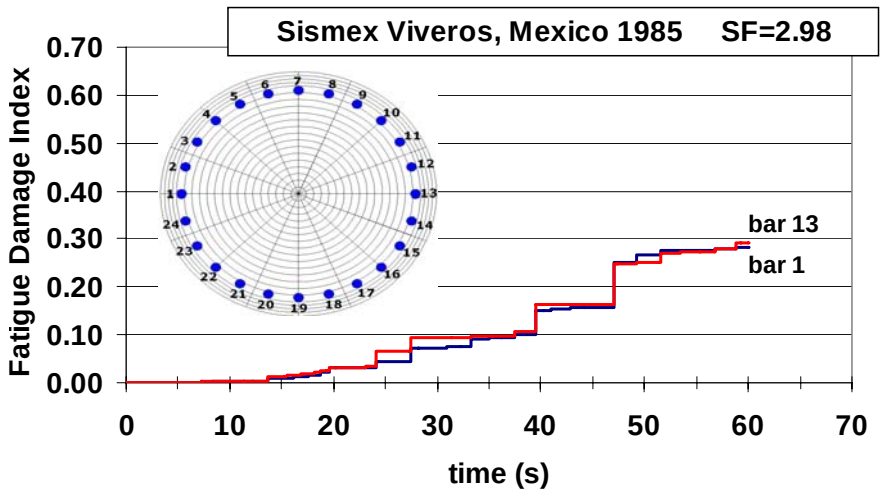

(d)

Figure C.6 (cont.) Column T=1.0s β_c for Sismex Viveros Record SF= 2.98

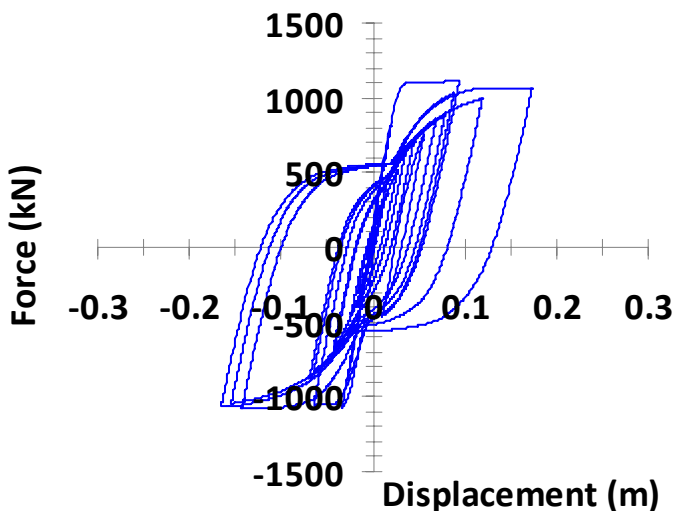

(a)

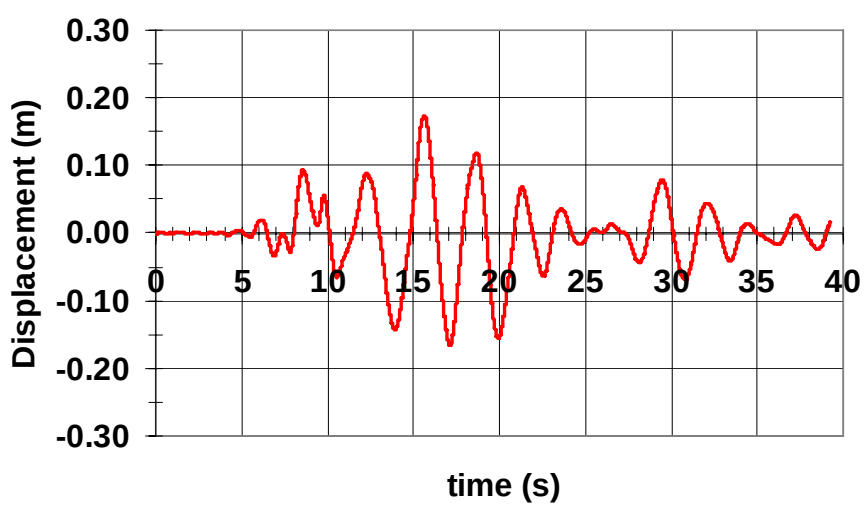

(b)

Figure C.7 Column T=1.0s β_c for Sunnyvale Record SF= 1.00

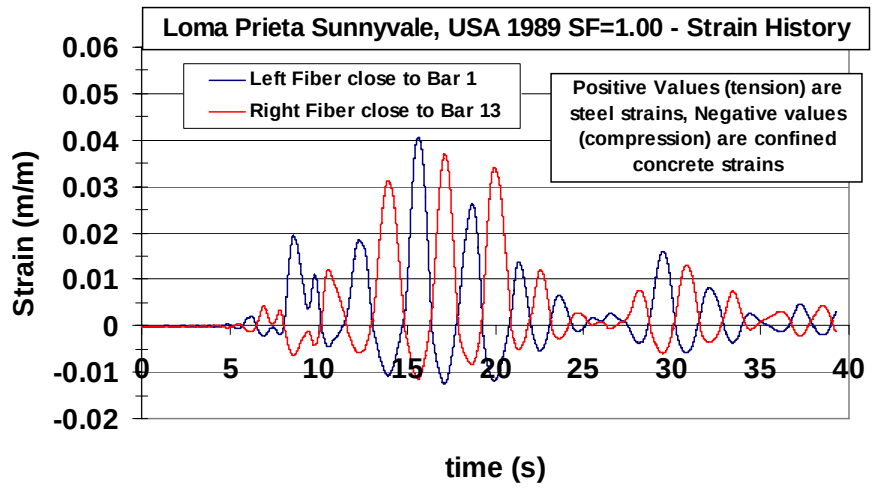

(c)

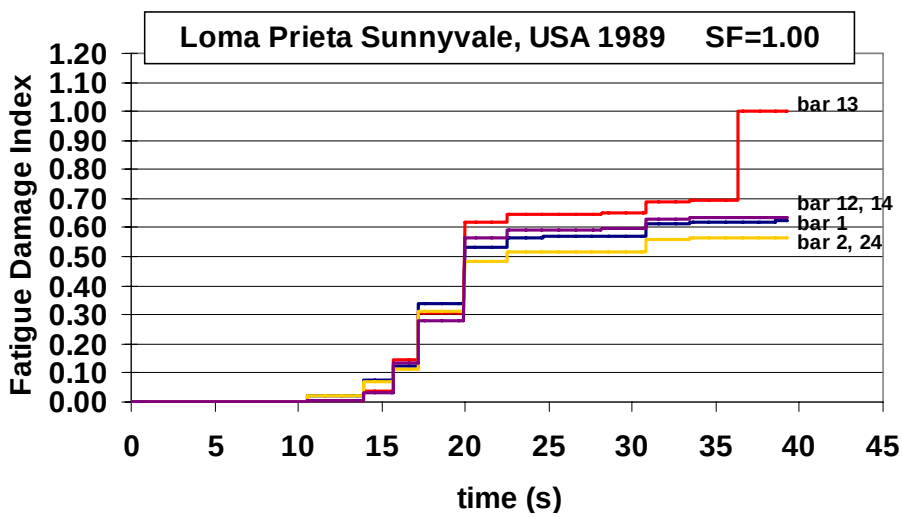

(d)

Figure C.7 (cont.) Column T=1.0s β_c for Sunnyvale Record SF= 1.00

C.5 β_c values for the T = 1.5s bridge column.

C.5.1 β_c values for subduction records and T = 1.5 s.

All these records induce SDPL by fracture of one or more bars due to low-cyclic fatigue.

For this column the β_c average value is 0.16. The maximum is 0.28 for the scaled Pisco record and the minimum is 0.09 for the Llolleo scaled record.

Figures C.8 a, and b show the hysteretic and time history responses of the T = 1.5 s bridge column for the Melipilla scaled record. It is observed in Figure C.8 d that at the SDPL three longitudinal bars fracture due to low-cyclic fatigue.

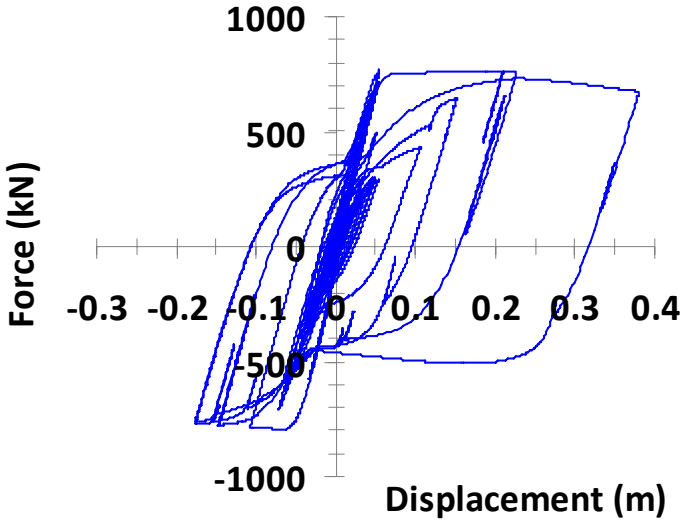

(a)

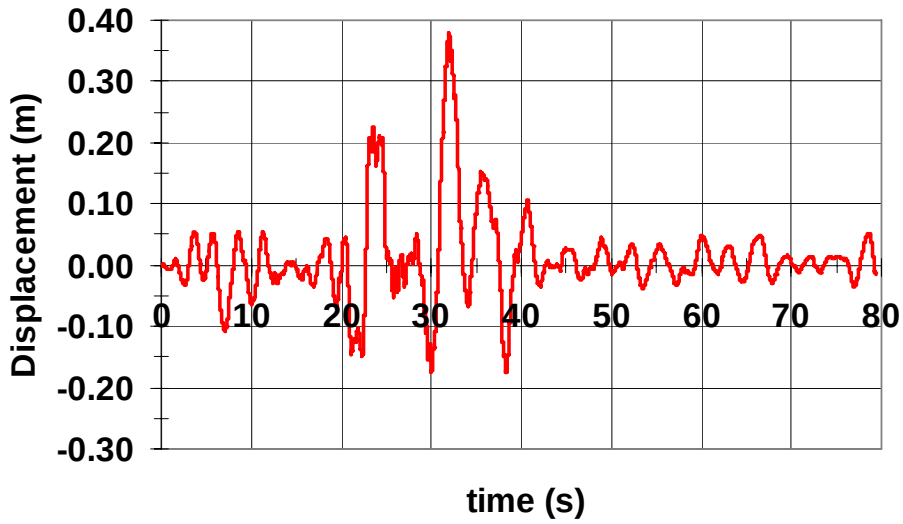

(b)

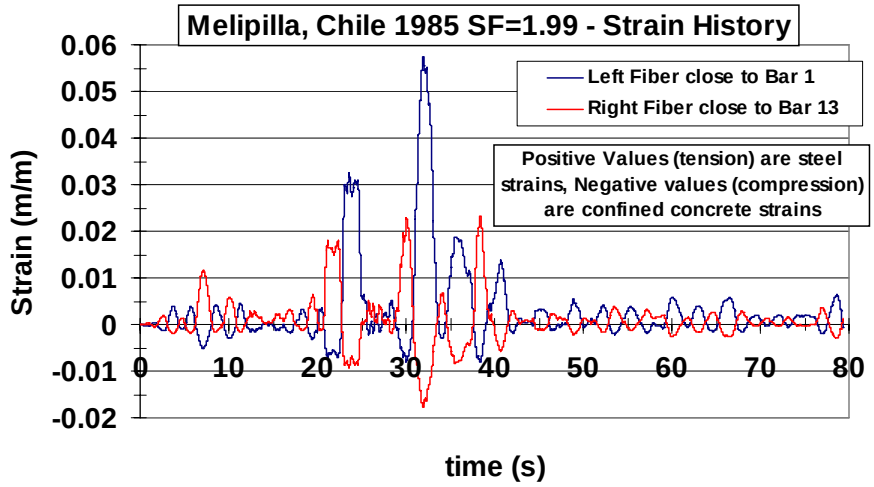

(c)

Figure C.8 Column T=1.5s β_c for Melipilla Record SF= 1.99

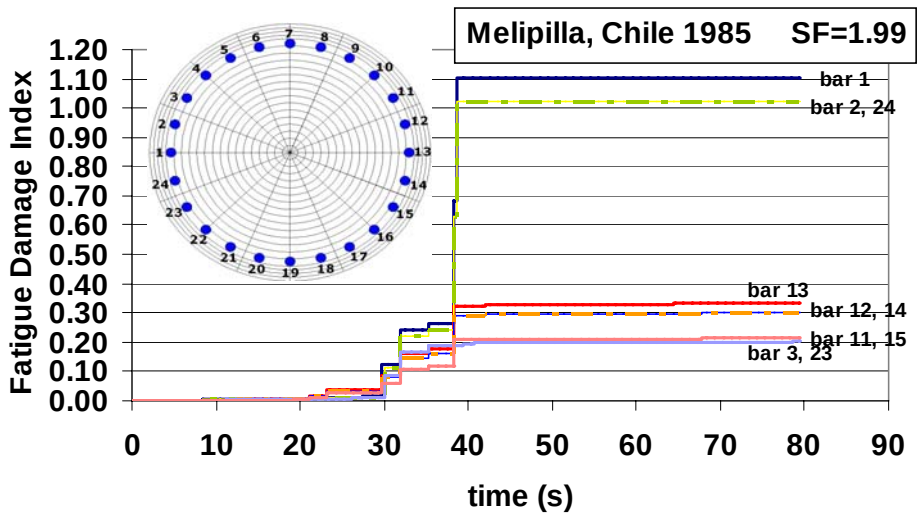

(d)

Figure C.8 (cont.) Column T=1.5s β_c for Melipilla Record SF= 1.99

C.5.2 β_c values for soft soil records and T = 1.5 s.

All records induce failure by low-cyclic fatigue in one bar.

The maximum β_c value is 0.28 for the scaled SCT-1 record and the minimum is 0.04 for the Sismex Viveros scaled record. The average value is 0.15.

Figure C.9 shows the responses of the T = 1.5 s to the SCT-1 scaled record. One bar fractures due to low-cyclic fatigue for this scaled record, as seen in Figure C.9 d.

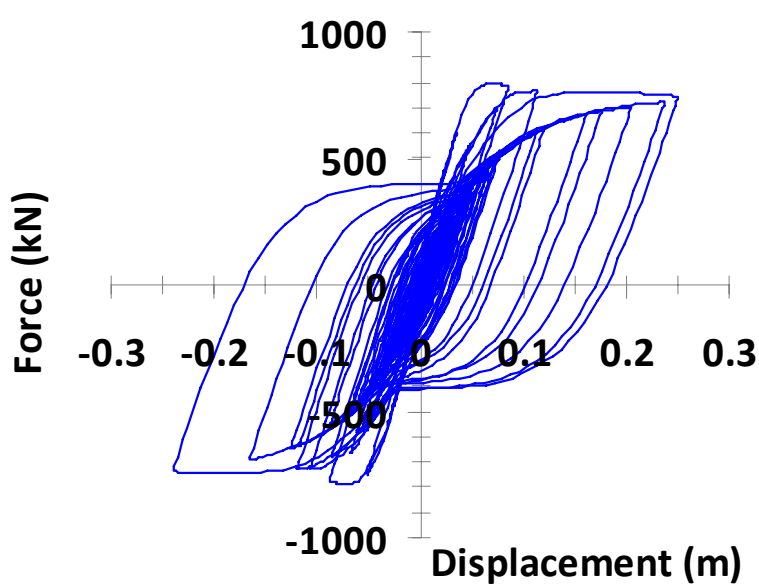

(a)

Figure C.9 Column T=1.5s β_c for SCT Record SF= 0.78

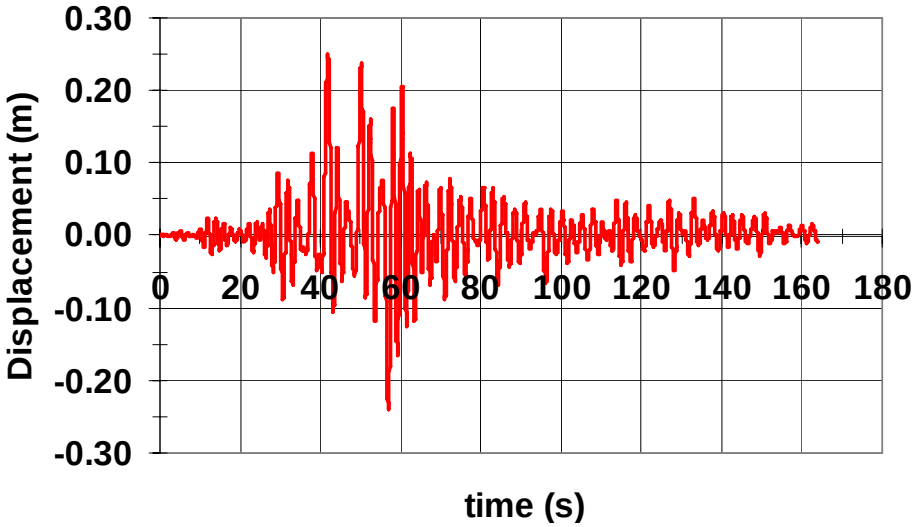

(b)

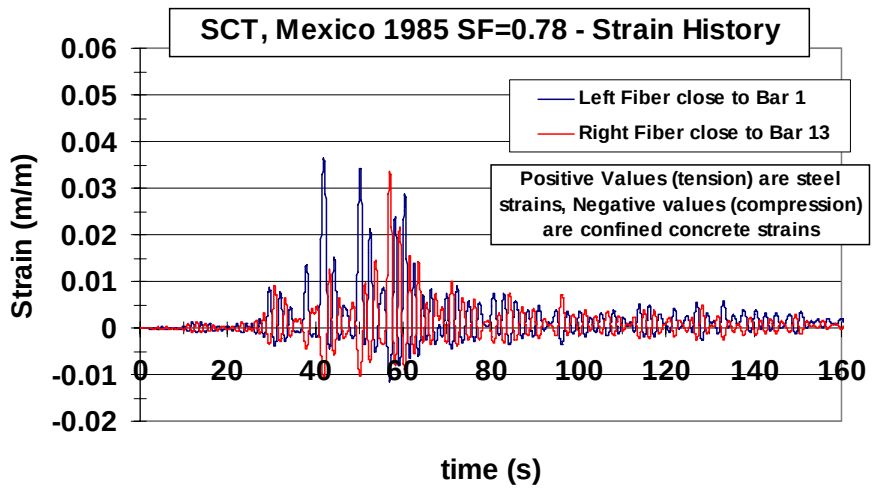

(c)

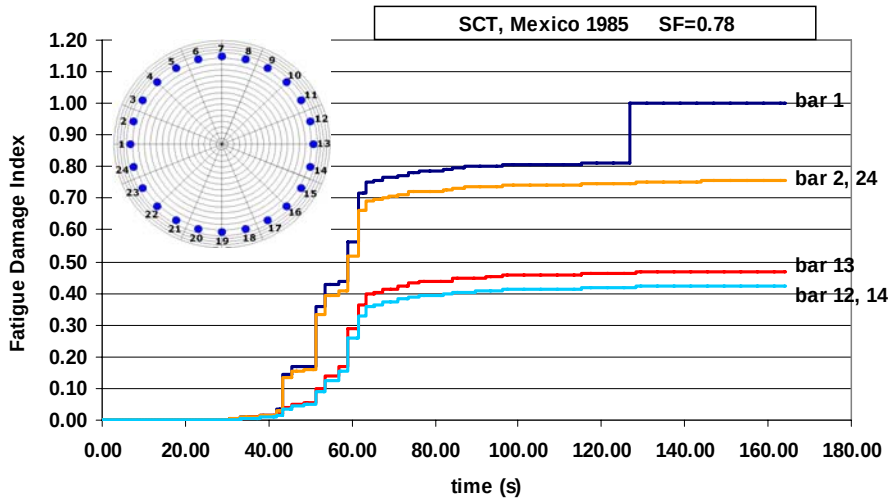

(d)

Figure C.9 (cont.) Column T=1.5s β_c for SCT Record SF= 0.78

C.5.3 β_c values for crustal records and T = 1.5s.

For six of the seven scaled records there is failure due to low-cyclic fatigue of one of the bars of the T = 1.5s column.

For the San Fernando-Hollywood storage scaled record the lateral displacement is 38cm equal to the displacement capacity prescribed by AASHTO therefore crushing of the concrete occurs since $\varepsilon_c = \varepsilon_{cu}$ as seen in Figure C.10 c.

The average β_c is 0.22 being the maximum 0.73 for the Hollywood storage scaled record and the minimum is 0.03 for the El Centro scaled record. For the Hollywood storage record the dissipated energy due to the repeated plastic displacements reaches a very low value.

Figure C.10 shows the responses for the scaled San Fernando-Hollywood records. Notice in the hysteretic response that there are few cycles of repeated displacement so this record appears more as a large pulse type of record.

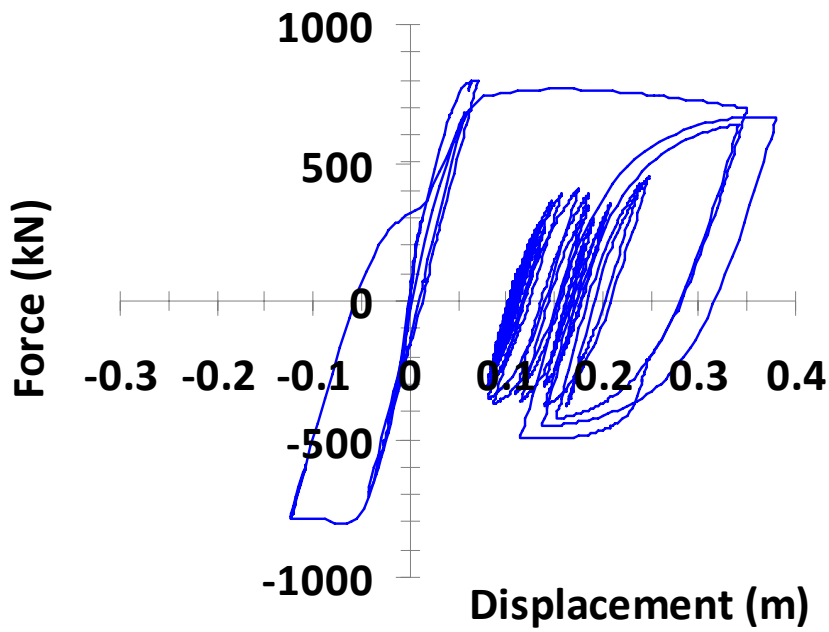

(a)

Figure C.10 Column T=1.5s β_c for San Fernando Hollywood Sto. Lot Record SF= 3.18

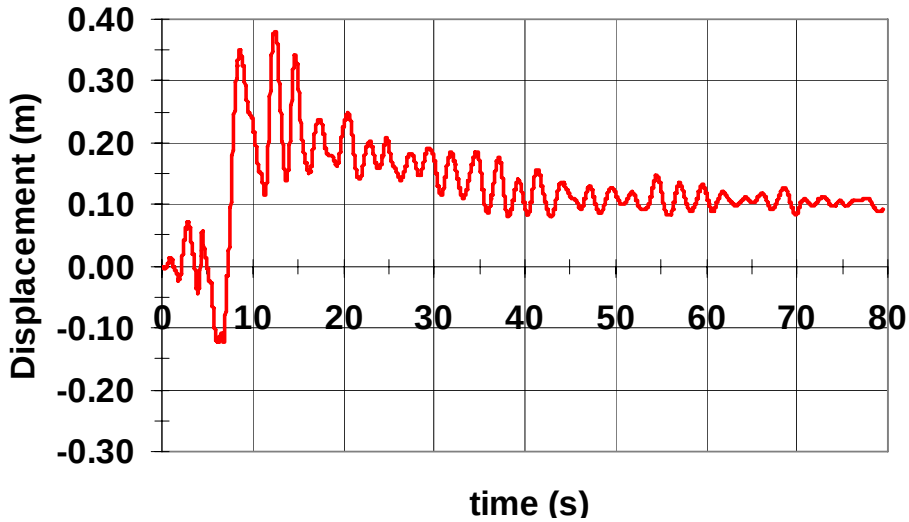

(b)

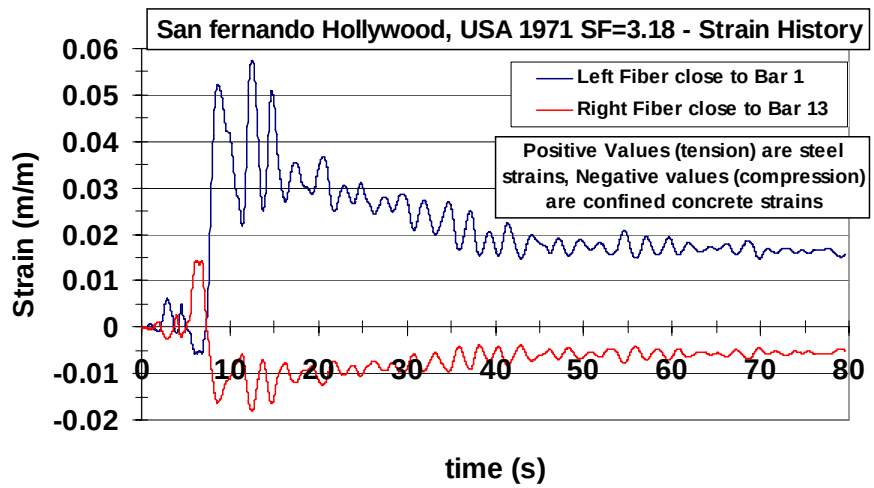

(c)

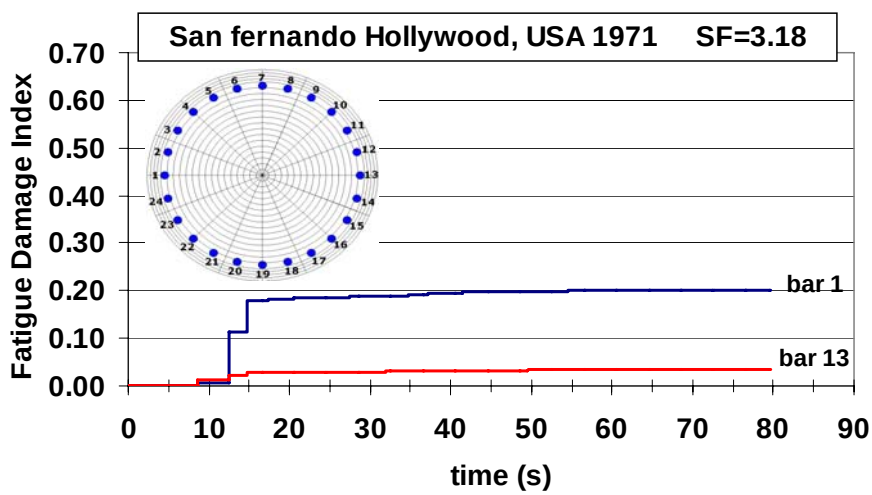

(d)

Figure C.10 (cont.) Column T=1.5s β_c for San Fernando Hollywood Storage Lot Record SF= 3.18

C.6 CDI for the T = 0.5 s bridge column.

C.6.1 CDI for T = 0.5s bridge column. Subduction records.

In Table 5.4 for the unscaled Llolleo record a total of three bars fracture due to low-cyclic fatigue and for the unscaled Llayllay record one bar fractures due to the same failure mechanism.

For the Pisco record at t = 18s the confined concrete strain reaches a larger value than the ultimate and later at t = 22s, two bars fracture due to low-cyclic fatigue and five more bars fracture due to the same mechanism between t = 22s to t= 26s as seen in Figures C.11 c, and d.

The above indicated damage is larger than the SDPL for these columns since the scale factors used on the same records to estimate SDPL are less than 1.0, Table 5.1. The Lolleo and Llayllay unscaled records carry the column to a CDI = 1.04 while Pisco has a CDI = 1.34.

The damage induced by the other four unscaled subduction records is less than the SDPL so the CDI values are less than 1.0.

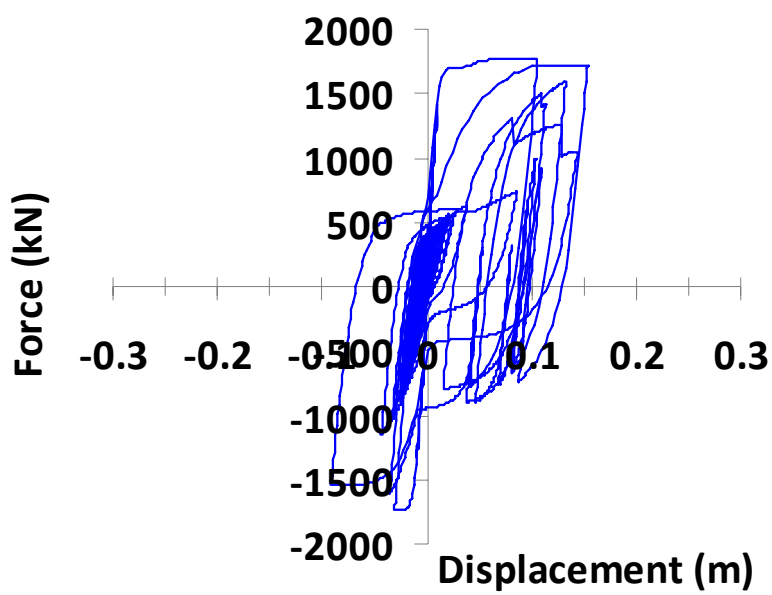

(a)

Figure C.11 Column T=0.5s CDI for Pisco Record SF=1.00

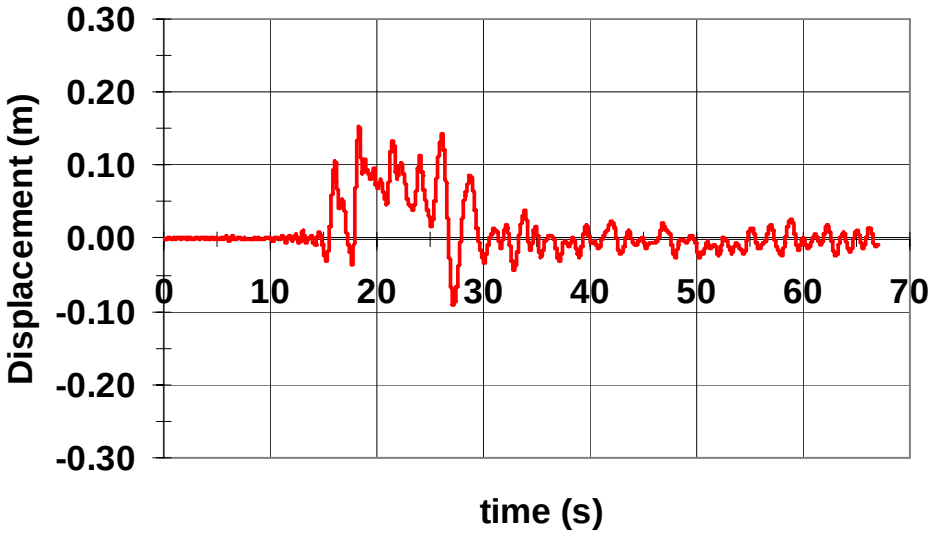

(b)

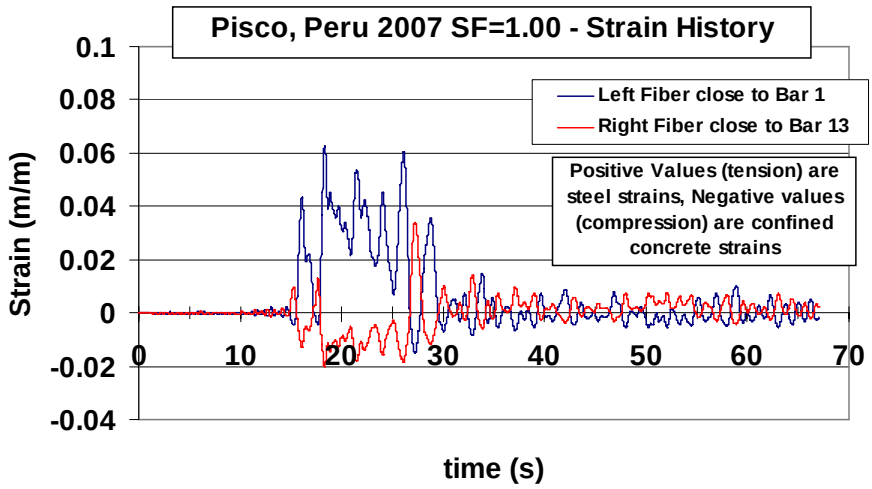

(c)

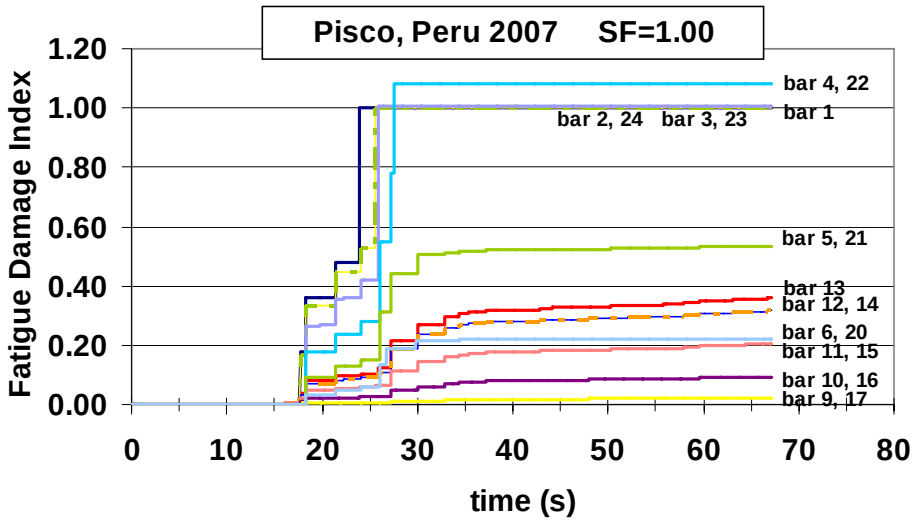

(d)

Figure C.11 (cont.) Column T=0.5s CDI for Pisco Record SF=1.00

C.6.2 CDI for T = 0.5s bridge column. Soft soil records.

The unscaled SCT and Tihuac Bombas records induce each one fatigue of one bar in the column then crushing of the confined concrete and finally more fracture of bars due to low cyclic fatigue. For the SCT unscaled record a total of 20 bars fracture and for the unscaled Tihuac Bombas record all the total reinforcing of 24 bars fracture.

Figures C.12 a, to C.12 d show the sequence of damage for the Tihuac Bombas record. At t = 59.0s two bars fracture due to low-cyclic fatigue. At t = 59.5s, the confined concrete strain is larger than ε_{cu} = 0.018 therefore the concrete crushes. Between t = 59.0s and t = 80s all bars fractured due to low-cyclic fatigue. During this same period of time the concrete reaches strains larger than 0.18 at least two times crushing continuously the confined concrete.

The hysteretic response let to observe the deterioration of the strength of this bridge column.
The increase in the E_{ucpr} values for the unscaled SCT and Tihuac Bombas records to 831.1kN-m and 723.5kN-m from those when SDPL is estimated causes the large number of fractured bars.

The unscaled TXSO record causes the fracture of 5 bars due to low-cyclic fatigue.
The damage caused by the other soft soil records is less than the one causing SDPL for this column so CDI values are less than 1.0.

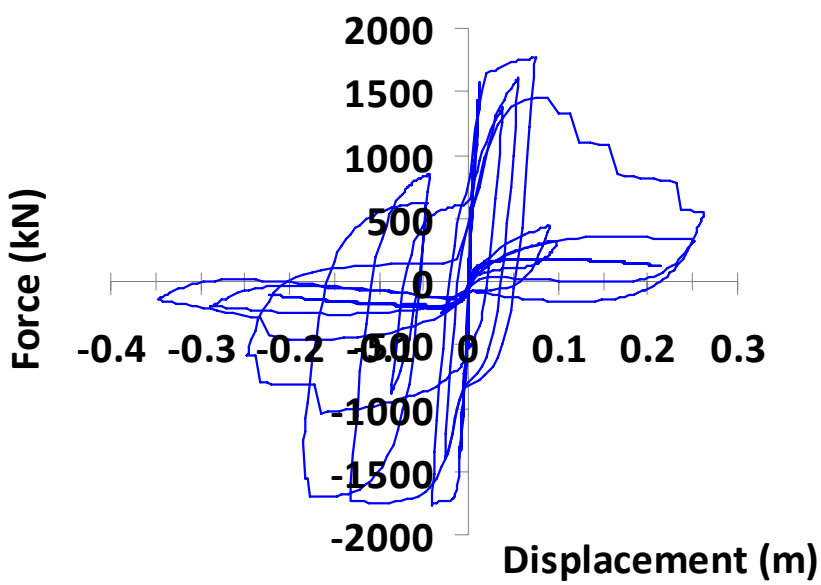

(a)

Figure C.12 Column T=0.5s CDI for Tihuac Bombas Record SF=1.00

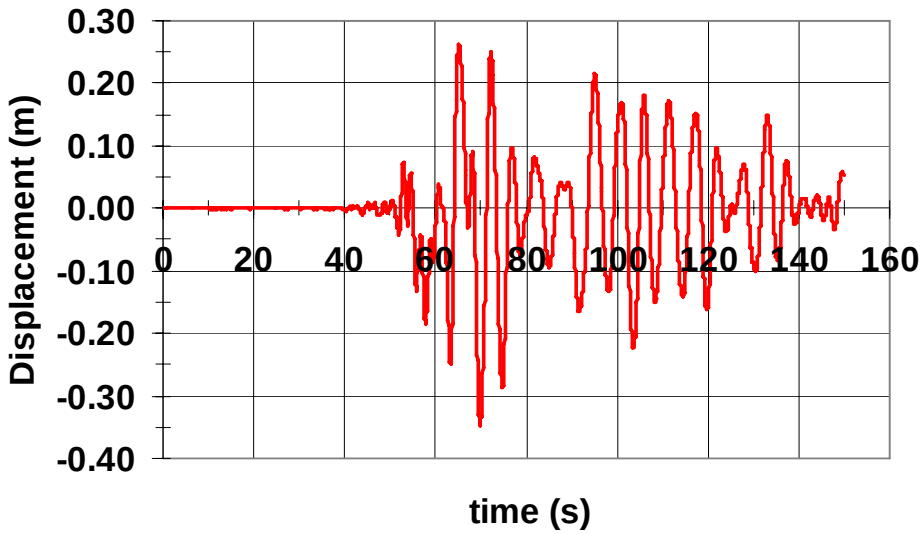

(b)

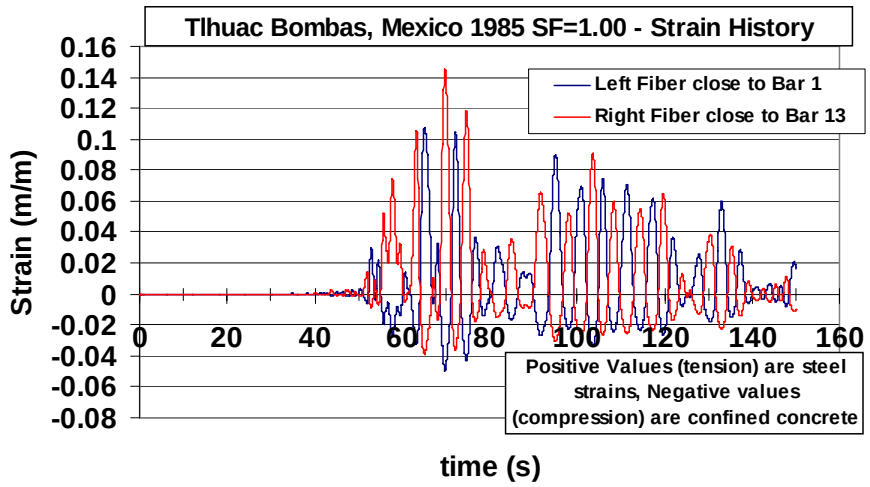

(c)

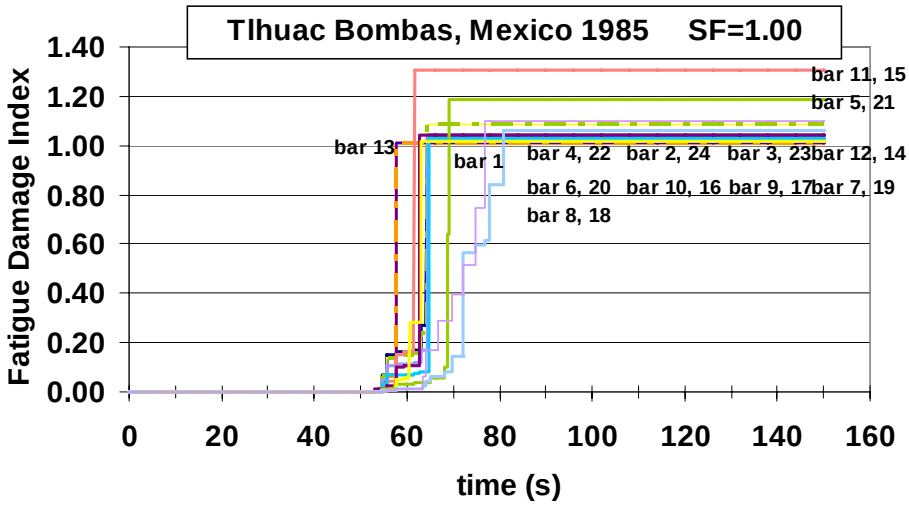

(d)

Figure C.12 (cont.) Column T=0.5s CDI for Tihuac Bombas Record SF=1.00

C.6.3 CDI for T = 0.5s bridge column. Crustal records.

There is no damage larger than the Significant Damage for any of the unscaled records on the column. Figure C.13 shows the responses of the T = 0.5s bridge column subjected to the Loma Prieta Hollister City Hall record. The displacements are less than the capacity and six bars have lost close to 20% of their fatigue life.

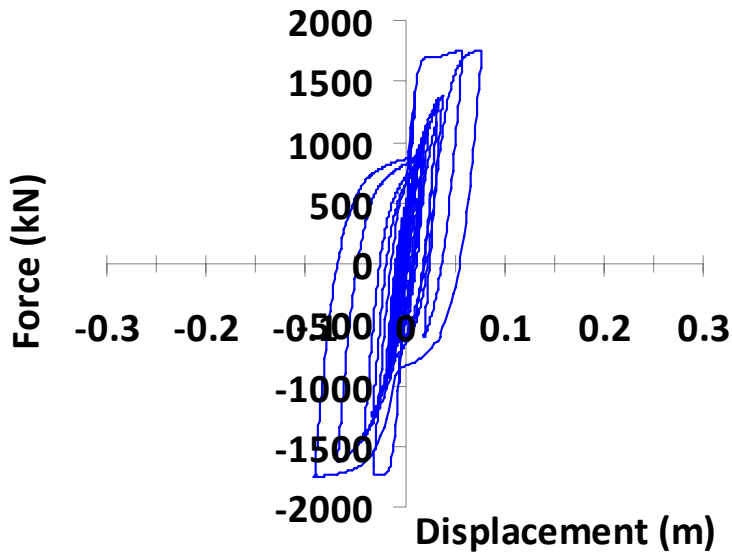

(a)

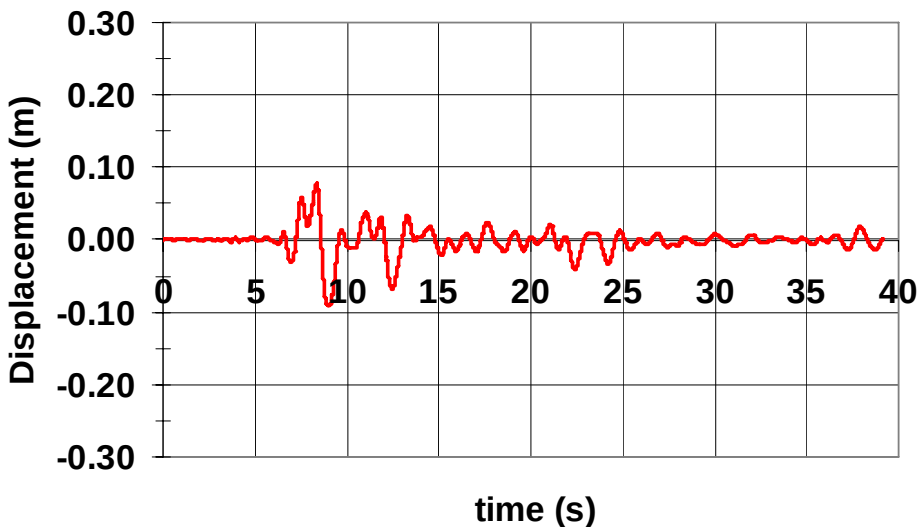

(b)

Figure C.13 Column T=0.5s CDI for Loma Prieta Hollister City Hall Record SF=1.00

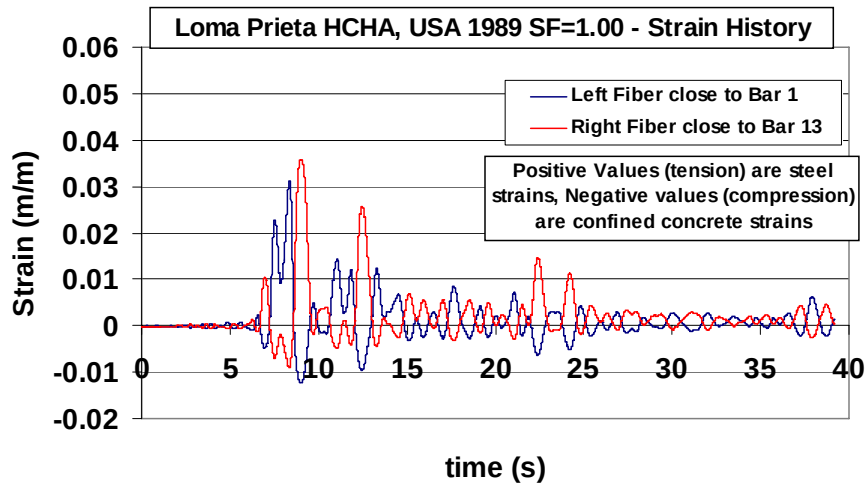

(c)

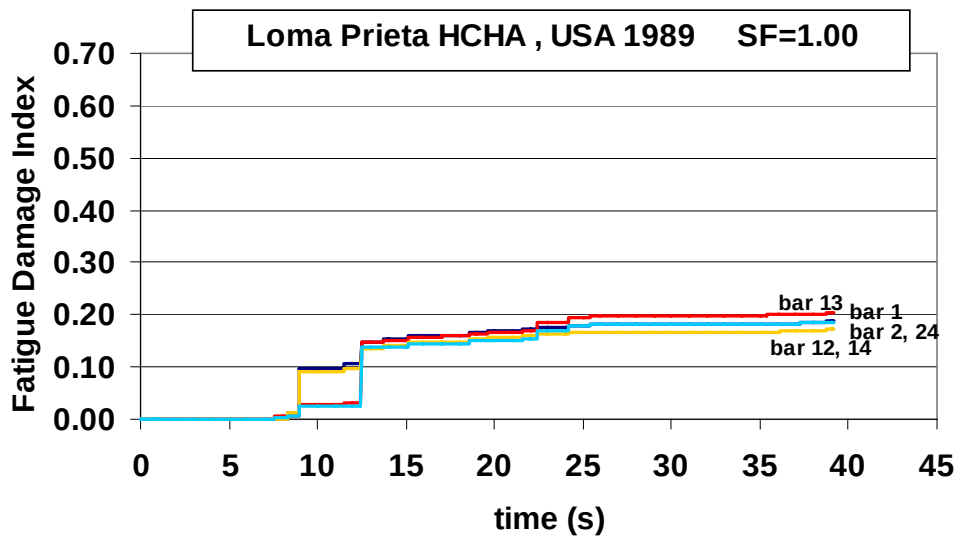

(d)

Figure C.13 (cont.) Column T=0.5s CDI for Loma Prieta Hollister City Hall Record SF=1.00

C.7 CDI for the T = 1.0 s bridge column.

C.7.1 CDI for T = 1.0 s bridge column. Subduction records.

The damage on the column for these records is lower than the Significant Damage. Figure C.14 shows the responses for the Pisco unscaled record. Six bars have lost between 42 and 49% of their fatigue life.

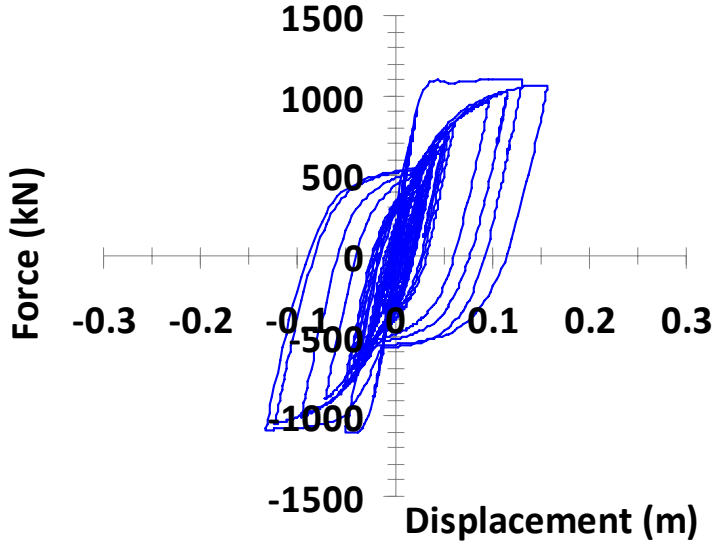

(a)

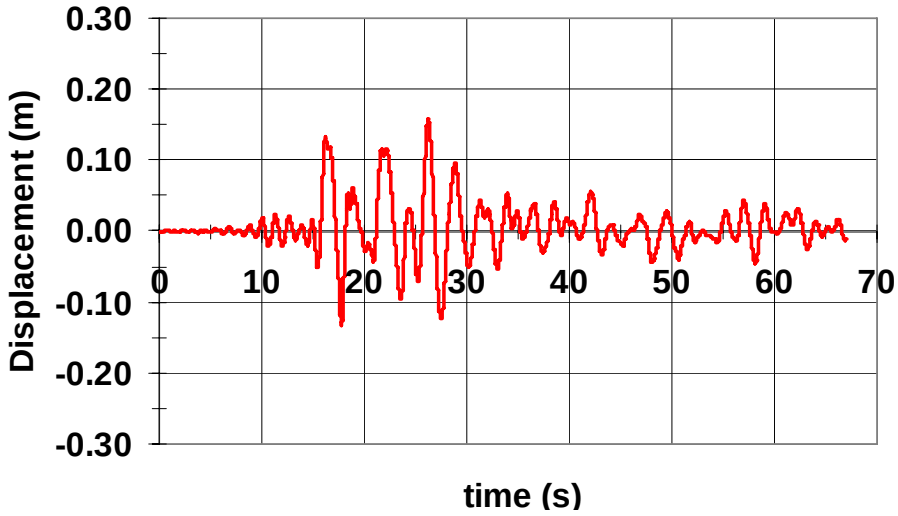

(b)

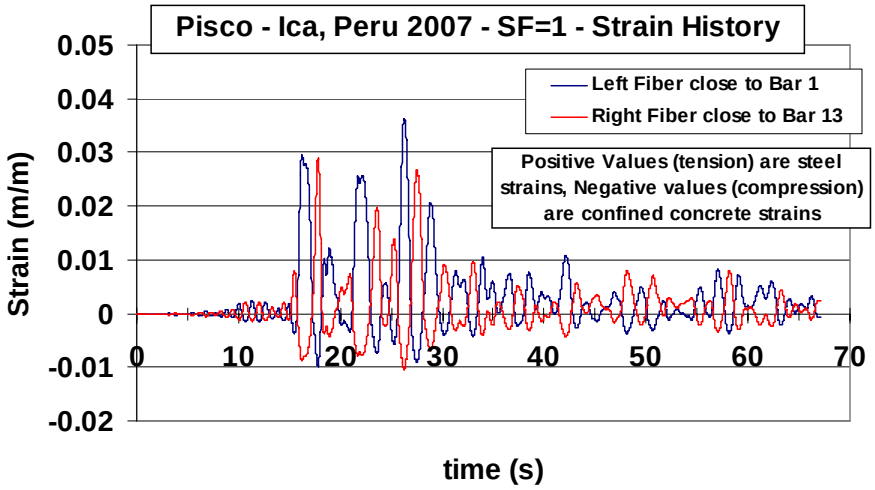

(c)

Figure C.14 Column T=1.0s CDI for Pisco Record SF=1.00

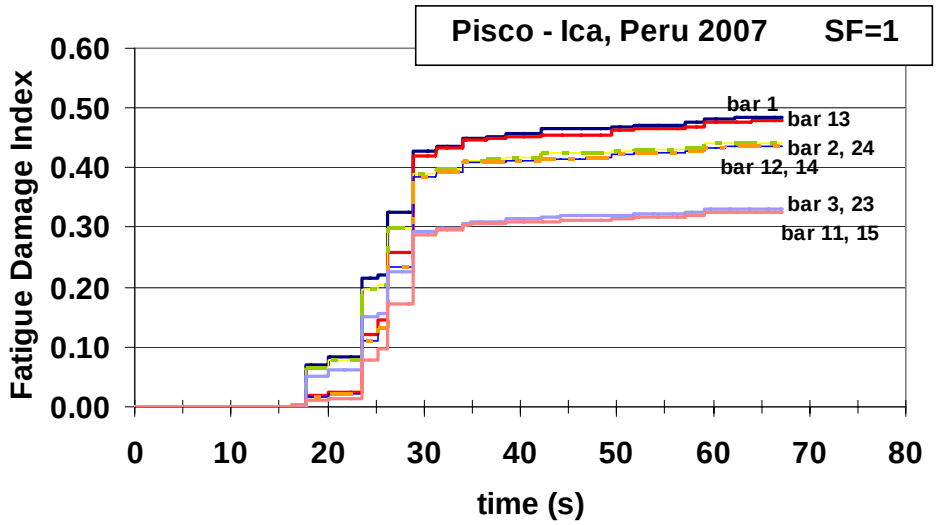

(d)

Figure C.14 (cont.) Column T=1.0s CDI for Pisco Record SF=1.00

C.7.2 CDI for T = 1.0s bridge column. Soft soil records.

The scale factor used to find the SDPL and β_c for the T = 1.0s column is less than 1.0 for the SCT-1, CDAO, CDAF and Tihuac-Bombas records. For the Tihuac Deportivo is 1.02, for the Sismex Viveros is 2.98 and for TXSO is 1.0. For six of the records the SDPL is the fracture of one bar due to low-cyclic fatigue. For the Sismex Viveros record the lateral displacement is larger than the capacity and the confined concrete strain results larger than the ultimate so the concrete crushes.

The results for the unscaled records as seen in Table 5.5 are fracture of 16 bars due to low-cyclic fatigue and later crushing of the confined concrete for the SCT-1 record that induces a displacement of 28cm larger than the 24cm capacity. Fracture of 3 bars for the CDAF record and fracture of 16 bars and crushing of the confined concrete for the CDAO record inducing 32cm displacement. No damage for the Tihuac-Bombas, Tihuac Deportivo and the Sismex Viveros records and, one bar fractured due to low-cyclic fatigue by the TXSO record.

This is a demonstration that if the scale used on the record to calculate the CDI of a column is larger than the one used on the same record to estimate SDPL, the damage will be larger than the SDPL. If the scaling for the CDI is lower than for the SDPL the damage is less than the SDPL and if the scaling for the CDI is equal to the one used for the SDPL, the damage is similar.

The hysteretic response, Figure C.15 a, shows the great deterioration of the bridge column due to the unscaled Tihuac-Bombas record that induces a large lateral displacement of about 32cm for the deteriorated column.

During the cycle that carries the bridge column to the first large displacement of 26cm the confined concrete crushes when the strain is larger than ε_{cu} =0.018. The cycle closes with a deteriorating strength.

In the following cycle the displacement reaches 32cm and the fracture of the bars due to low-cyclic fatigue begins. The hysteretic response shows a large decrease of the strength due to fracture of the bars.

At t = 55s due to the complete deterioration of the bridge column the OpenSees framework stops calculations.

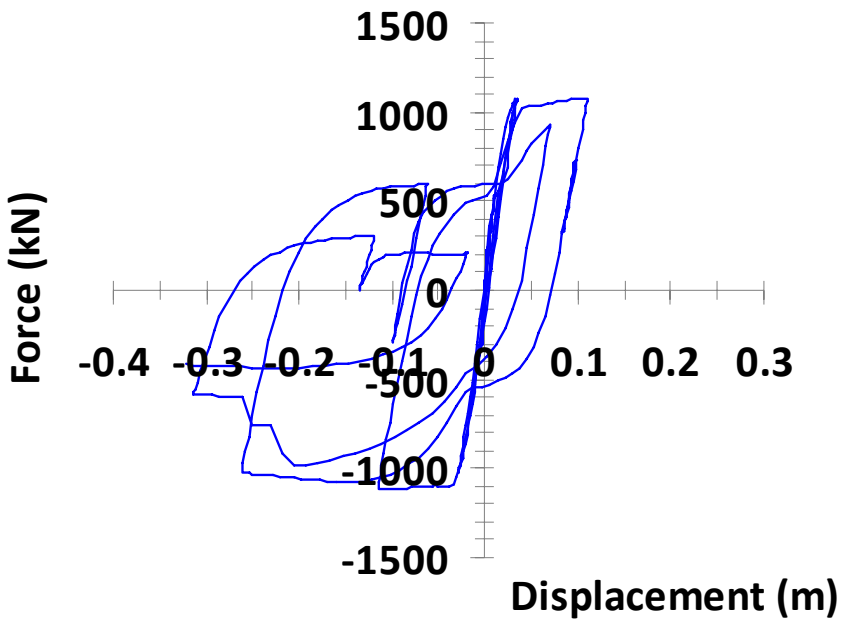

(a)

Figure C.15 Column T=1.0s CDI for Tlhuac Bombas Record SF=1.00

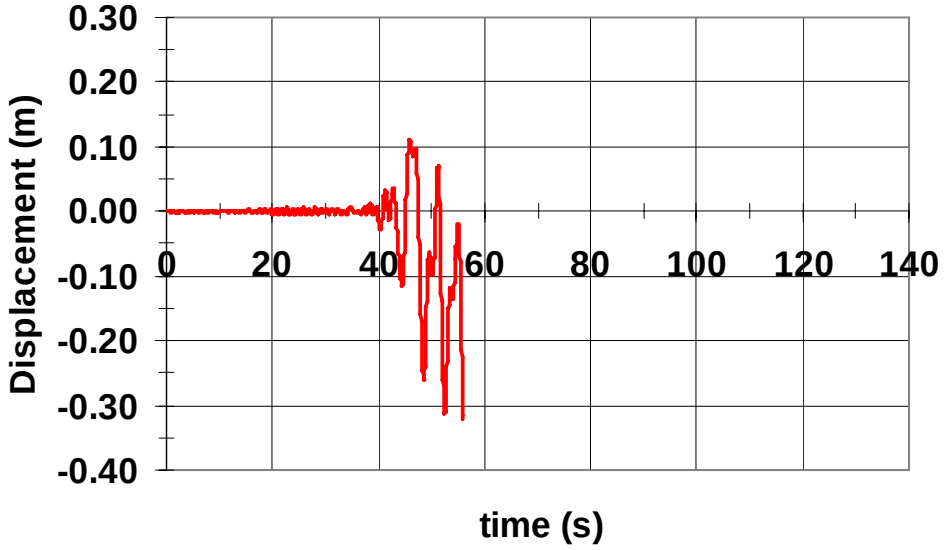

(b)

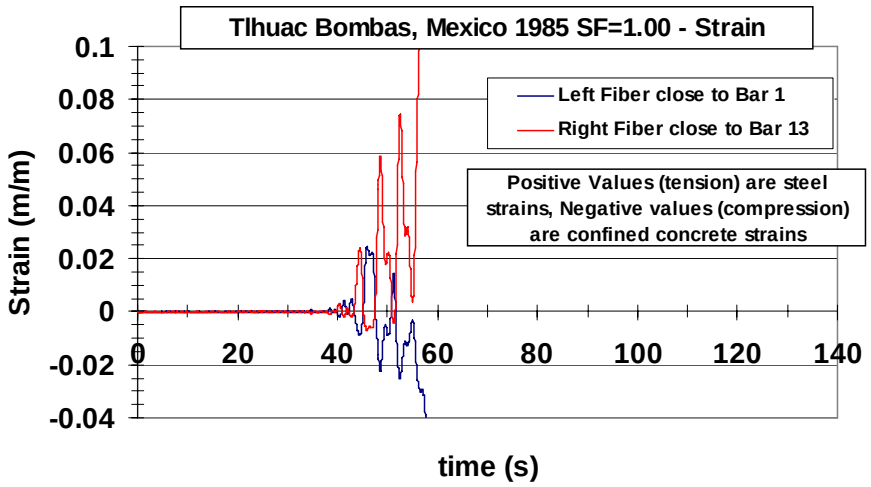

(c)

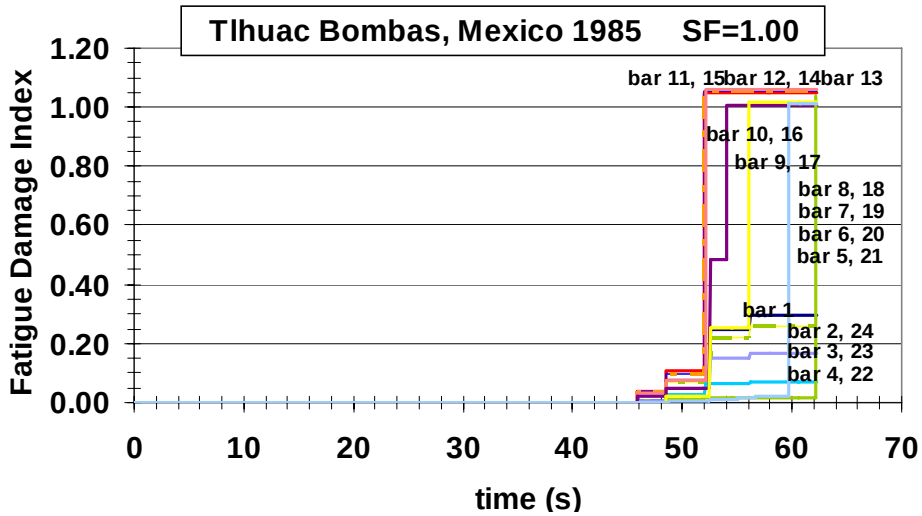

(d)

Figure C.15 (cont.) Column T=1.0s CDI for Tlhuac Bombas Record SF=1.00

C.7.3 CDI for T = 1.0s bridge column. Crustal records.

Except for the unscaled Loma Prieta-Sunnyvale record that induces fracture of one bar due to low-cyclic fatigue the other records do not cause any damage larger than the SDPL.

The scale factor for Sunnyvale to calculate β_c and reach SDPL is 1.0 and it is the same to calculate the CDI therefore the damage is the same.

Figure C.16 shows the responses for the T = 1.0s column subjected to the Loma Prieta Sunnyvale unscaled record. The CDI = 1.0 and there is only one bar that fractures due to low-cyclic fatigue.

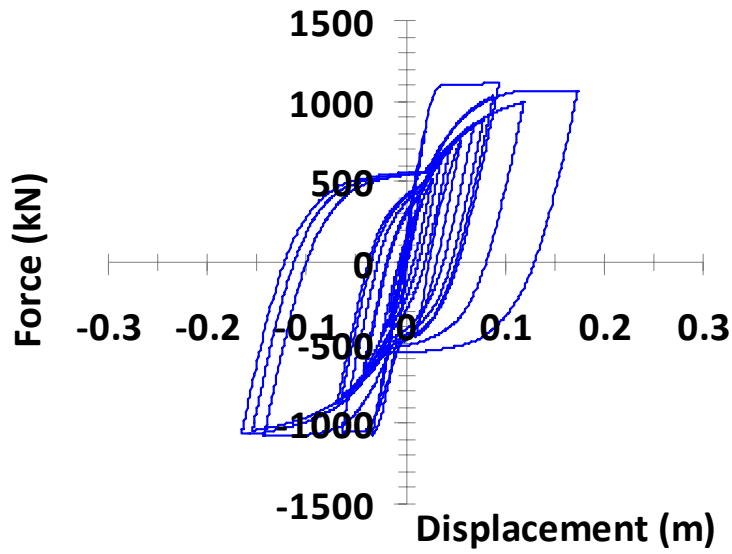

(a)

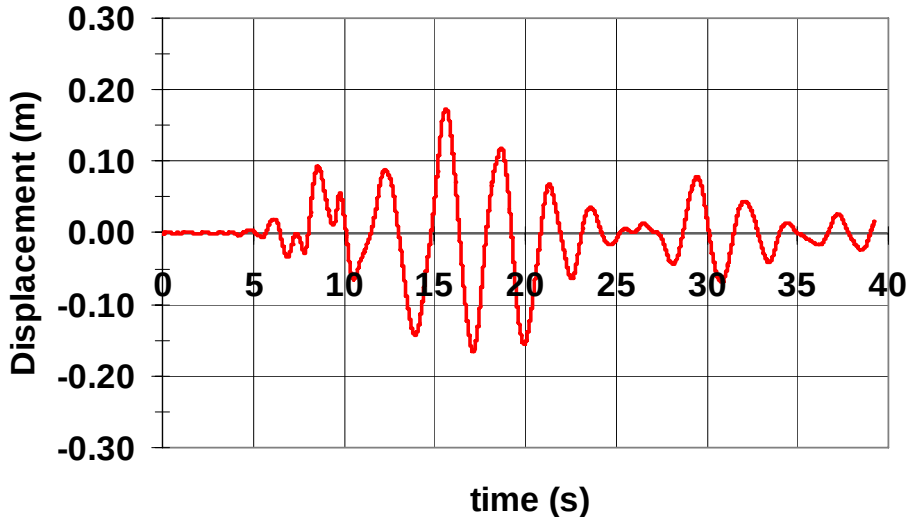

(b)

Figure C.16 Column T=1.0s CDI for Loma Prieta Sunnyvale Record SF=1.00

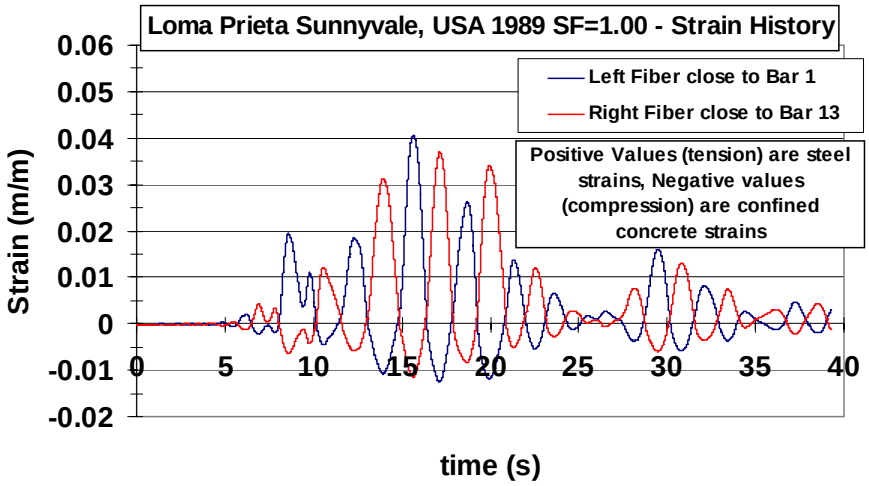

(c)

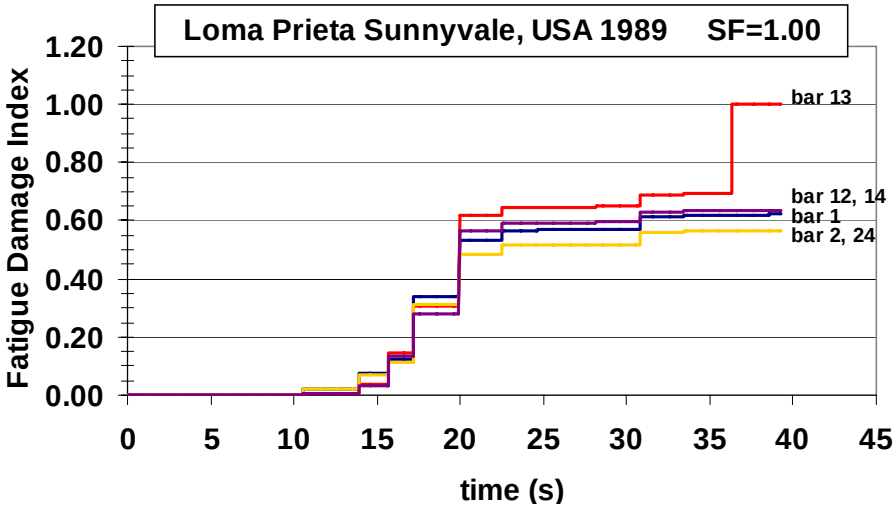

(d)

Figure C.16 (cont.) Column T=1.0s CDI for Loma Prieta Sunnyvale Record SF=1.00

C.8 CDI for the T = 1.5 s bridge column.

C.8.1 CDI for T = 1.5 s bridge column. Subduction records.

There is no flexural failure of the column for any of the unscaled records since the scale factors to reach Significant Damage are all larger than 1.0.

Figure C.17 show the responses for the Pisco unscaled record.

C.8.2 CDI for T = 1.5 s bridge column. Soft soil records.

Only three records induce damage for the column. To reach the SDPL fracture of one bar due to low-cyclic fatigue occurs for the SCT-1 record with scale factor of 0.78 as seen in Table 5.3.

Therefore, for the unscaled record there will be more damage. In effect, a total of seven bars fracture due to low-cyclic fatigue in this column for the unscaled record.

The CDAO record requires a scale factor of 0.65 to reach SDPL in the form of one bar fractured due to low-cyclic fatigue as seen in Table 5.3. For the unscaled record first, the maximum displacement reaches an extremely large value of 44cm so there is crushing of the concrete since the strain is larger than 0.018 as seen in Figure C.18 c. Immediately the fracture of the bars begins and a total of 14 bars fracture due to low-cyclic fatigue up to t = 115s as seen in Figure C.18 d.

The Tihuac Bombas with a scale factor of 0.63 provoked SDPL in the form of fracture of one bar as shown in Table 5.3. As shown in Figure C.19 the unscaled record induces the fracture of a total of 13 bars and then a large lateral displacement reaching 38cm that crushes the concrete.

The other four unscaled records do not cause any damage larger than the Significant Damage since the scaling to calculate β_c is larger than 1.0.

The deterioration of strength due to the fracture of the bars is seen in the hysteretic responses in Figures C.18 and C.19.

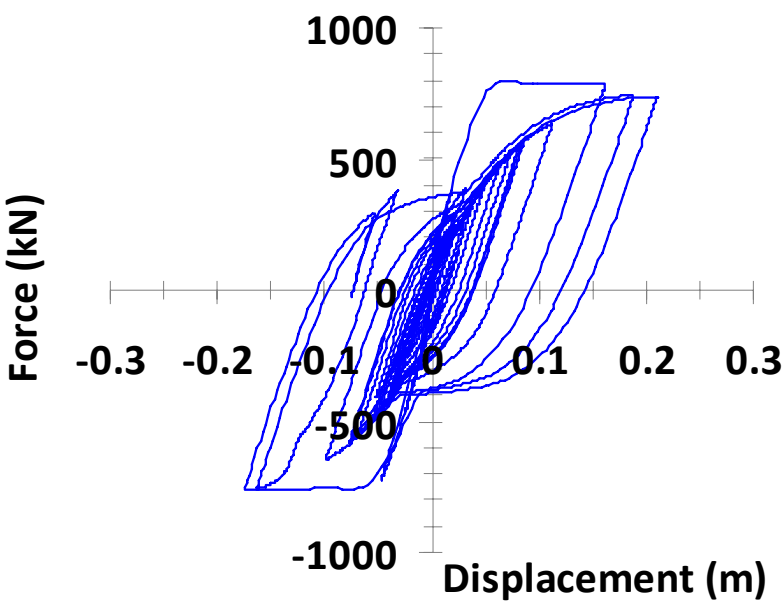

(a)

Figure C.17 Column T=1.5s CDI for Pisco Record SF=1.00

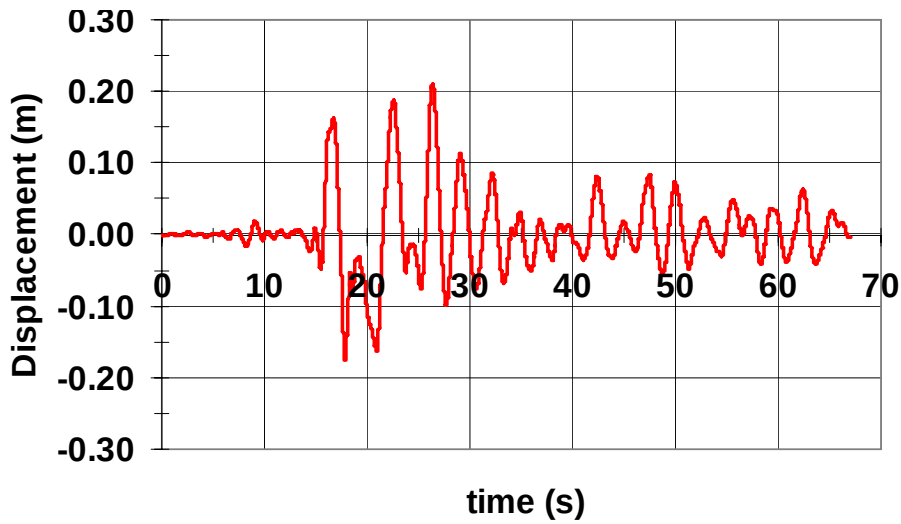

(b)

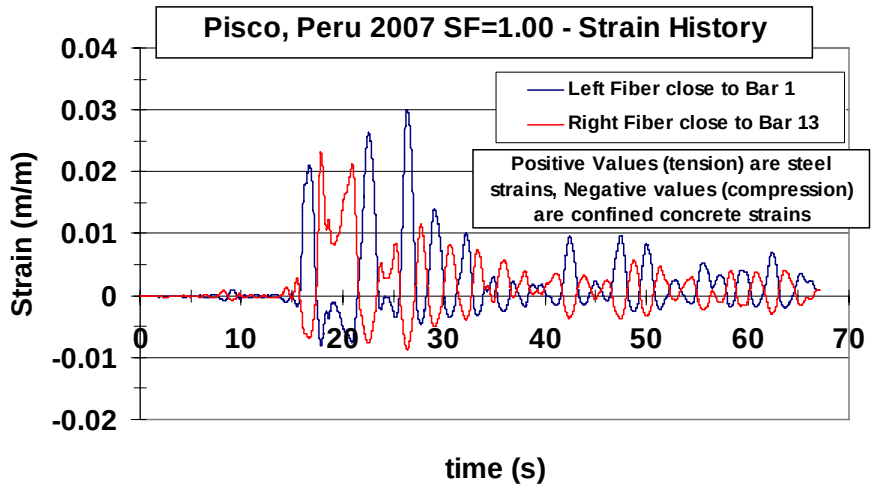

(c)

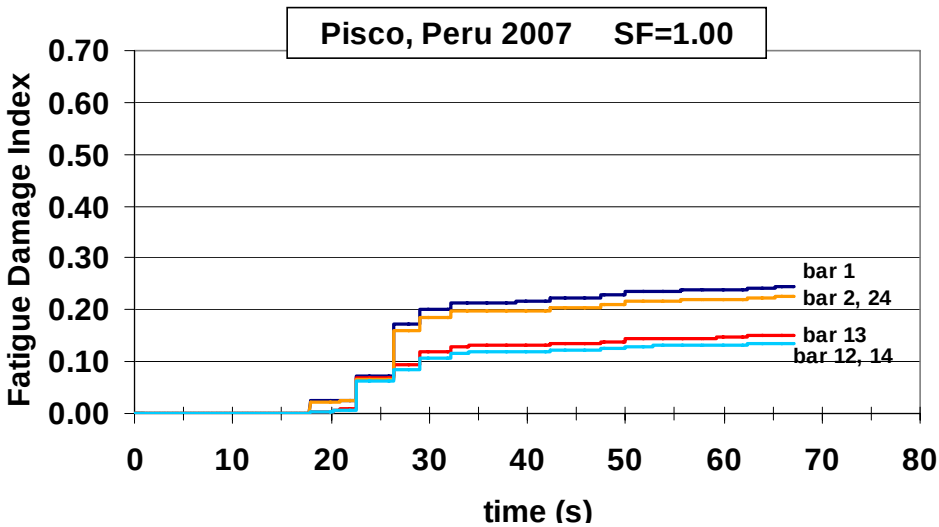

(d)

Figure C.17 (cont.) Column T=1.5s CDI for Pisco Record SF=1.00

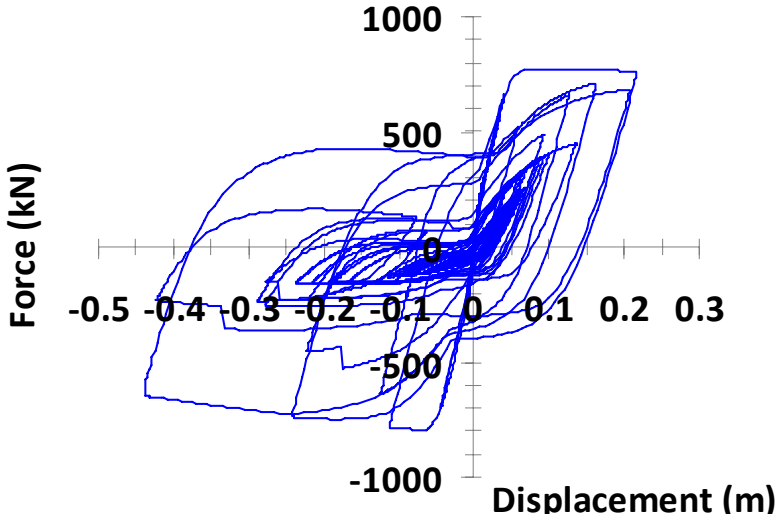

(a)

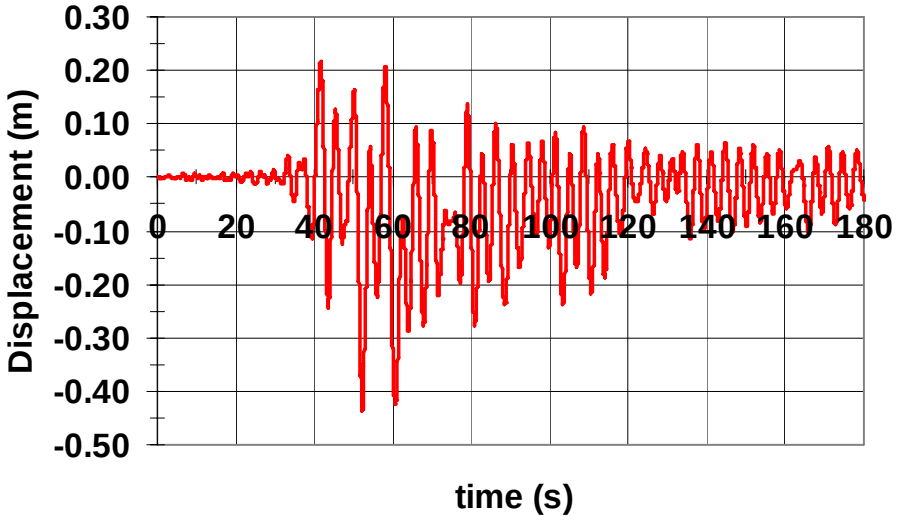

(b)

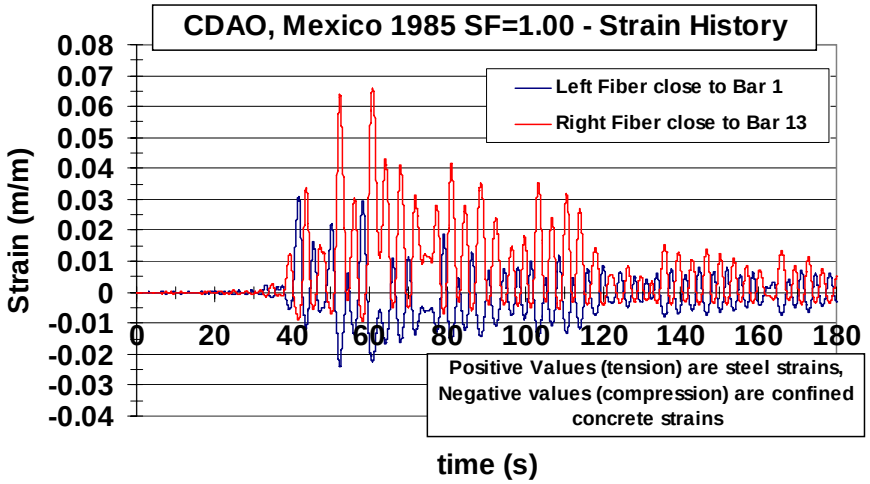

(c)

Figure C.18 Column T=1.5s CDAO Record SF=1.00

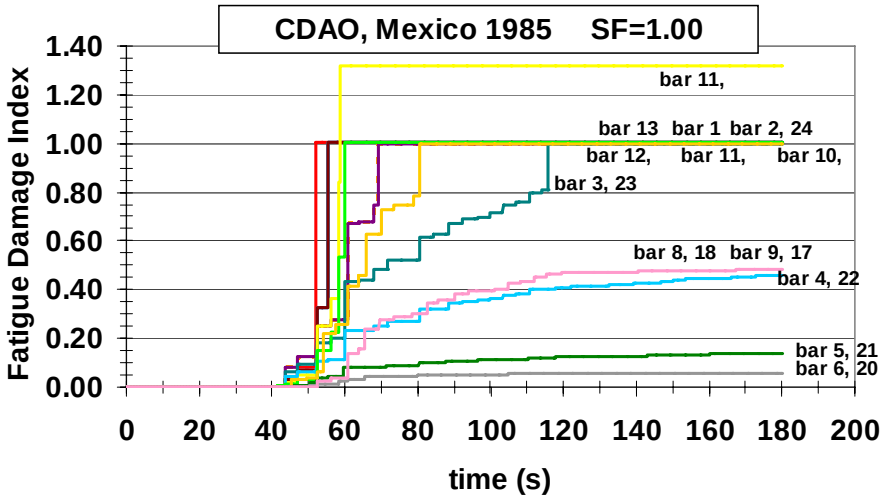

(d)

Figure C.18 (cont.) Column T=1.5s CDAO Record SF=1.00

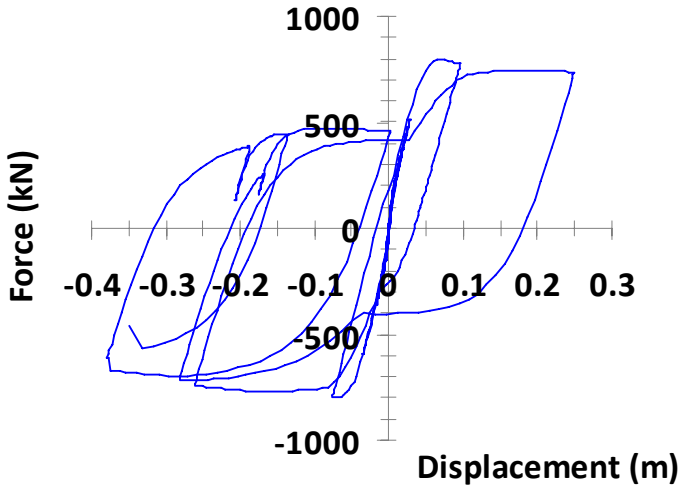

(a)

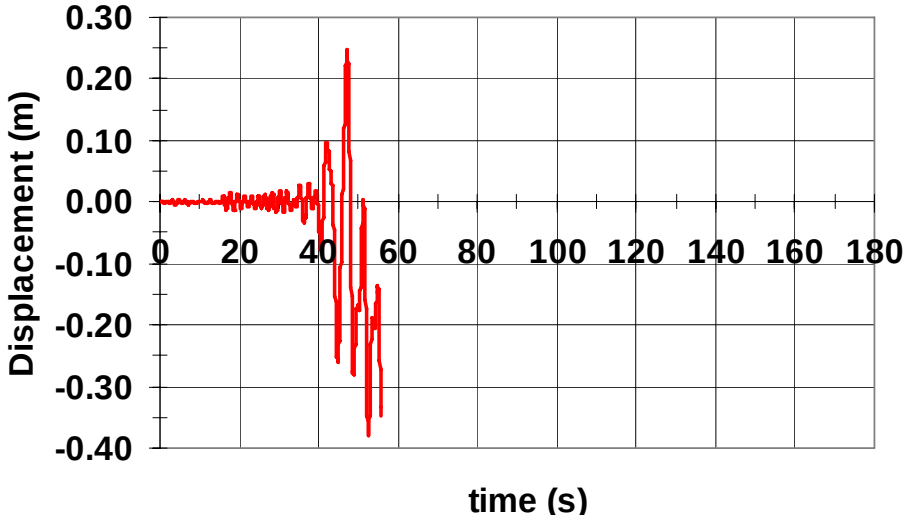

(b)

Figure C.19 Column T=1.5s CDI for Tlhuac Bombas Record SF=1.00

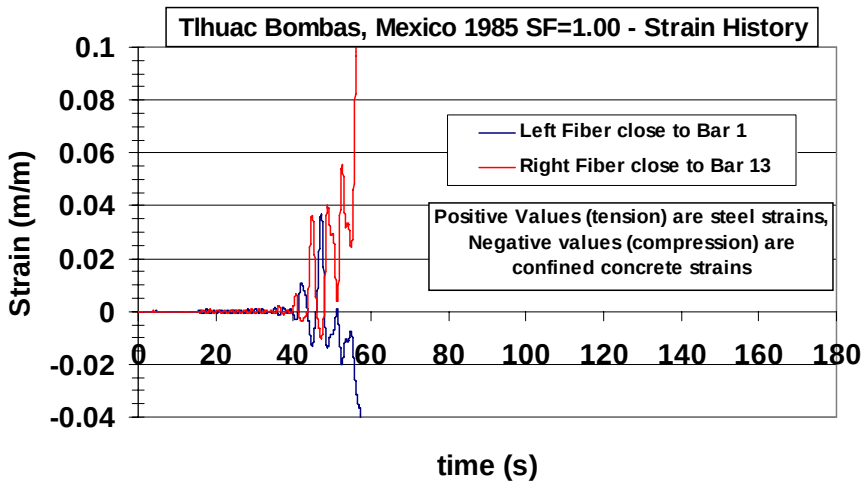

(c)

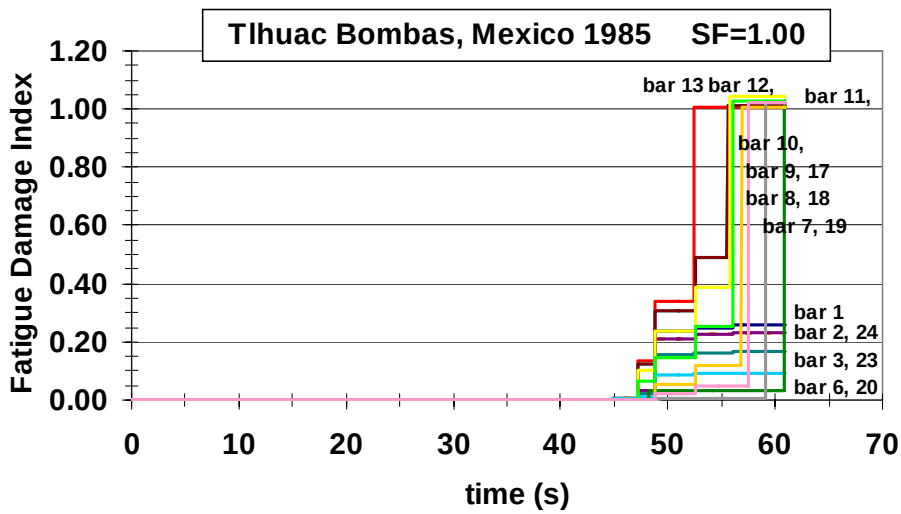

(d)

Figure C.19(cont.) Column T=1.5s CDI for Tlhuac Bombas Record SF=1.00

C.8.3 CDI for T = 1.5s bridge column. Crustal records.

The damage due to these unscaled records on the T = 1.5s column is less than the SDPL since to calculate β_c all records were scaled with values larger than 1.0.

Figure C.20 show results for the Loma Prieta Sunnyvale unscaled record. Bar 1 has lost about 40% of its fatigue life.

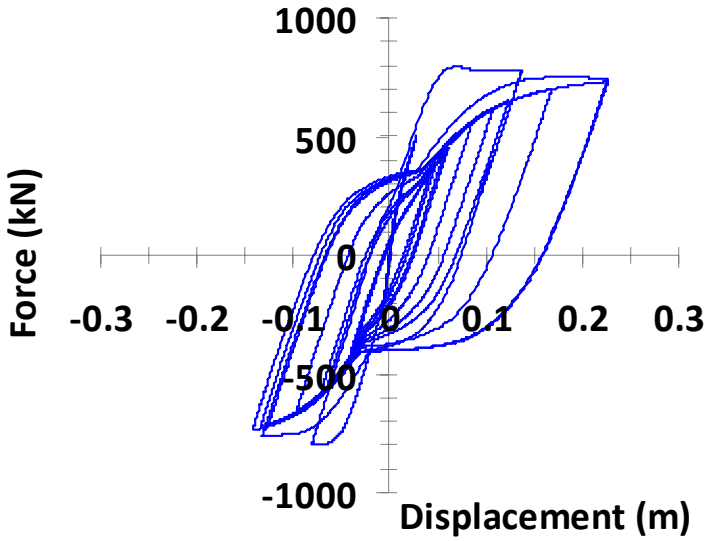

(a)

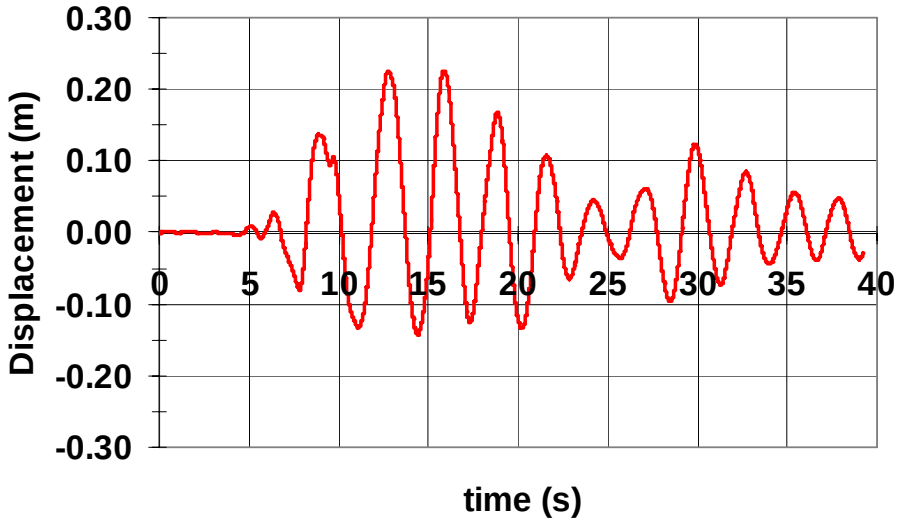

(b)

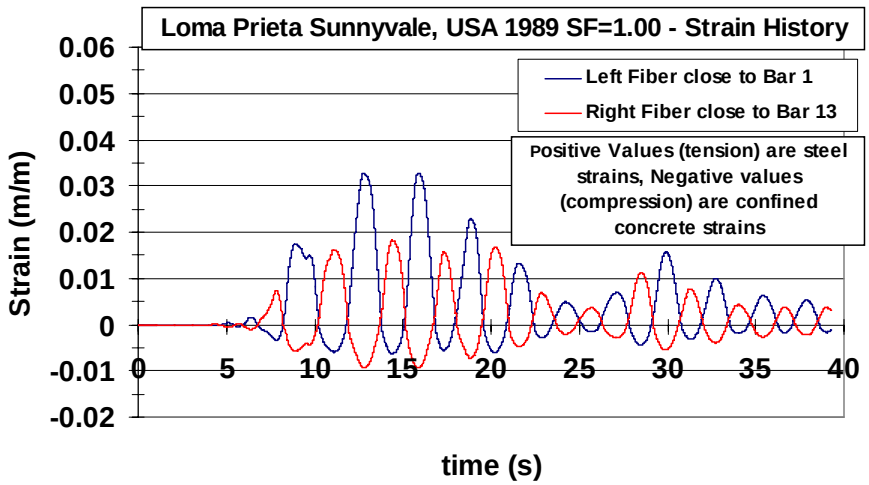

(c)

Figure C.20 Column T=1.5s CDI for Loma Prieta Sunnyvale Record SF=1.00

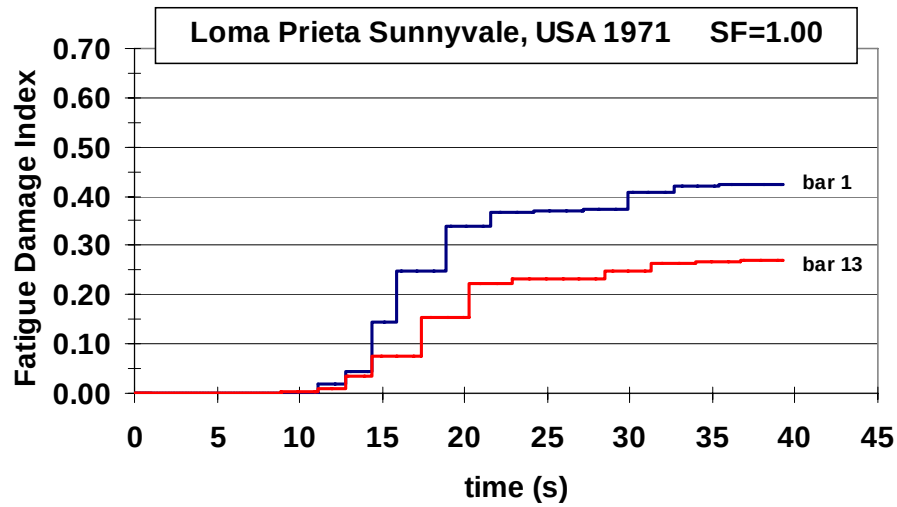

(d)

Figure C.20 (cont.) Column T=1.5s CDI for Loma Prieta Sunnyvale Record SF=1.00

C.9 Effects of aftershocks

C.9.1 Additional damage for T = 0.5s bridge column.

The unscaled Pisco earthquake is now the main shock and it is followed by an aftershock with intensity is equal to 60% of the main shock.

Table 5.7 shows that for the unscaled Pisco main shock 7 bars fracture due to low-cyclic fatigue and the aftershock causes an increase of the lateral displacement of 15.4cm that carries the bridge column to a compression concrete strain $\varepsilon_c = 0.020$ that is larger than $\varepsilon_{cu} = 0.018$ inducing crushing of the concrete. In addition, the increase in the number of cycles causes an increase in E_{ucpr} that induces the fracture of one more bar due to low-cyclic fatigue.

The unscaled Viña del Mar record transformed into the main shock induces lower damage than the SDPL but, an aftershock of the same intensity as the main shock induces the fracture of six bars due to low-cyclic fatigue.

For the unscaled Viña del Mar record the maximum strain demands for the main shock followed by the aftershock are lower than the confined concrete and steel strain capacities. The maximum lateral displacement demand is also lower than the displacement capacity.

The damage due to the Tihuac Deportivo unscaled record is less than the SDPL but an aftershock similar to the main shock causes the fracture of 10 bars due to low cyclic fatigue and later the

confined concrete strain increases to 0.02 that is a larger strain than ε_{cu} = 0.018 causing crushing of the confined concrete.

The Loma Prieta Hollister City unscaled record induced lower damage than the SDPL. The aftershock similar to the main shock does not induce any failure mechanism.

However, the Loma Prieta Hollister City as a main shock followed by two aftershocks of the same intensity as the main shock fracture six bars due to low-cyclic fatigue.

C.9.2 Additional damage for T = 1.0s Bridge column.

Table 5.8 shows the results of main shocks and aftershocks.

The unscaled Pisco record followed by an aftershock which intensity is 60% of the main shock increases the damage and one bar fractures due to low-cyclic fatigue.

The unscaled Tihuac Deportivo followed by 60% of the main shock as an aftershock both induce the fracture of three bars and if the aftershock were 80% of the main shock five bars will fracture by low-cyclic fatigue.

The strains in the confined concrete and in the steel are lower than the maximum allowed.

The unscaled TXSO and the Loma Prieta Sunnyvale records acting as main shocks already induced the fracture of one bar due to low-cyclic fatigue and the aftershocks with intensities of 60% of the main shocks induce much more damage. The aftershock of TXSO fractures five more bars and the Loma Prieta Sunnyvale aftershock fractures three more bars.

The strains in the confined concrete and in the steel bars are lower than the maximum allowed values.

C.9.3 Additional damage for T = 1.5s bridge column.

Table 5.9 show the results for unscaled records considered now as main shocks followed by percentages of them acting as aftershocks.

The Pisco, CDAF and Loma Prieta Sunnyvale main shocks induced less damage than the SDPL. However, these records followed by the corresponding aftershocks caused more damage in this bridge column.

The Pisco main shock followed by two aftershocks that amount each one 100% of the main shock induce the fracture of three bars due to low-cyclic fatigue.

The CDAF and the Loma Prieta Sunnyvale unscaled records followed each one by one aftershock with an intensity equal to 100% of the main shock induce the fracture of three bars in each case.

The SCT-1 unscaled record caused the fracture of seven bars due to low-cyclic fatigue. This record followed by an aftershock which intensity is 60% of the main shock induces the fracture of one more bar.

The strains in the confined concrete and in the steel are lower than the maximum allowed.